Dehydrohelicenes and Other Polycyclic Heteroaromatic Molecules: Electrochemical Syntheses, Derivatization, and Optical Properties

A Doctoral Thesis
Submitted to the Department of Chemistry
Graduate School of Science
Osaka University

By

Mohamed Salem

Synthetic Organic Chemistry
The Institute of Scientific and Industrial Research (SANKEN)
August 2022

Contents

List of Symbols and Abbreviations

Ac	acetyl group
Aq.	aqueous solution
Ar	aryl group
BINAP	2,2'-bis(diphenylphosphino)-1,1'-binaphthyl
BINOL	1,1'-bi-2-naphthol
Bn	benzyl group
B3LYP	the most famous hybrid DFT model, abbreviation for (Becke-3-parameter-Lee-Yang-Parr)
CD	circular dichroism
CE	cotton effect
CP	circularly polarized
CPL	circularly polarized luminescence
CV	cyclic voltammetry
D	electric dipole strength
DCM	dichloromethane
DDQ	2,3-dichloro-5,6-dicyano-1,4-benzoquinone
DFT	density functional theory
DMF	*N*,*N*-dimethylformamide
ΔI	differential emission intensity
ee	enantiomeric excess
Eq.	equation
Equiv.	equivalent
ESI	electrospray ionization
Et	ethyl group
FTO	fluorine doped tin oxide
G	magnetic dipole strength
g_{CD}	absorption dissymmetry factor
g_{CPL}	luminescence dissymmetry factor
HPLC	high-performance liquid chromatography
HRMS	high-resolution mass spectrometry
IPA	isopropyl alcohol
i-Pr	isopropyl group
IS	internal standard
Me	methyl group

MS	mass spectrometry
MTDM	magnetic transition dipole moments
MW	microwave
n-Bu	*normal*-butyl group
NIR	near infrared
NMR	nuclear magnetic resonance
OFET	organic field effect transistor
OLED	organic light emitting diode
OR	optical rotation
ORD	optical rotatory dispersion
OTf	triflate (trifluoromethanesulfonate) group
PCCs	polymeric cholesteric crystals
Ph	phenyl group
PHAs	polycyclic heteroaromatics
PL	photoluminescence
Quant	quantitatively
R	rotational strength or rotatory strength
Rac	racemic
ROA	raman optical activity
rt	room temperature
SET	single electron transfer
SOMs	small organic molecules
TBA	tetrabutylammonium group
t-Bu	*tert*-butyl group
TD-DFT	time dependent - density functional theory
TEDM	electric transition dipole moments $\|\boldsymbol{\mu}\|$
TFA	trifluoroacetic acid
THF	tetrahydrofuran
TMDM	magnetic transition dipole moments $\|\mathbf{m}\|$
TMEDA	*N*,*N*,*N*',*N*'-tetramethylethylenediamine
TMS	trimethylsilyl group
Ts	tosyl (*p*-toluenesulfonyl) group
UV-vis	ultraviolet–visible
VCD	vibrational circular dichroism

Chapter 1

1.1. Background

1.1.1. Polycyclic Heteroaromatic Compounds (PHAs)

The chemistry of PHA compounds, also described as heterocyclic nanographene, is a massive discipline, covering more than a hundred years of research. This area has progressed over time, including a mass of topics in physical chemistry, synthetic organic chemistry, molecular biology, synthesis of natural products, catalysis, and applied materials science.[1, 2] This rapidly growing field can be traced back to the earliest investigations and isolation of natural dyes. In 1907, Scholl achieved a quantum leap in this field by elucidating the unique structure of flavanthrone **2** which contains eight rings (**Scheme 1.1**).[3] However, the lack of analytical tools hindered the progress of the field for decades. The decisive determination of different structures like xylindein **1**, coerulein **3**, tricycloquinazoline **5**, and tetrabenzotetraoxa[8]circulene **4** had taken decades, although, most of these compounds were isolated earlier (**Scheme 1.1**). Even though these early examples were the first building blocks in this great building of PHA molecules, their applications are inexhaustible, and until recent years, their optical and electronic capabilities are being revisited and new directions are found for their implementations.[4] In the subsequent years, the field steadily extended from dyestuff exploration, to include new areas of theoretical as well as practical significance. In the 1950s, the PHA's field received a push forward due to the huge interest in exploring their mechanism of carcinogenicity.

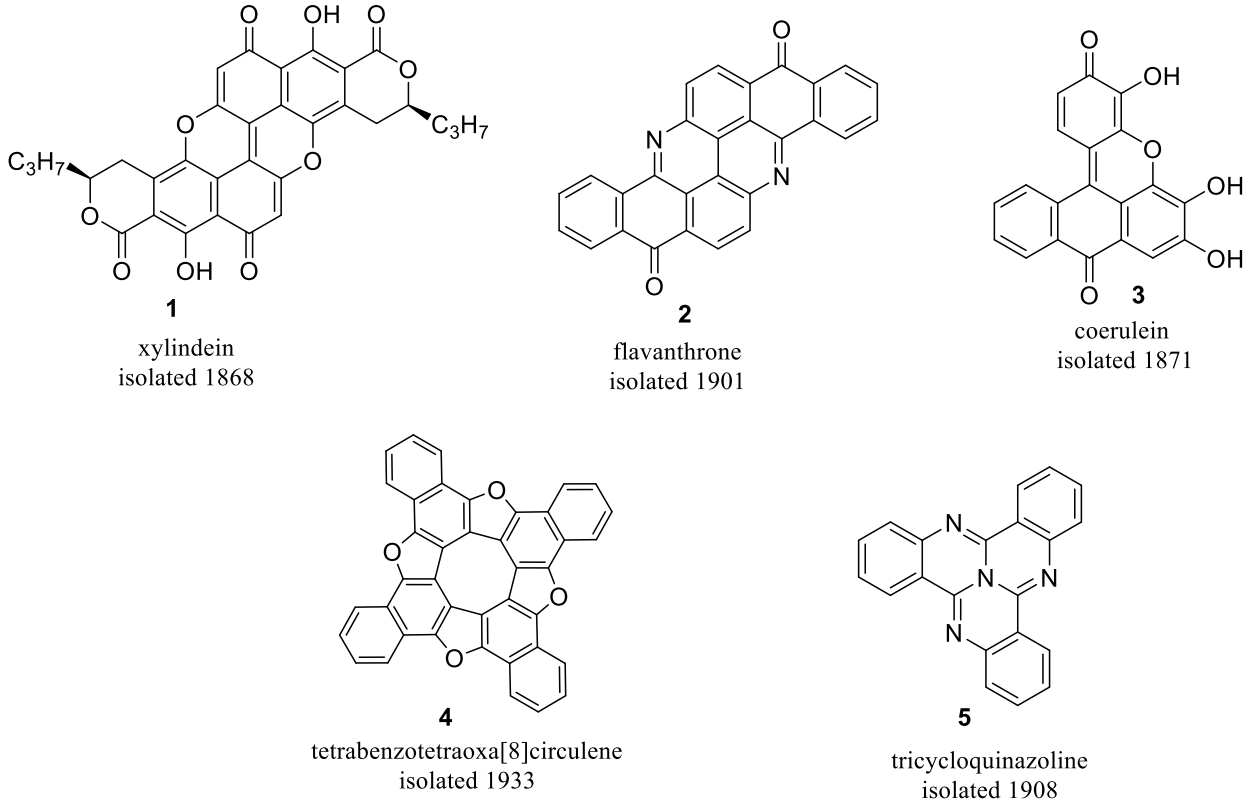

Scheme 1.1. Early examples of polycyclic heteroaromatic compounds PHAs

Due to their unique optical and electronic features, PHAs are debatably the most adjustable class of molecules to be implemented in numerous molecular post-silicon electronics, offering infinite potential in molecular design. This exceptional structural adjustability can be used for programming the desired characteristics into PHAs at molecular and even supramolecular levels opening new horizons in different applications. (**Scheme 1.2**) shows most of the active and hot topic applications nowadays in the field of PHAs chemistry.[1] These achievements have been made through significant and continuous improvements in the synthetic protocols, which principally reduced the harsh conditions in the early works. Hence, we were able to prepare different highly functionalized derivatives. At the beginning of the twenty-first century, the discovery of the amazing properties of nanographenes and their potential applications in molecular electronics especially as post-silicon semiconductors made a quantum leap in this field. Despite the tremendous progress made by nanographenes, their further application is still limited due to the pneumatic production and handling. So far, the available technologies do not provide straightforward access to structurally uniform material. Additionally, the necessity of a non-zero bandgap limits the applications of large-area graphene, especially its applications in the organic field-effect transistors.[5]

1.1.2. Heteroatoms open up new horizons for more applications

In the field of molecular electronics, doping of graphene with heteroatom has a key role, as it modifies and improves the electronic structure of graphene, opening new horizons for different applications. Various good properties, such as charge polarization, electro actelectroactivityap opening could be induced or enhanced *via* heteroatom doping.[6] In this context, PHAs combine both structural uniformity and tunable electronic features. By adjusting both topology and heteroatom content of the PHA molecule, various electronic features can be tuned including the optical absorption, redox behavior, band gap, and photoluminescence. Due to this advantage, many families of PHAs have been studied as Near infrared NIR active dyes,[7] fluorescence sensors, and two-photon absorbers.[8] Since the first days of PHAs, nitrogen has been considered the main "dopant", as a result of the availability of its synthetic methods and the stability of the *N*-containing scaffolds. Large effort is now being focused on the advance of large hetero-aromatics to magnify the portfolio of functional heteroatoms offering an extra variable in the design of PHA molecules.

The long history of this chemistry left us with a huge structural diversity that makes the classification of PHAs too difficult. With the variation of these compounds' size, number, and connectivity of constituting aromatic rings as well as the heteroatoms' types, numbers, and the way of their doping, there is no only one classification that can cover all PHAs. However, some attempts based on the connectivity between the rings, or the extent of benzenoid ring (graphene-like) fusion tried to afford some suggested classifications.[1,2,9] In the context of this introduction, we do not have opportunity to present in details the different classes of PHAs which cover coronenoids, perylenoids, pyrenoids, phenalenoids, and other classes with non-benzenoid fusion like circulenes. Instead, we will focus on few examples of PHAs that received a lot of attention lately due to their high potential to be implemented in various material-based applications, such as organic light-emitting diodes (OLEDs) and organic field-effect transistors (OFETs).

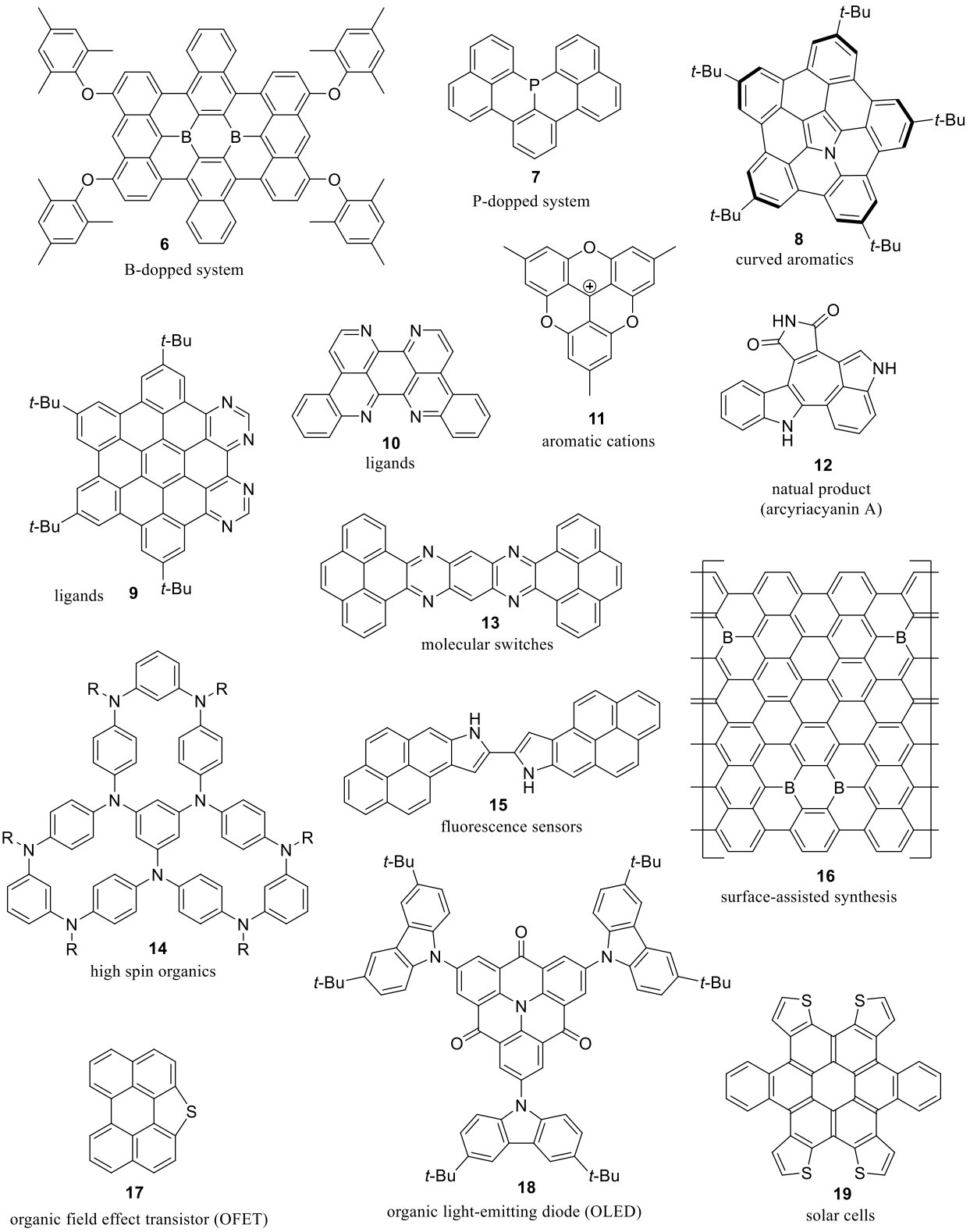

Scheme 1.2. Most active areas of modern PHAs research

1.2. Heterodehydrohelicenes as a noble example of PHAs

Dehydrohelicenes, sometimes described as quasi-circulenes, are polycyclic aromatic compounds in which the helical termini of the helicene precursor are connected *via* a sigma bond. Although there are many examples of heterohelicenes[10], and circulenes[11] that can be prepared *via* different methodologies, there remained a great deal of mystery surrounding dehydrohelicene scaffolds and only a few examples reported so far. In 1969, the first example of dehydrohelicenes was reported when Zander and Franke introduced diaza-dehydro[6]helicene **22** synthesized from the precursor diaza[6]helicene **21** through metal(Al)-mediated terminal ring closure at 150 °C (**Scheme 1.3**).[12] In all following schemes, the chemical transformation in which the two helical termini will form sigma bond affording dehydrohelicene was highlighted as the "key step" to be easily distinguished from other reactions.

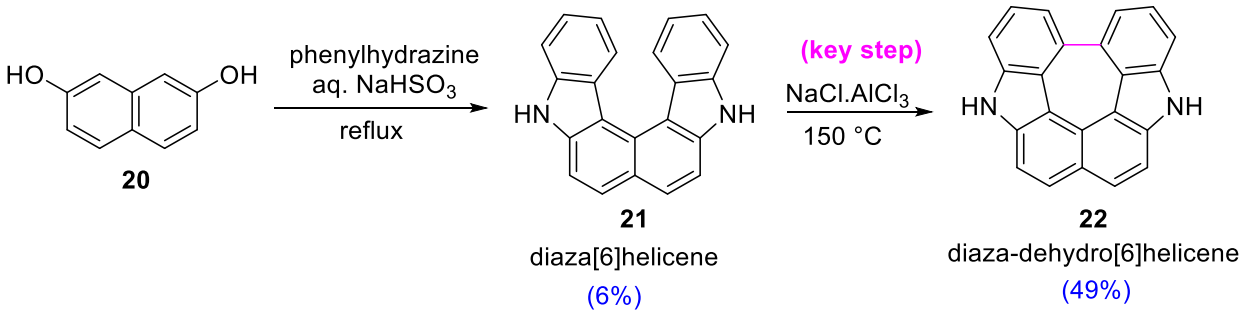

Scheme 1.3. First report of synthesizing dehydrohelicene using chloraluminate method

Therewith, Wynberg and co-workers used a similar protocol (Scholl-type reaction) to access the thiophene-based dehydrohelicenes **24** in high yields (up to 95%) from the corresponding helicenes **23** (**Scheme 1.4**). This intramolecular ring closure step is limited exclusively to hetero[5]helicenes and hetero[6]helicenes as concluded from some unsuccessful examples (**Scheme 1.5**).[13]

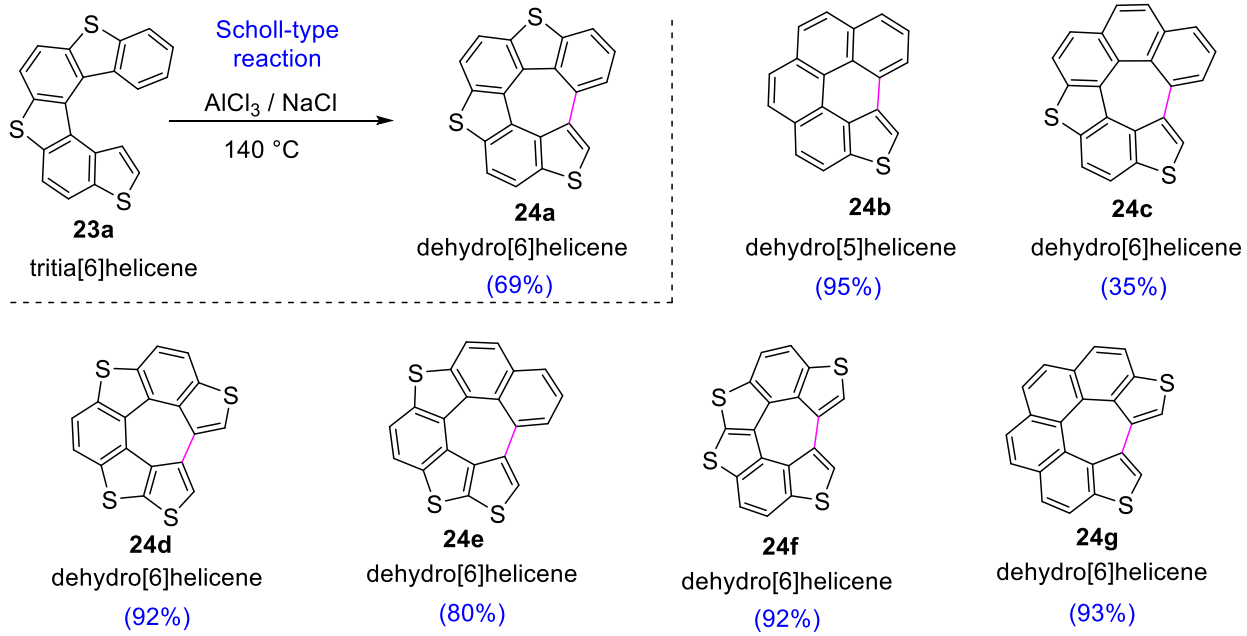

Scheme 1.4. Dehydrogenation of heterohelicenes by a Scholl-type reaction

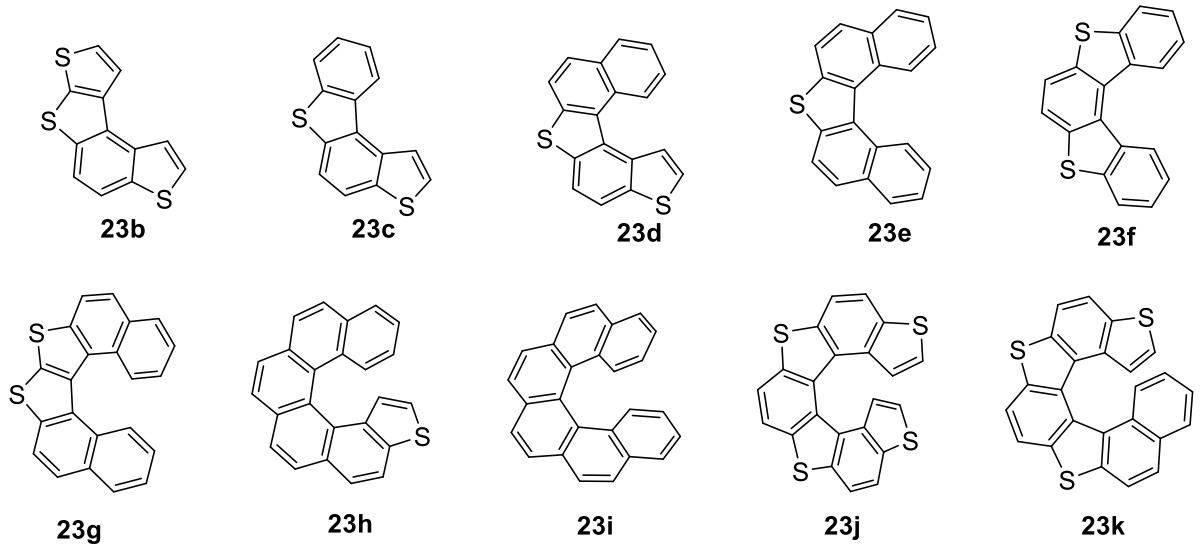

Scheme 1.5. Unsuccessful examples for the preparation of thiophene-based dehydrohelicenes

Generally, most of the early dehydrohelicenes were reported during the trials to prepare the circulenes as different class of PHAs. The importance and application of circulenes were realized at earlier stage compared to the dehydrohelicenes.[14] While seeking to prepare carbo[7]circulene **27**, Jessup and Reiss got the first carbodehydro[6]helicene **26a** upon irradiating a solution of the cyclophane diene **25a** in the presence of iodine as an oxidant (**Scheme 1.6**), but they did not study on its chiral properties.[15]

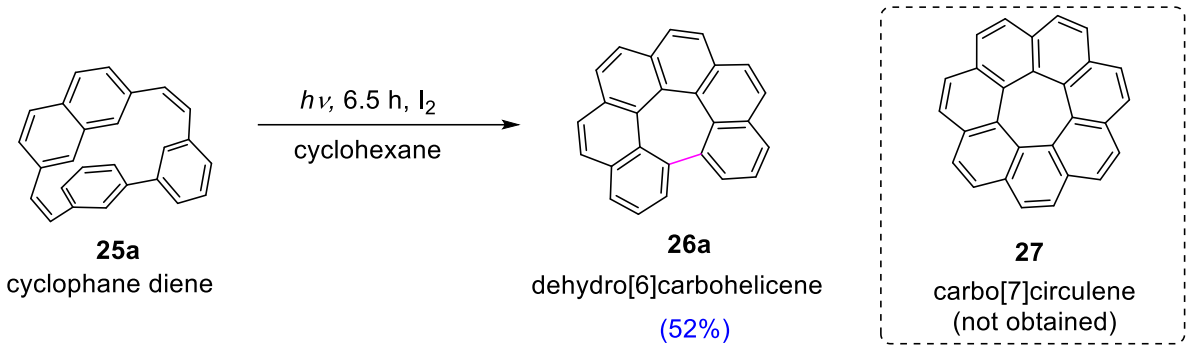

Scheme 1.6. Preparation of dehydro[6]carbohelicene

Later, Yamamoto and coworkers during their successful preparation of carbo[7]circulene **27**, confirmed the chiral nature of carbodehydro[6]helicen **26**, and introduced another three derivatives of chiral carbodehydro[6]helicenes **26b**-**26d** upon irradiation of diene **25** (**Scheme 1.7**). However, the low racemization barriers of these dehydro[6]helicenes **26** hindered their further study and investigation.[16]

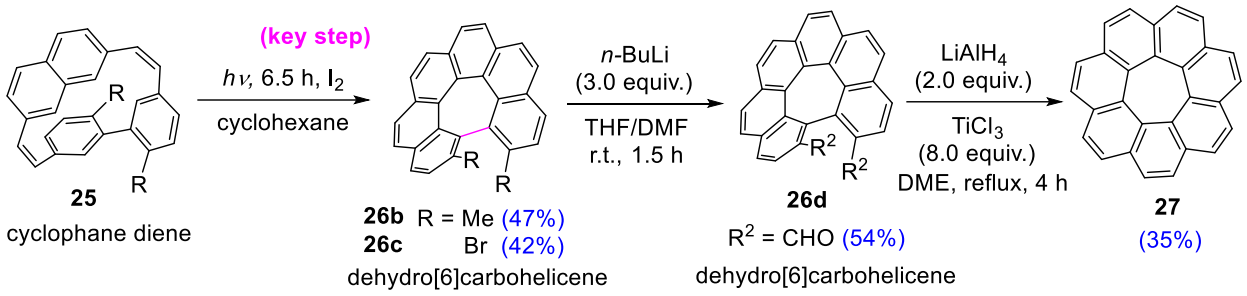

Scheme 1.7. preparation of [7]circulene and some dehydro[6]carbohelicene derivatives

In 2009, Rajca described dehydrohelicenes as quasi-circulene for the first time, after getting three novel thiophene-based dehydro[7]helicene **29** molecules from corresponding dibromohelicenes **28** by three different methods; pyrolysis, tin-mediated, or palladium-mediated carbon-carbon bond forming reactions (**Scheme 1.8**).[14]

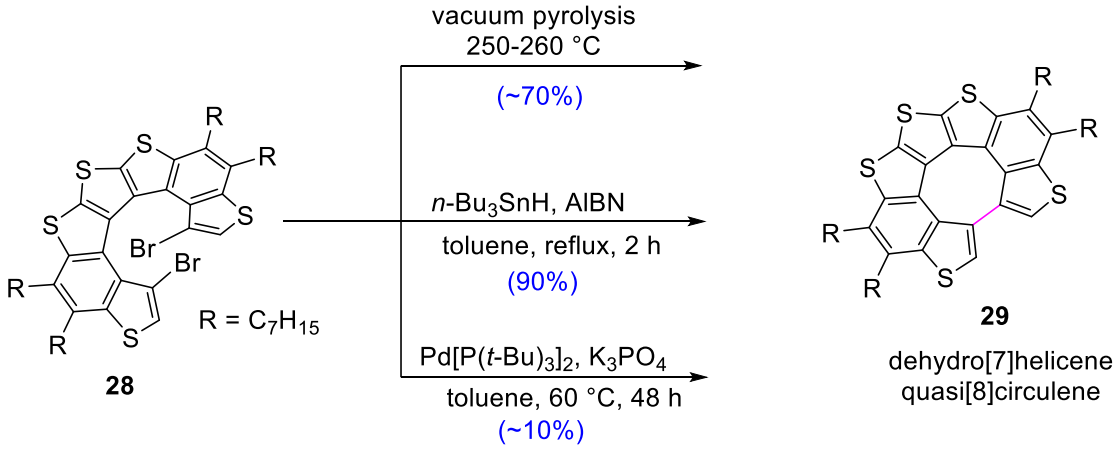

Scheme 1.8. Cyclization of thiophene-based [7]helicene at the two bromine-substituted termini

In 2013, Itami and Scott reported a grossly warped nanographene with a dehydrohelicene core **33**, that showed a superior behavior in terms of solubility, optical and electronic features compared to other planar nanographene. It can be prepared from its precursor corannulene derivative **30** *via* Scholl reaction using 10 equivalents of DDQ (**Scheme 1.9**). The cyclization process affixes the five polycyclic wing-like substituents to the hydrocarbon core then suture them together to generate ten new C–C bonds and five new seven-membered rings.[17]

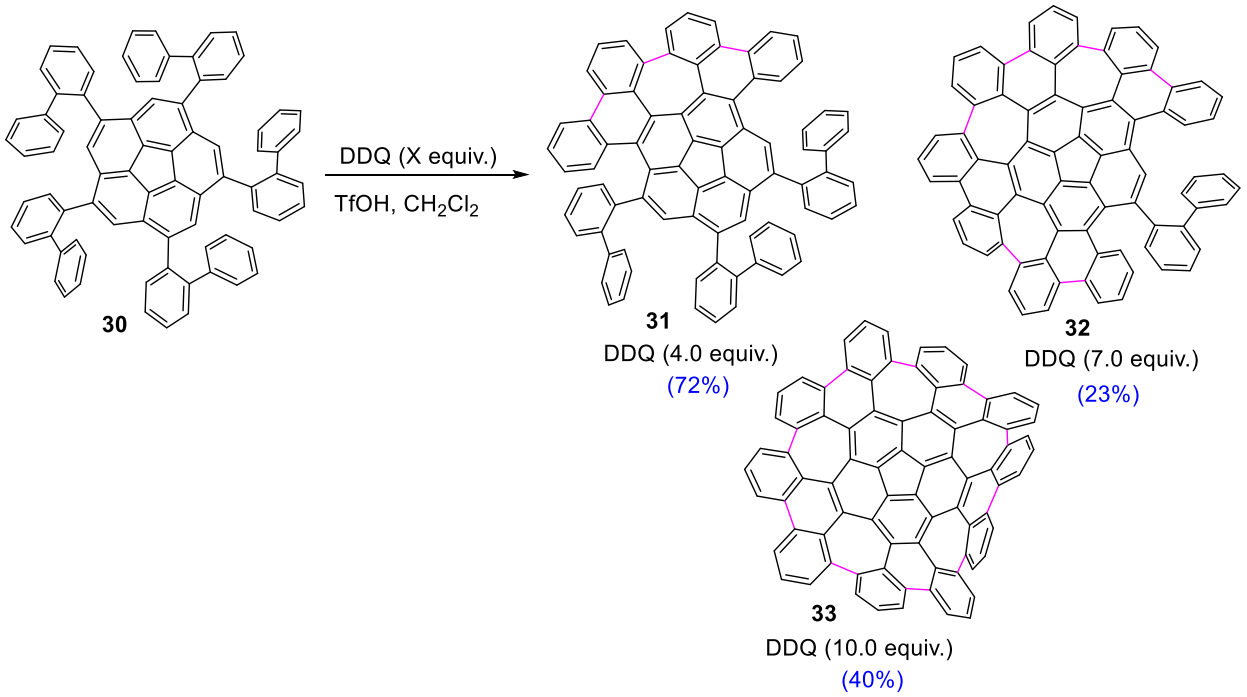

Scheme 1.9. Preparation of a grossly warped nanographene with dehydrohelicene core

Later, the same group reported two similar corannulene-based heptagons **32** and **33** with similar structural features and a high potential for application in functional materials. However, these compounds racemize rapidly in solution which hindered the study of their chiroptical properties.[18] To overcome this challenge, Itami and Segawa reported in 2017, a saddle-helix molecule **36** (**Scheme 1.10**), that showed higher racemization barrier which enabled the chiral HPLC resolution of dehydrohelicenes for the first time and subsequent study of their chiroptical features. This highly distorted molecule was prepared *via* a step wise sequence including a $MoCl_2$-mediated oxidative coupling of compound **34** involving capping of reactive sites by chlorination and a subsequent Pd-catalyzed dechlorination to afford compound **36**.[19]

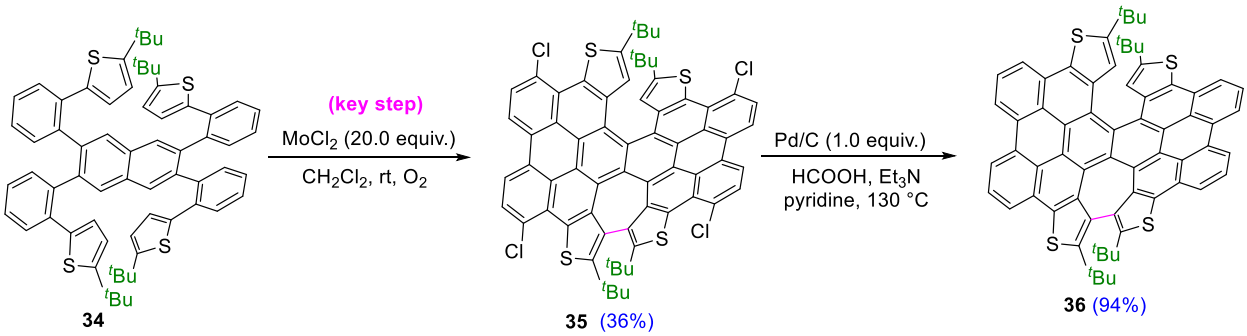

Scheme 1.10. Preparation of saddle-helix hybrid Molecule with dehydrohelicene core

Recently, Tanaka and Osuka introduced new dehydro[7]helicene and quasi-aza[8]circulene- molecules **38a** and **38b** with three pyrrole rings that exhibit interesting photophysical properties (**Scheme 1.11**). The oxidative fusion reaction of **37a** and **37b** was conducted with DDQ-$Sc(OTf)_3$ reagent in toluene

under reflux to afford **38a,b** in high yields. However, the fast racemization of these structures obstacle their further study.[20]

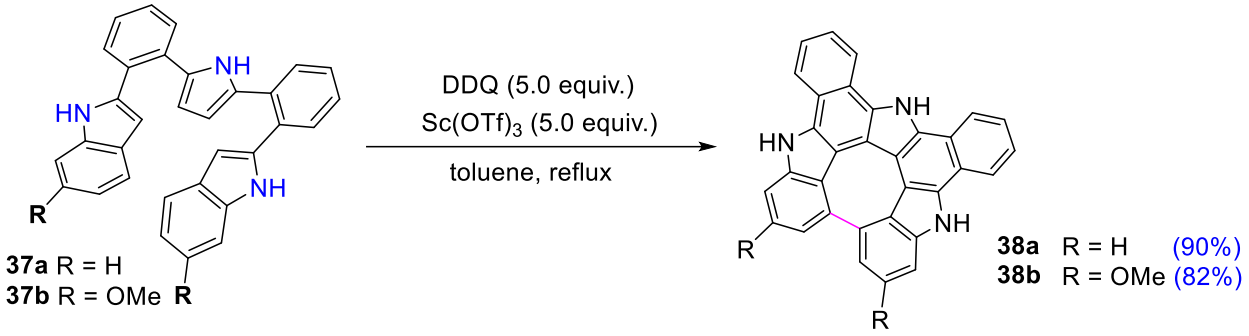

Scheme 1.11. Preparation of triaza-dehydro[7]helicene derivatives

One year later, the same group reported a modified version of their dehydro[7]helicene **39c** with a significantly higher racemization barrier (~40 kcal mol^{-1}), which enabled their chiral resolution using HPLC and investigating some of their promising chiroptical features such as CD spectra (**Scheme 1.12**).[21]

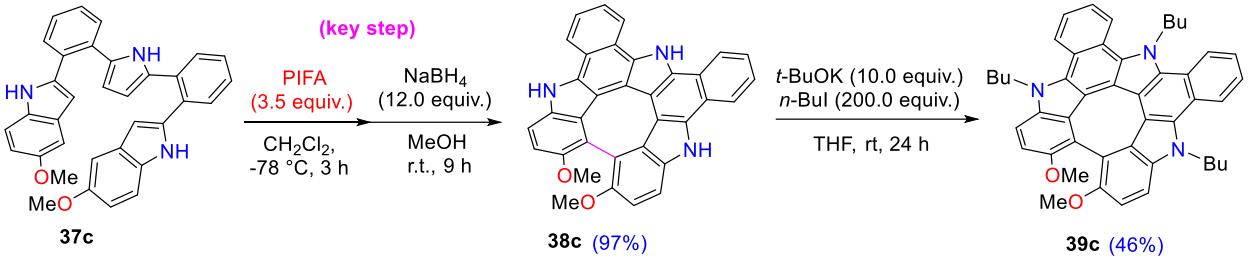

Scheme 1.12. Preparation of modified triaza-dehydro[7]helicene derivatives

Independently, Pittelkow reported two dehydro[7]helicenes **42a** and **42b** (**Scheme 1.13**) that showed improved optical and electro-chemical properties compared to the corresponding helicenes **41a** and **41b** and [8]circulenes. These two dehydro[7]helicenes **42a** and **42b** can be afforded in high yields *via* an intramolecular Scholl-type reaction upon treatment of the corresponding helicenes **41** with $BF_3{\cdot}OEt_2$ and chloranil. On the other hand, the precursor helicenes **41** need a long synthetic protocol to be prepared from readily available substrates over four steps and affording only 19% overall yield. In spite of their estimated high racemization barriers, all attempts for HPLC chiral resolution of these compounds **42a** and **42b** were unsuccessful which hindered their further study.[22]

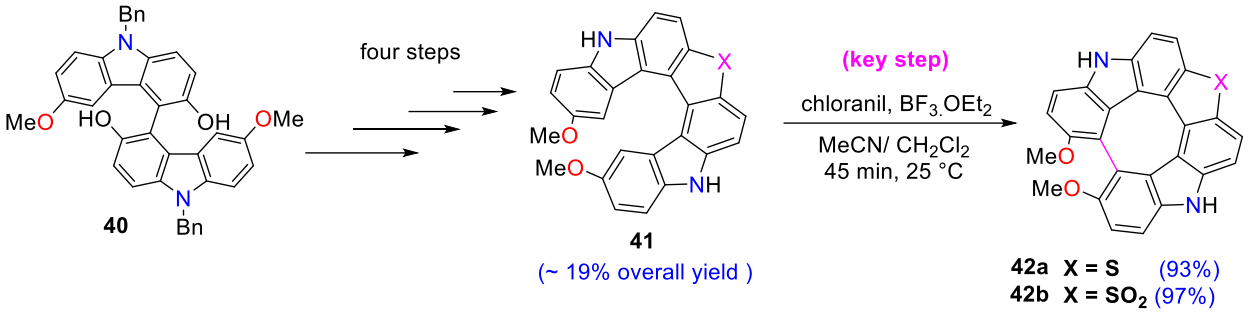

Scheme 1.13. Preparation of unique dehydro[7]helicene with three different heteroatoms

In 2021, Maeda and Ema reported another dehydro[7]helicene **44** that can be prepared *via* intramolecular $FeCl_3$-mediated Scholl-type reaction from the precursor **43** (**Scheme 1.14**).[23]

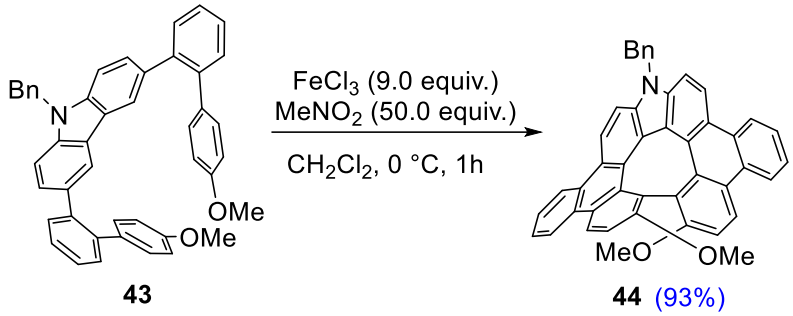

Scheme 1.14. Facile synthesis of dehydro[7]helicene *via* intramolecular Scholl-type reaction

Despite the immense potential exhibited by heterodehydrohelicenes, there are no reports so far on their straightforward construction including asymmetric synthesis. This could be due to the limitations associated with the synthetic steps: low total yields, harsh reaction conditions (such as high temperature), easy racemization of some examples, and/or overuse of oxidants (narrow functional group tolerance.

1.3. Optical properties of heterodehydrohelicenes

Even though the first example of dehydrohelicenes was reported 50 years ago, their chemistry, properties, and applications are not fully explored. This can be attributed to the fact that most of dehydrohelicenes did not attract attention until recently and have viewed for a long time as side products while trying to prepare the more valuable circulenes.[15,16,21,23] With the revolution occurred in the last twenty years in the field of renewable energy and the various applications of small organic molecules (SOMs) in materials science, there has been a tendency to revisit many scaffolds that were obtained earlier to reconsider their potential for different applications. Dehydrohelicenes are among the most important compounds that have been rehabilitated, especially with the recent progress made in some measuring tools and chiroptical methods, such as Raman optical activity (ROA), vibrational circular dichroism (VCD), and circularly polarized luminescence (CPL), that indorsed the study of both electronic and geometric structures more extensively. Heterodehydrohelicenes, such as those

incorporating sulfur, oxygen, and/or nitrogen, can afford further functionalities, exhibiting more diverse applications compared to their carbodehydrohelicene counterparts.[24] Among all their valuable features, come the photophysical and chiroptical properties as the prominent features that open the gate for their implementation in various material applications like OLEDs, and OFETs.[25]

1.3.1. Photophysical properties of heterodehydrohelicenes

Upon photoirradiation, heterodehydrohelicenes display a high degree of luminesce as a result of their structural rigidity that hinders the loss of thermal energy due to structural changes in the excited state. There are a lot of photophysical methods that deal with the interaction between matter and electromagnetic radiation. Among them we are focusing on the most common two methods that display a great value in characterizing the electronic and optical properties of different PHAs. These two methods are UV-Vis spectrophotometry and photoluminescence (PL). The integration between these two methods is the magic word in defining their real impact; as UV-Vis spectrophotometry refers to the quantitative optical absorption of a substance to an incident electromagnetic radiation, while photoluminescence describes the emission of the absorbed light. When an electromagnetic radiation is directed onto a substance, it absorbs the photons and gains some energy that excites electrons to a higher level. Subsequently, some excess energy is emitted again after electrons come back to their original energy levels, which can be quantified by PL methods.[26]

The interest in studying the photophysical properties of heterodehydrohelicenes dates back to 2009, when Rajca and coworkers studied the UV-Vis absorption of various thiophene-based dehydro[7]helicenes. The studied structures **29a-c** revealed good UV-Vis absorption spectra characterized by a red-shifting with the increasing number of benzene rings (**Figure 1.1**).[14]

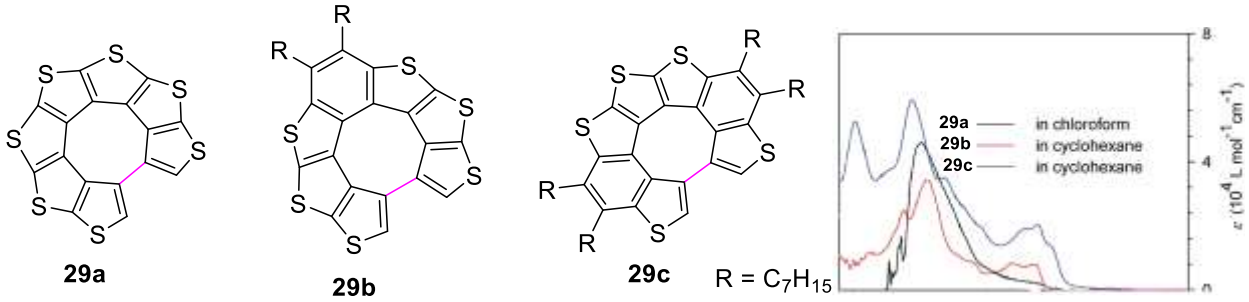

Figure 1.1. Photophyscial properties of some thiophene-based dehydrohelicenes

Lately, the interest in studying the photophysical properties of dehydrohelicenes have expanded more and more. In 2018, Tanka and Osuka studied their synthesized molecules that exhibited a red-shifted absorption reaching up to 470 nm. The emission bands were shifted in a bathochromic way at 462 and 476 nm for compounds **38a** and **38b** respectively (**Figure 1.2**).[20] Their modified dehydro[7]helicene scaffolds were studied as well and showed red-shifted absorption pattern. The absorption spectrum of **38c** is further shifted up to 474 nm compared to **38a** (433 nm).[21]

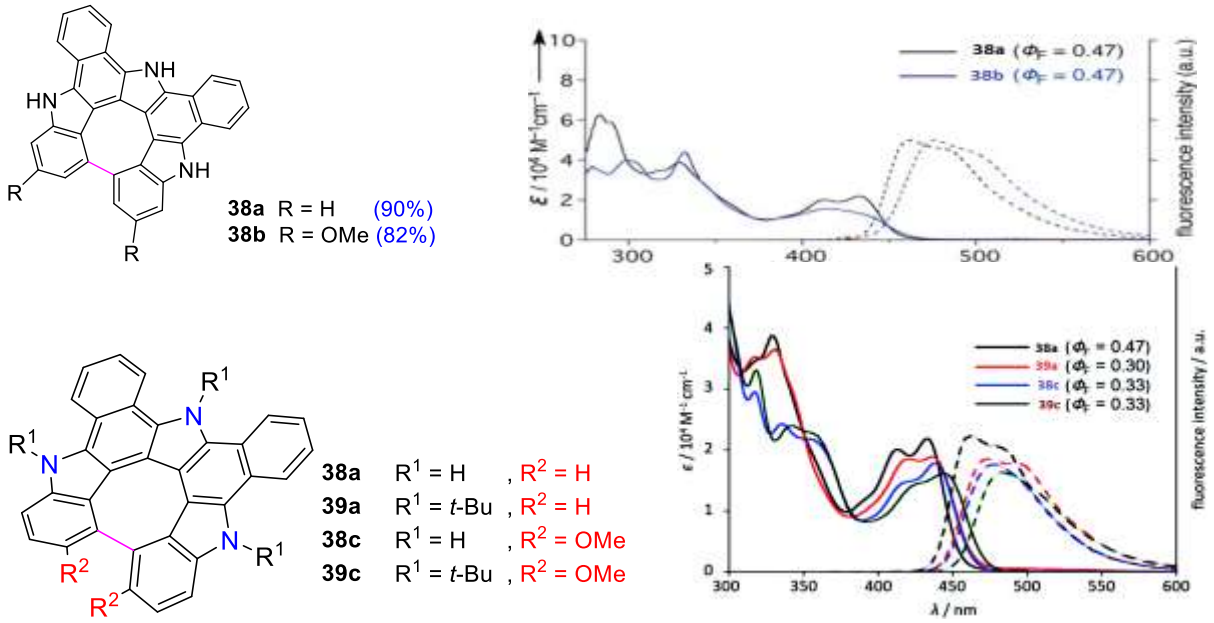

Figure 1.2. Photophysical properties (UV-vis spectroscopy/ PL) of some triaza-dehydro[7]helicenes

In 2020, Pittelkow and coworkers reported a series of PHAs that includes hetero[7]helicenes **41**, heterodehydro[7]helicenes **42**, and hetero[8]circulenes **45** as well. The photophysical properties (UV-vis & PL) of this series was investigated in THF (**Figure 1.3**). Planarization of the scaffold has a big impact on the photophysical properties which can be indicated by the bathochromic shift in the onset of absorption shown in circulene compared to dehydrohelicenens and helicenes.[22]

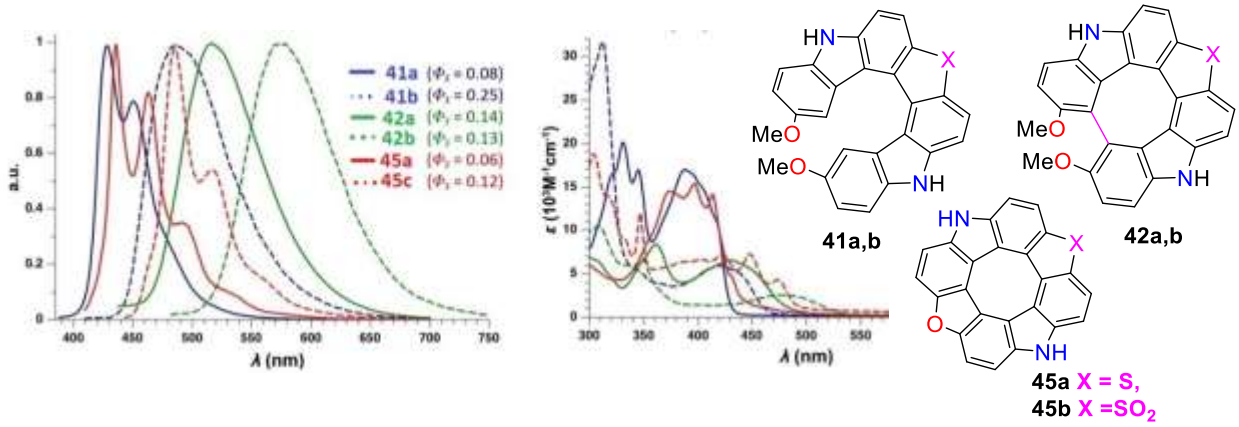

Figure 1.3. UV-vis and PL spectroscopy of various PHAs with three different heteroatoms

1.3.2. Chiroptical properties of heterodehydrohelicenes

The unique helical chirality of some PHAs especially helicenes and dehydrohelicenes has led to extraordinary chiroptical responses.[27] Among the various chiroptical properties, the high-level optical rotation (OR) and optical rotatory dispersion (ORD) considered as the most familiar features of small organic molecules.[28] However, recent reports ignore both ORD and OR due to their complex

dispersive properties from an analytical point of view.[29] Besides, there are other chiroptical methods that started to gain attention like Raman optical activity (ROA) and vibrational circular dichroism (VCD), due to their value in studying the configurational and conformational information of chiral molecules.[30] The only limitation related to these methods is their essential quantity and conditions required for the measurement that often stop them from being applied in routine spectral investigations. On the other hand, the electronic Circular Dichroism CD and Circularly Polarized Luminescence CPL have gained an increasing interest recently as the most common and favorable tools to study the chiroptical nature of small organic molecules. These two methods are superior compared to others in terms of simplicity and sensitivity, hence, they became the most utilized in recent routine spectral measurements. Moreover, these two methods, especially CPL, open the gate for studying the potential application in optical information storage and transfer, in such cases the level of CPL can promote a further dimension to the information content transported through light.[31]

1.3.2.1. Electronic circular dichroism (CD)

Electronic CD spectroscopy is the main tool used to define the difference between the absorption of left circularly polarized (CP) light and right CP light by chiral molecules, a phenomenon identified as the Cotton effect (CE).[32] CD is depends on the chirality in the ground state. In CD spectroscopy, the molar circular dichroism ($\Delta\varepsilon$) as a function of wavelength is a specific observable, which is the difference between the molar extinction coefficients for left CP light (ε_L) and right-CP light (ε_R); i.e., $\Delta\varepsilon = \varepsilon_L - \varepsilon_R$. For instrumental convenience, the molar ellipticity ([θ], in deg cm^2 dmol^{-1}) is also used but is mutually convertible with $\Delta\varepsilon$ (in M^{-1} cm^{-1}) by the following equation (Eq. 1).

$$[\theta] = 100 \times \frac{\mathrm{Ln}\,10}{4} + \frac{180}{\pi}\,\Delta\varepsilon = 3298\Delta\varepsilon \qquad \text{Eq. 1}$$

The molecular dissymmetry degree can be described *via* the absorption dissymmetry factor (g_{CD}), which is given by dividing the molar circular dichroism ($\Delta\varepsilon = \varepsilon_L - \varepsilon_R$) by the molar absorption coefficient (ε), that is average between ε_L and ε_R (Eq. 2).

$$g\mathrm{CD} = \frac{\varepsilon\mathrm{L} - \varepsilon\mathrm{R}}{\left(\frac{1}{2}\right)(\varepsilon\mathrm{L} + \varepsilon\mathrm{L})} = \frac{\Delta\varepsilon}{\varepsilon} \qquad \text{Eq. 2}$$

From the definition, the absorption dissymmetry factor (g_{CD}) should be between −2 and +2. Nevertheless, the (g_{CD}) values reported for the π–π* transition of many SOM, including helicenes and dehydrohelicenes, are much smaller (in absolute value) and typically in a range of 10^{-4} to 10^{-2}, leaving huge room for further improvements.

1.3.2.2. Circularly Polarized Luminescence (CPL)

CPL, sometimes described as luminescence/ or emission circular dichroism, is a chiroptical feature of chiral molecules that is related to their excited states. CPL is quantified as the difference in the intensity of left-CP and right-CP light emissions.[33,34] The recently growing interest of CPL can be attributed to the resolution of the circular polarization, that allows the development of smarter photonic materials for advanced technologies. For example; information storage and processing,[35] 3-D displays,[36] spintronics-based devices or ellipsometry-based tomography.[37] Moreover, the potential applications of chiral materials with high CPL activities can be extended to include different areas like stereoselective sensing, security inks, CPL lasers, and endoscope technologies. Generally, relatively high CPL has been observed for metamaterials, molecular assemblies, liquid crystals, supramolecular aggregates, and polymer systems, due to the chirality amplification effect, but this aggregation affects negatively on the emission wavelengths and intensities. Hence, the interest in CPL-responsive small organic molecules is growing exponentially in the last years due to their diversity and adjustability that can improve or fine-tune the CPL responses without decreasing the emission intensities.[34,38,39]

In CPL spectroscopy, the differential emission intensity (ΔI) of the left-handed CP luminescence (IL) and right-handed CP luminescence (IR) is recorded upon exposure to a beam of non-polarized excitation light. Since the absolute emission intensity depends on many factors and hardly reproducible, the luminescence dissymmetry is usually evaluated in terms of the luminescence dissymmetry factor (g_{CPL}) as a function of wavelength. By definition, the g_{CPL} values should be in the range: $-2 \leq g_{CPL} \leq +2$. Thus, it is a common practice to track larger absolute g_{CPL} values for superior CPL materials (Eq. 3).

$$g\mathrm{CPL} = \frac{I\mathrm{L} - I\mathrm{R}}{\left(\frac{1}{2}\right)(I\mathrm{L} + I\mathrm{L})} \qquad \text{Eq. 3}$$

Both CD and CPL can be described or defined in terms of the rotational strength (R) or the rotatory strength. R, according to Rosenfeld, is the imaginary quantity of the scalar product of the electric and magnetic transition dipole moments (ETDM and MTDM) of any transition between i and j states (Eq. 4).

$$R = \mathrm{Im}\, \boldsymbol{\mu}_{ij} \,.\, \boldsymbol{m}_{ij} \qquad \text{Eq. 4}$$

Both absorption intensity and emission intensity are proportional to the relevant dipole strength D, which is defined by the following equation (Eq. 5).

$$D = |\boldsymbol{\mu}_{ij}|^2 + |\boldsymbol{m}_{ij}|^2 \qquad \text{Eq. 5}$$

In isotropic solutions, the electric quadrupole moment is cancelled out in r and generally small and negligible for D. The dissymmetry factors g_{abs} and g_{lum} are thus given by the rotational and dipole

strengths, and thus dissymmetric factor, can be predicted by theory as will be discussed later (Eq. 6) (**Chapter 4**).[40]

$$g = \frac{4R}{D} \qquad \text{Eq. 6}$$

Until now, the highest CPL values have been chiefly accomplished from lanthanide complexes, which exhibit $|g_{lum}|$ values within the range of 0.05–0.5,[41] an outstanding value of 1.38 has been reported for a europium(III) complex.[42] Nonetheless, the emission efficiencies (quantum yields) of these complexes are typically small, due to their metal-centered electronic transitions. This fact hinders their implementation in many CPL applications (CPL lasing, for example). Some small chiral organic scaffolds afford CPL levels which is smaller compared to lanthanide complexes, but can jump exponentially when these molecules are hierarchically self-organized into non-racemic helical polymers or supramolecular aggregates ($|g_{lum}|$ typically within the 10^{-3}–10^{-1} range).[43] Even so, certain chiral superorganized polymeric cholesteric crystals (PCCs) can afford extraordinary levels of CPL (**Figure 1.4**).[44] As an example, an impressive $|g_{lum}|$ value of about 1.6 has been reported for an OLED involving a three-layered PCC reflector.[45]

Figure 1.4. Chiral super-organized polymeric cholesteric crystals (PCCs)

1.3.2.2.1. Helicene derivatives with CPL properties

Helicenes are ortho-fused aromatic polycyclic compounds with helical structures that can be distorted by steric hindrance between the terminal aromatic rings. Even though helicenes do not mainly show any asymmetric centers, their extended and twisted π-conjugated molecular scaffolds exhibit special helical chirality and excellent CPL properties. Accordingly, helicenes and their derivatives have been widely used in non-linear optical materials, optoelectronic devices, and so on.[46] In 2003, Venkataraman *et al.*[47] introduced the first helicene skeletons with CPL character (**Scheme 1.15**). The reported structures (*M*)/(*P*)-**46a** and (*M*)/(*P*)-**46b** showed CPL properties with the g_{lum} of $-1.1 \times 10^{-3}/0.9 \times 10^{-3}$

(λ_{em} = 453 nm) and $-0.7 \times 10^{-3}/0.8 \times 10^{-3}$ (λ_{em} = 478 nm), respectively. This pioneering work opened a new horizon for many new helicene derivatives with CPL properties. A lot of carbohelicenes and heterohelicenes were reported following this early example of Venkataraman and proved to have good CPL properties with g_{lum} up to 2.8×10^{-2}.[48]

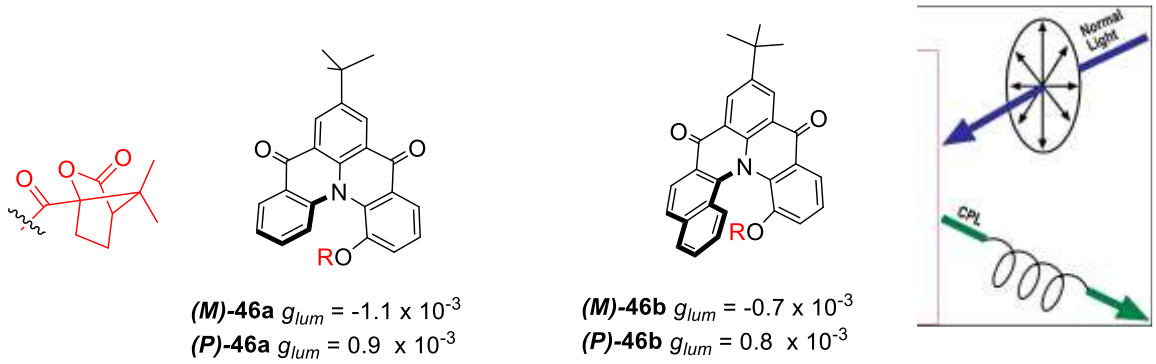

***(M)*-46a** g_{lum} = -1.1 x 10^{-3}
***(P)*-46a** g_{lum} = 0.9 x 10^{-3}

***(M)*-46b** g_{lum} = -0.7 x 10^{-3}
***(P)*-46b** g_{lum} = 0.8 x 10^{-3}

Scheme 1.15. First report of helicenes that show good CPL properties

Table 1.1 summarizes most of the reported heterohelicenes as represtitave examples of PHAs. A lot of carbohelicenes also reported to have such high CPL properties,[38,49] but I did not discuss here since it is excluded from the umbrella of PHAs.

Table 1.1. Most of the reported heterohelicenes that show CPL character

No.	Structure	Solvent	g_{lum} ($\times 10^{-3}$)	Year	Reference
47	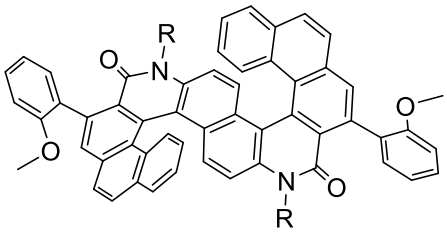 R = $CH_2C_6H_3$-4-$OC_{10}H_{21}$	$CHCl_3$ (1×10^{-6} M)	28.00	2014	48
48	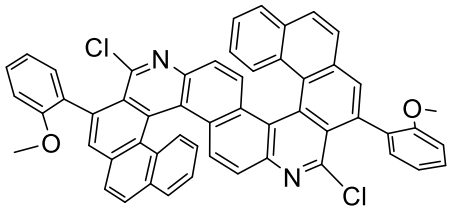	$CHCl_3$ (1×10^{-6} M)	11.00	2014	48

49	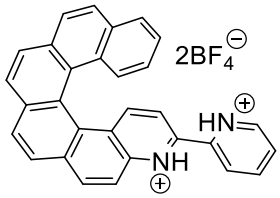	CH_2Cl_2	2.90	2015	50
50	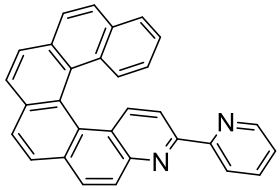	CH_2Cl_2	3.20	2015	51
51	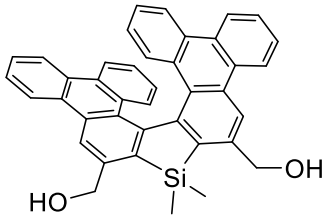	$CHCl_3$	16.00	2015	52
52	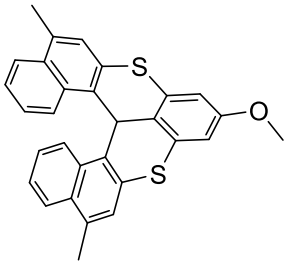	$CHCl_3$ (2×10^{-4} M)	9.00	2016	53
53	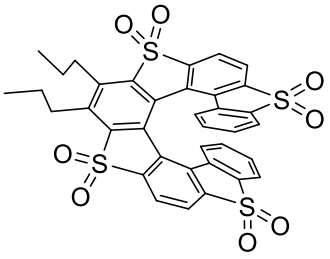	C_7H_8	0.83	2016	54
54	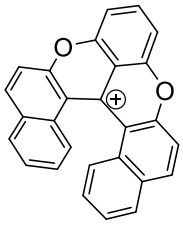	CH_2Cl_2 (2×10^{-3} M)	0.40	2016	55

55	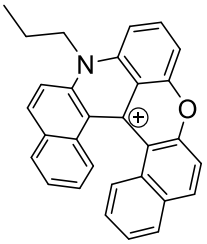	CH_2Cl_2 (2×10^{-3} M)	2.10	2016	55
56	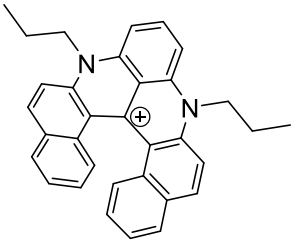	CH_2Cl_2 (2×10^{-3} M)	1.10	2016	55
57	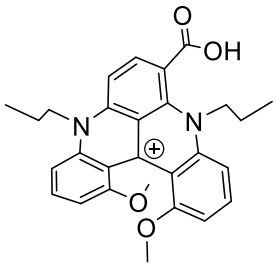	CH_3CN (1×10^{-5} M)	0.50	2016	56
58	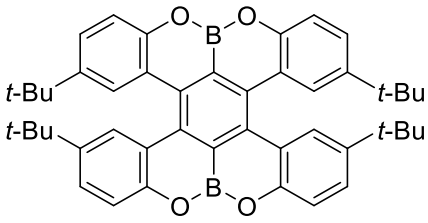	CH_2Cl_2 (2×10^{-3} M)	1.70	2016	57
59	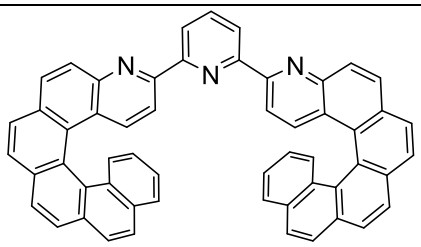	CH_2Cl_2 (2×10^{-3} M)	8.50	2016	58
60	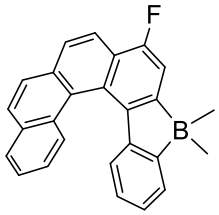	CH_2Cl_2	0.90	2017	59

61	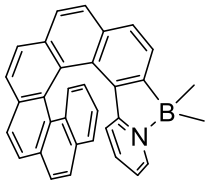	CH_2Cl_2	2.30	2017	59
62	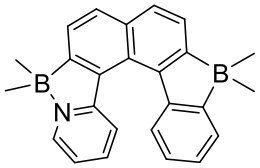	CH_2Cl_2	0.70	2017	59
63	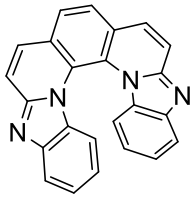	CH_2Cl_2 (1×10^{-5} M)	9.00	2017	60
64	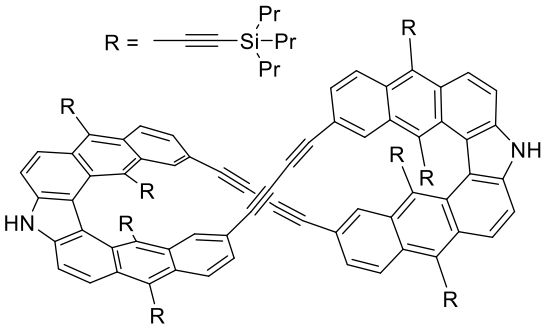	CH_2Cl_2	8.50	2017	61
65	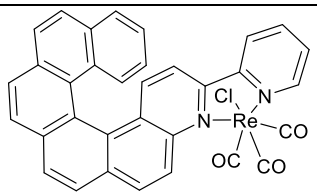	CH_2Cl_2 (1×10^{-3} M)	3.00	2015	51
66	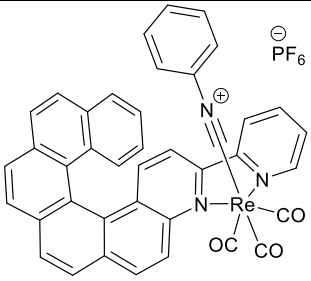	CH_2Cl_2 (1×10^{-3} M)	1.40	2015	51

67	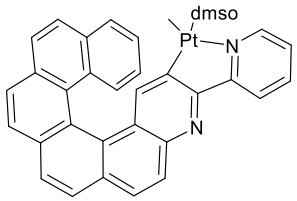	CH_2Cl_2	1.10	2015	50
68	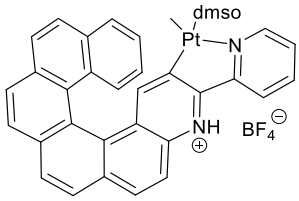	CH_2Cl_2	2.00	2015	50
69	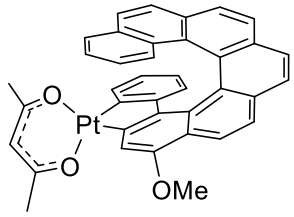	CH_2Cl_2 (1×10^{-3} M)	4.50	2014	62
70	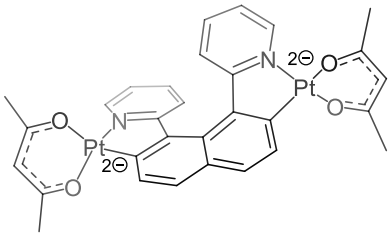	CH_2Cl_2 (1×10^{-3} M)	0.50	2014	62
71	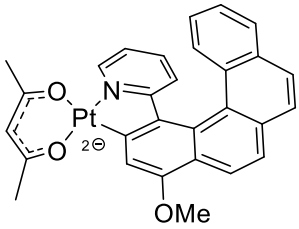	CH_2Cl_2 (1×10^{-3} M)	12.00	2014	62
72	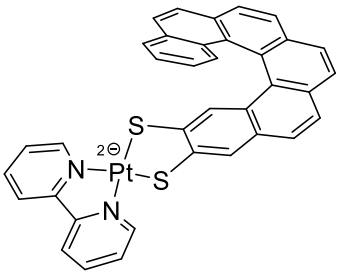	CH_3CN (3×10^{-4} M)	0.30	2017	63

73	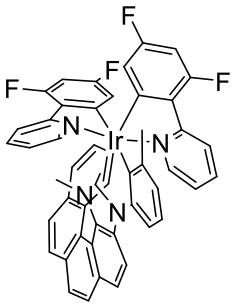	CH_2Cl_2 (5×10^{-5} M)	1.50	2017	64
74	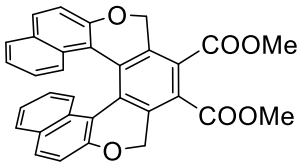	CH_2Cl_2 (2×10^{-5} M)	0.95	2017	65
75	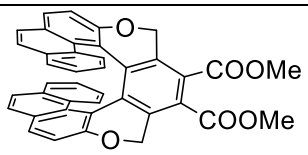	CH_2Cl_2 (2×10^{-5} M)	1.10	2017	65
76	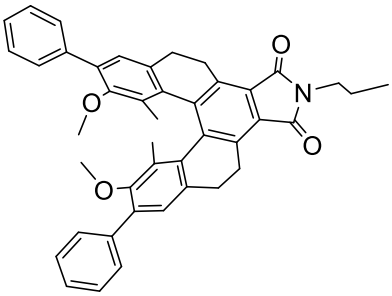	$(CH_2)_4O$ (1×10^{-5} M)	1.45	2016	66
77	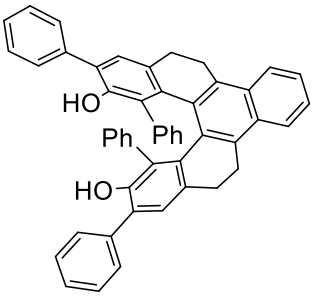	CH_2Cl_2 (1×10^{-5} M)	1.00	2017	67
78	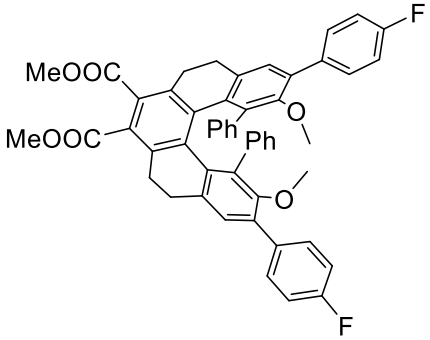	$(CH_2)_4O$ (5×10^{-5} M)	6.50	2017	68

1.3.2.2.2. Dehydrohelicene derivatives with CPL properties

The study of chiroptical properties of dehydrohelicenes is quite rare compared to the helicene scaffolds. The main reasons for this, is the lack of available chiral dehydrohelicenes and their challenging HPLC chiral resolution that was never achieved until 2017 by Itami and Segawa.[19] In 2021, Maeda, Ema and coworkers reported the only example of a CPL-responsive dehydrohelicene **44**, that showed g_{lum} of 0.25×10^{-3} (λ_{em} = 435 nm) (**Figure 1.5**).[23]

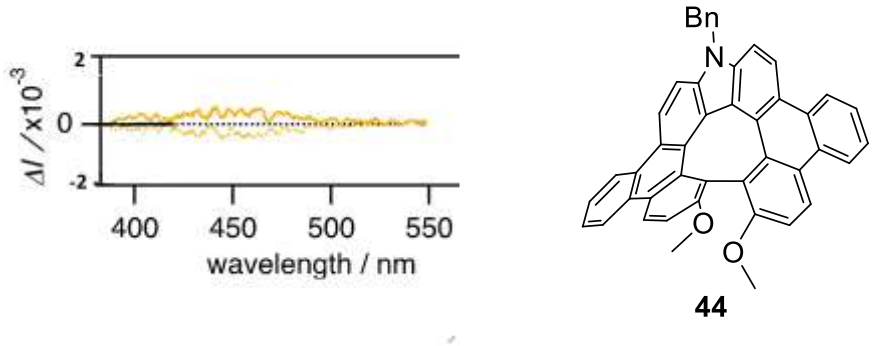

Figure 1.5. Only studied example about CPL of dehydro[7]helicene

In summary, we can realize that heterodehydrohelicenes represent an integrating scaffolds that show a lot of good photophyscial and chiroptical properties. These scaffolds so far are quite rare compared to other PHAs. Although of the recent progresses, still there are no reports on their straightforward construction including asymmetric synthesis. Moreover, most of the reported protocols have some synthetic limitations. This inspired us to start our study using an exceptionally new electrochemical approach to develop a facile sequential synthesis of aza-oxa-dehydro[7]helicenes and some other PHAs. After getting diverse molecules, we started to study their optical properties and design new scaffolds that can improve chiroptical responses.

In Chapter 2 of this thesis, we discuss the sequential synthesis of aza-oxa-dehydro[7]helicenes *via* an electrochemical oxidative hetero-coupling, dehydrative cyclization and intramolecular C-C bond formation (Scheme 1.16) and how varying the conditions can generate different PHAs.

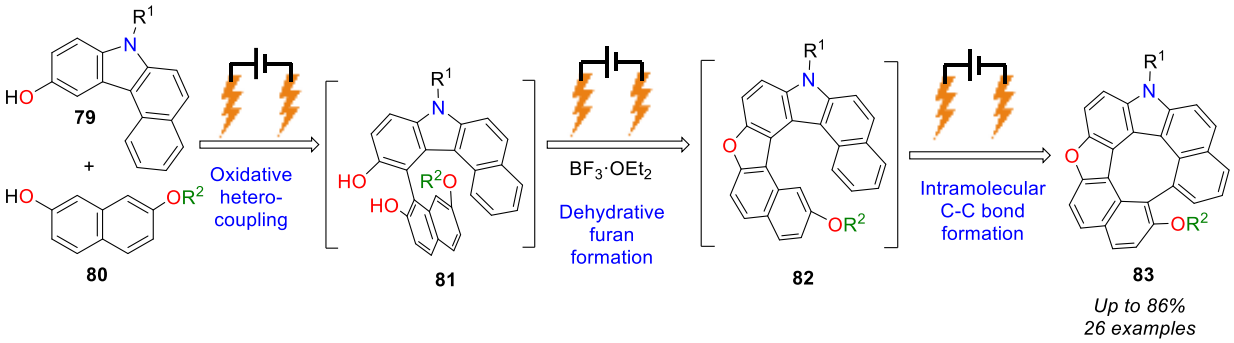

Scheme 1.16. Sequential synthesis of aza-oxa-dehydro[7]helicenes

In Chapter 3, we develop a stepwise enantioselective synthesis of aza-oxa-dehydro[7]helicenes that combines both vanadium chemistry and electrochemistry (Scheme 1.17).

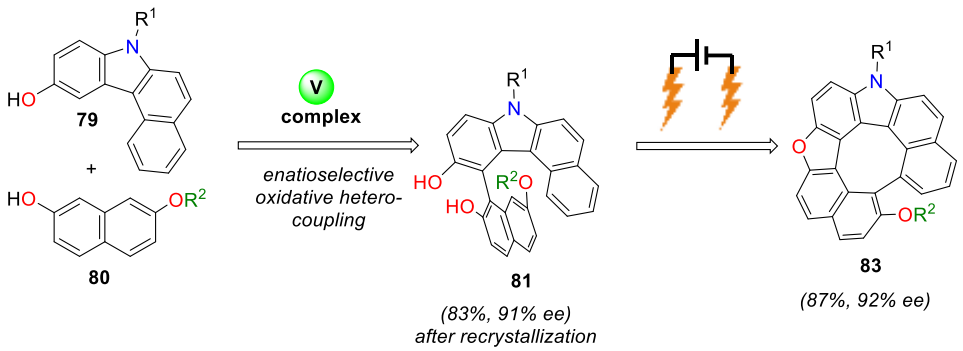

Scheme 1.17. Step-wise enantioselective synthesis of aza-oxa-dehydro[7]helicenes

In Chapter 4, we study the photophysical properties of all synthesized PHAs and the chiroptical characters of the chiral dehydrohelicenes, then design and synthesize some compounds that may boost these features.

References:

(1) Stepien, M.; Gonka, E.; Żyła, M.; Sprutta, N. Heterocyclic nanographenes and other polycyclic heteroaromatic compounds: synthetic routes, properties, and applications. *Chemical Reviews* **2017**, *117* (4), 3479-3716.

(2) Borissov, A.; Maurya, Y. K.; Moshniaha, L.; Wong, W.-S.; Żyła-Karwowska, M.; Stepien, M. Recent advances in heterocyclic nanographenes and other polycyclic heteroaromatic compounds. *Chemical Reviews* **2021**, *122* (1), 565-788.

(3) Scholl, R. Konstitution und synthese des flavanthrens. *Berichte der Deutschen Chemischen Gesellschaft* **1907**, *40* (2), 1691-1702.

(4) (a) Giesbers, G.; Van Schenck, J.; Quinn, A.; Van Court, R.; Vega Gutierrez, S. M.; Robinson, S. C.; Ostroverkhova, O. Xylindein: naturally produced fungal compound for sustainable (opto) electronics. *ACS Omega* **2019**, *4* (8), 13309-13318. (b) Petrov, N. G.; Chartier, P.; Maris, T.; Wuest, J. D. Designing tetraoxa[8]circulenes to serve as hosts and sensors. *Journal of the American Chemical Society* **2021**, *144* (1), 556-572. (c) Liu, J.; Yang, D.; Zhou, Y.; Zhang, G.; Xing, G.; Liu, Y.; Ma, Y.; Terasaki, O.; Yang, S.; Chen, L. Tricycloquinazoline-based 2D conductive metal-organic frameworks as promising electrocatalysts for CO_2 reduction. *Angewandte Chemie International Edition* **2021**, *60* (26), 14473-14479.

(5) Schwierz, F. Graphene transistors. *Nature Nanotechnology* **2010**, *5* (7), 487-496.

(6) (a) Wang, X.; Sun, G.; Routh, P.; Kim, D.-H.; Huang, W.; Chen, P. Heteroatom-doped graphene materials: syntheses, properties and applications. *Chemical Society Reviews* **2014**, *43* (20), 7067-7098. (b) Maiti, U. N.; Lee, W. J.; Lee, J. M.; Oh, Y.; Kim, J. Y.; Kim, J. E.; Shim, J.; Han, T. H.; Kim, S. O. 25th anniversary article: chemically modified/doped carbon nanotubes & graphene for optimized nanostructures & nanodevices. *Advanced Materials* **2014**, *26* (1), 40-67. (c) Duan, J.; Chen, S.; Jaroniec, M.; Qiao, S. Z. Heteroatom-doped graphene-based materials for energy-relevant electrocatalytic processes. *ACS Catalysis* **2015**, *5* (9), 5207-5234.

(7) (a) Qian, G.; Wang, Z. Y. Near-infrared organic compounds and emerging applications. *Chemistry–An Asian Journal* **2010**, *5* (5), 1006-1029. (b) Sun, Z.; Wu, J. Higher order acenes and fused acenes with near-infrared absorption

and emission. *Australian Journal of Chemistry* **2011**, *64* (5), 519-528.

(8) Pawlicki, M.; Collins, H. A.; Denning, R. G.; Anderson, H. L. Two-photon absorption and the design of two-photon dyes. *Angewandte Chemie International Edition* **2009**, *48* (18), 3244-3266.

(9) Tanaka, T. Synthesis of novel heteronanographenes via Fold-in Approach. *Bulletin of the Chemical Society of Japan* **2022**, *95* (4), 602-610.

(10) (a) Stará, I. G.; Starý, I. Helically chiral aromatics: the synthesis of helicenes by [2+ 2+ 2] cycloisomerization of π-electron systems. *Accounts of Chemical Research* **2019**, *53* (1), 144-158. (b) Kinoshita, S.; Yamano, R.; Shibata, Y.; Tanaka, Y.; Hanada, K.; Matsumoto, T.; Miyamoto, K.; Muranaka, A.; Uchiyama, M.; Tanaka, K. Rhodium-catalyzed highly diastereo-and enantioselective synthesis of a configurationally stable S-shaped double helicene-like molecule. *Angewandte Chemie International Edition* **2020**, *59* (27), 11020-11027. (c) Gauthier, E. S.; Rodríguez, R.; Crassous, J. Metal-based multihelicenic architectures. *Angewandte Chemie* **2020**, *132* (51), 23036-23052. (d) Anetai, H.; Takeda, T.; Hoshino, N.; Kobayashi, H.; Saito, N.; Shigeno, M.; Yamaguchi, M.; Akutagawa, T. Ferroelectric alkylamide-substituted helicene derivative with two-dimensional hydrogen-bonding lamellar phase. *Journal of the American Chemical Society* **2019**, *141* (6), 2391-2397.

(11) (a) Pedersen, S. K.; Eriksen, K.; Ågren, H.; Minaev, B. F.; Karaush-Karmazin, N. N.; Hammerich, O.; Baryshnikov, G. V.; Pittelkow, M. A. Fully conjugated planar heterocyclic[9]circulene. *Journal of the American Chemical Society* **2020**, *142* (33), 14058-14063. (b) Nakamura, K.; Li, Q. Q.; Krejčí, O. e.; Foster, A. S.; Sun, K.; Kawai, S.; Ito, S. On-surface synthesis of a π-extended diaza [8] circulene. *Journal of the American Chemical Society* **2020**, *142* (26), 11363-11369. (c) Karaush, N. N.; Baryshnikov, G. V.; Minaeva, V. A.; Ågren, H.; Minaev, B. F. Recent progress in quantum chemistry of hetero[8]circulenes. *Molecular Physics* **2017**, *115* (17-18), 2218-2230. (d) Dadvand, A.; Cicoira, F.; Chernichenko, K. Y.; Balenkova, E. S.; Osuna, R. M.; Rosei, F.; Nenajdenko, V. G.; Perepichka, D. F. Heterocirculenes as a new class of organic semiconductors. *Chemical Communications* **2008**, (42), 5354-5356.

(12) Zander, M.; Franke, W. H. Über Carbazolo-carbazole. *Chemische Berichte* **1969**, *102* (8), 2728-2738.

(13) (a) Wynberg, H.; Groen, M.; Schadenberg, H. Synthesis and resolution of some heterohelicenes. *The Journal of Organic Chemistry* **1971**, *36* (19), 2797-2809. (b) Dopper, J.; Oudman, D.; Wynberg, H. Dehydrogenation of heterohelicenes by a Scholl type reaction. dehydrohelicenes. *The Journal of Organic Chemistry* **1975**, *40* (23), 3398-3401.

(14) Rajca, A.; Miyasaka, M.; Xiao, S.; Boratyński, P. J.; Pink, M.; Rajca, S. Intramolecular cyclization of thiophene-based[7]helicenes to quasi-[8] circulenes. *The Journal of Organic Chemistry* **2009**, *74* (23), 9105-9111.

(15) Jessup, P. J.; Reiss, J. A. Cyclophanes. V. Biphenylnaphthalenophanes and the synthesis of hexa[7]circulene. *Australian Journal of Chemistry* **1976**, *29* (1), 173-178.

(16) Yamamoto, K.; Harada, T.; Okamoto, Y.; Chikamatsu, H.; Nakazaki, M.; Kai, Y.; Nakao, T.; Tanaka, M.; Harada, S.; Kasai, N. Synthesis and molecular structure of [7] circulene. *Journal of the American Chemical Society* **1988**, *110* (11), 3578-3584.

(17) Kawasumi, K.; Zhang, Q.; Segawa, Y.; Scott, L. T.; Itami, K. A grossly warped nanographene and the consequences of multiple odd-membered-ring defects. *Nature Chemistry* **2013**, *5* (9), 739-744.

(18) Kato, K.; Segawa, Y.; Scott, L. T.; Itami, K. Synthesis, properties, and packing structures of corannulene-based π -systems containing heptagons. *Chemistry–An Asian Journal* **2015**, *10* (8), 1635-1639.

(19) Fujikawa, T.; Segawa, Y.; Itami, K. Laterally π-extended dithia[6]helicenes with heptagons: saddle-helix hybrid molecules. *The Journal of Organic Chemistry* **2017**, *82* (15), 7745-7749.

(20) Chen, F.; Tanaka, T.; Mori, T.; Osuka, A. Synthesis, structures, and optical properties of azahelicene derivatives and unexpected formation of azahepta[8]circulenes. *Chemistry–A European Journal* **2018**, *24* (29), 7489-7497.

(21) Matsuo, Y.; Chen, F.; Kise, K.; Tanaka, T.; Osuka, A. Facile synthesis of fluorescent hetero[8]circulene analogues with tunable solubilities and optical properties. *Chemical Science* **2019**, *10* (48), 11006-11012.

(22) Lousen, B.; Pedersen, S. K.; Bols, P.; Hansen, K. H.; Pedersen, M. R.; Hammerich, O.; Bondarchuk, S.; Minaev, B.; Baryshnikov, G. V.; Ågren, H. Compressing a non-planar aromatic heterocyclic [7] helicene to a planar hetero [8] circulene. *Chemistry–A European Journal* **2020**, *26* (22), 4935-4940.

(23) Maeda, C.; Nomoto, S.; Akiyama, K.; Tanaka, T.; Ema, T. Facile Synthesis of azahelicenes and diaza[8]circulenes through the intramolecular Scholl reaction. *Chemistry–A European Journal* **2021**, *27* (63), 15699-15705.

(24) Yavari, K.; Delaunay, W.; De Rycke, N.; Reynaldo, T.; Aillard, P.; Srebro-Hooper, M.; Chang, V. Y.; Muller, G.; Tondelier, D.; Geffroy, B. Phosphahelicenes: from chiroptical and photophysical properties to OLED applications. *Chemistry–A European Journal* **2019**, *25* (20), 5303-5310.

(25) Demissie, T. B.; Sundar, M. S.; Thangavel, K.; Andrushchenko, V.; Bedekar, A. V.; Bouř, P. Origins of optical activity in an oxo-helicene: experimental and computational studies. *ACS Omega* **2021**, *6* (3), 2420-2428.

(26) Baruah, R. Study of optical absorption and photoluminescence (PL) of hexa thiobenzene acid. *Indian Academy of Sciences*. http://reports.ias.ac.in/report/20872/study-of-optical-absorption-and-photoluminescence-pl-of-hexa-thiobenzene-acid

(27) Mori, T. Chiroptical properties of symmetric double, triple, and multiple helicenes. *Chemical Reviews* **2021**, *121* (4), 2373-2412.

(28) (a) Aharon, T.; Caricato, M. Configuration space analysis of the specific rotation of helicenes. *The Journal of Physical Chemistry A* **2019**, *123* (20), 4406-4418. (b) Barron, L. D. Theoretical optical rotation of oriented hexahelicene. *Journal of the Chemical Society, Faraday Transactions 2: Molecular and Chemical Physics* **1975**, *71*, 293-300. (c) Martin, R.; Marchant, M.-J. Resolution and optical properties ([α] max, ORD and CD) of hepta-, octa- and nonahelicene. *Tetrahedron* **1974**, *30* (2), 343-345.

(29) (a) Petrovic, A. G.; Berova, N.; Alonso-Gómez, J. L. Absolute configuration and conformational analysis of chiral compounds via experimental and theoretical prediction of chiroptical properties: ORD, ECD, and VCD. *Structure Elucidation in Organic Chemistry: The Search for the Right Tools* **2015**. (b) Friese, D. H.; Hättig, C. Optical rotation calculations on large molecules using the approximate coupled cluster model CC2 and the resolution-of-the-identity approximation. *Physical Chemistry Chemical Physics* **2014**, *16* (13), 5942-5951. (c) Yamamoto, H.; Carreira, E. M. *Comprehensive Chirality: Online*; Elsevier Science, 2012. (d) Srebro, M.; Autschbach, J. Tuned range-separated time-dependent density functional theory applied to optical rotation. *Journal of Chemical Theory and Computation* **2012**, *8* (1), 245-256. (e) Naaman, R.; Beratan, D. N.; Waldeck, D. *Electronic and Magnetic Properties of Chiral Molecules and Supramolecular Architectures*; Springer Science & Business Media, 2011.

(30) (a) Yubuta, A.; Hosokawa, T.; Gon, M.; Tanaka, K.; Chujo, Y.; Tsurusaki, A.; Kamikawa, K. Enantioselective synthesis of triple helicenes by cross-cyclotrimerization of a helicenyl aryne and alkynes via dynamic kinetic resolution. *Journal of the American Chemical Society* **2020**, *142* (22), 10025-10033. (b) Shen, C.; Srebro-Hooper, M.; Weymuth, T.; Krausbeck, F.; Navarrete, J. T. L.; Ramírez, F. J.; Nieto-Ortega, B.; Casado, J.; Reiher, M.; Autschbach, J. Redox-Active Chiroptical Switching in Mono-and Bis-Iron Ethynylcarbo[6]helicenes Studied by Electronic and Vibrational Circular Dichroism and Resonance Raman Optical Activity. *Chemistry–A European Journal* **2018**, *24* (56), 15067-15079. (c) Abbate, S.; Longhi, G.; Lebon, F.; Castiglioni, E.; Superchi, S.; Pisani, L.; Fontana, F.; Torricelli, F.; Caronna, T.; Villani, C. Helical sense-responsive and substituent-sensitive features in vibrational and electronic circular dichroism, in circularly polarized luminescence, and in Raman spectra of some simple optically active hexahelicenes. *The Journal of Physical Chemistry C* **2014**, *118* (3), 1682-1695.

(31) (a) Peeters, E.; Christiaans, M. P.; Janssen, R. A.; Schoo, H. F.; Dekkers, H. P.; Meijer, E. Circularly polarized electroluminescence from a polymer light-emitting diode. *Journal of the American Chemical Society* **1997**, *119* (41), 9909-9910. (b) Kraft, A.; Grimsdale, A. C.; Holmes, A. B. Electroluminescent conjugated polymers-seeing polymers in a new light. *Angewandte Chemie International Edition* **1998**, *37* (4), 402-428.

(32) (a) Berova, N.; Nakanishi, K.; Woody, R. W. *Circular Dichroism: Principles and Applications*; John Wiley & Sons, 2000. (b) Lightner, D. A.; Gurst, J. E. *Organic Conformational Analysis and Stereochemistry from Circular Dichroism Spectroscopy*; John Wiley & Sons, 2000. (c) Berova, N.; Polavarapu, P. L.; Nakanishi, K.; Woody, R. W. *Comprehensive Chiroptical Spectroscopy, Volume 1: Instrumentation, Methodologies, and Theoretical Simulations*; John Wiley & Sons, 2011. (d) Berova, N.; Polavarapu, P. L.; Nakanishi, K.; Woody, R. W. *Comprehensive Chiroptical Spectroscopy, Volume 2: Applications in Stereochemical Analysis of Synthetic Compounds, Natural Products, and Biomolecules*; John Wiley & Sons, 2012. (e) Eyring, H.; Liu, H.-C.; Caldwell, D. Optical rotatory dispersion and circular dichroism. *Chemical Reviews* **1968**, *68* (5), 525-540. (f) Pescitelli, G.; Di Bari, L.; Berova, N. Conformational aspects in the studies of organic compounds by electronic circular dichroism. *Chemical Society Reviews* **2011**, *40* (9), 4603-4625. (g) Gillard, R. Circular dichroism. A review. *Analyst* **1963**, *88* (1052), 825-828.

(33) (a) Ma, J. L.; Peng, Q.; Zhao, C. H. Circularly polarized luminescence switching in small organic molecules. *Chemistry–A European Journal* **2019**, *25* (68), 15441-15454. (b) Longhi, G.; Castiglioni, E.; Koshoubu, J.; Mazzeo, G.; Abbate, S. Circularly polarized luminescence: a review of experimental and theoretical aspects. *Chirality* **2016**, *28* (10), 696-707. (c) Kumar, J.; Nakashima, T.; Kawai, T. Circularly polarized luminescence in chiral molecules and supramolecular assemblies. *The Journal of Physical Chemistry Letters* **2015**, *6* (17), 3445-3452.

(34) Sánchez-Carnerero, E. M.; Agarrabeitia, A. R.; Moreno, F.; Maroto, B. L.; Muller, G.; Ortiz, M. J.; de la Moya, S. Circularly polarized luminescence from simple organic molecules. *Chemistry–A European Journal* **2015**, *21* (39), 13488-13500.

(35) (a) Wagenknecht, C.; Li, C.; Reingruber, A.; Bao, X.; Goebel, A.; Chen, Y.; Zhang, Q.; Chen, K.; Pan, J. *Nature Photonics* **2010**, *4*, 549–552. (b) Carr, R.; Evans, N. H.; Parker, D. *Chemical Society Reviews* **2012**, *41*, 7673-7686.

(36) Schadt, M. Liquid crystal materials and liquid crystal displays. *Annual Review of Materials Science* **1997**, *27* (1), 305-379.

(37) (a) Farshchi, R.; Ramsteiner, M.; Herfort, J.; Tahraoui, A.; Grahn, H. Optical communication of spin information between light emitting diodes. *Applied Physics Letters* **2011**, *98* (16), 162508. (b) Jan, C. M.; Lee, Y. H.; Wu, K. C.; Lee, C. K. Integrating fault tolerance algorithm and circularly polarized ellipsometer for point-of-care applications. *Optics Express* **2011**, *19* (6), 5431-5441.

(38) Tanaka, H.; Inoue, Y.; Mori, T. Circularly polarized luminescence and circular dichroisms in small organic molecules: correlation between excitation and emission dissymmetry factors. *ChemPhotoChem* **2018**, *2* (5), 386-402.

(39) Mori, T. *Circularly Polarized Luminescence of Isolated Small Organic Molecules*; Springer, 2020.

(40) (a) Srebro-Hooper, M.; Autschbach, J. Calculating natural optical activity of molecules from first principles. *Annual Review of Physical Chemistry* **2017**, *68*, 399-420. (b) Polavarapu, P. L.; Covington, C. L. Comparison of experimental and calculated chiroptical spectra for chiral molecular structure determination. *Chirality* **2014**, *26* (9), 539-552. (c) Autschbach, J. Computing chiroptical properties with first-principles theoretical methods: background and illustrative examples. *Chirality: The Pharmacological, Biological, and Chemical Consequences of Molecular Asymmetry* **2009**, *21* (1), 116-152.

(41) (a) De Bettencourt-Dias, A. *Luminescence of Lanthanide Ions in Coordination Compounds and Nanomaterials*; John Wiley & Sons, 2014. (b) Zinna, F.; Di Bari, L. Lanthanide circularly polarized luminescence: bases and applications. *Chirality* **2015**, *27* (1), 1-13. (c) Muller, G. *Luminescence of Lanthanide Ions in Coordination Compounds and Nanomaterials*. John Wiley & Sons, Chichester, UK **2014**, 77-124. (d) Heffern, M. C.; Matosziuk, L. M.; Meade, T. J. Lanthanide probes for bioresponsive imaging. *Chemical Reviews* **2014**, *114* (8), 4496-4539. (e) Muller, G. Luminescent chiral lanthanide (III) complexes as potential molecular probes. *Dalton Transactions* **2009**, (44), 9692-9707.

(42) Lunkley, J. L.; Shirotani, D.; Yamanari, K.; Kaizaki, S.; Muller, G. Extraordinary circularly polarized luminescence activity exhibited by cesium tetrakis (3-heptafluoro-butylryl-(+)-camphorato) Eu (III) complexes in EtOH and CHCl3 solutions. *Journal of the American Chemical Society* **2008**, *130* (42), 13814-13815.

(43) Inouye, M.; Hayashi, K.; Yonenaga, Y.; Itou, T.; Fujimoto, K.; Uchida, T. a.; Iwamura, M.; Nozaki, K. A doubly alkynylpyrene-threaded [4] rotaxane that exhibits strong circularly polarized luminescence from the spatially restricted excimer. *Angewandte Chemie* **2014**, *126* (52), 14620-14624.

(44) Gong, Z. L.; Li, Z. Q.; Zhong, Y. W. Circularly polarized luminescence of coordination aggregates. *Aggregate* **2022**, 177.

(45) Jeong, S. M.; Ohtsuka, Y.; Ha, N. Y.; Takanishi, Y.; Ishikawa, K.; Takezoe, H.; Nishimura, S.; Suzaki, G. Highly circularly polarized electroluminescence from organic light-emitting diodes with wide-band reflective polymeric cholesteric liquid crystal films. *Applied Physics Letters* **2007**, *90* (21), 211106.

(46) (a) Zhao, Z. H.; Zhang, M.-Y.; Liu, D. H.; Zhao, C.-H. Modification of [5] helicene with dimesitylboryl: one way to enhance the fluorescence efficiency. *Organic Letters* **2018**, *20* (23), 7590-7593. (b) Fang, L.; Lin, W.; Chen, C. Tetrahydrobenzo[5]helicenediol derivatives as additives for efficient proline-catalyzed asymmetric List-Lerner-Barbas aldol reactions of bulky aldehyde substrates. *Chinese Chemical Letters* **2018**, *29* (8), 1223-1225.

(47) Field, J. E.; Muller, G.; Riehl, J. P.; Venkataraman, D. Circularly polarized luminescence from bridged triarylamine helicenes. *Journal of the American Chemical Society* **2003**, *125* (39), 11808-11809.

(48) Nakamura, K.; Furumi, S.; Takeuchi, M.; Shibuya, T.; Tanaka, K. Enantioselective synthesis and enhanced circularly polarized luminescence of S-shaped double azahelicenes. *Journal of the American Chemical Society* **2014**, *136* (15), 5555-5558.

(49) Chen, N.; Yan, B. Recent theoretical and experimental progress in circularly polarized luminescence of small organic molecules. *Molecules* **2018**, *23* (12), 3376.

(50) Saleh, N.; Moore, B.; Srebro, M.; Vanthuyne, N.; Toupet, L.; Williams, J. G.; Roussel, C.; Deol, K. K.; Muller, G.; Autschbach, J. Acid/base-triggered switching of circularly polarized luminescence and electronic circular dichroism in organic and organometallic helicenes. *Chemistry–A European Journal* **2015**, *21* (4), 1673-1681.

(51) Saleh, N.; Srebro, M.; Reynaldo, T.; Vanthuyne, N.; Toupet, L.; Chang, V. Y.; Muller, G.; Williams, J. G.; Roussel, C.; Autschbach, J. Enantioenriched CPL-active helicene-bipyridine-rhenium complexes. *Chemical Communications* **2015**, *51* (18), 3754-3757.

(52) Murayama, K.; Oike, Y.; Furumi, S.; Takeuchi, M.; Noguchi, K.; Tanaka, K. Enantioselective Synthesis, Crystal Structure, and Photophysical Properties of a 1, 1′ -Bitriphenylene-Based Sila [7] helicene. *European Journal of Organic Chemistry* **2015**, *2015* (7), 1409-1414.

(53) Longhi, G.; Castiglioni, E.; Villani, C.; Sabia, R.; Menichetti, S.; Viglianisi, C.; Devlin, F.; Abbate, S. Chiroptical properties of the ground and excited states of two thia-bridged triarylamine heterohelicenes. *Journal of Photochemistry and Photobiology A: Chemistry* **2016**, *331*, 138-145.

(54) Yamamoto, Y.; Sakai, H.; Yuasa, J.; Araki, Y.; Wada, T.; Sakanoue, T.; Takenobu, T.; Kawai, T.; Hasobe, T. Controlled excited-state dynamics and enhanced fluorescence property of tetrasulfone [9] helicene by a simple synthetic process. *The Journal of Physical Chemistry C* **2016**, *120* (13), 7421-7427.

(55) Bosson, J.; Labrador, G. M.; Pascal, S.; Miannay, F. A.; Yushchenko, O.; Li, H.; Bouffier, L.; Sojic, N.; Tovar, R. C.; Muller, G. Physicochemical and Electronic Properties of Cationic [6] Helicenes: from Chemical and Electrochemical Stabilities to Far-Red (Polarized) Luminescence. *Chemistry–A European Journal* **2016**, *22* (51), 18394-18403.

(56) Pascal, S.; Besnard, C.; Zinna, F.; Di Bari, L.; Le Guennic, B.; Jacquemin, D.; Lacour, J. Zwitterionic [4] helicene: a water-soluble and reversible pH-triggered ECD/CPL chiroptical switch in the UV and red spectral regions. *Organic & Biomolecular Chemistry* **2016**, *14* (20), 4590-4594.

(57) Katayama, T.; Nakatsuka, S.; Hirai, H.; Yasuda, N.; Kumar, J.; Kawai, T.; Hatakeyama, T. Two-step synthesis of boron-fused double helicenes. *Journal of the American Chemical Society* **2016**, *138* (16), 5210-5213.

(58) Isla, H.; Srebro-Hooper, M.; Jean, M.; Vanthuyne, N.; Roisnel, T.; Lunkley, J. L.; Muller, G.; Williams, J. G.; Autschbach, J.; Crassous, J. Conformational changes and chiroptical switching of enantiopure bis-helicenic terpyridine upon Zn 2+ binding. *Chemical Communications* **2016**, *52* (35), 5932-5935.

(59) Shen, C.; Srebro-Hooper, M.; Jean, M.; Vanthuyne, N.; Toupet, L.; Williams, J. G.; Torres, A. R.; Riives, A. J.; Muller, G.; Autschbach, J. Synthesis and chiroptical properties of hexa-, octa-, and deca-azaborahelicenes: influence of helicene size and of the number of boron atoms. *Chemistry–A European Journal* **2017**, *23* (2), 407-418.

(60) Otani, T.; Tsuyuki, A.; Iwachi, T.; Someya, S.; Tateno, K.; Kawai, H.; Saito, T.; Kanyiva, K. S.; Shibata, T. Facile two-step synthesis of 1, 10-phenanthroline-derived polyaza [7] helicenes with high fluorescence and CPL efficiency. *Angewandte Chemie International Edition* **2017**, *56* (14), 3906-3910.

(61) Ushiyama, A.; Hiroto, S.; Yuasa, J.; Kawai, T.; Shinokubo, H. Synthesis of a figure-eight azahelicene dimer with high emission and CPL properties. *Organic Chemistry Frontiers* **2017**, *4* (5), 664-667.

(62) Shen, C.; Anger, E.; Srebro, M.; Vanthuyne, N.; Deol, K. K.; Jefferson, T. D.; Muller, G.; Williams, J. G.; Toupet, L.; Roussel, C. Straightforward access to mono-and bis-cycloplatinated helicenes displaying circularly polarized phosphorescence by using crystallization resolution methods. *Chemical Science* **2014**, *5* (5), 1915-1927.

(63) Biet, T.; Cauchy, T.; Sun, Q.; Ding, J.; Hauser, A.; Oulevey, P.; Bürgi, T.; Jacquemin, D.; Vanthuyne, N.; Crassous, J. Triplet state CPL active helicene–dithiolene platinum bipyridine complexes. *Chemical Communications* **2017**, *53* (66), 9210-9213.

(64) Hellou, N.; Srebro-Hooper, M.; Favereau, L.; Zinna, F.; Caytan, E.; Toupet, L.; Dorcet, V.; Jean, M.; Vanthuyne, N.; Williams, J. G. Enantiopure cycloiridiated complexes bearing a pentahelicenic *N*-heterocyclic carbene and displaying long-lived circularly polarized phosphorescence. *Angewandte Chemie* **2017**, *129* (28), 8348-8351.

(65) Yamano, R.; Hara, J.; Murayama, K.; Sugiyama, H.; Teraoka, K.; Uekusa, H.; Kawauchi, S.; Shibata, Y.; Tanaka, K. Rh-mediated enantioselective synthesis, crystal structures, and photophysical/chiroptical properties of phenanthrenol-based [9] helicene-like molecules. *Organic Letters* **2017**, *19* (1), 42-45.

(66) Li, M.; Lu, H.-Y.; Zhang, C.; Shi, L.; Tang, Z.; Chen, C.-F. Helical aromatic imide based enantiomers with full-color circularly polarized luminescence. *Chemical Communications* **2016**, *52* (64), 9921-9924.

(67) Fang, L.; Li, M.; Lin, W.-B.; Shen, Y.; Chen, C.-F. Synthesis, structures, and photophysical properties of optically stable 1, 16-diphenyl-3, 14-diaryl-substituted tetrahydrobenzo [5] helicenediol derivatives: enantioselective recognition toward tryptophan methyl esters. *The Journal of Organic Chemistry* **2017**, *82* (14), 7402-7409.

(68) He, D.-Q.; Lu, H.-Y.; Li, M.; Chen, C.-F. Intense blue circularly polarized luminescence from helical aromatic esters. *Chemical Communications* **2017**, *53* (45), 6093-6096.

Chapter 2

Electrochemical Sequential Synthesis of Aza-oxa-dehydro[7]helicenes and Other PHAs

2.1. Introduction

Heterodehydrohelicenes derivatives represent a particular category of PHAs, and such molecular systems show a high potential to be implemented in a wide variety of materials science applications.[1] Despite the immense potential exhibited by heterodehydrohelicenes, there are no reports on their straightforward construction. This could be due to the limitations associated with the synthetic steps: low total yields,[2] harsh reaction conditions (such as high temperature),[3] easy racemization,[4] and/or overuse of oxidants (narrow functional group tolerance).[2]

In 2016, we reported an efficient vanadium-catalyzed synthesis of oxa[9]helicenes *via* the oxidative coupling of arenols followed by intramolecular dehydrative cyclization.[5] Recently we also developed the catalytic enantioselective oxidative hetero-coupling of arenols using a chiral vanadium(v) complex.[6] Based on this radical-anion coupling mechanism, we envisioned applying an organic electrochemical method to develop more environmentally benign syntheses of heterodehydrohelicenes. Recently, the electrochemical metal-catalyzed C–H functionalization process has received extensive attention as a useful strategy to construct PHAs.[7] Electrochemical domino processes are one of the most sustainable methods to construct multiple chemical bonds with a single operation; they reduce the requirement of chemicals and time for isolation and/or purification of synthetic intermediates, enabling environmentally benign synthetic processes.[8] Indeed, many metal- and oxidant-free electrochemical oxidative coupling reactions of arenols have been reported.[9] However, there have been no reports of heterodehydrohelicenes and other related PHAs synthesis using arenol as a starting material under electrochemical conditions. Herein, I describe the electrochemical synthesis of aza-oxa-dehydro[7]helicenes **83** possessing multiple heteroaromatic rings through the oxidative hetero-coupling of readily available arenols **79** and **80**, followed by dehydrative cyclization and intramolecular C-C bond formation sequence (**Scheme 2.1**).

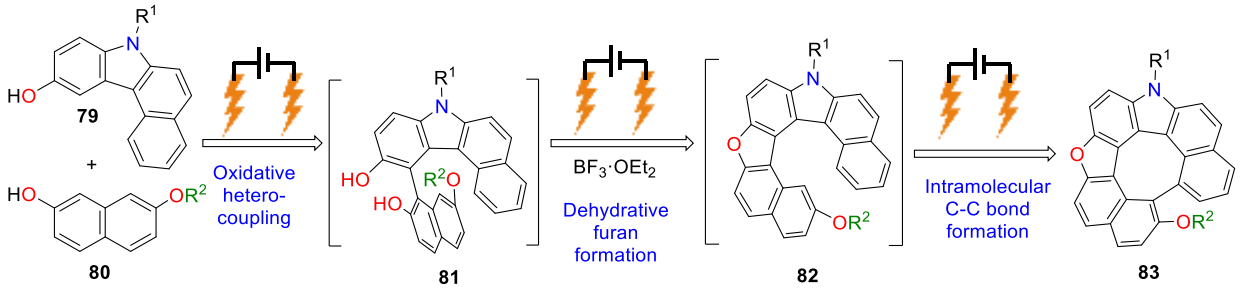

Scheme 2.1. Sequential synthesis of aza-oxa-dehydro[7]helicenes

2.2. Preliminary results

To investigate the electrochemical synthesis of aza-oxa-dehydro[7]helicenes **83**, hydroxybenzo[c] carbazole **79a** and 7-methoxy-2-naphthol (**80a**) were selected as the model starting materials. We assumed that single electron transfer (SET) from **79a** would occur first to generate the electrophilic

radical species at the anode because **79a** is more easily oxidized than **80a**. From cyclic voltammetry studies of arenols at (MeCN) with Bu_4NPF_6 (0.1 M): $E_{\mathbf{79a}(ox)}$ = 0.69 eV; $E_{\mathbf{80a}(ox)}$ = 1.05 eV (**Figure 2.1**). After radical-anion coupling between the radical cation species and **80a**, followed by dehydrative cyclization and intramolecular C-C bond formation sequence, aza-oxa-dehydro[7]helicenes **83aa** would be formed. Our preliminary optimization afforded aza-oxa-dehydro[7]helicenes **83aa** in 61% yield upon using CH_2Cl_2 as a solvent (1.25 mM) with Pt-electrodes and Bu_4NPF_6 as electrolyte (0.1 M) at 25 °C for 3 hours (**Scheme 2.2**).

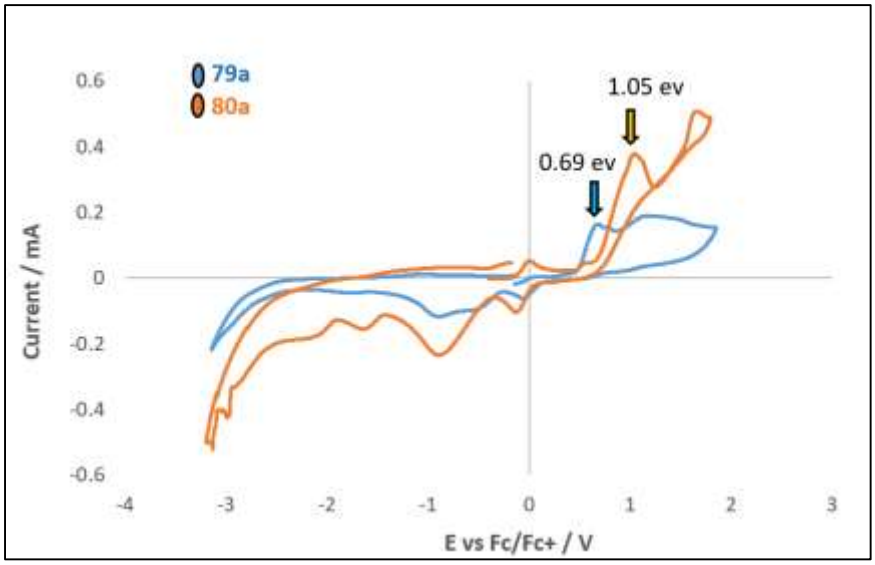

Figure 2.1. CV experiments of **79a** and **80a** (MeCN) as a solvent with Bu_4NPF_6 (0.1 M) as electrolyte.

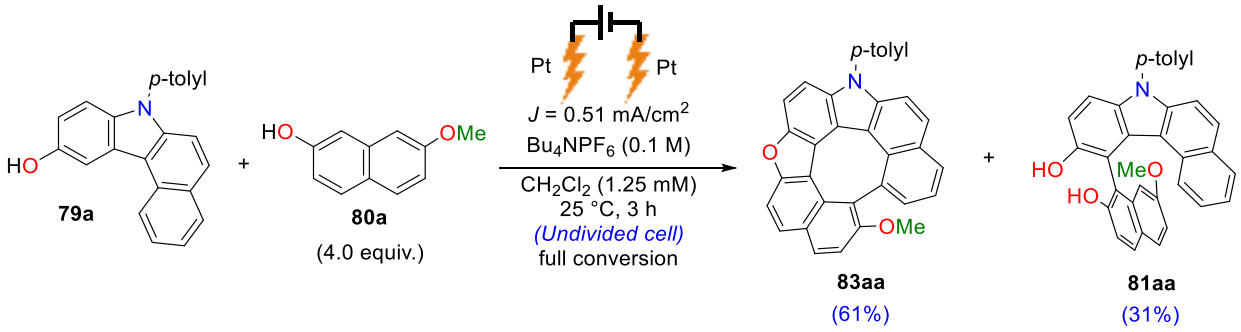

Scheme 2.2. Preliminary results for sequential synthesis of aza-oxa-dehydro[7]helicenes

Despite aza-oxa-dehydro[7]helicenes **83aa** was afforded in a moderate yield, we had to use excess amount (4.0 equiv.) of 7-methoxy-2-naphthol (**80a**) to supress the formation of side products. Decreasing the amount of 1.0 equiv. of **80a** produced low yield of aza-oxa-dehydro[7]helicene **83aa** (Diol **81aa** was isolated as the major side product 64%) as shown in (**Scheme 2.3**).

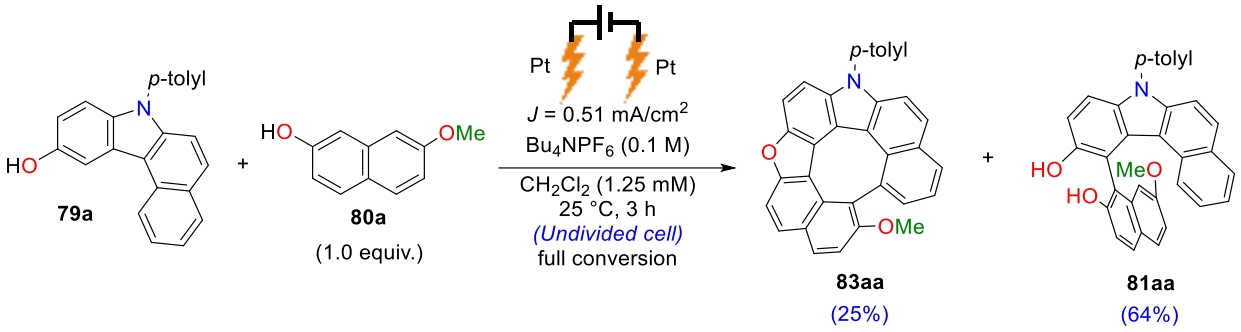

Scheme 2.3. Synthesis of aza-oxa-dehydro[7]helicenes using 1/1 ratio of coupling partners

So far, the role played by the excess amount of 7-methoxy-2-naphthol (**80a**) to suppress the formation of diol **81aa** and encourage the formation of dehydro[7]helicene **83aa** still elusive. But what baffled us more at first is the nature of this side product **81aa**, as our initial understanding of this reaction was based on the assumption of diol **81** to be an intermediate that can be converted under our conditions to the corresponding dehydro[7]helicene **83aa**. The thing which does not seem to be correct in our case. In order to shed some light on the nature of this sequential reaction, we have done some control experiments before suggesting the most plausible reaction mechanism.

2.3. Control experiments and plausible reaction mechanism

The diol **81aa** did not afford the corresponding dehydro[7]helicene **83aa** under our electrochemical conditions which supoorts that diol **81aa** is not an intermediate in this sequential pathway (**Scheme 2.4**). However, it is possible to convert this diol **81aa** to the corresponding [7]helicene **82aa** *via* an acid-mediated dehydrative cyclization which can be followed by an anodic oxidation to form dehydro[7]helicene **83aa** smoothly (**Scheme 2.5**).

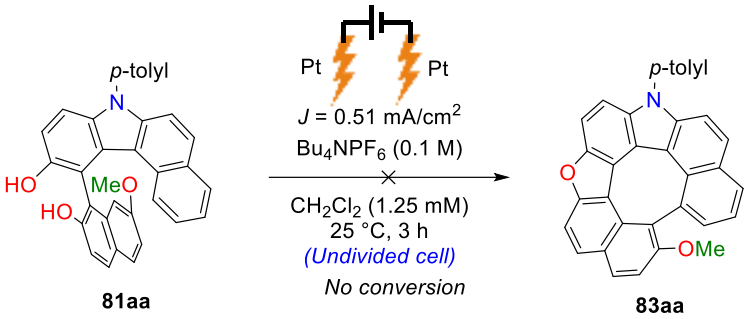

Scheme 2.4. Control experiment: study the conversion of diol under electrochemical conditions

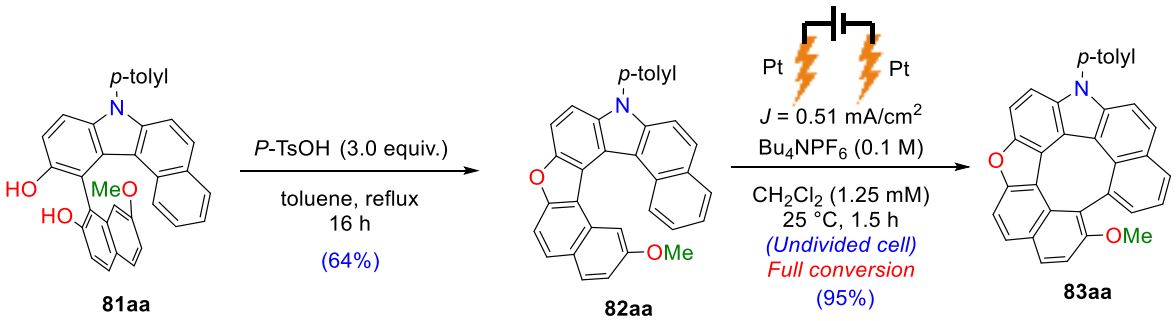

Scheme 2.5. Control experiment: acid-mediated dehydrative cyclization

Based on the previous experiments (**Schemes 2.4** and **2.5**), and cyclic voltammetry studies (**Figure 2.1**), we can suggest the anodic oxidation of **79a** to be the onset of this reaction. After that, single electron transfer (SET) would occur to generate the electrophilic radical species **II** at the anode that undergo radical-anion coupling with the more nucleophilic **80a**. Further anodic oxidations can afford intermediate **IV** that can either tautomerize to generate diol **81aa** side product or readily undergoes dehydrative cyclization to afford [7]helicene **82aa**, followed by intramolecular C-C bond formation to afford **83aa** (**Schemes 2.6**).

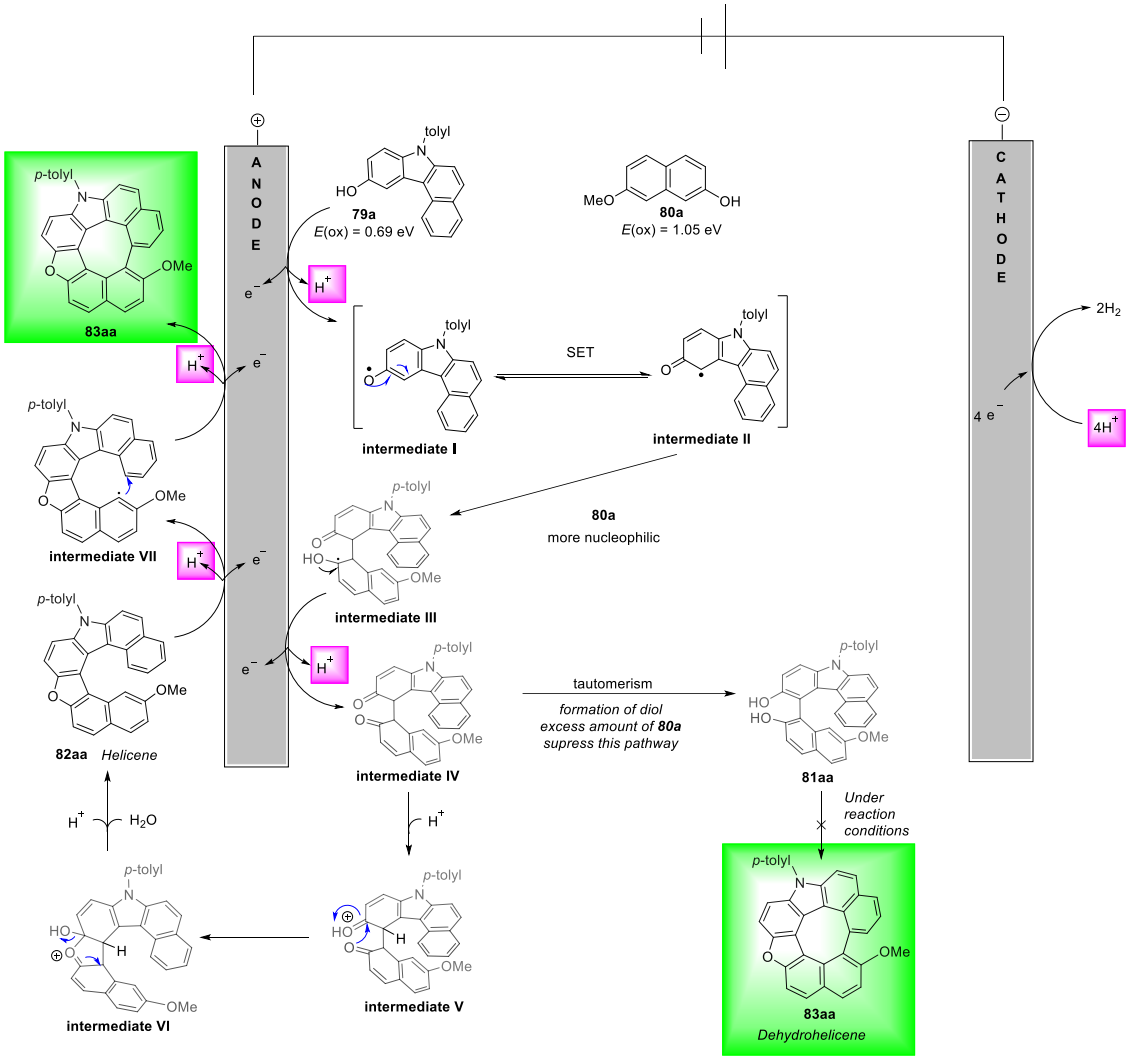

Scheme 2.6. Plausible reaction mechanism

Although we reached around 61% yield of dehydro[7]helicene **83aa** under our preliminary optimized conditions, we couldn't push this yield forward anymore. We envitionisoed based on our understanding to the mechanism that addition of some acid additives (such as $BF_3.OEt_2$) to our protocol, may help the conversion of diol to the corresponding helicene **82aa**, and subsequently dehydrohelicene **83aa**. In other words, we can modify the conditions to bring this side product diol **81aa** back to the sequential reaction as an intermediate. Besides, we can reoptimize some parameters to overcome other drawbacks or limitations in the preliminary conditions associated with using excess amount of 7-methoxy-2-naphthol (**80a**: 4.0 equiv.), super dilute concentration (1.25 mM) which hinders the scaling up of this reaction, and surely the absence of enantioselective version of this reaction.

2.4. Reoptimization of the reaction conditions to promote the efficiency

As we mentioned above, in an effort to overcome some of the reaction limitations and promote its efficiency, we decided to screen some different reaction parameters like solvents (**Table 2.1**), electrochemical parameters such as electrodes and electrolytes (**Table 2.2**), concentration and current density (**Table 2.3**), and some additives (**Table 2.4**).

Table 2.1. Screening of solvents.[a]

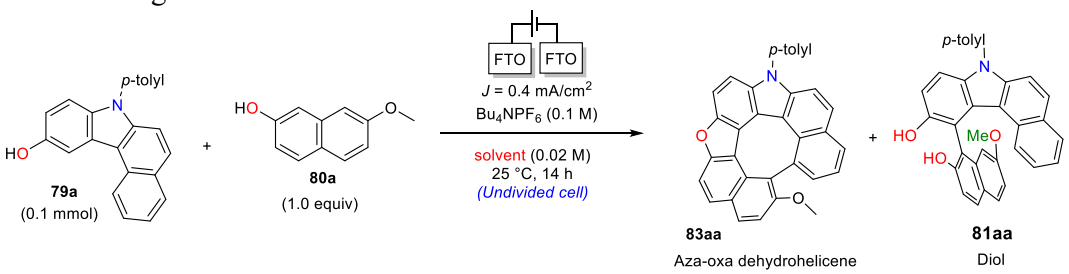

entry	solvent	yield of **83aa** (%)[b]	yield of **81aa** (%)[b]
1	CH_2Cl_2	28	68
2	THF	17	70
3	CH_3CN	14	50
4	CH_3OH	12	57

[a] The reaction of **79a** (0.1 mmol) and **80a** (0.1 mmol) was carried out in the corresponding solvent (5 mL) at 25 °C under air (1 atm). [b] Yields were determined by ^{1}H NMR spectroscopy using 1,3,5-trimethoxybenzene as an internal standard.

Table 2.2. Screening of electrodes, and electrolytes.[a]

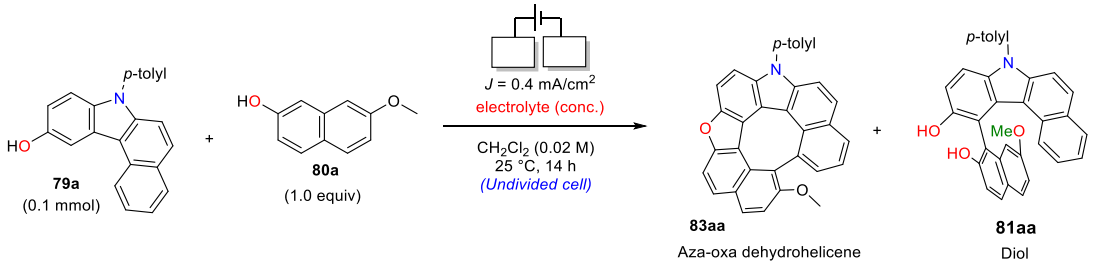

entry	electrode	electrolyte (conc. M)	yield of **83aa** (%)[b]	yield of **81aa** (%)[b]
1	Pt(+)-Pt(-)	Bu_4NPF_6 (0.1)	25	64
2	Pt(+)–C(-)	Bu_4NPF_6 (0.1)	22	55
3	Pt(+)–FTO(-)	Bu_4NPF_6 (0.1)	24	62
4	FTO(+)–FTO(-)	Bu_4NPF_6 (0.1)	28	68
5	FTO(+)–FTO(-)	$LiClO_4$ (0.1)	15	50
6	FTO(+)–FTO(-)	Bu_4NClO_4 (0.1)	20	54
7	FTO(+)–FTO(-)	Bu_4NPF_6 (0.05)	15	60
8	FTO(+)–FTO(-)	Bu_4NPF_6 (0.2)	26	68

[a] The reaction of **79a** (0.1 mmol) and **80a** (0.1 mmol) was carried out in dichloromethane (DCM: 5 mL) at 25 °C under air (1 atm). [b] Yields were determined by ^{1}H NMR spectroscopy using 1,3,5-trimethoxybenzene as an internal standard.

Table 2.3. Screening of concentration of **79a** and current density.[a]

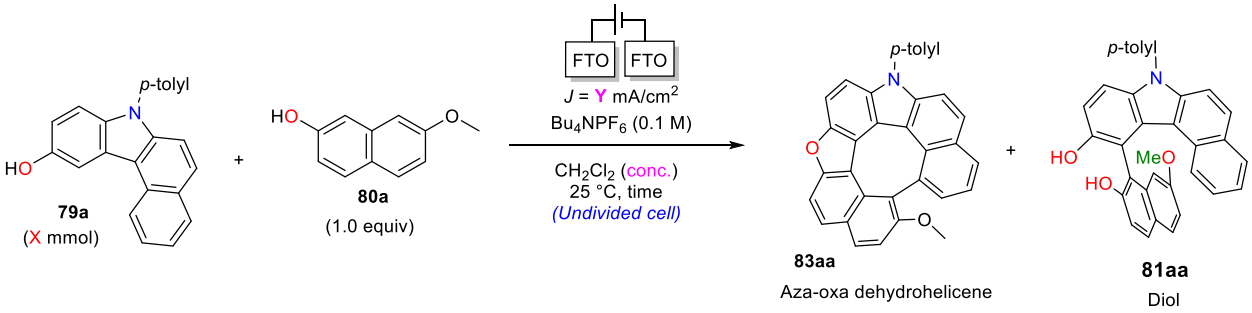

entry	**79a** (X mmol)	J = Y mA/cm^2	time (h)	yield of **83aa** (%)[b]	yield of **81aa** (%)[b]
1	0.025	0.4	3.0	22	63
2	0.05	0.4	6.5	25	64
3	0.1	0.4	14.0	28	68
4	0.1	0.8	12.5	32	64
5	0.1	1.2	10.0	37	60
6	0.1	1.6	7.0	30	55

[a] The reaction of **79a** (X mmol) and **80a** (X mmol) was carried out in DCM (5 mL) at 25 °C under air (1 atm). [b] Yields were determined by ^{1}H NMR spectroscopy using 1,3,5-trimethoxybenzene as an internal standard.

Table 2.4. Screening of additives.[a]

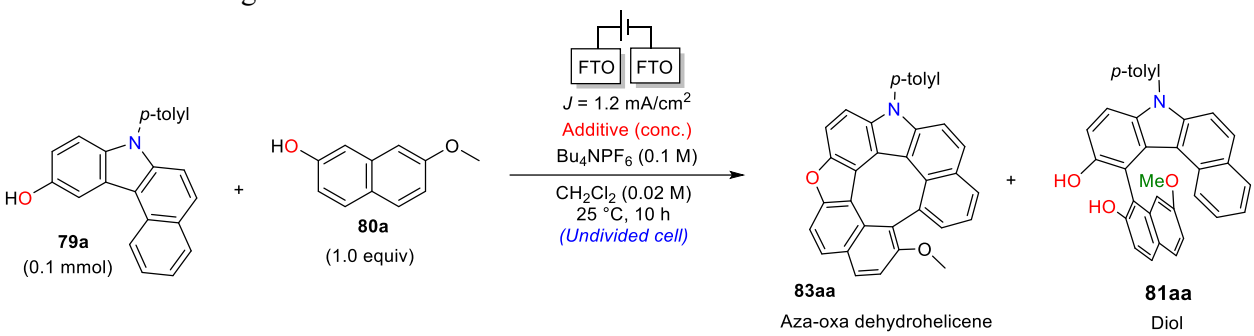

entry	additive	(conc. M)	yield of **83aa** (%)[b]	yield of **81aa** (%)[b]
1	acetic acid	0.05	50	35
2	TFA	0.05	55	21
3	$BF_3.OEt_2$	0.05	57	28
4	$BF_3.OEt_2$	0.1	68	20
5	$BF_3.OEt_2$	0.2	84	0
6	$BF_3.OEt_2$	0.3	76	0

[a] The reaction of **79a** (0.1 mmol) and **80a** (0.1 mmol) was carried out in DCM (5 mL) in presence of additive (conc.) at 25 °C under air (1 atm). [b] Yields were determined by ^{1}H NMR spectroscopy using 1,3,5-trimethoxybenzene as an IS.

After examining various conditions and performing sedulous optimization (**Tables 2.1-2.4**), a sequential protocol generating aza-oxa-dehydro[7]helicenes **83aa** in 84% yield (81% isolated yield, current efficiency = 30%) was developed; fluorine-doped tin oxide (FTO) was used as electrodes and Bu_4NPF_6 as the electrolyte (0.1 M) at 25 °C, in the presence of $BF_3{\cdot}OEt_2$ (as an additive) in CH_2Cl_2. The structure of **83aa** was confirmed by X-ray crystallography (**Figure 2.2**).

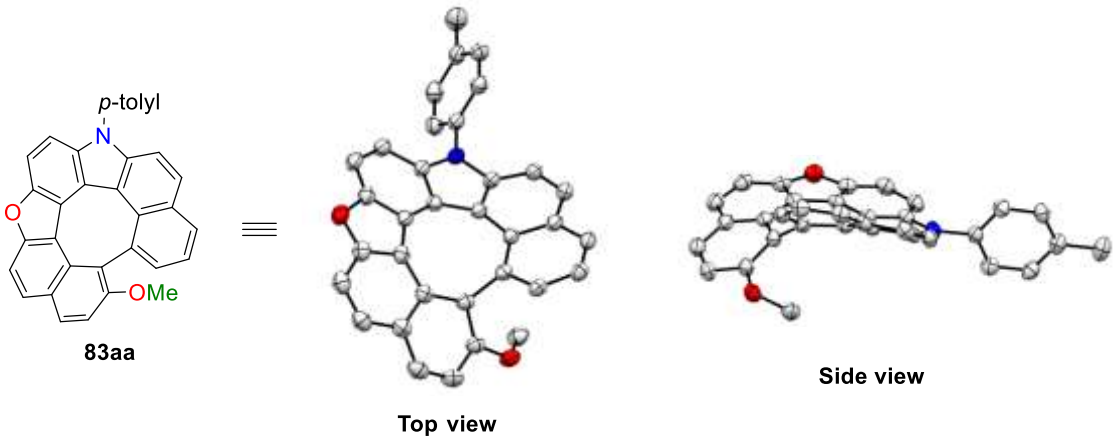

Figure 2.2. X-ray structure of **83aa** with ellipsoids at 30% probability (H atoms were omitted for clarity).

A series of control experiments were subsequently conducted to understand the role of each reactant (**Table 2.5**). To our delight, fluorine-doped tin oxide FTO electrodes showed the best performance compared to others (entries 2-3). The FTO electrodes are commercially available, recyclable (>5 times) and cheap.[10] Doubling the current density reduced the yield of **83aa** to 65% (entry 4); its reduction to 0.8 mA/cm^2 did not significantly affect the yield but prolonged the reaction time (entry 5). High concentrations of the electrolyte, other solvents [THF, MeCN, and MeOH (5 mL)], and other electrolytes such as $LiClO_4$ (0.1 M) formed diol **81aa** as the major side product in 9 to 22% yields (entries 6–10). Decreasing the amount of $BF_3{\cdot}OEt_2$ or replacing it with other Brønsted acids (as acidic additives) produced low yields of aza-oxa-dehydro[7]helicene **83aa** (**81aa** was isolated as the major side product in 5 to 20% yields) (entries 11–13). $BF_3{\cdot}OEt_2$ transformed diol **81aa** to helicene intermediate **82aa**, which underwent facile anodic oxidation to form **83aa**. No reaction occurred in the absence of electricity (entry 14). Finally, to generalize this protocol, **83aa** was synthesized using ElectraSyn® 2.0 (designed by IKA);[11] it exhibited comparable results (entry 15).

Table 2.5. Variation from standard conditions.[a]

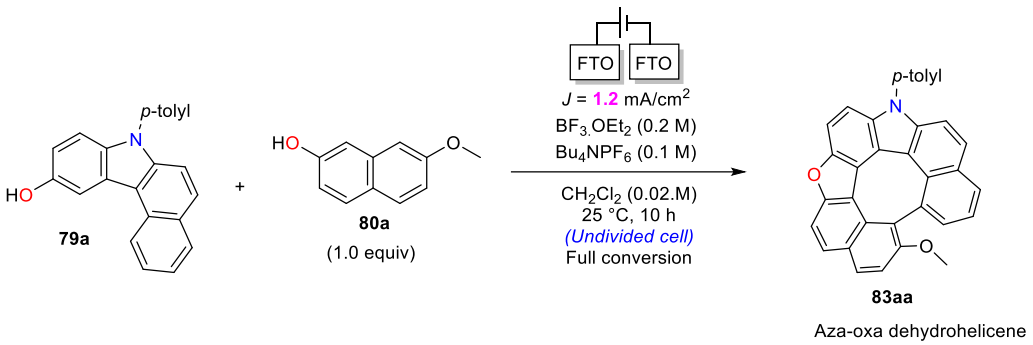

entry	variation from standard conditions	yield of **83aa** (%)
1	None	84 (81)
2	With C(+) / FTO(-)	42
3	With FTO(+) / Pt(-)	55
4	J = 2.4 mA/cm^2	65
5	J = 0.8 mA/cm^2	77 [b]
6	0.2 M of Bu_4NPF_6	65
7	$LiClO_4$ instead of Bu_4NPF_6	47
8	THF instead of CH_2Cl_2	21
9	MeCN instead of CH_2Cl_2	36
10	MeOH instead of CH_2Cl_2	45
11	Without $BF_3{\cdot}OEt_2$	37
12	Using 0.1 M of $BF_3{\cdot}OEt_2$	68
13	Using TFA instead of $BF_3{\cdot}OEt_2$	67
14	No electricity	No reaction [c]
15	ElectraSyn® 2.0 with Pt(+) / Pt(-)	75

[a] Electrolysis conditions: FTO anode, FTO cathode, constant current = 3 mA, **79a** and **80a** (0.1 mmol), Bu_4NPF_6 (0.1 M), $BF_3{\cdot}OEt_2$ (0.2 M), CH_2Cl_2 (5 mL), 25 °C, 10 h. [b]12.5 h. [c] No conversion.

2.5. Substrate scope

Subsequently, the substrate scope of various hydroxycarbazoles **79** and 2-naphthols **80** were investigated under the optimal reaction conditions (**Scheme 2.7**). *N*-Aryl- and *N*-alkyl-substituted derivatives **79a–79f** underwent facile conversion to aza-oxa-dehydro[7]helicenes **83aa–83fa** in 78-86% yields. Different combinations of **80** with 7-benzyloxy or allyloxy groups **80b–80c** were used to synthesize aza-oxa-dehydro[7]helicenes **83ab–83fc** in 71-84% yields. A series of compounds **79** substituted by Me, Ph, and OMe groups at various positions on the aromatic ring formed products **83ga–83la** in 76-84% yields. π-Expanded substrate **79i** also reacted with **80a** to form **83ia** in 80% yield. Hydroxycarbazole **79m** with an electron withdrawing cyano group afforded **83ma** in 67% yield.

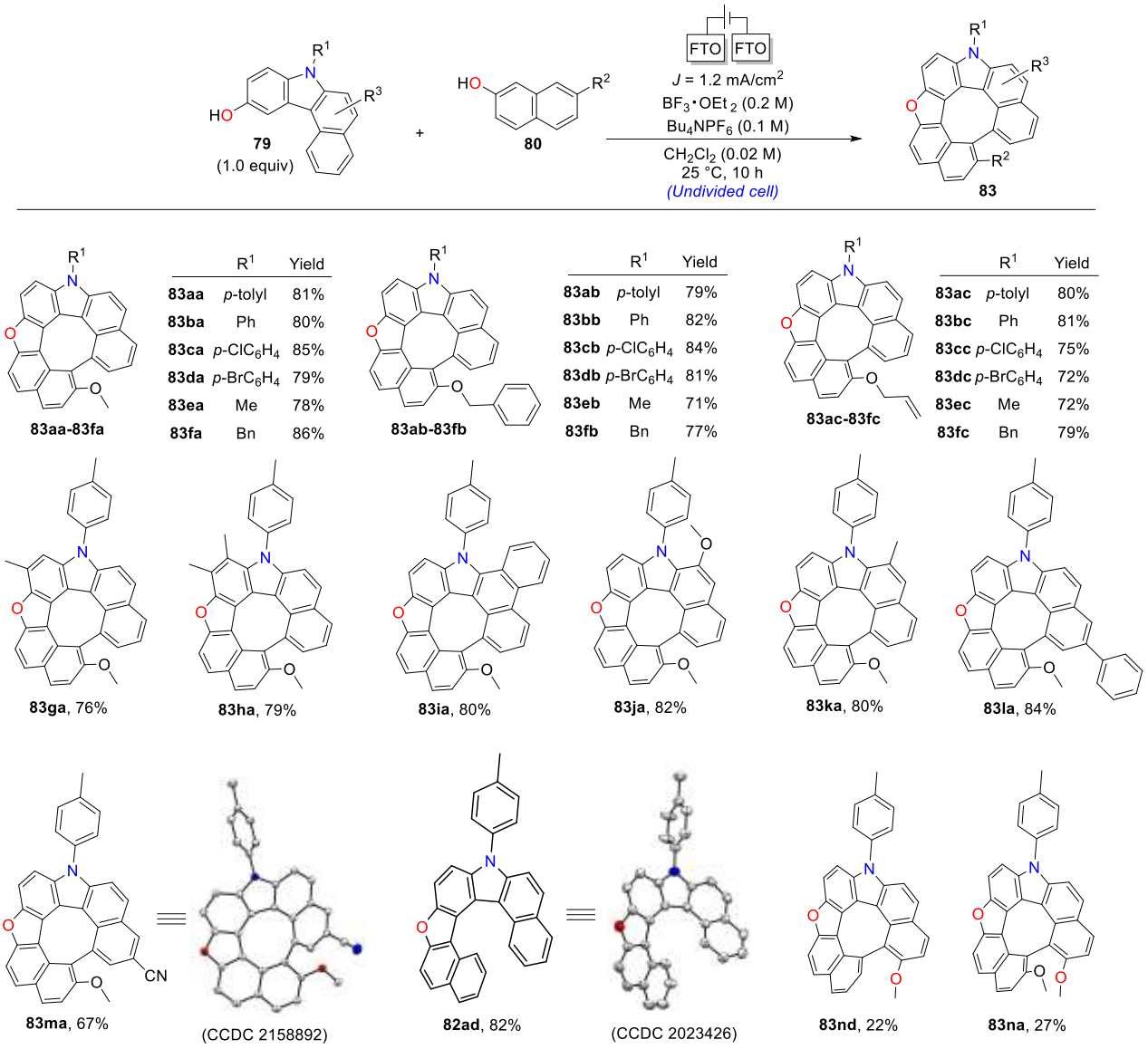

	R^1	Yield
83aa	*p*-tolyl	81%
83ba	Ph	80%
83ca	*p*-ClC_6H_4	85%
83da	*p*-BrC_6H_4	79%
83ea	Me	78%
83fa	Bn	86%

	R^1	Yield
83ab	*p*-tolyl	79%
83bb	Ph	82%
83cb	*p*-ClC_6H_4	84%
83db	*p*-BrC_6H_4	81%
83eb	Me	71%
83fb	Bn	77%

	R^1	Yield
83ac	*p*-tolyl	80%
83bc	Ph	81%
83cc	*p*-ClC_6H_4	75%
83dc	*p*-BrC_6H_4	72%
83ec	Me	72%
83fc	Bn	79%

Scheme 2.7. Substrate-scope studies

In the absence of 7-alkoxy group from **80**, aza-oxa-dehydro[7]helicenes cannot be afforded and only the corresponding aza-oxa[7]helicene **82ad** was afforded. This highlights the critical role of these

groups to maintain the electron density at the helical termini that makes dehydro[7]helicene formation possible. To our delight, the presence of this alkoxy group at the carbazole moiety instead of 2-naphthol moiety allowed the formation of dehydro[7]helicene **83nd** at low yield. Keeping the methoxy groups at both helical termini did not eliminate the possibility of dehydro[7]helicene formation, but it decreased the yield of **83na** (27%). Although the low yield of the last two substrates **83nd** and **83na** compared to others, they show the possibility of the dehydro[7]helicene formation with broader scope of substrates, and possibly their yields could be further improved with more optimization.

2.6. Two-pot synthesis of aza-oxa-dehydro[7]helicenes

To establish the applicability of this method for concise synthesis, a two-pot protocol using commercially available substrates *p*-benzoquinone **84** and *N*-phenyl-2-naphthylamine **85** was tested; it produced aza-oxa-dehydro[7]helicene **83ba** in 55% overall yield (**Scheme 2.8**).

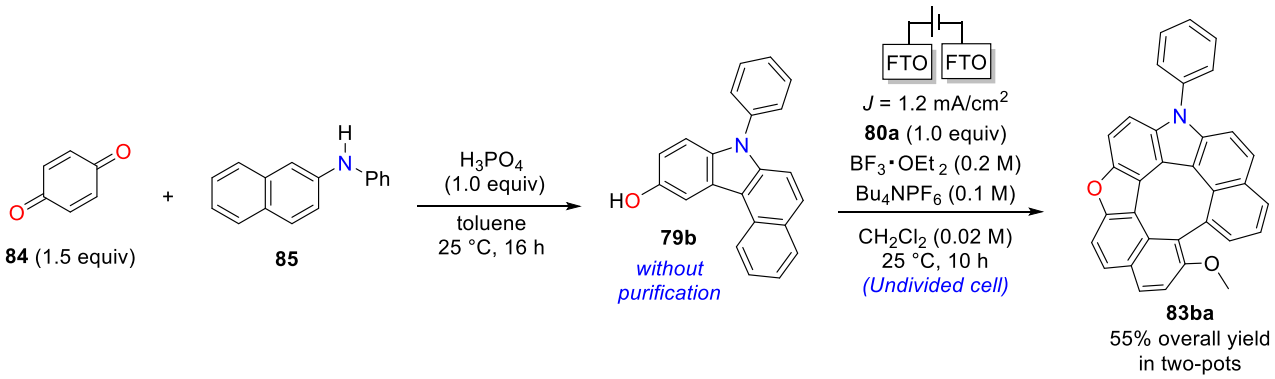

Scheme 2.8. Two-pot synthesis of **83ba** from commercially available substrates **84** and **85**.

2.7. Chemical transformations of aza-oxa-dehydro[7]helicenes

Transformations for the introduction of functional groups were subsequently investigated using various aza-oxa-dehydro[7]helicenes **83**. The benzyl group on the nitrogen of **83fa** was removed using $AlCl_3$ to give **83oa**, which underwent Pd-catalyzed *N*-arylation to form **83ba** (**Scheme 2.9.A**). The carboxylic acid derivative **83pa** was formed after the hydrolysis of **83ma** under basic conditions (**Scheme 2.9.B**). Furthermore, a treatment of **83na** with BBr_3 at 25 °C afforded corresponding aza-oxa[8]circulene **86** in 92% yield (**Scheme 2.9.C**). This aza-oxa[8]circulene **86** considered as a new type of [8]circulenes. All reported [8]circulenes belong to one of these three types; type I, II, and III (**Figure 2.3**).[12]

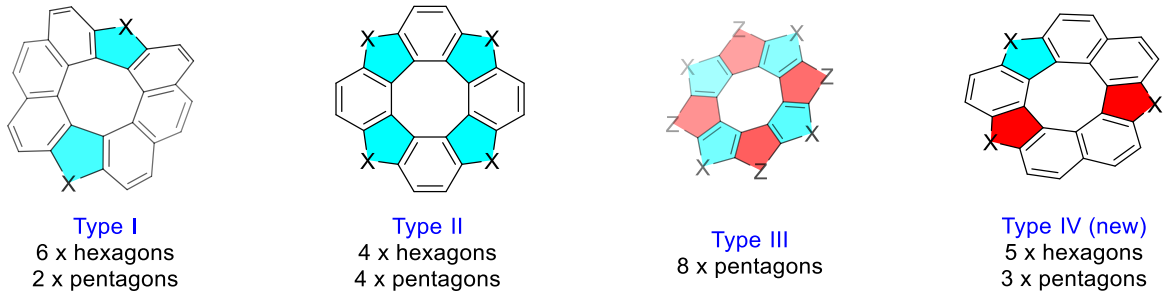

Figure 2.3. Types of hetero[8]circulenes

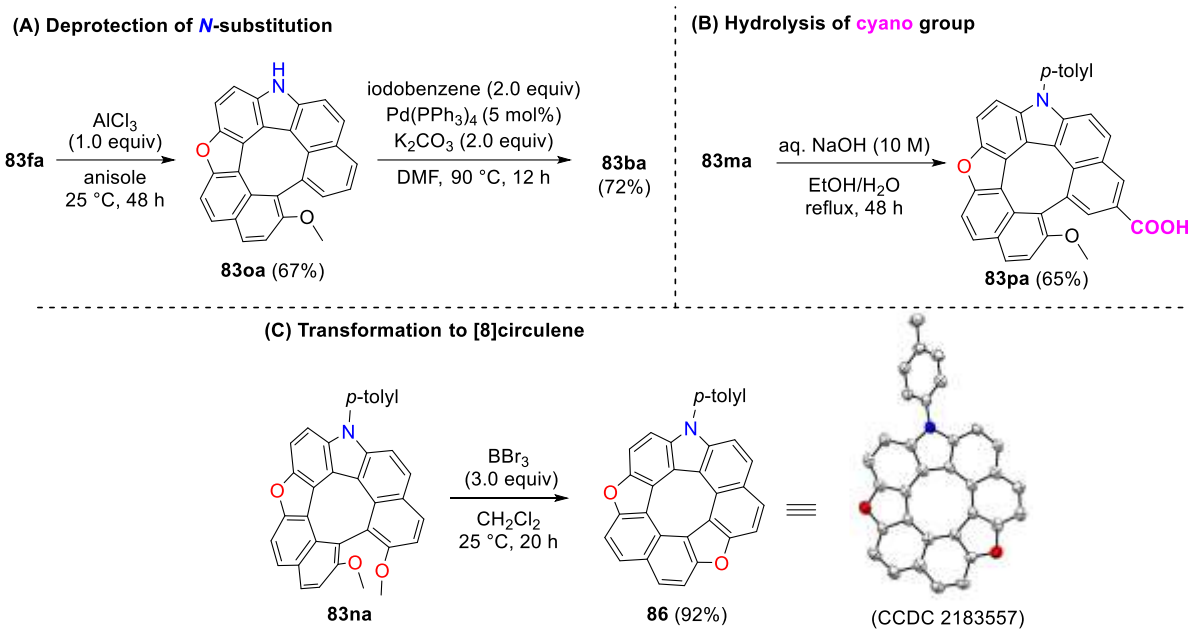

Scheme 2.9. Derivatization of aza-oxa-dehydro[7]helicenes

2.8. Electrochemical synthesis of other PHAs

When the transformation of **81aa** to heterodehydro[7]helicene **83aa** was carried out in the absence of $BF_3.OEt_2$, the double C-O insertions occurred to afford **87aa** in 83% yield. The structure of **87aa** was confirmed *via* X-ray crystallographic analysis (**Scheme 2.10**).

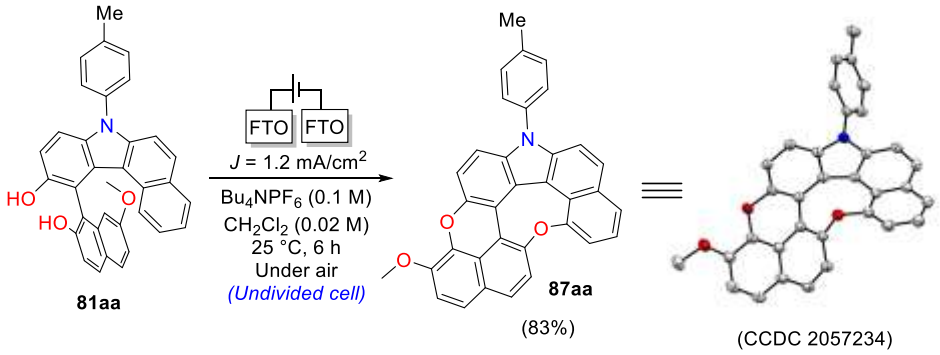

Scheme 2.10. Electrochemical synthesis of compound **87aa**

The homo-coupling of **79a** was not possible under low intensities of electric current. However, after modifying the electrochemical parameters (current density and electrodes), homo-coupling diol product **88a** was obtained which subsequently underwent double C-O insertions to afford **89a** in 62% yield (analogue of **87aa**) under the same conditions. The structure of **89a** was confirmed *via* X-ray crystallographic analysis (**Scheme 2.11**).

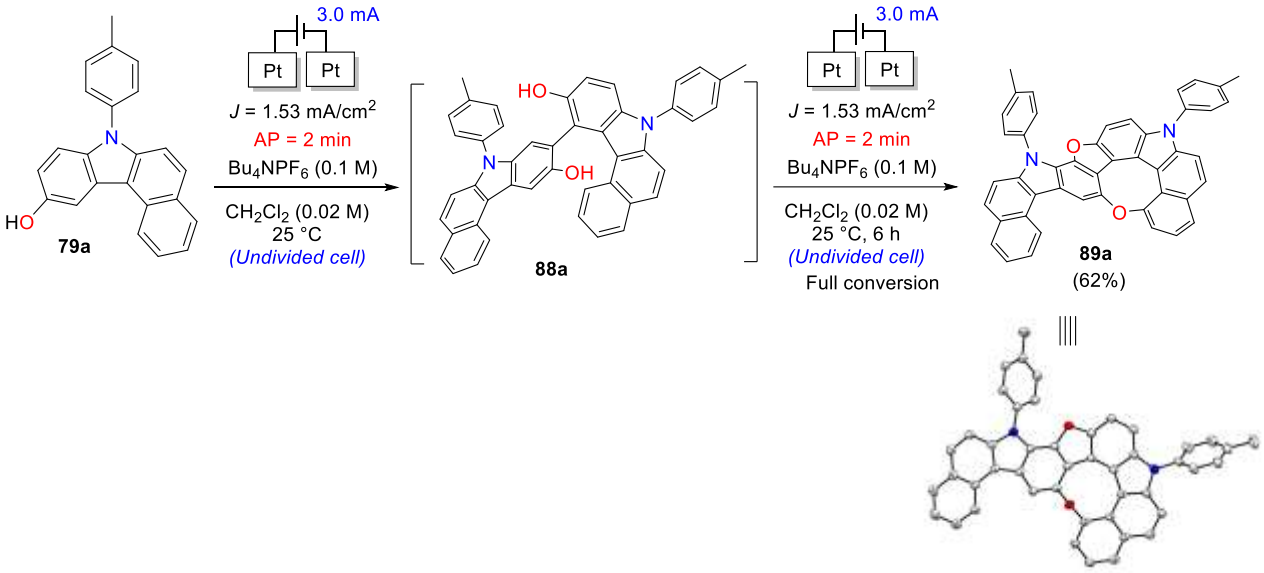

Scheme 2.11. Electrochemical synthesis of compound **89a**

By increasing the intensity of electric current (up to 6.0 mA/ J = 3.06 mA/cm^2), we observed the formation of another homo-coupling product **90** (**Scheme 2.12**). After spectral analysis, we realized that diol **88a** afforded a new helicene **91** that subsequently underwent a chlorination to afford **90** in 24% yield. The structure of **90** was confirmed *via* X-ray crystallographic analysis. The only source of this chloro- is CH_2Cl_2, which is quite rare to be a chlorinating agent. Compound **89a** was also afforded as a major product under these conditions in 52% yield. Further studies are going on right now to understand the reaction mechanism, improve the yield of **90**, and explore its potential applications in different fields.

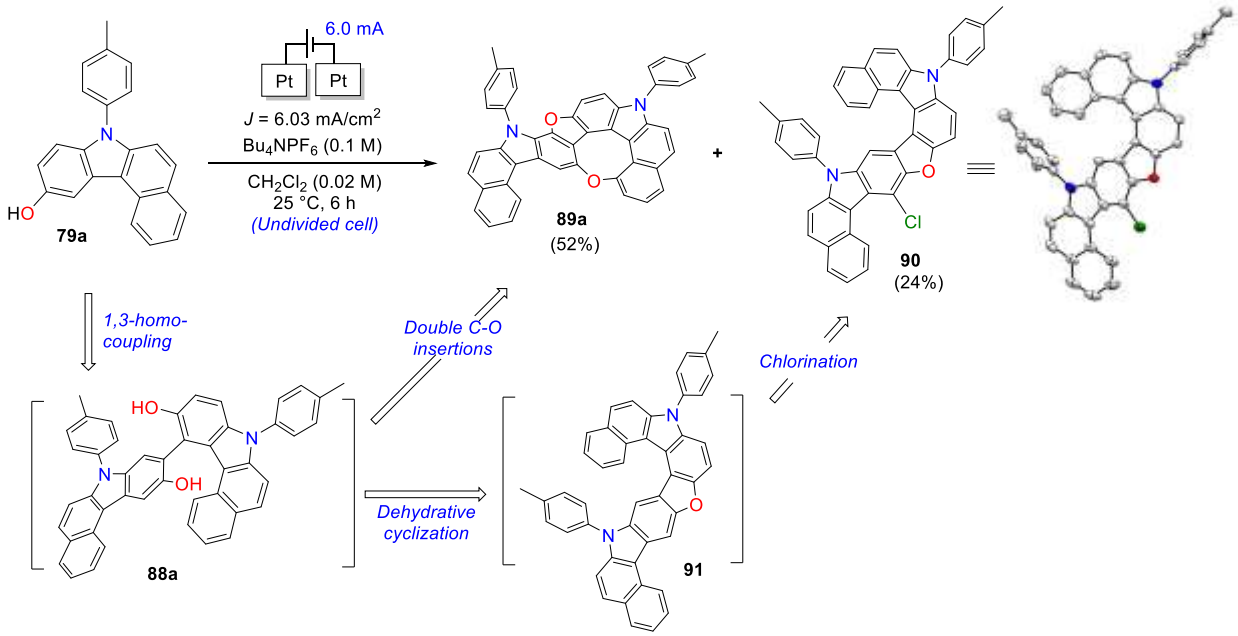

Scheme 2.12. Electrochemical synthesis of compounds **89a** and **90**

References

(1) Borissov, A.; Maurya, Y. K.; Moshniaha, L.; Wong, W.-S.; Żyła-Karwowska, M.; Stepien, M. Recent advances in heterocyclic nanographenes and other polycyclic heteroaromatic compounds. *Chemical Reviews* **2021**, *122* (1), 565-788.

(2) (a) Pedersen, S. K.; Eriksen, K.; Ågren, H.; Minaev, B. F.; Karaush-Karmazin, N. N.; Hammerich, O.; Baryshnikov, G. V.; Pittelkow, M. A fully conjugated planar heterocyclic [9] circulene. *Journal of the American Chemical Society* **2020**, *142* (33), 14058-14063. (b) Matsuo, Y.; Chen, F.; Kise, K.; Tanaka, T.; Osuka, A. Facile synthesis of fluorescent hetero[8]circulene analogues with tunable solubilities and optical properties. *Chemical Science* **2019**, *10* (48), 11006-11012.

(3) (a) Dopper, J.; Oudman, D.; Wynberg, H. Dehydrogenation of heterohelicenes by a Scholl type reaction dehydrohelicenes. *The Journal of Organic Chemistry* **1975**, *40* (23), 3398-3401. (b) Zander, M.; Franke, W. H. Über carbazolo-carbazole. *Chemische Berichte* **1969**, *102* (8), 2728-2738.

(4) (a) Chen, F.; Tanaka, T.; Mori, T.; Osuka, A. Synthesis, structures, and optical properties of azahelicene derivatives and unexpected formation of azahepta [8] circulenes. *Chemistry–A European Journal* **2018**, *24* (29), 7489-7497. (b) Kato, K.; Segawa, Y.; Scott, L. T.; Itami, K. Synthesis, properties, and packing structures of corannulene-based π-systems containing heptagons. *Chemistry-An Asian Journal* **2015**, *10* (8), 1635-1639. (c) Kawasumi, K.; Zhang, Q.; Segawa, Y.; Scott, L. T.; Itami, K. A grossly warped nanographene and the consequences of multiple odd-membered-ring defects. *Nature Chemistry* **2013**, *5* (9), 739-744.

(5) Sako, M.; Takeuchi, Y.; Tsujihara, T.; Kodera, J.; Kawano, T.; Takizawa, S.; Sasai, H. Efficient enantioselective synthesis of oxahelicenes using redox/acid cooperative catalysts. *Journal of the American Chemical Society* **2016**, *138* (36), 11481-11484.

(6) Sako, M.; Higashida, K.; Kamble, G. T.; Kaut, K.; Kumar, A.; Hirose, Y.; Zhou, D.-Y.; Suzuki, T.; Rueping, M.; Maegawa, T. Chemo- and enantioselective hetero-coupling of hydroxycarbazoles catalyzed by a chiral vanadium(v) complex. *Organic Chemistry Frontiers* **2021**, *8* (17), 4878-4885.

(7) (a) Malapit, C. A.; Prater, M. B.; Cabrera-Pardo, J. R.; Li, M.; Pham, T. D.; McFadden, T. P.; Blank, S.; Minteer, S. D. Advances on the merger of electrochemistry and transition metal catalysis for organic synthesis. *Chemical Reviews* **2021**, *122* (3), 3180-3218. (b) Zhu, C.; Ang, N. W.; Meyer, T. H.; Qiu, Y.; Ackermann, L. Organic electrochemistry: molecular syntheses with potential. *ACS Central Science* **2021**, *7* (3), 415-431. (c) Kakiuchi, F.; Kochi, T. New strategy for catalytic oxidative C–H functionalization: efficient combination of transition-metal catalyst and electrochemical oxidation. *Chemistry Letters* **2020**, *49* (10), 1256-1269.

(8) (a) Murray, P. R.; Cox, J. H.; Chiappini, N. D.; Roos, C. B.; McLoughlin, E. A.; Hejna, B. G.; Nguyen, S. T.; Ripberger, H. H.; Ganley, J. M.; Tsui, E. Photochemical and electrochemical applications of proton-coupled electron transfer in organic synthesis. *Chemical Reviews* **2022**, *122* (2), 2017-2291. (b) Tay, N. E.; Lehnherr, D.; Rovis, T. Photons or electrons? A critical comparison of electrochemistry and photoredox catalysis for organic synthesis. *Chemical Reviews* **2022**, *122* (2), 2487-2649. (c) Qian, P.; Xu, L.; Wang, W.; Zhang, L.; Tang, L.; Liu, J.; Sheng, L. Electrochemical synthesis of dipyrazolo/dipyrimidine-fused pyridines *via* oxidative domino cyclization of C (sp^3)-H bonds. *Organic Chemistry Frontiers* **2022**, *9* (6), 1662-1667.

(9) (a) Röckl, J. L.; Pollok, D.; Franke, R.; Waldvogel, S. R. A decade of electrochemical dehydrogenative C-C coupling of aryls. *Accounts of Chemical Research* **2019**, *53* (1), 45-61. (b) Röckl, J. L.; Schollmeyer, D.; Franke, R.; Waldvogel, S. R. Dehydrogenative anodic C-C coupling of phenols bearing electron-withdrawing groups. *Angewandte Chemie International Edition* **2020**, *59* (1), 315-319. (c) Selt, M.; Mentizi, S.; Schollmeyer, D.; Franke, R.; Waldvogel, S. R. Selective and scalable dehydrogenative electrochemical synthesis of 3,3',5,5'-Tetramethyl-2,2'-biphenol. *Synlett* **2019**, *30* (18), 2062-2067.

(10) Zhang, L.; Hu, X. Nickel catalysis enables convergent paired electrolysis for direct arylation of benzylic C-H bonds. *Chemical Science* **2020**, *11* (39), 10786-10791.

(11) https://www.ika.com/en/Products-Lab-Eq/Electrochemistry-Kit-csp-516/ElectraSyn-20-pro-Package-cpdt-40003261/

(12) Miyake, Y.; Shinokubo, H. Hetero[8]circulenes: synthetic progress and intrinsic properties. *Chemical Communications* **2020**, *56* (100), 15605-15614.

Chapter 3

Stepwise Enantioselective Synthesis of Aza-oxa-dehydro[7]helicenes

3.1. Introduction

Although many reports are found on the enantioselective synthesis of helicenes,[1] there are no such reports for dehydrohelicenes. Success in such a challenge will represent a quantum leap in this field. Not only it can provide an easier and more efficient way to get the desired enantiomer, but also restore hope for many stopped attempts to study the chiroptical properties due to the difficulty of HPLC chiral resolution.[2] An efficient chemo- and enantioselective protocol for the oxidative hetero-coupling of hydroxycarbazoles **79o** and naphthols **80d** using a chiral vanadium(v) complex **92**, producing axially chiral biaryl derivatives, has been previously reported (**Scheme 3.1**);[3] based on this study, a stepwise enantioselective synthesis of diol **81ba** was examined, which was followed by electrochemical transformation to the corresponding heterodehydrohelicenes (**Scheme 3.2**).

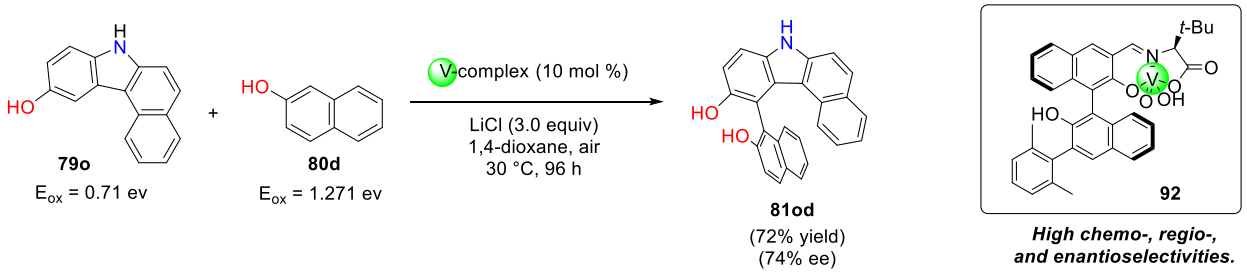

Scheme 3.1. Vanadium-catalyzed hetero-coupling of hydroxycarbazole with 2-naphthol

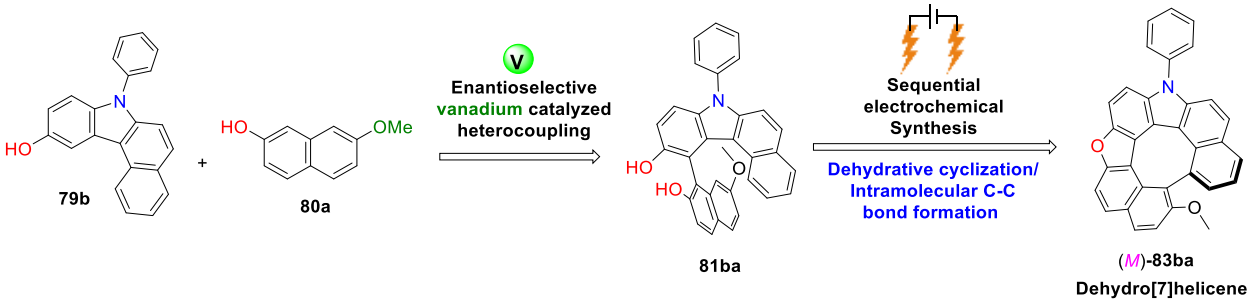

Scheme 3.2. Stepwise enantioselective synthesis of aza-oxa-dehydro[7]helicenes

3.2. Optimization of reaction conditions (first step)

3.2.1. Screening of vanadium complexes

Initially, chiral vanadium(v) catalysts were screened for oxidative hetero-coupling employing a 1:1 molar ratio of 3-hydroxycarbazole (**79b**) and 7-methoxy-2-naphthol (**80a**) under air (**Scheme 3.3**). The

catalyst (R_a,*S*)-**92a** having a (*R*)-BINOL skeleton and a tert-leucine moiety afforded the axially chiral hetero-coupling diol **81ba** in good yield (85%) with a moderate enantiomeric excess (50% ee).

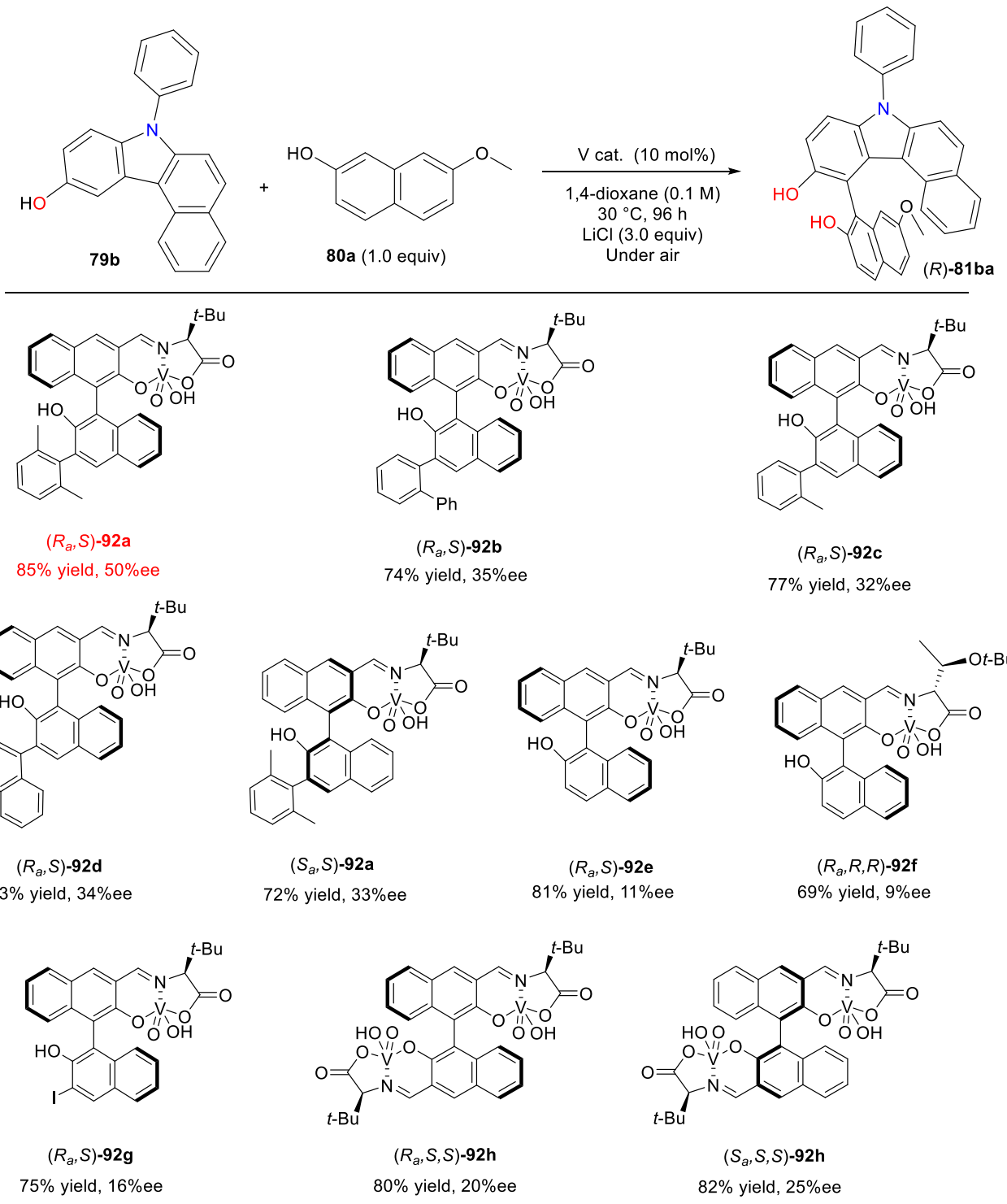

Scheme 3.3. Effects of vanadium complexes

3.2.2. Effects of temperatures and solvents

We tried to further improve the enantioselectivity through screening of different temperatures and solvents (**Table 3.1**). CCl_4 was found to be the optimum solvent for this reaction that can afford diol (*R*)-**81ba** in good yield (83%) and moderate enantioselectivity (59% ee) at 30 °C under air (entry 18). Screening lower temperatures did not improve the enantioselectivity, but decreased the yield and prolonged the reaction time (entries 19-20).

Table 3.1. Screening of different solvents and temperatures.[a]

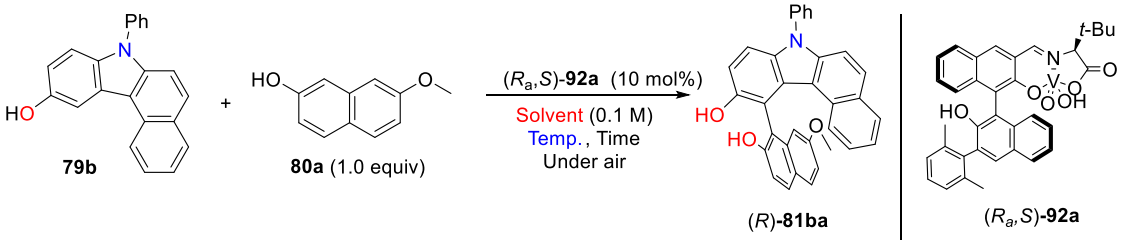

entry	temp. (°C)	solvent	time (h)	yield of **81ba** (%)[b]	ee of **81ba** (%)[c]
1	10	$ClCH_2CH_2Cl$	24	45	36
2	20	$ClCH_2CH_2Cl$	24	56	34
3	30	$ClCH_2CH_2Cl$	24	60	33
4	30	$ClCH_2CH_2Cl$	48	84	33
5	40	$ClCH_2CH_2Cl$	24	71	30
6[d]	50	$ClCH_2CH_2Cl$	24	75	25
7	30	$Cl_2C{=}CCl_2$	48	75	39
8	30	PhCl	48	81	39
9	30	1,4-dioxane	48	85	44
10	30	toluene	48	80	43
11	30	*o*-xylene	48	80	Rac.
12	30	*p*-xylene	48	81	10
13	30	THF	48	65	35
14	30	Et_2O	48	60	29
15	30	EtOAc	48	75	42
16	30	CH_2Cl_2	48	90	36
17	30	$CHCl_3$	48	87	36
18[d]	30	CCl_4	48	83	59
19[e]	0	CCl_4	48	57	59
20	-10	CCl_4	96	45	61

[a] The reaction of **79b** (0.05 mmol) and **80a** (0.05 mmol) with 10% mol of (R_a,*S*)-**92a** (0.005 mmol) was carried out in different solvents (0.5 mL) at different temperatures under air (1 atm). [b] Yields were determined by ^{1}H NMR spectroscopy using 1,3,5-trimethoxybenzene as an internal standard. [c] Determined by HPLC (Daicel Chiralpak IB, hexane / EtOH = 2/1, flow rate 1.0 mL/min, T = 25 ºC, 280 nm): t_{maj} = 5.6 min, t_{min} = 6.9 min. [d] Under these conditions trace amount of the corresponding helicene **82ba** was observed to be formed.

3.2.3. Recrystallization of diol (*R*)-81ba

Science there was no real improvement in the ee% values upon trying lower temperatures (**Table 3.1**, entries 19-20), we decided to apply the conditions in (entry 18), and try to improve the ee% of resulting diol (*R*)-**81ba** *via* recrystallization (**Scheme 3.4**). After screening different crystallization conditions, we decided to the layering between *n*-hexane and $CHCl_3$ which improved the enantiopurity of (*R*)-**81ba** to 91% ee (**Figure 3.1**).

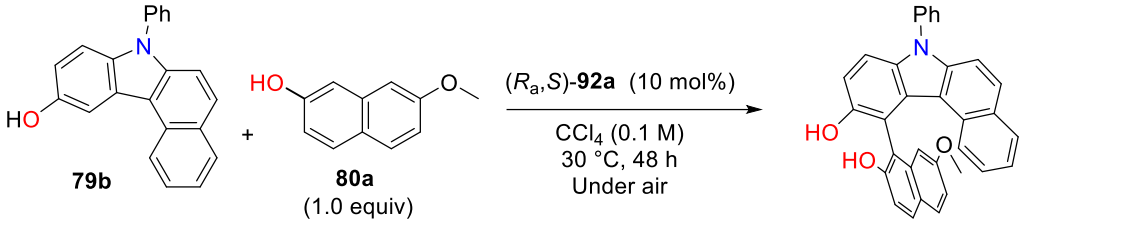

(*R*)-**81ba**
83%, 59% ee (91% ee)[a]
[a] Recrystallization from *n*-hexane/$CHCl_3$

Scheme 3.4. Enantioselective synthesis of diol (*R*)-**81ba**

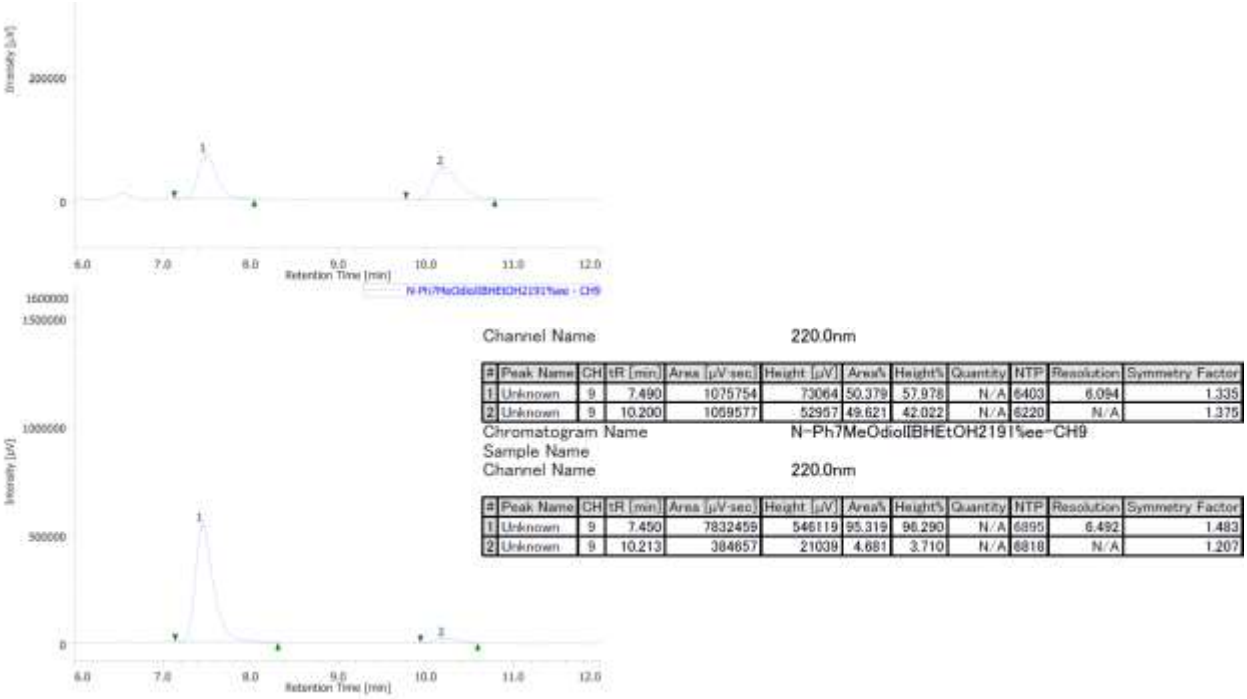

#	Peak Name	CH	tR [min]	Area [μV·sec]	Height [μV]	Area%	Height%	Quantity	NTP	Resolution	Symmetry Factor
1	Unknown	9	7.490	1075754	73064	50.379	57.978	N/A	6403	6.094	1.335
2	Unknown	9	10.200	1059577	52957	49.621	42.022	N/A	6220	N/A	1.375

#	Peak Name	CH	tR [min]	Area [μV·sec]	Height [μV]	Area%	Height%	Quantity	NTP	Resolution	Symmetry Factor
1	Unknown	9	7.450	7832459	546119	95.319	96.290	N/A	6895	6.492	1.483
2	Unknown	9	10.213	384657	21039	4.681	3.710	N/A	6818	N/A	1.207

Determined by HPLC (Daicel Chiralpak IB, hexane / EtOH = 3/1, flow rate 1.0 mL/min, T = 25 ºC, 280 nm): t_{maj} = 7.5 min, t_{min} = 10.2 min.

Figure 3.1. HPLC chromatogram of diol (*R*)-**81ba** after recrystallization: Rac. (Above chart), 91% ee (Below chart).

3.3. Mechanism of vanadium-catalyzed hetero-coupling

A plausible catalytic cycle for the oxidative hetero-coupling of hydroxycarbazoles **79b** with 7-methoxy-2-naphthol (**80a**) is illustrated in (**Scheme 3.5**). The condensation of the mononuclear vanadium(v) complex (R_a,*S*)-**92a** with **79b** generates intermediate A. Then, intermediate A undergoes a single electron transfer (SET) from the carbazole moiety to vanadium (v) to generate the conceivable electrophilic radical intermediate B, since **79b** is more easily oxidized than **80a**. This is followed by an intermolecular radical–anion coupling to afford intermediate C with the formation of a new carbon-carbon bond through the nucleophilic attack of **80a**. Reoxidation of vanadium(iv) to vanadium(v) by molecular oxygen proceeds in air followed by exchange with **79b**, the hetero-coupling product **81ba** is obtained and **intermediate A** is regenerated.

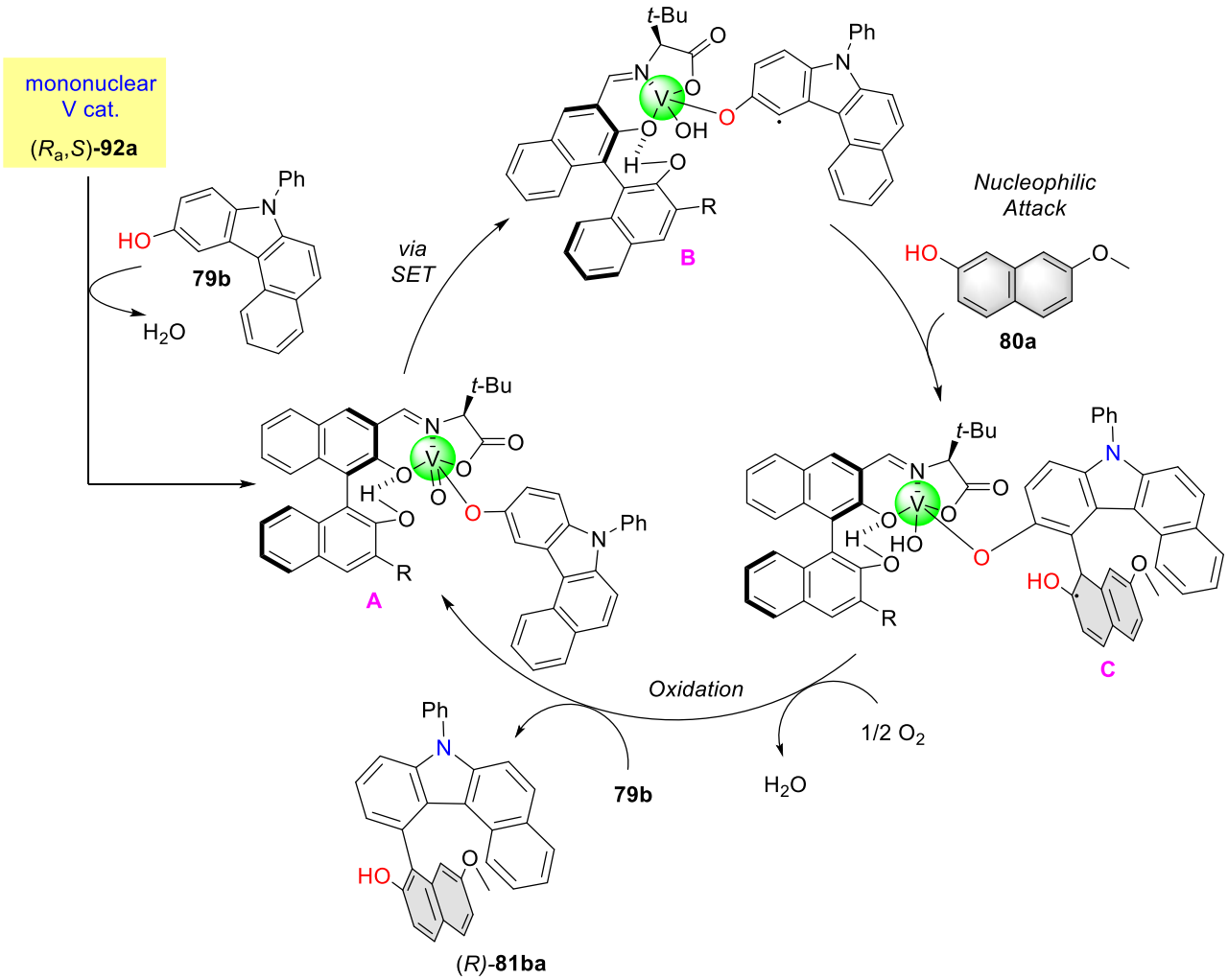

Scheme 3.5. Plausible reaction mechanism for the oxidative hetero-coupling of 3-hydroxycarbazole **79b** with 7-methoxy-2-naphthol (**80a**).

3.4. Second step: electrochemical conversion of 81ba to dehydro[7]helicene 83ba

To our delight, applying our optimized electrochemical conditions on the diol (*R*)-**81ba** gave the corresponding dehydrohelicene (*M*)-**83ba** in 87% yield without affecting on the optical purity (<92% ee) (**Scheme 3.6**). To the best of our knowledge, this is the first example of the enantioselective synthesis of any kind of dehydrohelicene derivatives.

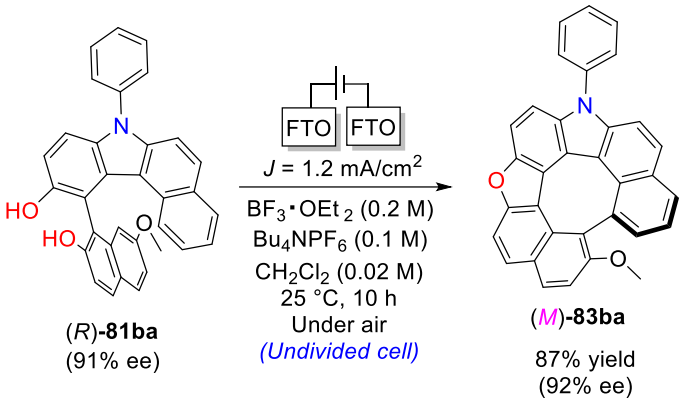

Scheme 3.6. Stepwise enantioselective synthesis of dehydro[7]helicene (*M*)-**83ba**

3.5. Determination of the absolute configuration of (*M*)-83ba

The configuration of (*M*)-**83ba** was determined after comparing the CD spectrum of **83ba** with that of previously assigned (*M*)- and (*P*)-**83aa** *via* X-ray crystallographic analysis, and found the pattern of **83ba** is matching with the (*M*) configuration (**Figure 3.2**). Hence, we can understand that **81ba** has an (*R*)-configuration; i.e. (*R*)-**81ba** will give exclusively (*M*)-**83ba** and vice versa. Moreover, these results matching with our previous work[3] in which similar substrates gave (*R*)-diols using this vanadium complex (R_a,*S*)-**92a**.

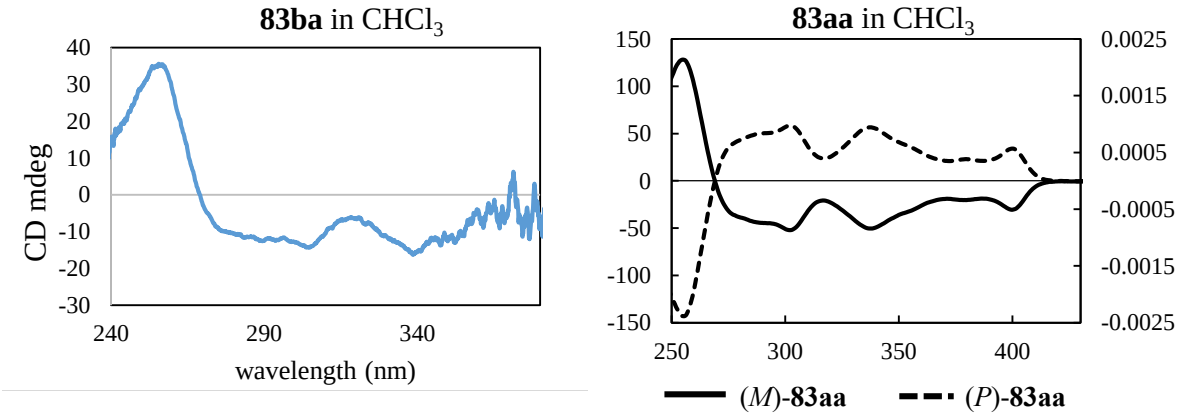

Figure 3.2. CD spectrum of **83ba** and **83aa**

3.6. Scale up the stepwise enantioselective synthesis of dehydrohelicene (*M*)-83ba

Taking one more step towards industrial implementation, we scaled up our enantioselective stepwise protocol to the semi-gram scale as depicted in (**Scheme 3.7**). Using (3.23 mmol) of both **79b** and **80a**, the diol (*R*)-**81ba** was afforded in 83% yield and 85% ee (after recrystallization). (*R*)-**81ba** can undergo

the subsequent electrochemical transformation using larger FTO electrodes (4.5 × 5 cm^2) with a little higher intensity of electric current (5.0 mA) to partially compensate the decreased current density (*J*) without affecting significantly the potential of the cell. The corresponding dehydro[7]helicene (*M*)-**83ba** was afforded in 72% yield, and 85% ee (98% ee after recrystallization from *n*-hexane/EtOAc) (**Figure 3.3**).

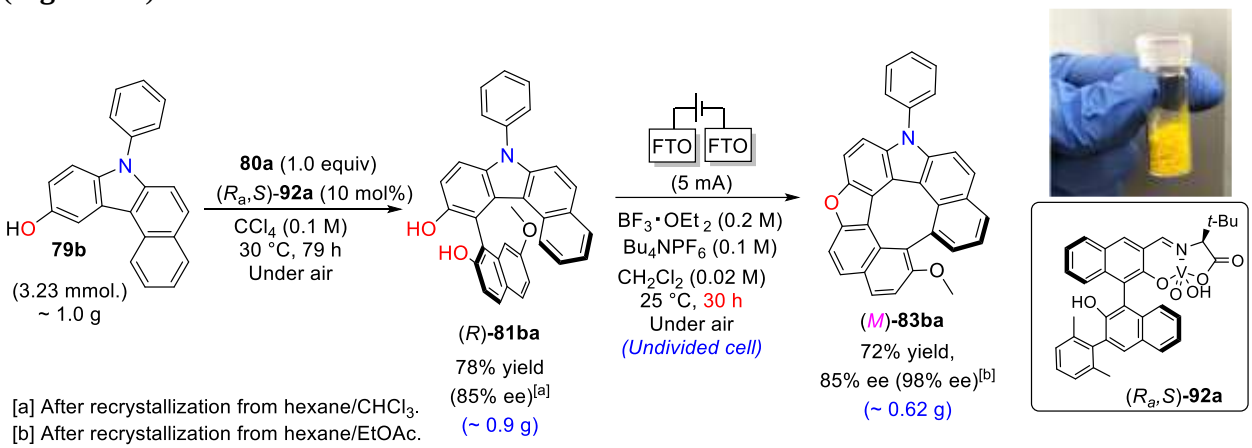

[a] After recrystallization from hexane/$CHCl_3$.
[b] After recrystallization from hexane/EtOAc.

Scheme 3.7. Reaction scalability

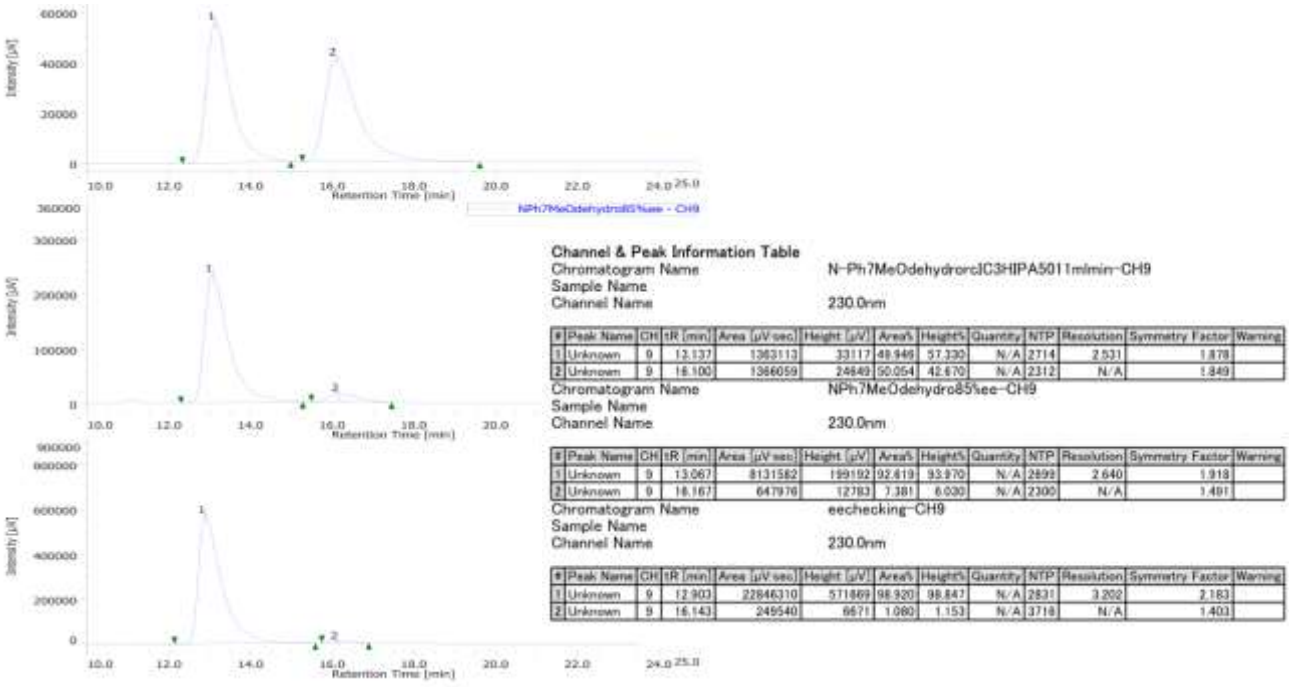

Determined by HPLC (Daicel Chiralpak IC-3, hexane/*i*-PrOH = 50/1, flow rate 1.0 mL/min, T = 25 ºC, 230 nm): t_{maj} = 12.9 min, t_{min} = 16.1 min.

Figure 3.3. HPLC chromatogram of diol (*M*)-**83ba** after recrystallization; Rac. (Above chart); 85% ee (Middle chart), 98% ee (Bottom chart)

References

(1) (a) Pelliccioli, V.; Hartung, T.; Simon, M.; Golz, C.; Licandro, E.; Cauteruccio, S.; Alcarazo, M. Enantioselective Synthesis of Dithia [5] helicenes and their Postsynthetic Functionalization to Access Dithia [9] helicenes. *Angewandte Chemie International Edition* **2022**, *61* (6), e202114577. (b) Wang, Q.; Zhang, W.-W.; Zheng, C.; Gu, Q.; You, S.-L. Enantioselective synthesis of azoniahelicenes by Rh-catalyzed C–H annulation with alkynes. *Journal of the American Chemical Society* **2020**, *143* (1), 114-120. (c) Stará, I. G.; Starý, I. Helically Chiral Aromatics: The Synthesis of Helicenes by [2+ 2+ 2] Cycloisomerization of π-Electron Systems. *Accounts of Chemical Research* **2019**, *53* (1), 144-158. (d) Yubuta, A.; Hosokawa, T.; Gon, M.; Tanaka, K.; Chujo, Y.; Tsurusaki, A.; Kamikawa, K. Enantioselective synthesis of triple helicenes by cross-cyclotrimerization of a helicenyl aryne and alkynes *via* dynamic kinetic resolution. *Journal of the American Chemical Society* **2020**, *142* (22), 10025-10033. (e) Dhbaibi, K.; Favereau, L.; Crassous, J. Enantioenriched helicenes and helicenoids containing main-group elements (B, Si, N, P). *Chemical Reviews* **2019**, *119* (14), 8846-8953.

(2) Lousen, B.; Pedersen, S.; Bols, P.; Hansen, K.; Pedersen, M.; Hammerich, O.; Bondarchuk, S.; Minaev, B.; Baryshnikov, G. V.; Ågren, H.; Pittelkow, M. Compressing a Non-Planar Aromatic Heterocyclic [7] Helicene to a Planar Hetero [8] Circulene. *Chemistry-A European Journal* **2020**, *26* (22), 4935-4940.

(3) Sako, M.; Higashida, K.; Kamble, G. T.; Kaut, K.; Kumar, A.; Hirose, Y.; Zhou, D.-Y.; Suzuki, T.; Rueping, M.; Maegawa, T. Chemo-and enantioselective hetero-coupling of hydroxycarbazoles catalyzed by a chiral vanadium (v) complex. *Organic Chemistry Frontiers* **2021**, *8* (17), 4878-4885.

Chapter 4

Optical Properties of Aza-oxa-dehydro[7]helicenes and Other PHAs

4.1. Photophysical properties of different PHAs

There are a lot of photophysical methods that deal with the interaction between matter and electromagnetic radiation. Among them, we are focusing on the most common two methods that display a great value in characterizing the electronic and optical properties of different PHAs. These two methods are UV-Vis spectrophotometry and photoluminescence (PL), whose integration plays a key role in defining their real impact.[1]

4.1.1. Photophysical properties of aza-oxa-dehydro[7]helicenes

Upon photoirradiation, heterodehydro[7]helicenes **83** display a high degree of luminescence as a result of their structural rigidity that hinders the loss of thermal energy due to structural changes in the excited state. All the helical dyes showed absorption in the wavelength range of 399-420 nm and fluorescence maxima at 450 nm. Heterodehydrohelicene **83aa**, for example, exhibited a maximum absorption at the wavelength of 399 nm in $CHCl_3$ (20 µM) (**Figure 4.1A**). PL spectra of **83aa** were shifted in a bathochromic way to 412 nm and 431 nm when investigated in $CHCl_3$ (20 µM) (**Figure 4.1B**). Remarkably, heterodehydrohelicenes exhibited a high solubility in various solvents like halogenated ($CHCl_3$), polar aprotic (THF), and non-polar solvents (*n*-hexane) which enabled the study of solvent effect on their optical properties. Generally, all solvents showed similar absorption and emission patterns, with relatively larger Stokes shift in $CHCl_3$ and improved absorption in *n*-hexane.

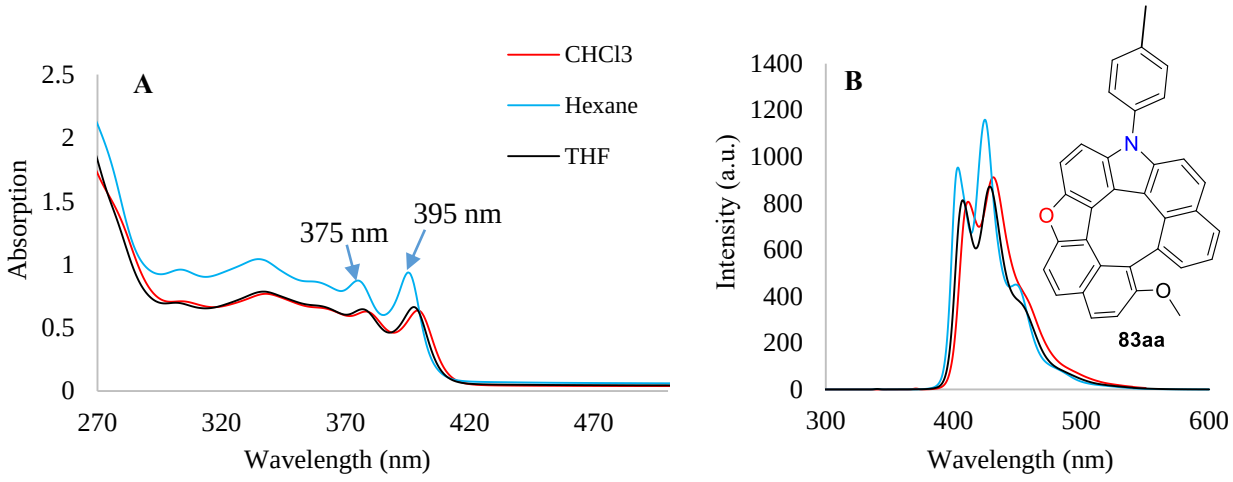

Figure 4.1. Photophysical properties of heterodehydro[7]helicene **83aa**: **(A)** UV spectra of **83aa** in ($CHCl_3$, *n*-hexane, and THF) 20 µM solutions **(B)** PL spectra of **83aa** in ($CHCl_3$, *n*-hexane, and THF) 20 µM solutions.

The photophysical properties (UV-vis & PL) of other aza-oxa-dehydro[7]helicenes **83ea** and **83ab** were also investigated in $CHCl_3$ (20 µM), and exhibited a red-shifted absorption reaching up to 404 nm and 399 nm respectively. Moreover, their emission maxima were shifted in a bathochromic way at 412 nm and 435 nm for compound **83ea** (**Figure 4.2**), and 416 nm and 432 nm for compound **83ab** (**Figure 4.3**).

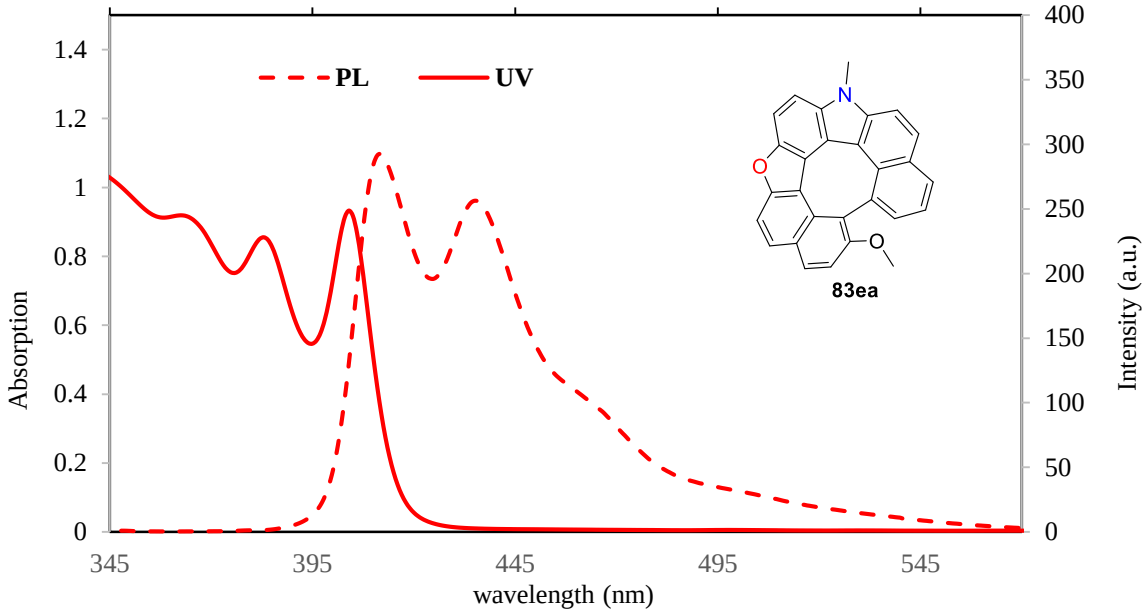

Figure 4.2. Photophysical properties (UV & PL) of **83ea** in $CHCl_3$ (20 µM) solutions.

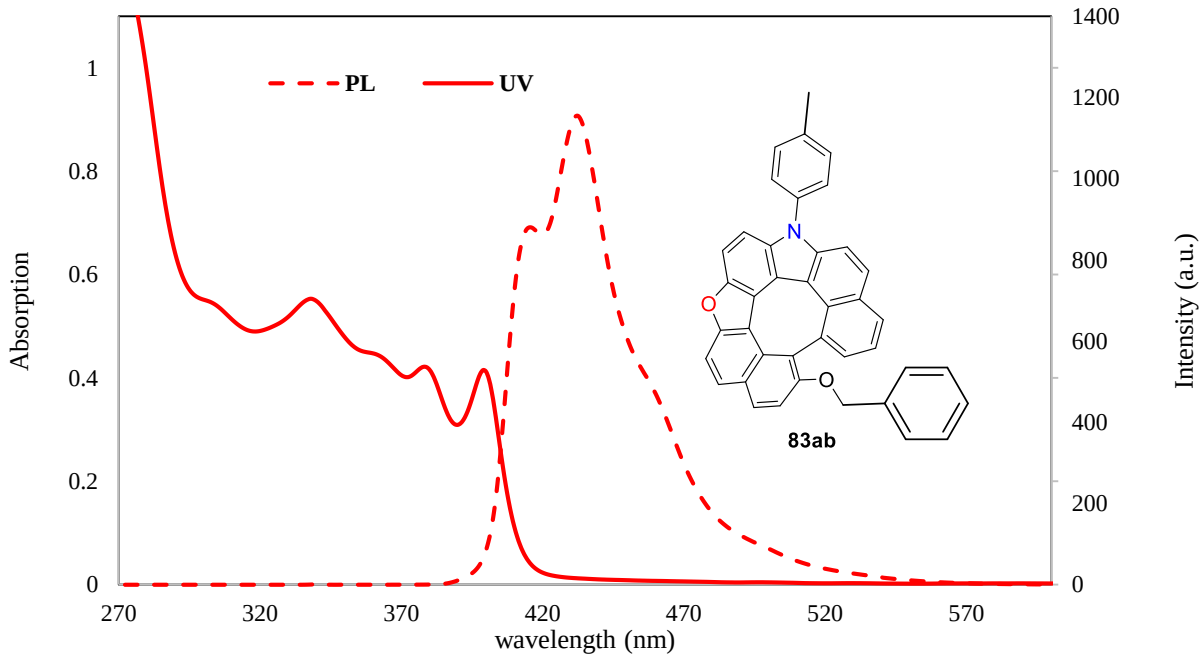

Figure 4.3. Photophysical properties (UV & PL) of **83ab** in $CHCl_3$ (20 µM) solutions.

4.1.2. Photophysical properties of other PHAs

Next, we started to study the photophysical properties (UV and PL) of other PHAs: for example, hetero[7]helicene derivative **82ad** revealed a maximum absorption at 406 nm and fluorescence maxima at the wavelengths of 418 nm and 440 nm (**Figure 4.4**).

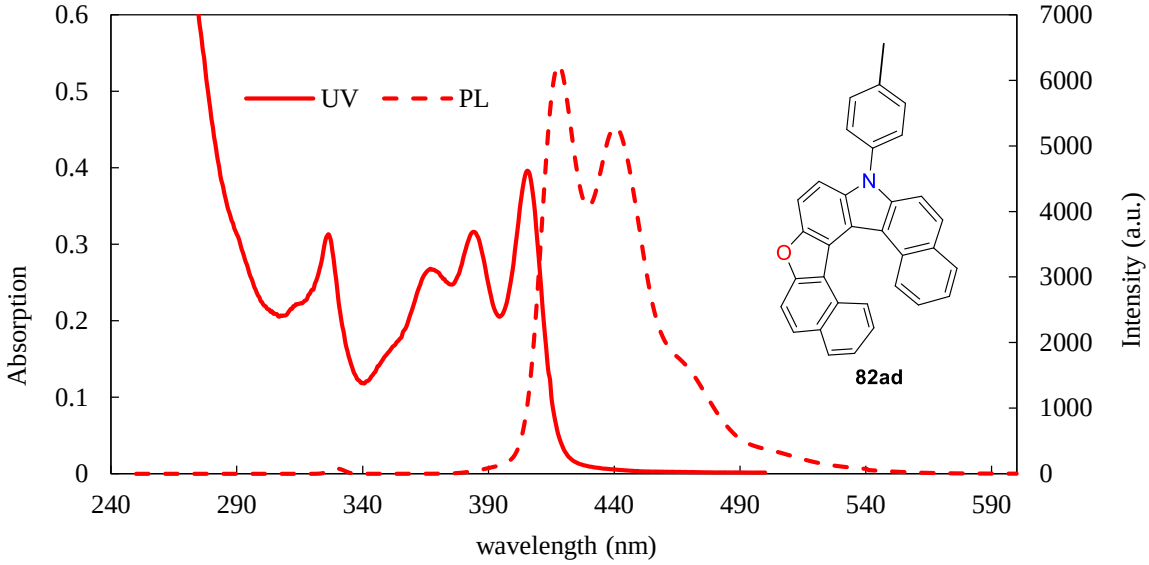

Figure 4.4. Photophysical properties (UV & PL) of **82ad** in $CHCl_3$ (20 μM) solutions.

Compounds **87aa** and **89a** showed analogous photophysical properties with red-shifted absorption maxima reaching up to 405 nm and 406 nm, respectively. Also, their emission maxima were shifted in a bathochromic way to 407 nm and 434 nm for compound **87aa** (**Figure 4.5**), and 412 nm and 437 nm for compound **89a** (**Figure 4.6**).

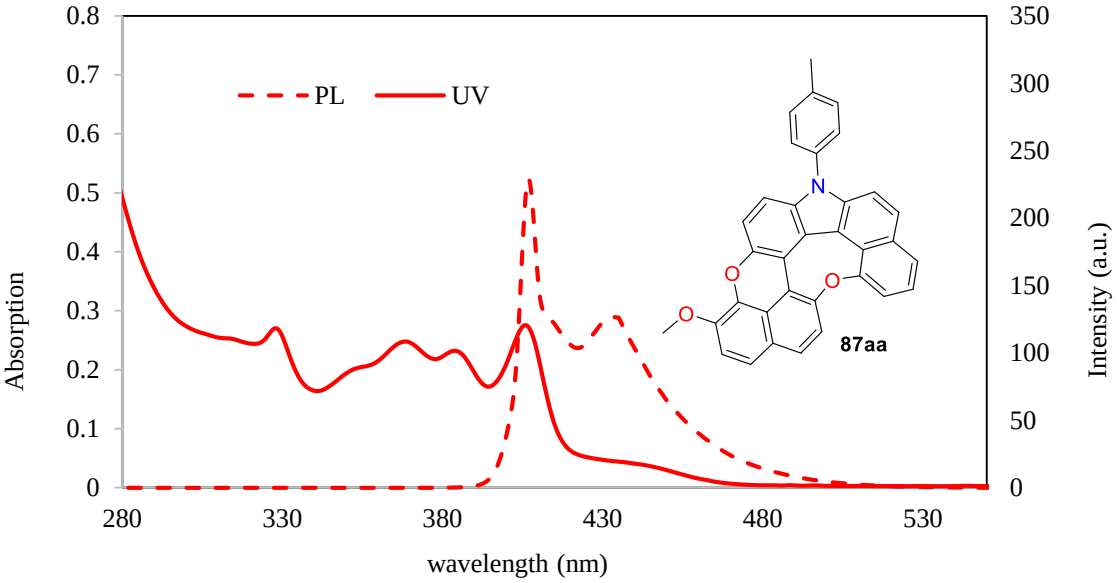

Figure 4.5. Photophysical properties (UV & PL) of **87aa** in $CHCl_3$ (20 μM) solutions.

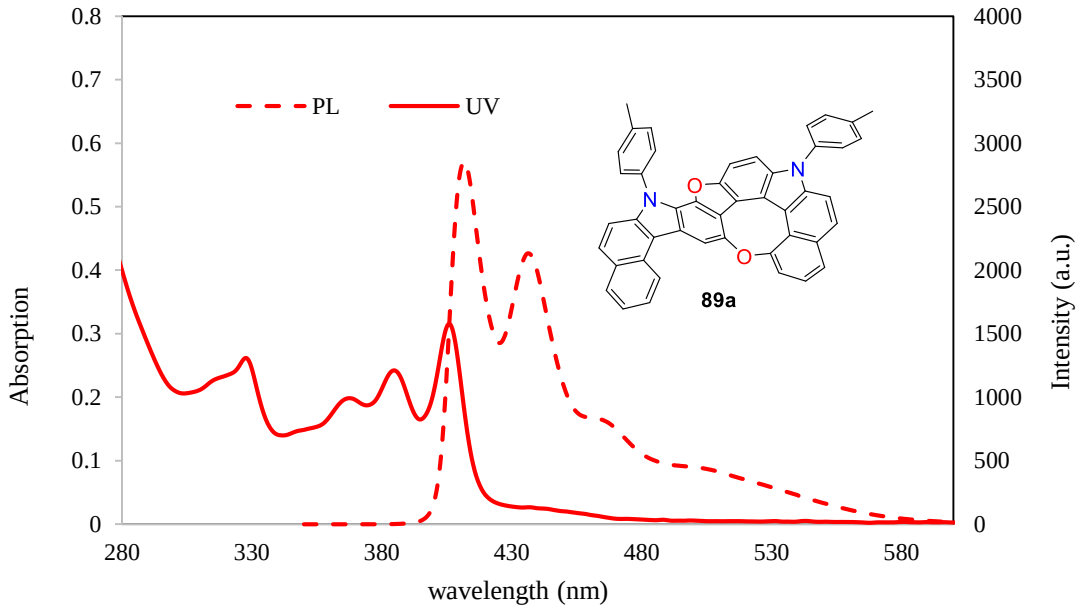

Figure 4.6. Photophysical properties (UV & PL) of **89a** in $CHCl_3$ (20 μM) solutions.

More red-shifting was observed upon studying compound **90** which exhibited an absorption maximum upon photoirradiation at the wavelength of 418 nm. With a very small Stock-shift in $CHCl_3$ solvent, compound **90** showed emission maxima at 427 nm and 450 nm (**Figure 4.7**).

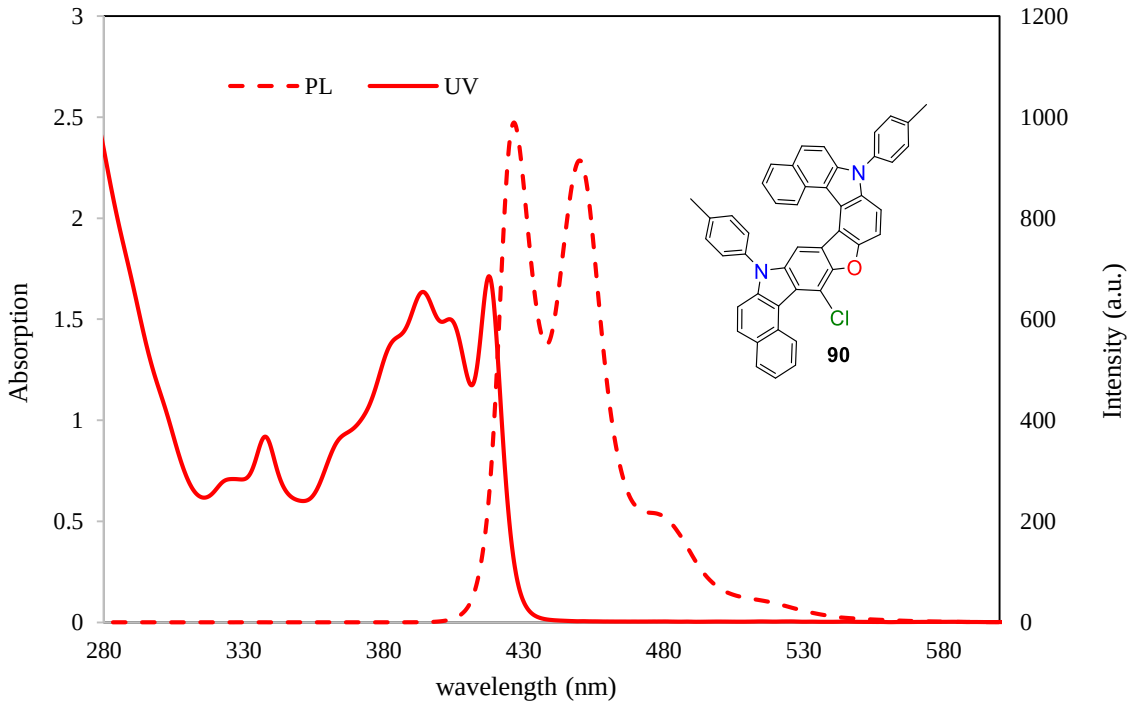

Figure 4.7. Photophysical properties (UV & PL) of **90** in $CHCl_3$ (20 μM) solutions.

4.2. Chiroptical properties of PHAs

The unique helical chirality of some PHAs (especially helicenes **82** and dehydrohelicenes **83**) has led to extraordinary chiroptical responses. As shown in chapter 1, these photophysical and chiroptical properties play a key role in opening the gate for future implementation of PHAs in material science applications like OLEDs, and OFETs.[2] Chiral molecules have the ability to interact with left and right circularly polarized (CP) light in a different manner. This variance in the interaction between the left and right CP light can be defined in terms of molecular dissymmetry which can vary with many known and obscure parameters.[3] However, before taking a few steps in this direction, it is more reasonable to study the chiral stability of our scaffolds. Molecules with low racemization barriers are less valuable and cannot be applied in optical materials as they will lose their chiroptical merits rapidly. Hence, we decided to conduct thermodynamic and kinetic studies for the racemization of the dehydro[7]helicenes **83** before studying their chiroptical features.

4.3. Racemization of dehydro[7]helicenens

The remarkably warped structure of our dehydro[7]helicenes **83** provoked us to study their enantiomeric separation. Through screening of different chiral stationary phases and eluents, we successfully separated dehydro[7]helicenes **83aa**, **83ca**, and **83fa** -as representative examples to study their racemization barriers- by HPLC using chiral stationary phase column (CHIRALPAK IC, *n*-hexane/i-PrOH = 30:1, 10 mL/min.

4.3.1. Racemization barrier of 83aa

Since racemization is a first-order process, we could monitor the change in the enantiomeric excess ratio (ee) with time at three different temperatures of 100, 130, and 150 °C (**Figures 4.8**). This tracking could be achieved using optically pure (-) **83aa** or (+) **83aa** dissolved in DMF at concentration of 1.0 mg/mL, and ee% values were calculated using chromatographic peak area (Daicel Chiralpak IC-3, hexane / IPA = 30/1, flow rate 1.0 mL/min, T = 25 ºC, 230 nm): t_{maj} = 9.3 min, t_{min} = 10.4 min).

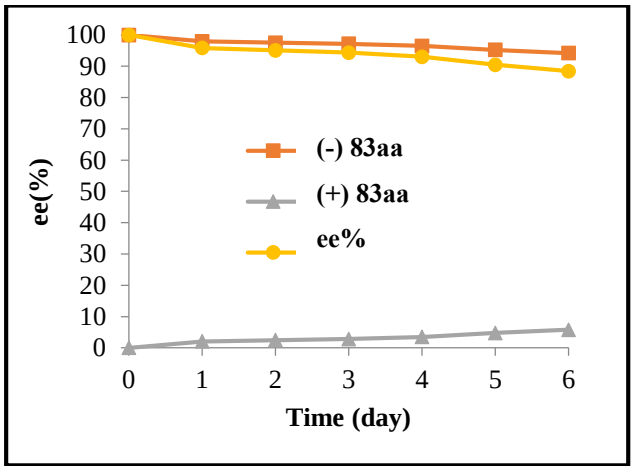

Figure 4.8 (a): Racemization of (-) **83aa** at 100 °C

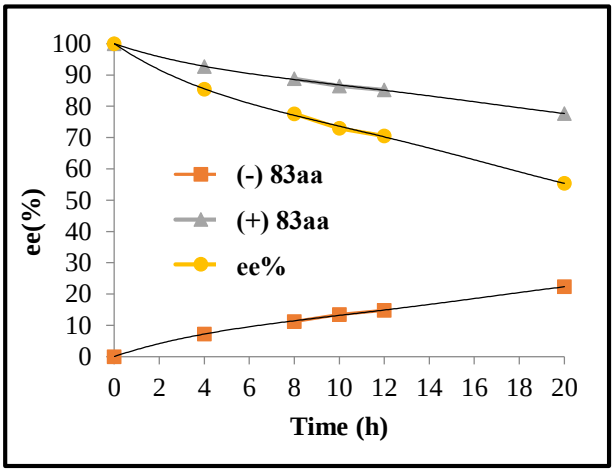

Figure 4.8 (b): Racemization of (+) **83aa** at 130 °C

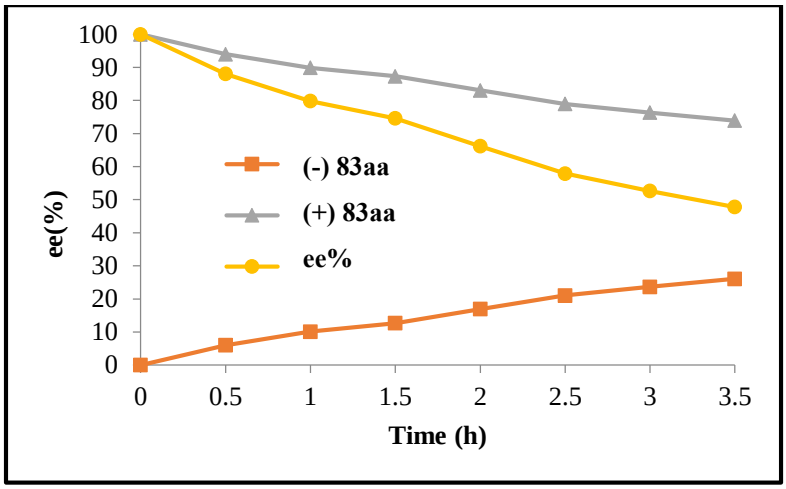

Figure 4.8 (c): Racemization of (+) **83aa** at 150 °C

Plotting the ln of (ee) versus time produced a straight line whose slope can give the racemization rate constant *k* at each temperature (**Figure 4.9**). Once we had the *k* values at different temperatures we could draw the Eyring plot that shows the change in ln(*k*/2T) versus 1/T (**Figure 4.10**). Using Erying equation (**Eq. 4.1**), we calculated the thermodynamic parameters of dehydro[7]helicene **83aa** racemization, including the racemization barrier $\Delta G^{\ddagger}$ and its constituent entropy $\Delta S^{\ddagger}$, and enthalpy $\Delta H^{\ddagger}$.

$$\mathrm{Ln}(k/2T) = -\Delta H^{\ddagger}/R(1/T) + \ln(k_b/h) + \Delta S^{\ddagger}/R \quad \textbf{(Eq. 4.1)}$$

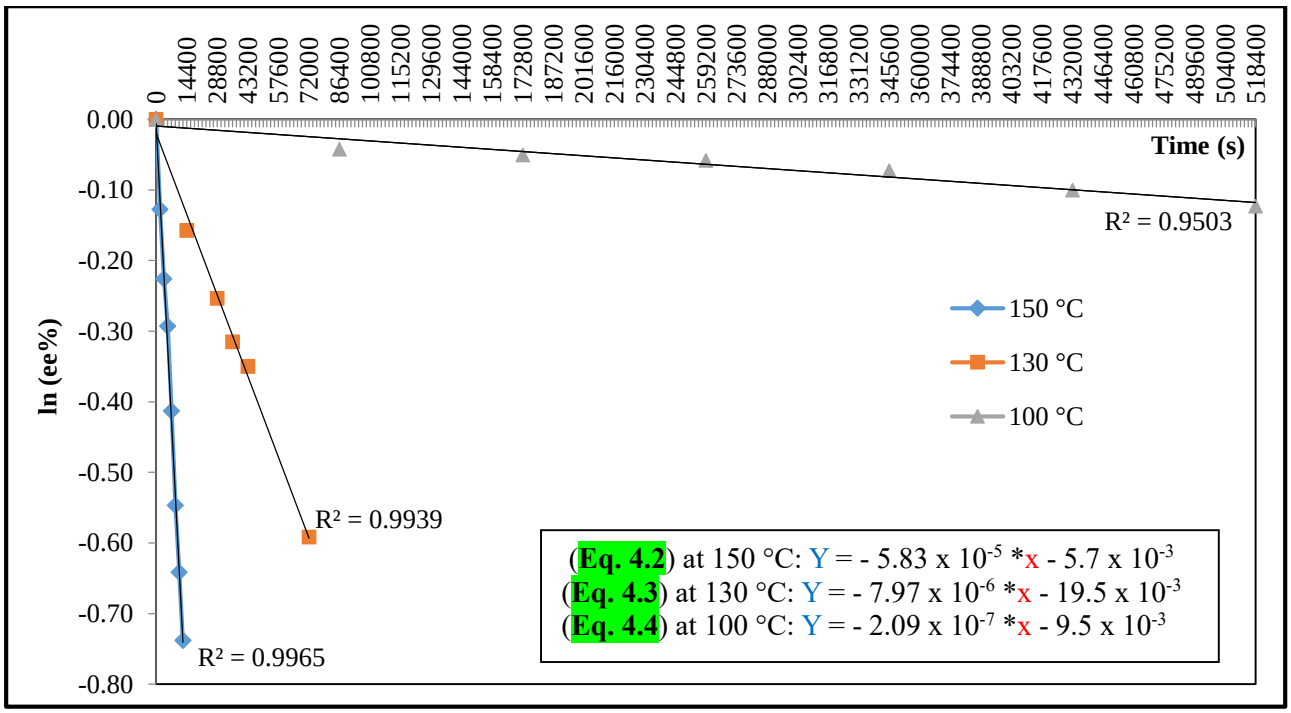

Figure 4.9. A plot showing ln(ee) versus time in seconds to show racemization rate of (+) **83aa** as it was heated at 100, 130, and 150 °C, at 1.0 mg/mL concentration in DMF

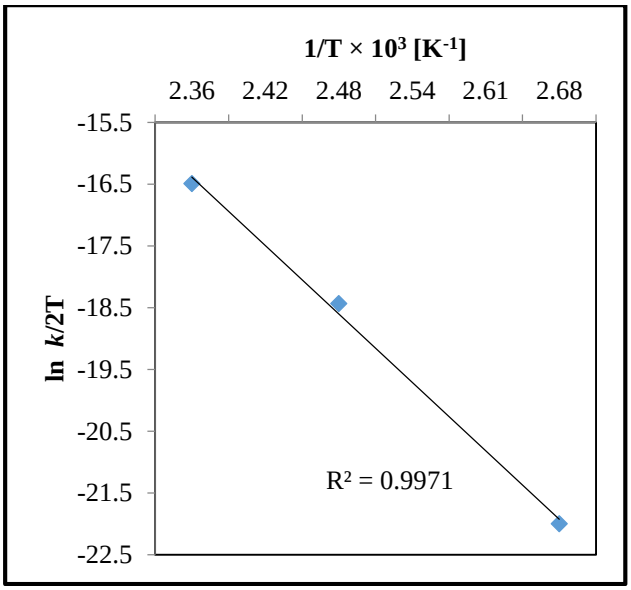

Eyring plot: $Y = -1.74 \times 10^4 * X + 24.8$

(**Eq. 4.5**): $\ln(k/2T) = -1.74 \times 10^4 * (1/T) + 24.8$

$-\Delta H^{\ddagger}/R = -1.74 \times 10^4$ & $\ln(k_b/h) + \Delta S^{\ddagger}/R = 24.8$

$\mathbf{\Delta H^{\ddagger}}$ = 145.0 kJ.mol^{-1} as (R = 8.31 J/mol.K)

$\mathbf{\Delta S^{\ddagger}}$ = 8.30 J.mol^{-1} K^{-1} as kB (Boltzmann const. = 1.38 × 10^{-23} J/K) & h (Planck's const. = 6.63 × 10^{-34} J.s)

$\mathbf{\Delta G^{\ddagger} = \Delta H^{\ddagger} - T\,\Delta S^{\ddagger}}$

$\mathbf{\Delta G^{\ddagger}}$ = 141.7 ± 0.209

$\mathbf{\Delta G^{\ddagger}}$ at 100 °C = 141.9 kJ.mol^{-1}

$\mathbf{\Delta G^{\ddagger}}$ at 130 °C = 141.6 kJ.mol^{-1}

$\mathbf{\Delta G^{\ddagger}}$ at 150 °C = 141.5 kJ.mol^{-1}

$t_{1/2}$ at 25 °C = ln 2 /*k*

k at 25 °C = 1.34 x 10^{-12}

$t_{1/2}$ at 25 °C = 1.6 x 10^4 years

Figure 4.10. Eyring plot of **83aa** showing the change in ln(*k*/2T) versus 1/T

After calculating the thermodynamic parameters of dehydro[7]helicenes **83aa**, we realized that our scaffold can exhibits a high racemization barrier > 141 kJ mol^{-1} (~ 33.5 kcal mol^{-1}). Next, we calculated the racemization half lifetime at 25 °C that depends on the activation enthalpy $\Delta H^{\ddagger}$ and entropy $\Delta S^{\ddagger}$ as well, using Erying equation (**Eq. 4.5**). The $t_{1/2}$ of compound **83aa** was more than 16,350 years which reflects the high chiral stability and low entropy ($\Delta S^{\ddagger}$).

4.3.2. Racemization barrier of 83ca and 83fa

Similarly, we studied the racemization barriers of dehydrohelicenes **83ca** and **83fa**. After chiral resolution of **83ca** and **83fa** using HPLC (CHIRALPAK IC, *n*-hexane/i-PrOH = 30:1, 10 mL/min flow rate), the racemization of optically pure (+) **83ca** and (+) **83fa** was tracked at three different temperatures of 100, 130, and 150 °C. Plotting the ln of (ee) versus time produced a straight line whose slope can give the racemization rate constant *k* at each temperature (**Figure 4.11** and **4.13**). Once we had the *k* values at different temperatures we could draw the Eyring plot that shows the change in ln(*k*/2T) versus 1/T (**Figure 4.12** and **4.14**). Using Erying equation (**Eq. 4.1**), we calculated the thermodynamic parameters of dehydro[7]helicenes **83ca** and **83fa** racemization, including the racemization barrier $\Delta G^{\ddagger}$ and its constituent entropy $\Delta S^{\ddagger}$, and enthalpy $\Delta H^{\ddagger}$.

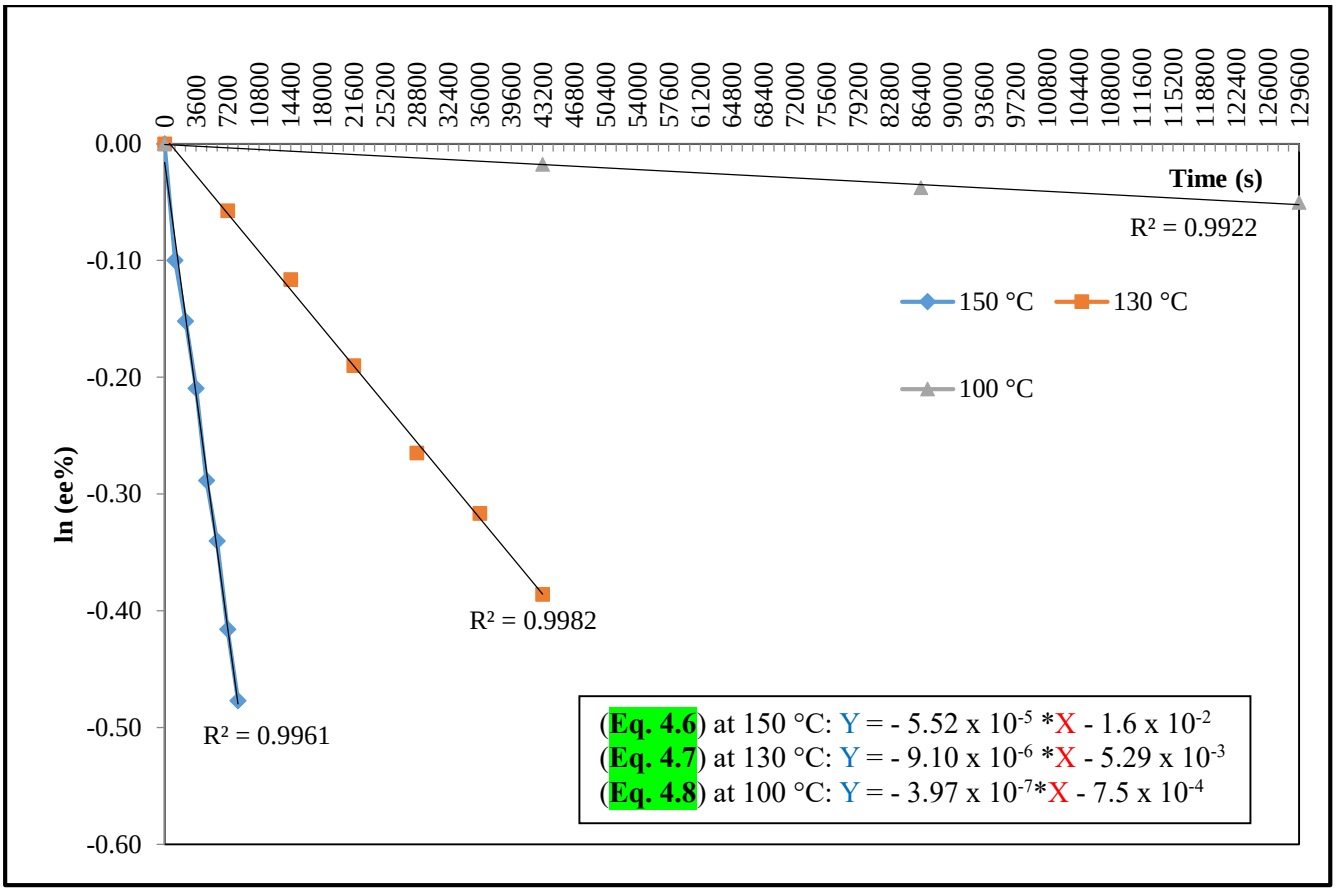

Figure 4.11. A plot showing ln(ee) versus time in seconds to show racemization rate of (+) **83ca** as it was heated at 100, 130, and 150 °C, at 1.0 mg/mL concentration in DMF

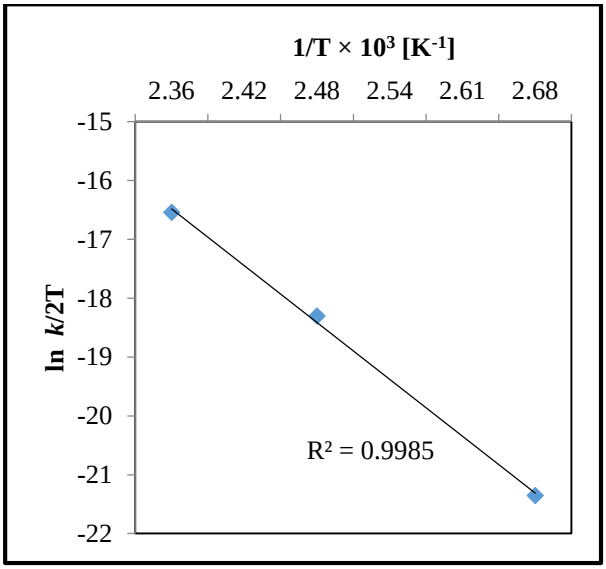

Eyring plot: Y = -1.52 x 10^4 *X + 19.4
(**Eq. 4.9**): $\ln(k/2T) = -1.52 \times 10^4 * (1/T) + 19.4$
$-\Delta H^{\ddagger}/R = -1.52 \times 10^4$ & $\ln(k_b/h) + \Delta S^{\ddagger}/R = 19.4$

$\Delta H^{\ddagger}$ = 126.4 kJ.mol^{-1} as (R = 8.31 J/mol.K)

$\Delta S^{\ddagger}$ = -36.3 J.mol^{-1} K^{-1} as kB (Boltzmann const. = 1.38 × 10^{-23} J/K) & h (Planck's const. = 6.63 × 10^{-34} J.s)

$\Delta G^{\ddagger} = \Delta H^{\ddagger} - T\Delta S^{\ddagger}$

$\Delta G^{\ddagger}$ = 140.9 ± 0.914

$\Delta G^{\ddagger}$ at 100 °C = 140.0 kJ.mol^{-1}

$\Delta G^{\ddagger}$ at 130 °C = 141.0 kJ.mol^{-1}

$\Delta G^{\ddagger}$ at 150 °C = 141.8 kJ.mol^{-1}

$t_{1/2}$ at 25 °C = ln 2 /k
k at 25 °C = 1.13 x 10^{-11}
$t_{1/2}$ at 25 °C = 1.9 x 10^3 years

Figure 4.12. Eyring plot of **83ca** showing the change in ln(k/2T) versus 1/T.

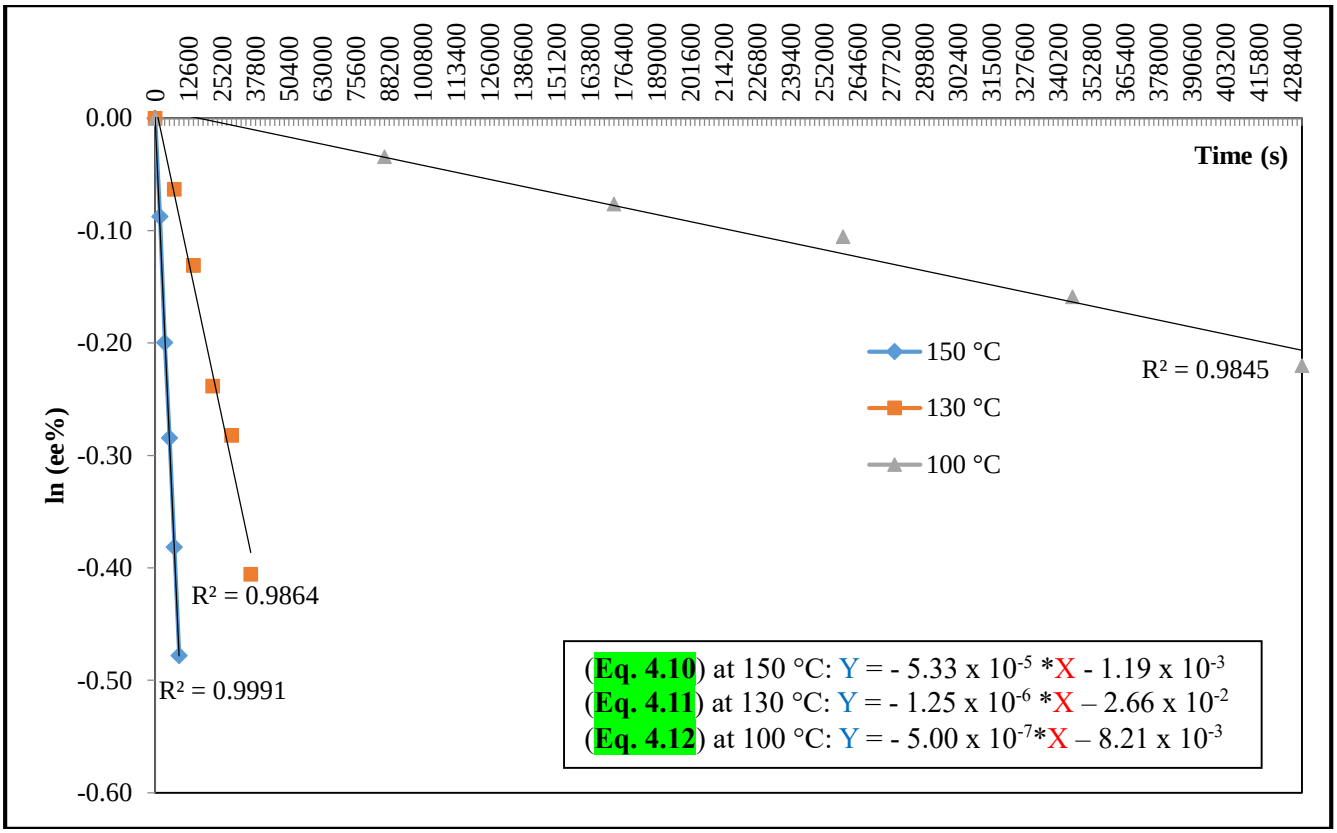

Figure 4.13. A plot showing ln(ee) versus time in seconds to show racemization rate of (+) **83fa** as it was heated at 100, 130, and 150 °C, at 1.0 mg/mL concentration in DMF

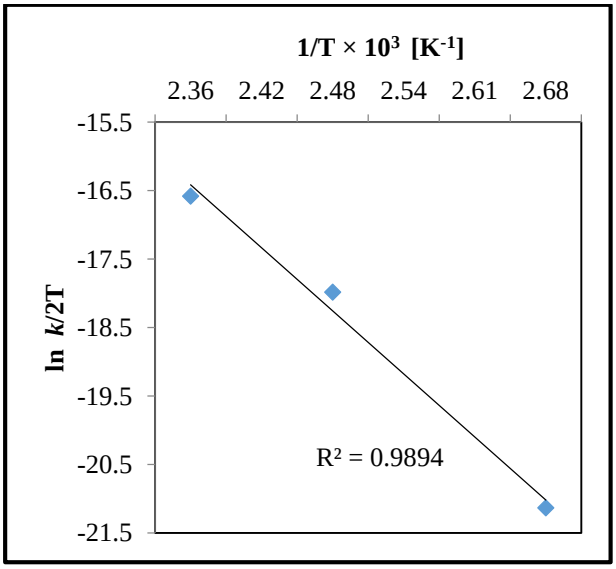

Eyring plot: Y = -1.45 x 10^4 *X + 17.8
(**Eq. 4.13**): $\ln(k/2T) = -1.45 \times 10^4 * (1/T) + 17.8$
$-\Delta H^{\ddagger}/R = -1.45 \times 10^4$ & $\ln(k_b/h) + \Delta S^{\ddagger}/R = 17.8$

$\Delta H^{\ddagger}$ = 120.7 kJ.mol^{-1} as (R = 8.31 J/mol.K)
$\Delta S^{\ddagger}$ = -49.2 J.mol^{-1} K^{-1} as kB (Boltzmann const. = 1.38 × 10^{-23} J/K) & h (Planck's const. = 6.63 × 10^{-34} J.s)

$\Delta G^{\ddagger} = \Delta H^{\ddagger} - T\,\Delta S^{\ddagger}$
$\Delta G^{\ddagger}$ = 140.4 ± 1.24
$\Delta G^{\ddagger}$ at 100 °C = 139.1 kJ.mol^{-1}
$\Delta G^{\ddagger}$ at 130 °C = 140.5 kJ.mol^{-1}
$\Delta G^{\ddagger}$ at 150 °C = 141.5 kJ.mol^{-1}

$t_{1/2}$ at 25 °C = ln 2 /*k*
k at 25 °C = 2.39 x 10^{-11}
$t_{1/2}$ at 25 °C = 9.2 x 10^2 years

Figure 4.14. Eyring plot of **83fa** showing the change in ln(*k*/2T) versus 1/T.

4.3.3. Racemization barrier of helicene 82aa

After the chiral resolution of **82aa** using HPLC (CHIRALPAK IC, *n*-hexane/i-PrOH = 50:1, 10 mL/min), the racemization of enantioenriched (83% ee) (+) **82aa** was tracked following the same protocol to draw the Eyring plot (**Figure 4.16**) and calculate thermodynamic parameters $\Delta G^{\ddagger}$, $\Delta S^{\ddagger}$, and $\Delta H^{\ddagger}$ from Eyring equation.

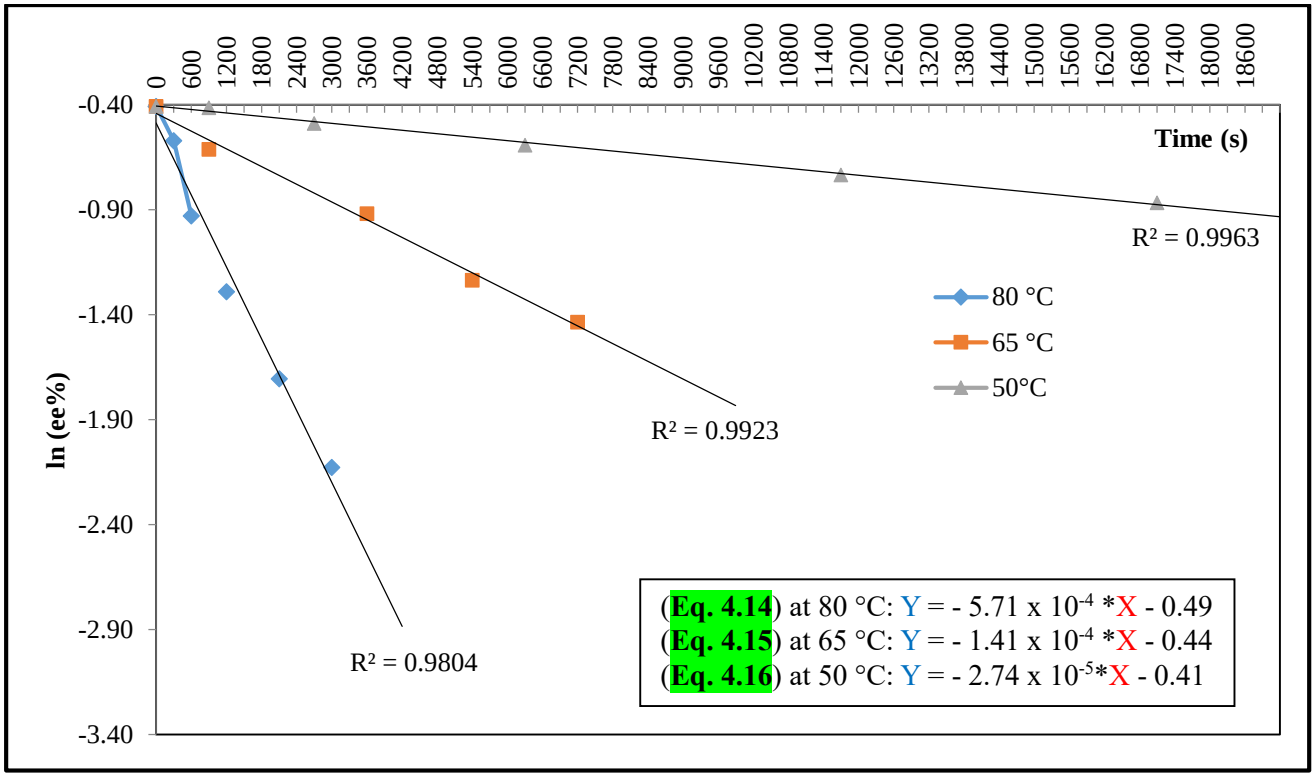

Figure 4.15. A plot showing ln(ee) versus time in seconds to show racemization rate of (+) **82aa** as it was heated at 50, 65, and 80 °C, at 1 mg/mL concentration in toluene

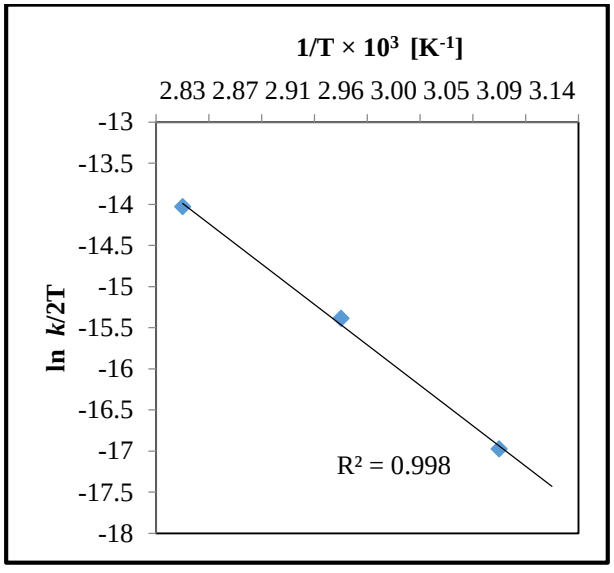

Eyring plot: $Y = -1.12 \times 10^4 * X + 17.8$

(**Eq. 4.17**): $\ln(k/2T) = -1.12 \times 10^4 * (1/T) + 17.8$

$-\Delta H^{\ddagger}/R = -1.12 \times 10^4$ & $\ln(k_b/h) + \Delta S^{\ddagger}/R = 17.8$

$\mathbf{\Delta H^{\ddagger}}$ = 93.3 kJ.mol^{-1} as (R = 8.31 J/mol.K)

$\mathbf{\Delta S^{\ddagger}}$ = -49.8 J.mol^{-1} K^{-1} as kB (Boltzmann const. = 1.38 × 10^{-23} J/K) & h (Planck's const. = 6.63 × 10^{-34} J.s)

$\mathbf{\Delta G^{\ddagger} = \Delta H^{\ddagger} - T\,\Delta S^{\ddagger}}$

$\mathbf{\Delta G^{\ddagger}}$ = 110.2 ± 0.74

$\mathbf{\Delta G^{\ddagger}}$ at 50 °C = 109.4 kJ.mol^{-1}

$\mathbf{\Delta G^{\ddagger}}$ at 65 °C = 110.3 kJ.mol^{-1}

$\mathbf{\Delta G^{\ddagger}}$ at 80 °C = 110.9 kJ.mol^{-1}

$t_{1/2}$ at 25 °C = ln 2 /*k*

k at 25 °C = 1.40 x 10^{-6}

$t_{1/2}$ at 25 °C = 5.74 days

Figure 4.16. Eyring plot of **82aa** showing the change in ln(*k*/2T) versus 1/T.

4.3.4. Analyzing the thermodynamic parameters (helicene vs dehydrohelicene)

After comparing the thermodynamic parameters of dehydro[7]helicenes **83aa**, **83ca**, and **83fa**, we realized that our scaffolds can exhibit a high racemization barrier > 140 kJ mol^{-1} (~ 33.5 kcal mol^{-1}) opening the gate for wide applications that require significantly high chiral stability and sustained racemization half-life time. The $t_{1/2}$ of compound **83aa** at 25 °C was more than 1.6 x 10^4 years which reflects the high chiral stability and low entropy ($\Delta S^{\ddagger}$). Although changing the *N*-substituents of dehydrohelicene **83**, has no great effect on $\Delta G^{\ddagger}$ values, other thermodynamic parameters showed considerable variations, especially the $\Delta S^{\ddagger}$ values which are revealed on the lower racemization half-life times (**Figure 4.17**). Compounds **83** showed considerably higher barriers than most of the previously investigated dehydrohelicenes by Itami and Scott in 2013 (1.7 kcal mol^{-1}),[4] or by Tanaka and Osuka in 2018 (5.2-6.0 kcal mol^{-1}).[5] The calculated energy barriers $\Delta G^{\ddagger}$ also showed comparable results to the estimated $\Delta G^{\ddagger}$ values of the reported quasi-aza[8]circulene by Tanaka and Osuka in 2019 (~40 kcal mol^{-1}).[6] To further show the superior chiral stability of dehydrohelicene **83aa**, we wanted to compare it with the corresponding helicene **82aa**; hence we isolated that compound and separated its two enantiomers by HPLC. After checking the racemization rate at different temperatures, and drawing the Eyring plot, we observed the lower racemization barrier of **82aa** =110 kJ mol^{-1} (~ 26.3 kcal mol^{-1}) and the dramatically shorter $t_{1/2}$ at 25 °C (only 5.74 days). In other words, compound **82aa** racemizes more than million times faster compared to the corresponding dehydrohelicene **83aa**.

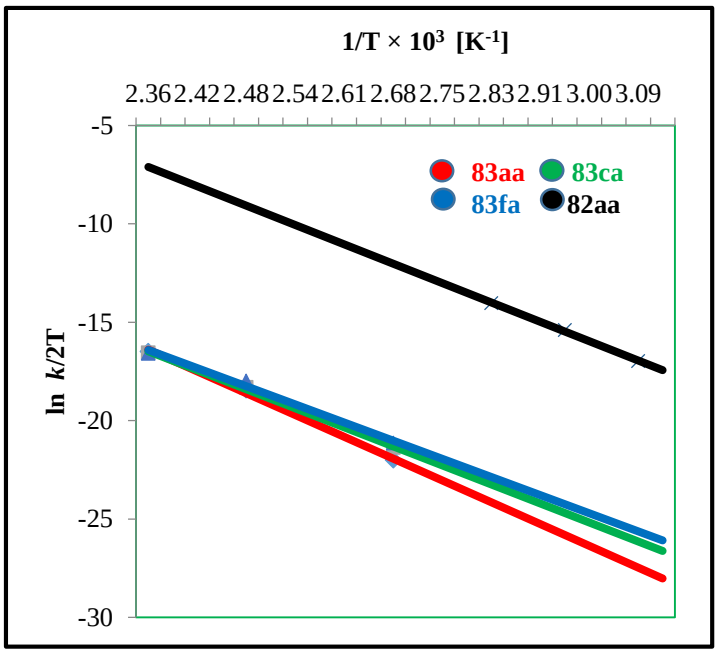

	83aa	82aa
R^2	0.997	0.998
Slope	-1.74 x 10^4	-1.12 x 10^4
intercept	24.8	17.8
k/s^{-1} at 25°C	1.34 X 10^{-12}	1.40 X 10^{-6}

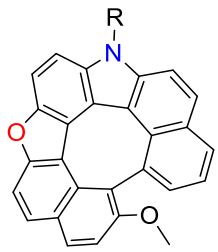

83

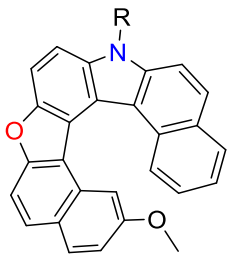

82aa

	R	$\Delta H^{\neq}$	$\Delta S^{\neq}$	$\Delta G^{\neq}$	$t_{1/2}$ at 25 °C
83aa	*p*-tolyl	145.0 kJ.mol^{-1}	8.30 J.mol^{-1}K^{-1}	141.7 ± 0.21 kJ.mol^{-1}	1.6 x 10^4 years
83ca	*p*-ClC$_6$H$_4$	126.4 kJ.mol^{-1}	-36.3 J.mol^{-1}K^{-1}	140.9 ± 0.91 kJ.mol^{-1}	1.9 x 10^3 years
83fa	Bn	120.7 kJ.mol^{-1}	-49.2 J.mol^{-1}K^{-1}	140.4 ± 1.24 kJ.mol^{-1}	9.2 x 10^2 years
82aa	*p*-tolyl	93.3 kJ.mol^{-1}	-49.8 J.mol^{-1}K^{-1}	110.2 ± 0.75 kJ.mol^{-1}	5.7 days

Figure 4.17. Eyring plot for the racemization of dehydro[7]helicenes **83aa**, **83ca**, **83fa**, and helicene **82aa.**

4.4. Chiroptical properties of dehydro[7]helicenes 83

Among various chiroptical methods, the electronic circular dichroism CD and circularly polarized luminescence CPL showed superior performance in terms of simplicity and sensitivity.[7] Hence, they became the most favorable tools to study the chiroptical nature of small organic molecules in recent routine spectral measurements. These tools are used to define the difference between the absorption of left circularly polarized (CP) light and right CP light by chiral molecules, a phenomenon identified as the Cotton effect (CE).[8] The magnitude of CD and CPL can be quantified by the absorptive (g_{abs}) and luminescence dissymmetry factors (g_{lum}). In quantum chemistry, both CD and CPL are expressed by a single electronic parameter, i.e. rotational strength *R* which is the imaginary part of the scalar product of the electric and magnetic transition dipole moments of a given electronic transition between *i* and *j* state (**Eq. 4.18**).[3]

$$R = \mathrm{Im}\, \boldsymbol{\mu}_{ij} \,.\, \boldsymbol{m}_{ij} \qquad \textbf{(Eq. 4.18)}$$

Both absorption intensity and emission intensity are proportional to the relevant dipole strength *D*, which is defined by the following equation (**Eq. 4.19**).

$$D = |\boldsymbol{\mu}_{ij}|^2 + |\boldsymbol{m}_{ij}|^2 \qquad \textbf{(Eq. 4.19)}$$

In isotropic solutions, the electric quadrupole moment is canceled out in *R* and generally small and negligible for *D*. The dissymmetry factors g_{abs} and g_{lum} are thus given by the rotational and dipole strengths, and thus dissymmetric factor can be predicted by theory (**Eq. 4.20**).[9]

$$g = \frac{4R}{D} \qquad \textbf{(Eq. 4.20)}$$

Although CD and CPL share most of the common elements discussed above, there are some key differences that exist between them. The information obtained from CD can describe the thermally equilibrated electronic ground state, while CPL describes the emissive excited state. CPL has gained an increasing interest recently due to its value in defining the information content transported through the light, as its higher level can promote further dimensions for optical information storage and transfer. From the above equations, we can understand that the luminescence dissymmetry factor (g_{lum}) becomes stronger for electronically hindered and magnetically allowed transitions. Hence, most of the earlier CPL observations are for Laporte-forbidden *f-f* transition of lanthanide complexes.[10] Very recently the CPL of SOMs has been investigated. Although most of the reports so far show lower g_{lum} values compared to lanthanide complexes for example, they show better photophysical features, higher quantum yields and broader molecular diversity. Among most of chiral SOMs, helicenes with their unique helical chirality showed special excellent CPL properties (**see chapter 1**). On the other hand, dehydrohelicenes are less investigated and only one example of a CPL-responsive dehydrohelicene **44**, that showed g_{lum} of 0.25×10^{-3} (λ_{em} = 435 nm) was reported last year by Maeda, Ema.[11]

4.4.1. Chiroptical properties of some dehydro[7]helicenes **83aa**, **83ea**, and **83ab**

After HPLC chiral resolution as discussed before, the chiroptical properties (CD and CPL) of the optically pure aza-oxa-dehydro[7]helicenes **83aa**, **83ea**, and **83ab** were investigated. All the helical dyes **83** showed Cotton effect and simmilar CD and CPL signals (**Figure 4.19**). Among the aza-oxa-dehydro[7]helicenes, **83aa** exhibited significant CPL activity with $g_{lum} = 2.5\times10^{-3}$ at λ_{em}= 433 nm (>10 times higher than Maeda, Ema reported dehydrohelicene **44**). CPL of dehydrohelicene **83aa** was studied in different solvents (*n*-hexane, THF, and $CHCl_3$) showing equivalent luminescence patterns with almost the same dissymmetry factors g_{lum} values (**Figure 4.20**). g_{lum} values slightly decrease when replacing the methoxy group in **83aa** with benzyloxy group in **83ab** (2.2×10^{-3}). Besides, upon replacement of the *p*-tolyl *N*-substitution with a smaller methyl group, the g_{lum} value almost halved as shown in **83ea** (1.1×10^{-3}).

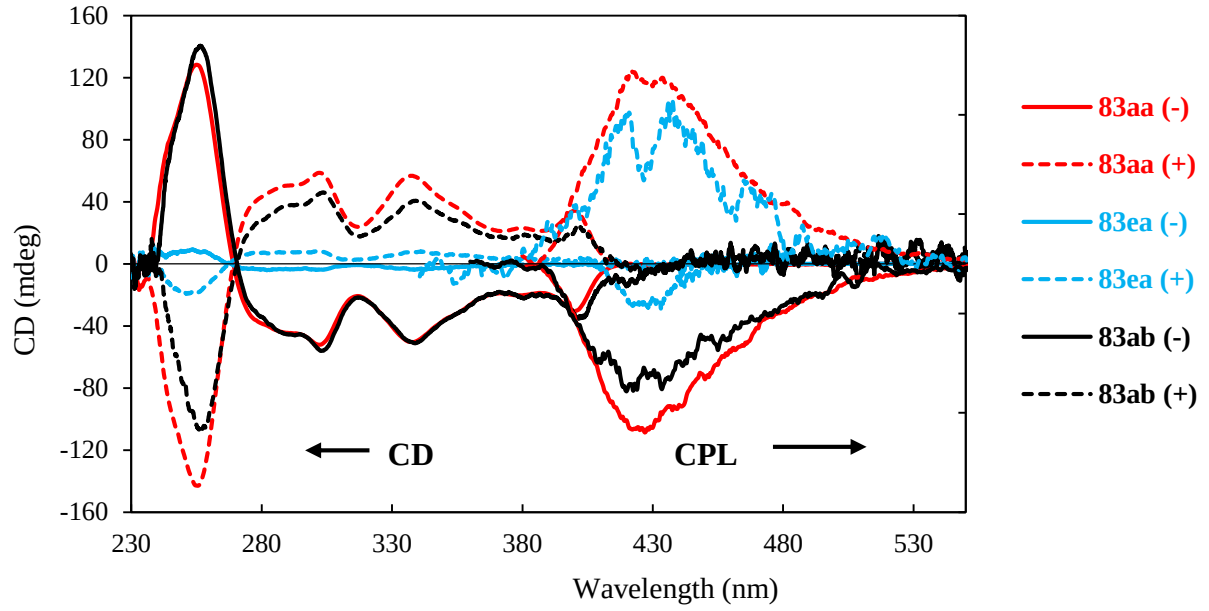

Figure 4.19. CD and CPL spectra of some dehydro[7]helicenes (**83aa**/**83ea**/**83ab**) in $CHCl_3$ (2×10^{-5} M).

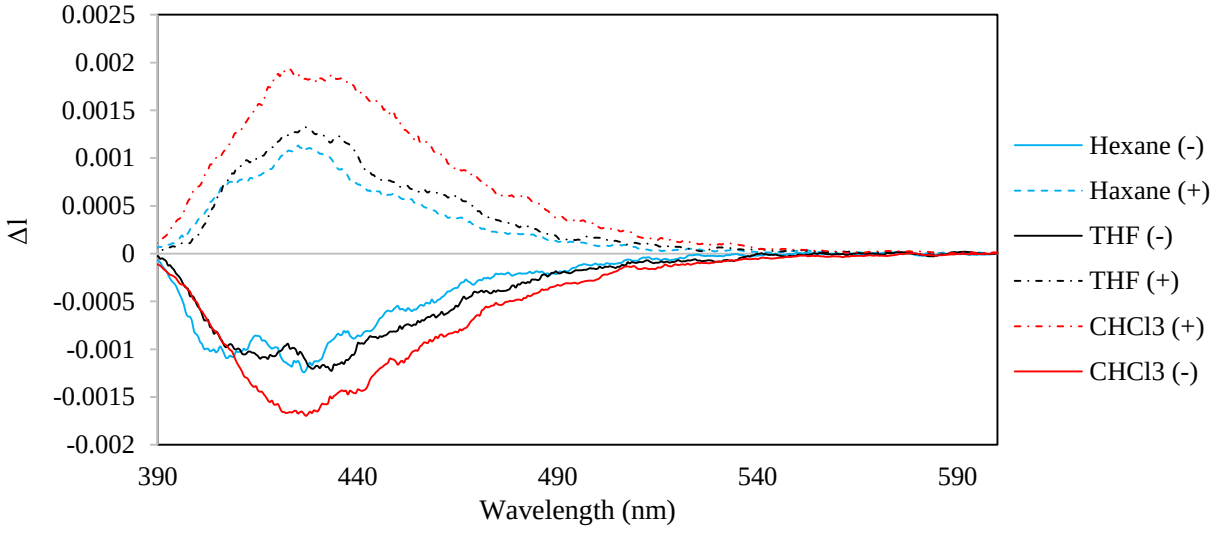

Figure 4.20. CPL spectra of compound **83aa** in ($CHCl_3$, hexane and THF) 20 µM solutions. g_{lum} = (2.5×10^{-3}, 2.25×10^{-3}, and 2.2×10^{-3} in $CHCl_3$, *n*-hexane, and THF respectively).

4.4.2. Chiroptical properties of the corresponding [7]helicene 82aa

On the other hand, the Cotton effects and CPL intensities of the corresponding helicene **82aa** proved to be weaker and the g_{lum} value dramatically dropped to around (6.0×10^{-4}) (**Figure 4.21**).

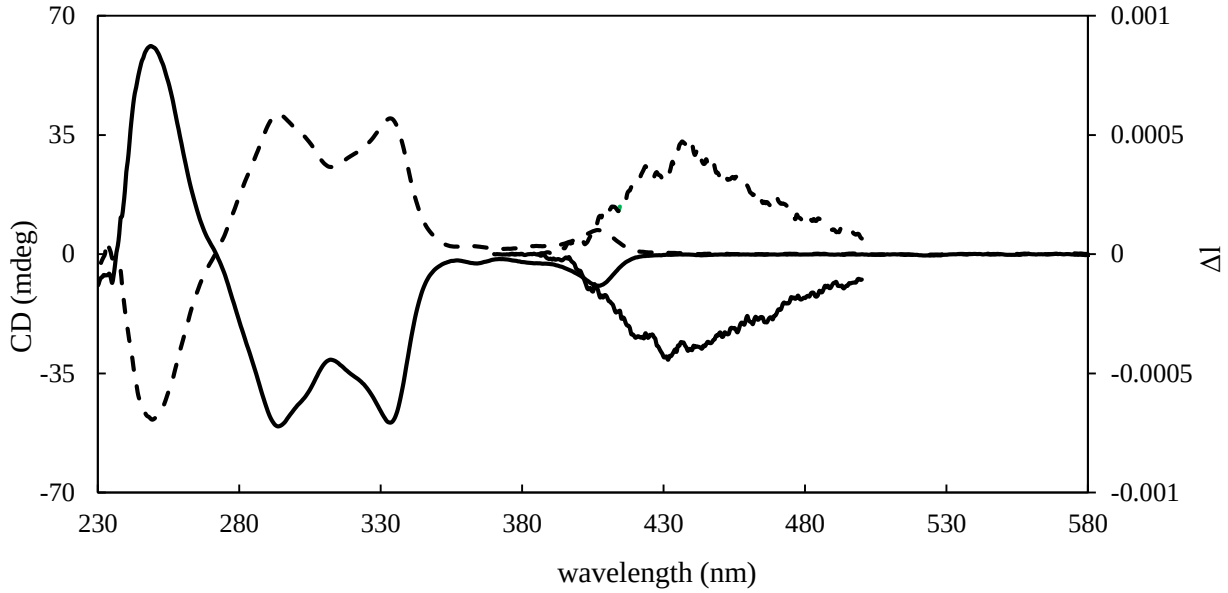

Figure 4.21. CD and CPL spectra of [7]helicenes (**82aa**) in $CHCl_3$ (2×10^{-5} M).

4.5. Design multiple helicene/dehydrohelicenes towards boosting chiroptical features

4.5.1. Introduction and inspiration

Theortically, all chiroptical properties are dependant on the rotational strenght *R*, however, the factors and mechanisms that control these properties in real molecules are not well explored. So far, there are no reliable well established strategy for the rationale design of excellent CPL-responsive molecules.[3, 12] Thus, the occasional successes in improving the chiroptical properties of SOMs mostly depends on trial-and-error basis through inspiration or by chance.[13] A few trials showed that assembling or fusing helicenes in specific arrangements affects positively on boosting their chiroptical properties. Tanaka and coworkers showed this potential when they studied the CPL of their *S*-shaped double azahelicenes **48** in comparison with azahelicene monomers **93** (**Scheme 4.1**).[14]

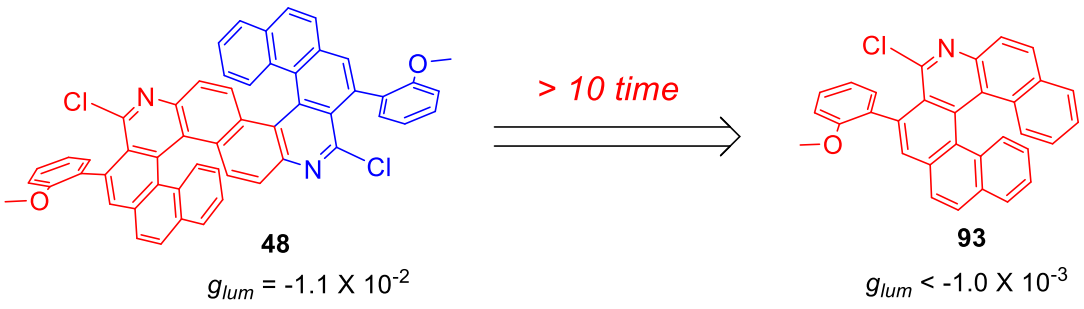

Scheme 4.1. Enhanced CPL of *S*-shaped double azahelicenes **48**

Very recently, Mori and coworkers introduced a general protocol for a symmetry-based design of multiple chiral units to boost the chiroptical responses. Based on this study, the alignment of two hexahelicene monomers in a dimeric form (S-shaped or X-shaped) improved the CPL values at least twice compared to the corresponding monomer **94** (**Scheme 4.2**).[12]

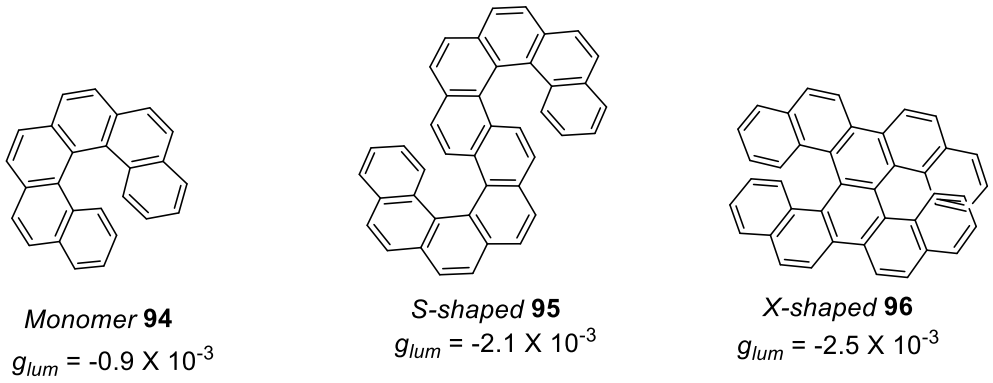

Scheme 4.2. Enhanced CPL of S-shaped and X-shaped double hexahelicenes

In 2019, Di Bari and Diederich presented a double helicene with a thiophene linker that showed one of the highest g_{lum} values reported so far among helicenes (**Scheme 4.3**). They used various techniques to improve the chiroptical properties, trying to benefit from the accumulated experience in this field. Through designed symmetrical dimer molecules incorporating some chemical entities to explore the push-pull effects they achieved g_{lum} value up to 0.025.[15]

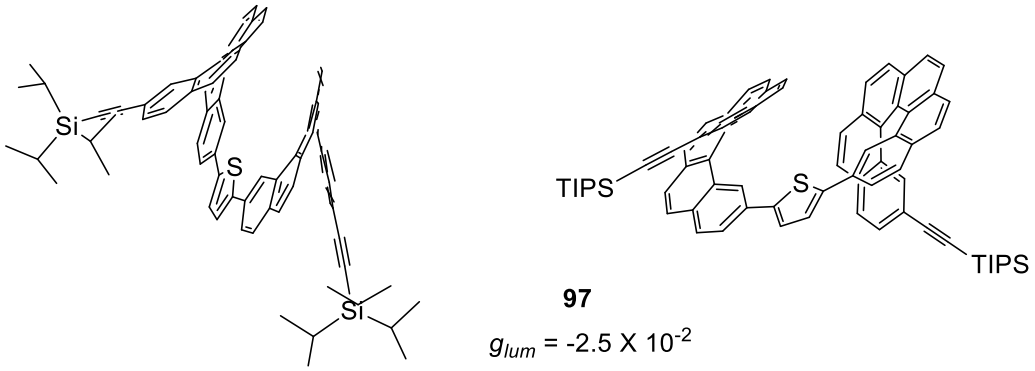

Scheme 4.3. High CPL of helicene dimer **97**

4.5.2. Design novel multiple helicenes and dehydrohelicenes to boost the chiroptical features

Although this field have gained more attention recently, we still have a lot to understand and discover. Based on the previous available studies [2, 12, 14, 15] and in an attempt to apply the concepts of symmetry[2] and assembly of chiral chromophores in multiple scaffolds, we put some preliminary designs of multiple helicenes and dehydrohelicnes in order to push their chiroptical properties to another level (**Scheme 4.4**).

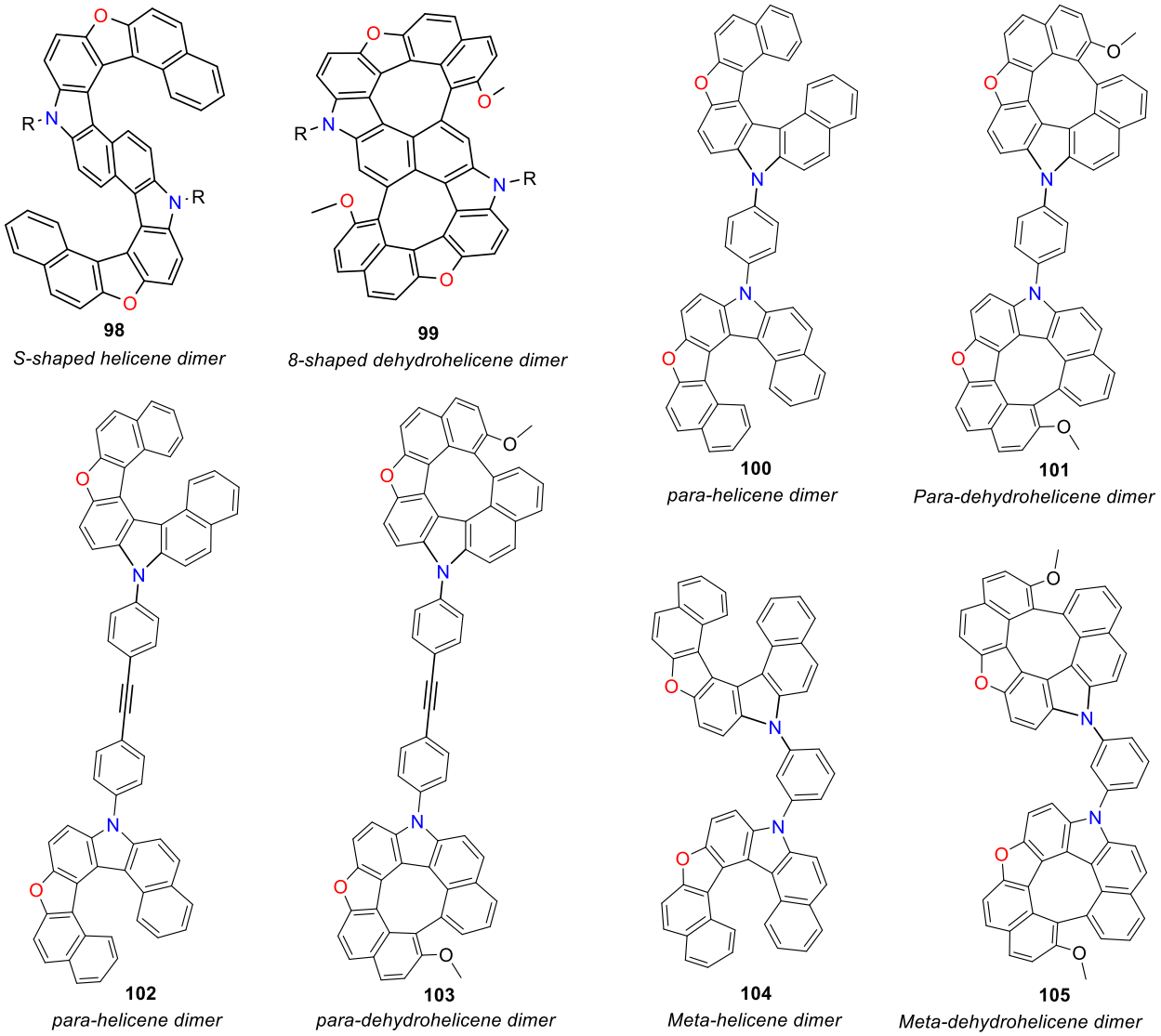

Scheme 4.4. Designed multiple helicenes and dehydrohelicenes to improve CPL properties

4.5.3. Synthesis of multiple helicenes and dehydrohelicenes

All the trials to prepare compounds **98** and **99** did not succeed as we couldn't get their di-carbazole precursor **109** (**Scheme 4.5**). Although, I tried to screen different conditions, reagents, and even completely different synthetic approaches (**Scheme 4.6**), this precursor **109** was not afforded at all. Hence, I decided to prepare other helicene and dehydrohelicene dimers **100-105**. To our fortunate, these compounds could be prepared from their precursors **118a**, **118b**, and **119** smoothly at low to moderate yields (**Scheme 4.7 - 7.9**). The structures of these dimers was confirmed by all spectral data and compound **100** was further confirmed by X-ray crystallographic analysis.

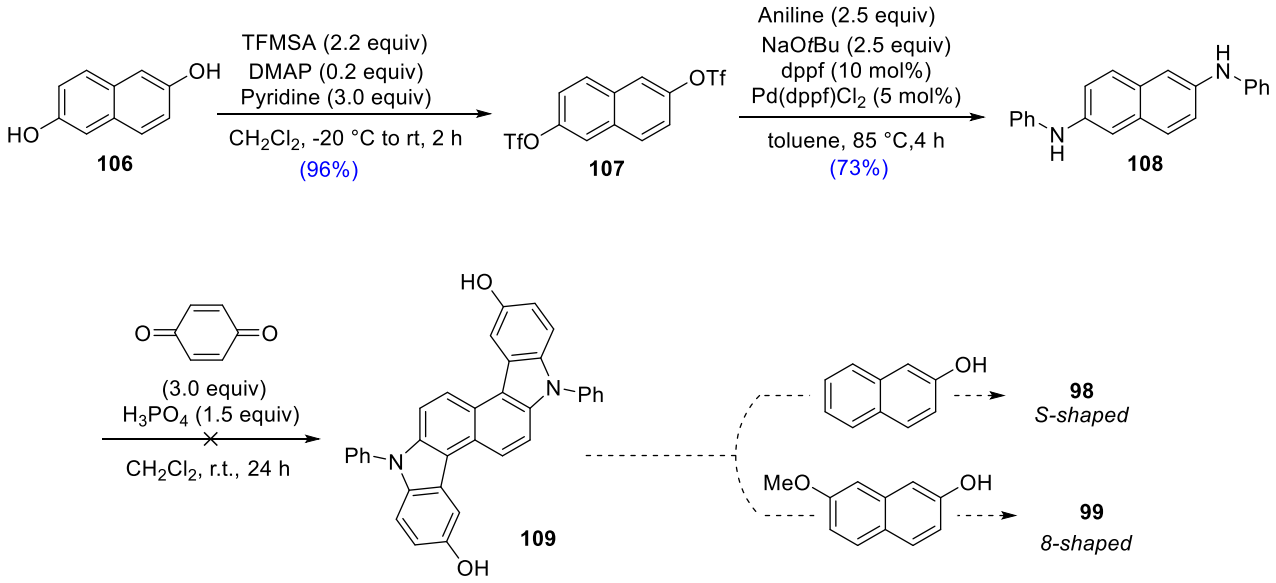

Scheme 4.5. Unsuccessful trial to prepare helicene dimer **98** and dehydrohelicene dimer **99**

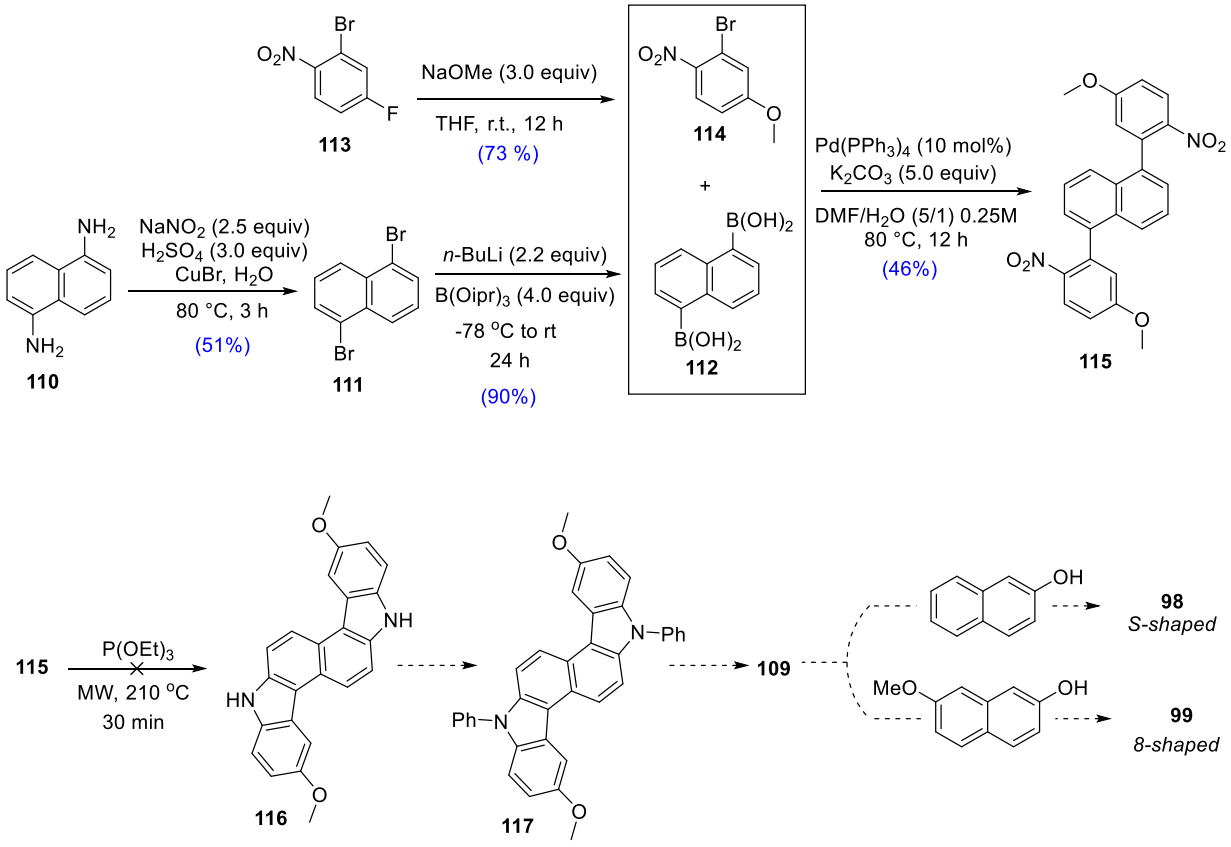

Scheme 4.6. Another unsuccessful trial to prepare helicene and dehydrohelicene dimers **98** and **99**

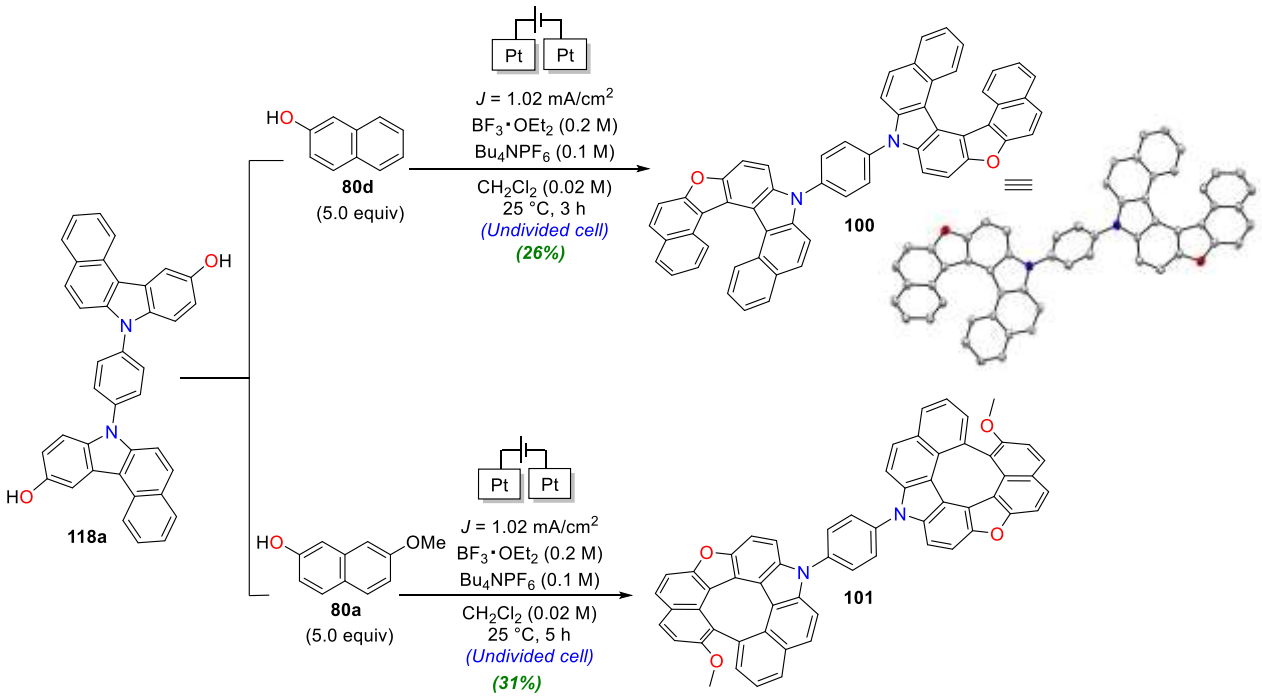

Scheme 4.7. Preparation of helicene dimer **100** and dehydrohelicene dimer **101**

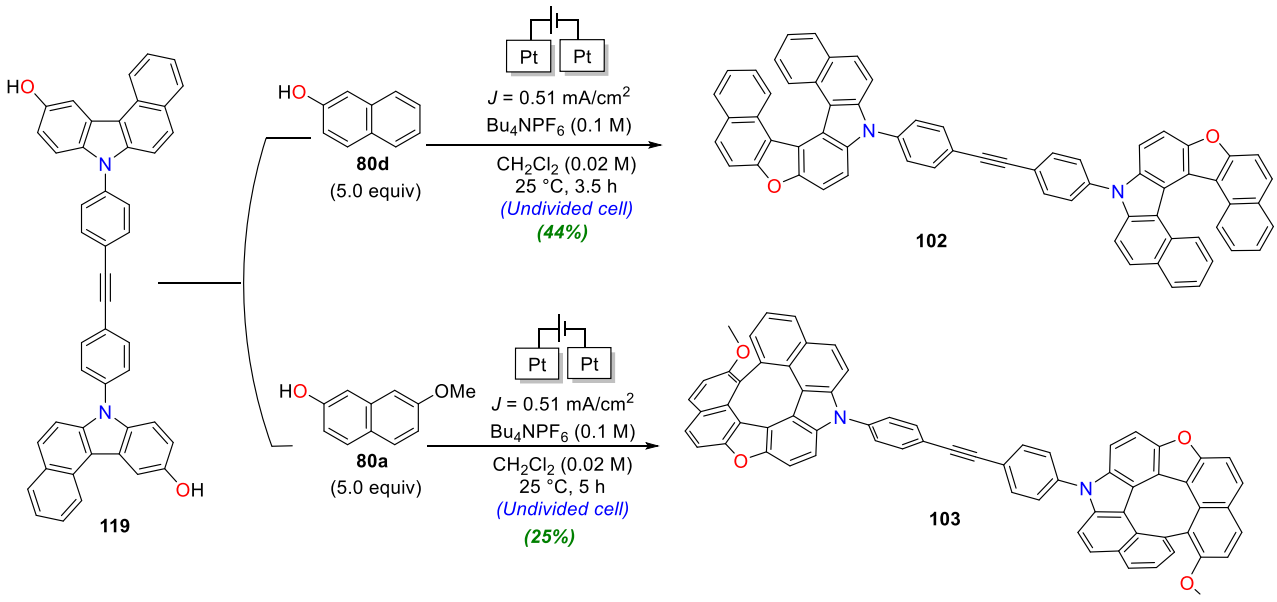

Scheme 4.8. Preparation of helicene dimer **102** and dehydrohelicene dimer **103**

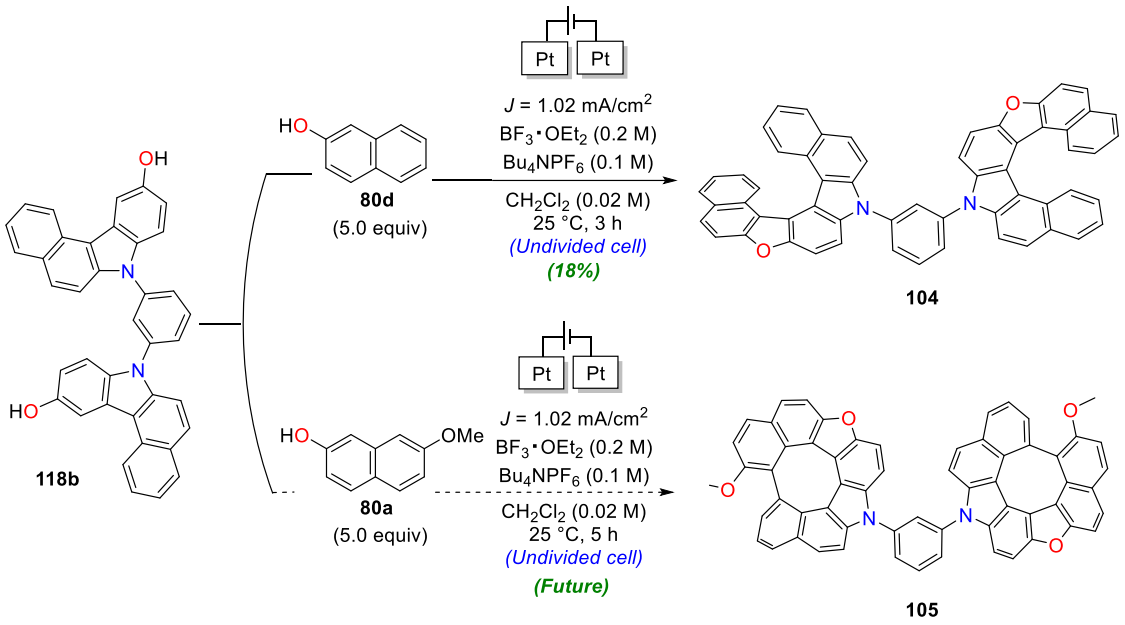

Scheme 4.9. Preparation of helicene dimer **104**

4.5.4. Optical properties of some dimers

The photophysical properties (UV-vis & PL) of some helicene dimers **100** and **120** were investigated in $CHCl_3$ (20 µM), and exhibited a red-shifted absorption reaching up to 406 nm and 407 nm respectively. Moreover, their emission maxima were shifted in a bathochromic way at 415 nm and 439 nm for compound **100**, and 417 nm and 440 nm for compound **120** (**Figure 4.22**).

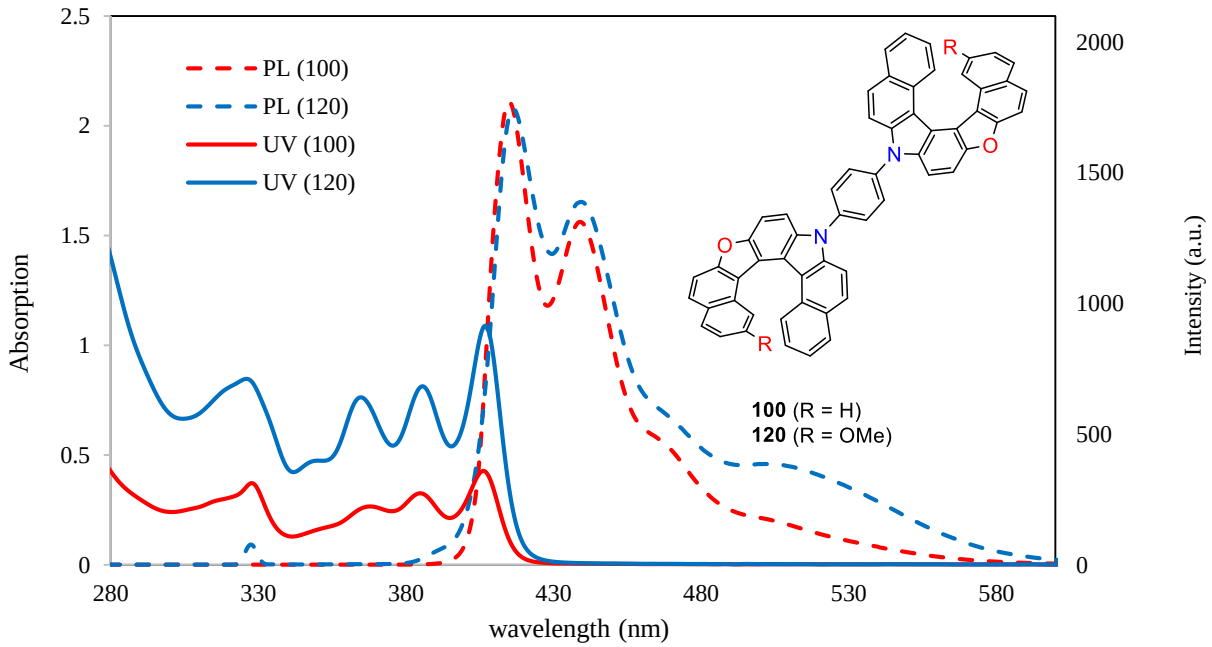

Figure 4.22. Photophysical properties (UV & PL) of **100** and **120** in $CHCl_3$ (20 µM) solutions.

In spite of the promising photophysical properties of the prepared dimers, we couldn't investigate their chiroptical features so far. The HPLC resolution on chiral columns was challenging at this stage, as we couldn't find the appropriate conditions to isolate and study one optically pure isomer. This can be attributed to the big number of isomers in each case (four isomers), which makes the separation more challenging. Consequently, we decided to conduct a theoretical study based on TD-DFT calculations to predict the luminescence dissymmetry factor g_{lum} of these dimers as a quick measure until we can separate them and evaluate their experimental g_{lum} values. This theoretical study gives us an additional advantage to correlate the higher g_{lum} values to the structural features and trying to find the trend in which the CPL properties will improve. Also, we can design new molecules with expected outstanding CPL values and try to synthesize them in the future.

4.5.5. Theoretical calculations of g_{lum} values of multiple helicenes and dehydrohelicenes

The theory of optical activity was well documented by Schellman in 1975, according to this theory the luminescence dissymmetry factor g_{lum} can be defined according to (**Eq. 4.21**).[16] Where **μ** and **m** are the TEDM and TMDM vectors, respectively, and $\boldsymbol{\theta_{\mu,m}}$ is the angle between these two vectors. Based on this key equation, CPL spectra can be predicted theoretically using time-dependent density functional theory (TD-DFT) calculations in which the rotational strength R and the dipole strength D are calculated in the excited state. This method (TD-DFT) showed comparable calculated g_{lum} values to the experimental values as reported previously.[12, 17]

$$g_{lum} = \frac{4\,|\mu|.|\mathbf{m}|.\cos\theta_{\mu,m}}{|\mu|^2 + |\mathbf{m}|^2} \qquad \textbf{(Eq. 4.21)}$$

By applying TD-DFT calculations at the TD-B3LYP/6-31G(d) basis set in the Gaussian 16 package, we were able to calculate the parameters corresponding to the transition electric and magnetic dipole moments (TEDM) and (TMDM). Based on these parameters and using (**Eq. 4.21**), we calculated the rotational strength R and the dipole strength D of our dimers **98**-**105** in the excited states (**Table 4.1**). These calculations enabled us finally to predict the g_{lum} values of our designed scaffolds (**Figure 4.23**).

Table 4.1. Electronic transition properties of helicene and dehydrohelicene dimers **98**-**105**

Cpd	$\lvert\boldsymbol{\mu}\rvert$ 10^{-20} esu.cm	$\lvert\mathbf{m}\rvert$ 10^{-20} erg.G^{-1}	cos $\theta_{\mu,m}$	D 10^{-40} esu^2.cm^2	R 10^{-40} erg.esu.cm.G^{-1}	G 10^{-40} erg^2.G^{-2}	$g_{CPL,\ calcd}$
(*M*,*P*)-**98**	632	0.00	0.070	399877	0.0	0	0
(*M*,*P*)-**99**	398	0.28	0.510	158049	5.8	0.08	1.5×10^{-4}
(*M*,*P*)-**100**	679	0.52	-0.590	460922	-208.6	0.27	-1.8×10^{-3}
(*M*,*P*)-**101**	532	1.82	-0.014	283094	-13.5	3.32	-1.9×10^{-4}
(*M*,*P*)-**102**	736	0.00013	-0.078	540949	-0.0076	2.0×10^{-8}	-5.6×10^{-8}
(*P*,*M*)-**103**	746	0.24	0.283	555874	50.5	0.057	3.6×10^{-4}
(*P*,*M*)-**104**	704	0.78	0.277	495778	151.3	0.603	1.2×10^{-3}
(*P*,*M*)-**105**	471	1.53	0.423	221878	305.7	2.354	5.5×10^{-3}

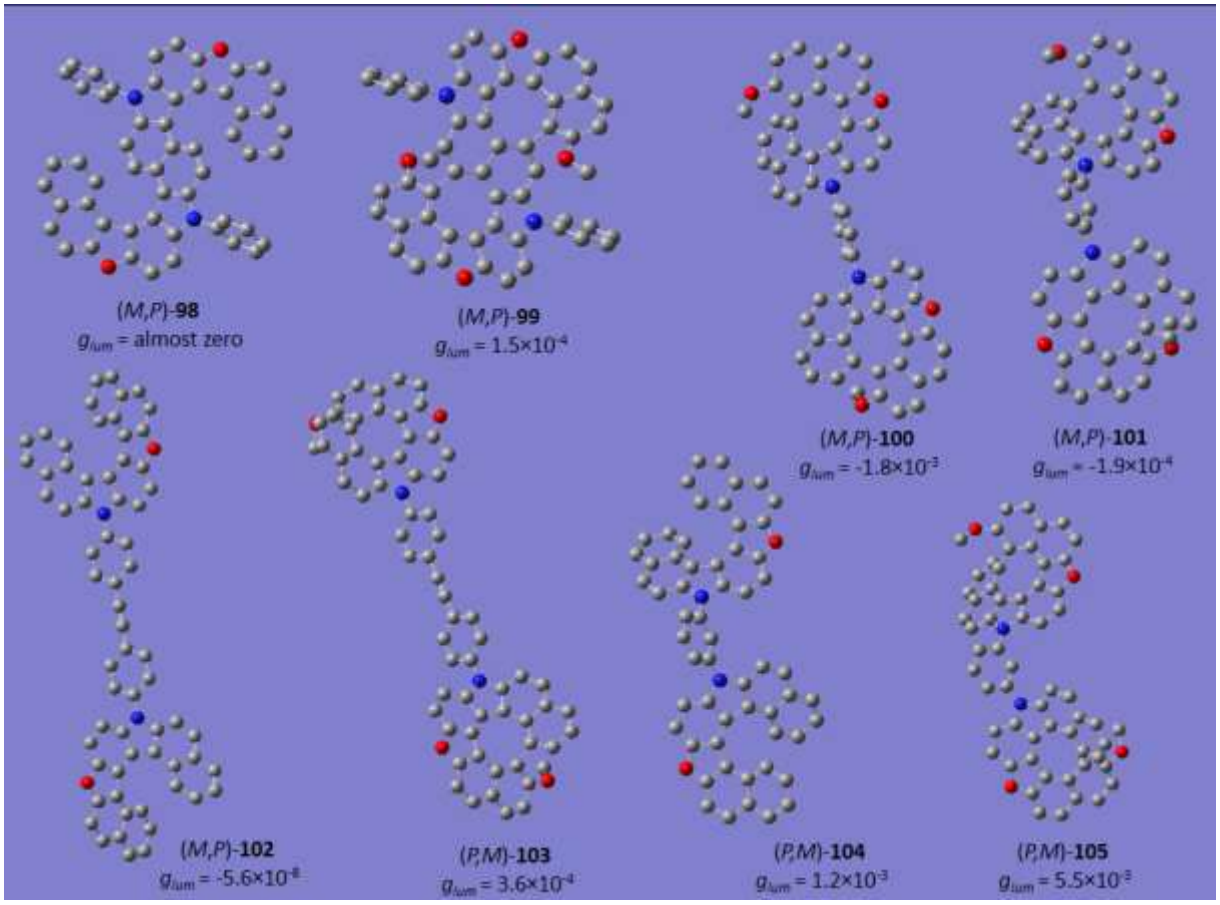

Figure 4.23. Calculated g_{CPL} values for multiple helicenes and dehydrohelicenes

Apart from compound **105**, unfortunately most of the designed dimers did not show promising CPL properties, even some of these scaffolds showed lower g_{CPL} values than the corresponding monomers. However, we were able to design some other multiple helicene or dehydrohelicenes whose transitions are electrically hindered and magnetically allowed. The new designs showed more promising g_{CPL} values and some of them exceeds the highest CPL for all reported SOMs (**Scheme 4.10**). In the future, we hope the preparation of these designed molecules can afford extraordinary CPL-sensitive materials that will represent a quantum leap in the field of material science and application in optical devices.

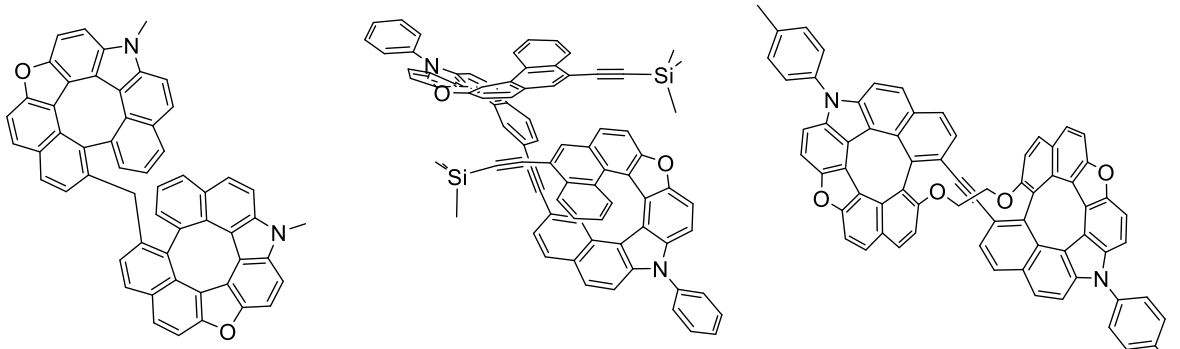

Scheme 4.10. New designs that show high g_{lum} values

References

(1) Baruah, R. Study of optical absorption and photoluminescence (PL) of hexa thiobenzene acid. *Indian Academy of Sciences*. http://reports.ias.ac.in/report/20872/study-of-optical-absorption-and-photoluminescence-pl-of-hexa-thiobenzene-acid

(2) Mori, T. Chiroptical properties of symmetric double, triple, and multiple helicenes. *Chemical Reviews* **2021**, *121* (4), 2373-2412.

(3) Tanaka, H.; Inoue, Y.; Mori, T. Circularly polarized luminescence and circular dichroisms in small organic molecules: correlation between excitation and emission dissymmetry factors. *ChemPhotoChem* **2018**, *2* (5), 386-402.

(4) Kawasumi, K.; Zhang, Q.; Segawa, Y.; Scott, L. T.; Itami, K. A grossly warped nanographene and the consequences of multiple odd-membered-ring defects. *Nature Chemistry* **2013**, *5* (9), 739-744.

(5) Chen, F.; Tanaka, T.; Mori, T.; Osuka, A. Synthesis, structures, and optical properties of azahelicene derivatives and unexpected formation of azahepta [8] circulenes. *Chemistry–A European Journal* **2018**, *24* (29), 7489-7497.

(6) Matsuo, Y.; Chen, F.; Kise, K.; Tanaka, T.; Osuka, A. Facile synthesis of fluorescent hetero [8] circulene analogues with tunable solubilities and optical properties. *Chemical Science* **2019**, *10* (48), 11006-11012.

(7) (a) Peeters, E.; Christiaans, M. P.; Janssen, R. A.; Schoo, H. F.; Dekkers, H. P.; Meijer, E. Circularly polarized electroluminescence from a polymer light-emitting diode. *Journal of the American Chemical Society* **1997**, *119* (41), 9909-9910. (b) Kraft, A.; Grimsdale, A. C.; Holmes, A. B. Electroluminescent conjugated polymers-seeing polymers in a new light. *Angewandte Chemie International Edition* **1998**, *37* (4), 402-428.

(8) Pescitelli, G.; Di Bari, L.; Berova, N. Conformational aspects in the studies of organic compounds by electronic circular dichroism. *Chemical Society Reviews* **2011**, *40* (9), 4603-4625.

(9) (a) Srebro-Hooper, M.; Autschbach, J. Calculating natural optical activity of molecules from first principles. *Annual Review of Physical Chemistry* **2017**, *68*, 399-420. (b) Polavarapu, P. L.; Covington, C. L. Comparison of experimental and calculated chiroptical spectra for chiral molecular structure determination. *Chirality* **2014**, *26* (9), 539-552. (c) Autschbach, J. Computing chiroptical properties with first-principles theoretical methods: background and illustrative examples. *Chirality: The Pharmacological, Biological, and Chemical Consequences of Molecular Asymmetry* **2009**, *21* (1E), E116-E152.

(10) Muller, G. Luminescence of lanthanide ions in coordination compounds and nanomaterials. *John Wiley & Sons, Chichester, UK* **2014**, 77-124.

(11) Maeda, C.; Nomoto, S.; Akiyama, K.; Tanaka, T.; Ema, T. Facile synthesis of azahelicenes and diaza [8] circulenes through the intramolecular Scholl reaction. *Chemistry–A European Journal* **2021**, *27* (63), 15699-15705.

(12) Tanaka, H.; Ikenosako, M.; Kato, Y.; Fujiki, M.; Inoue, Y.; Mori, T. Symmetry-based rational design for boosting chiroptical responses. *Communications Chemistry* **2018**, *1* (1), 1-8.

(13) (a) Dhbaibi, K.; Favereau, L.; Srebro-Hooper, M.; Jean, M.; Vanthuyne, N.; Zinna, F.; Jamoussi, B.; Di Bari, L.; Autschbach, J.; Crassous, J. Exciton coupling in diketopyrrolopyrrole–helicene derivatives leads to red and near-infrared circularly polarized luminescence. *Chemical Science* **2018**, *9* (3), 735-742. (b) Nakakuki, Y.; Hirose, T.; Sotome, H.; Miyasaka, H.; Matsuda, K. Hexa-*peri*-hexabenzo [7] helicene: Homogeneously π-extended helicene as a primary substructure of helically twisted chiral graphenes. *Journal of the American Chemical Society* **2018**, *140* (12), 4317-4326.

(14) Nakamura, K.; Furumi, S.; Takeuchi, M.; Shibuya, T.; Tanaka, K. Enantioselective synthesis and enhanced circularly polarized luminescence of S-shaped double azahelicenes. *Journal of the American Chemical Society* **2014**, *136* (15), 5555-5558.

(15) Schaack, C.; Arrico, L.; Sidler, E.; Górecki, M.; Di Bari, L.; Diederich, F. Helicene monomers and dimers: chiral chromophores featuring strong circularly polarized luminescence. *Chemistry–A European Journal* **2019**, *25* (34), 8003-8007.

(16) Schellman, J. A. Circular dichroism and optical rotation. *Chemical Reviews* **1975**, *75* (3), 323-331.

(17) (a) Kubo, H.; Hirose, T.; Nakashima, T.; Kawai, T.; Hasegawa, J.-y.; Matsuda, K. Tuning transition electric and magnetic dipole moments:[7] helicenes showing intense circularly polarized luminescence. *The Journal of Physical Chemistry Letters* **2021**, *12* (1), 686-695. (b) Chen, N.; Yan, B. Recent theoretical and experimental progress in circularly polarized luminescence of small organic molecules. *Molecules* **2018**, *23* (12), 3376.

Chapter 5: Conclusion

This study represents the first electrochemical approach for synthesizing heterodehydro[7]helicenes *via* a sequential protocol of chemoselective hetero-coupling of hydoxycarbazoles and 2-naphthols, followed by dehydrative cyclization, and intramolecular carbon-carbon bond formation. Dehydrohelicenes are some of the most attractive chiroptical materials with unique helical chirality that can be implemented in various material-based applications, such as organic light-emitting diodes (OLEDs) and organic field-effect transistors (OFETs). However, there are no prior reports on their direct construction involving asymmetric methods. In this thesis, I introduced one of the most efficient and facile methods to prepare these scaffolds under mild conditions using an electrochemical domino approach.

Also, I introduced the first efficient enantioselective synthesis of heterodehydro[7]helicene *via* a hybrid chiral vanadium-catalyzed hetero-coupling and electrochemical oxidative transformations. The synthesized heterodehydro[7]helicenes exhibited several interesting properties: intense blue-colored circularly polarized luminescence ($|g_{lum}| \approx 2.5 \times 10^{-3}$ at 433 nm) (highest CPL for all dehydrohelicenes) and significant chiral stability (studies on the racemization barrier indicated $\Delta G^{\ddagger} > 140$ kJ mol^{-1} and $t_{1/2} >$ ca. 1.6 x 10^4 years at 25 °C).

Various polycyclic heteroaromatics PHAs were accessible using electrochemical approaches in high yields. Some of these PHAs present unique chemical features with great opportunities to study them and further improve their properties. In this thesis, I introduced for example a new type of hetero[8]circulene, the first dehydrohelicene dimer, and new scaffolds afforded *via* double C-O insertions. All these exceptional PHAs showed good photophysical properties with high potential for optical material-based applications.

As a conclusion of my thesis, a new efficient approach for synthesizing PHAs, especially aza-oxa-dehydro[7]helicenes, was introduced representing a significant contribution to the literature because it shows an exceptional efficiency of electrochemistry in affording one of the key scaffolds in material science applications. Also, the concepts of electrochemistry and chiral vanadium catalysis were combined together to present the first enantioselective approach to heterodehydro[7]helicene. Most of the prepared PHAs showed good photophysical and chiroptical properties with exceptional chiral stability of dehydrohelicenes. Based on the current achievements, new designs of multiple helicene and dehydrohelicenens were placed to boost the chiroptical features, and some of these suggested designs showed exceptional result according to TD-DFT calculations.

Chapter 6: Experimental Section

General information

The electrochemical reactions were performed in a 10 mL reaction vessel equipped with two FTO electrodes (1.0 × 2.5 cm^2) connected to Cu wire (**Figure 6.1a** and **6.1b**). The two electrodes are connected to DC power supply (KIKUSUI PMX 35-1A) (**Figure 6.1c**). The reactions were carried out at rt, under air (1 atm.), and at a constant current of 3 mA. Constant current mode of electrolysis –in the case of our substrates- offers many advantages over constant potential mode; related to its easier setup and full conversion of the substrates.

Figure 6.1a: FTO electrodes

Figure 6.1b: Rx vessel

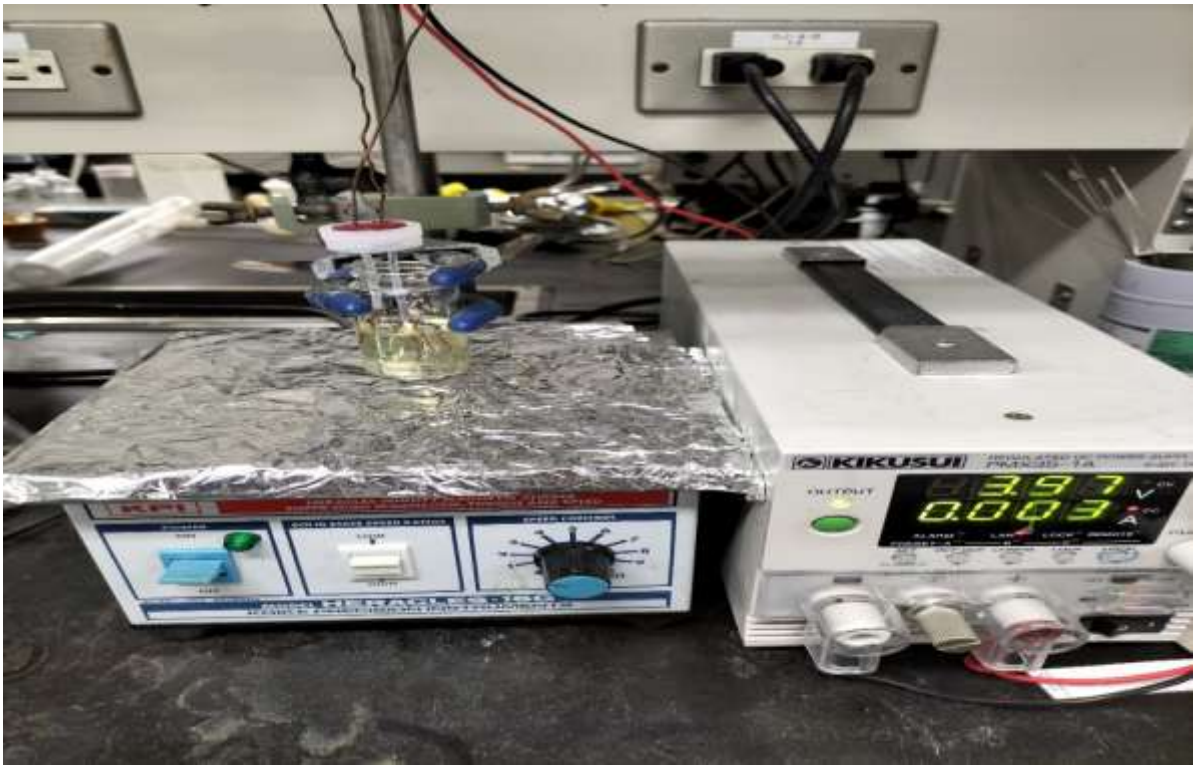

Figure 6.1c: DC power supply (KIKUSUI PMX 35.0-1.0A)

Experimental procedures for the synthesis of 79

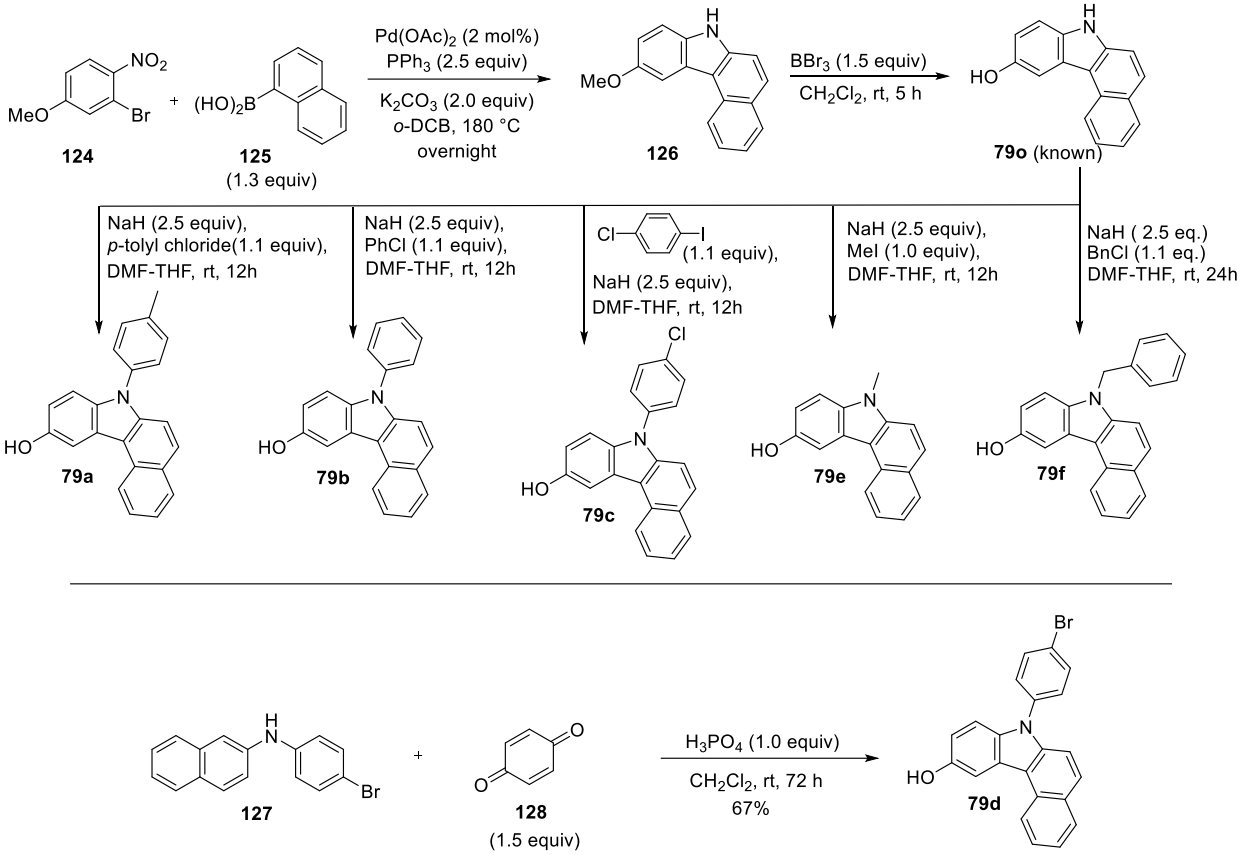

7*H*-Benzo[*c*]carbazol-10-ol **79o**

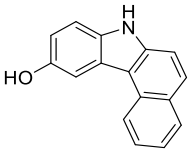

A mixture of 2-bromo-4-methoxy-1-nitrobenzene **124** (574.6 mg, 2.48 mmol), naphthalen-1-boronic acid **125** (553.7 mg, 3.22 mmol), $Pd(OAc)_2$ (11.1 mg, 0.05 mmol), PPh_3 (1.62 g, 6.19 mmol) and K_2CO_3 (684.5 mg, 4.95 mmol) in *o*-DCB (5.0 mL) was heated at 180 °C (oil bath temperature). After stirring for 20 h at the same temprature, the reaction mixture was filtrated through celite and concentrated in vacuo. The residue was purified by silica-gel column chromatography to afford 10-methoxy-7*H*-benzo[*c*]carbazole (**126**, 71% yield) as a deep green solid. Then, BBr_3 (1.0 M in CH_2Cl_2, 4.5 mL, 4.5 mmol) was added to a solution of **126** (592 mg, 3.00 mmol) in CH_2Cl_2 (30 mL) at 0 °C, and then the mixture was stirred for 5 h at rt. The reaction was quenched with sat. $NaHCO_3$ at 0 °C and the resulting mixture was extracted with EtOAc, drying over anhydrous Na_2SO_4, filtered, and evaporated *in vacuo.* The residue was purified by silica-gel column chromatography to afford **79o** (85% yield) as a brown solid (60% overall yield in 2 steps). **^{1}H NMR** (400 MHz, $(CD_3)_2CO$): δ 10.58 (s, 1H), 8.67 (d, J = 8.7 Hz, 1H), 7.99-8.02 (m, 3H), 7.85 (d, J = 8.7 Hz, 1H), 7.72 (d, J = 8.7 Hz, 1H), 7.68 (ddd, J = 7.8, 7.3, 0.9 Hz, 1H), 7.50 (d, J = 8.2 Hz, 1H), 7.43 (ddd, J = 7.8, 7.3, 0.9 Hz, 1H), 7.02 (ddd, J = 8.7, 2.3, 0.9 Hz, 1H). **^{13}C NMR** (100 MHz, $(CD_3)_2CO$): δ 152.33, 139.33, 134.40, 131.07, 129.97, 129.85, 127.66, 127.43, 125.16, 123.52, 123.20, 115.27, 114.59, 114.23, 112.76, 107.37. **HRMS** (APCI): calcd for $C_{16}H_{12}NO$: *m/z* 234.0913 $[M + H]^+$, found 234.0910. **IR** (KBr): 3524, 3400, 3348, 1492, 1209, 1164, 832, 803, 753, 737 cm^{-1}. **mp**: 212-214 °C.

7-(*p*-Tolyl)-7*H*-benzo[*c*]carbazol-10-ol **79a**

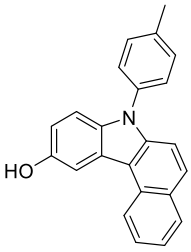

To a stirring solution of DMF (0.27 mL) and NaH (171.5 mg, 4.29 mmol) was added a solution of **1'** (401.2 mg,1.72 mmol) in THF (8.6 mL) at 0 °C. After stirring for 10 min at rt, *p*-tolyl chloride (217.7 mg, 1.72 mmol) was added to the solution and the reaction mixture was allowed to stir at 50 ºC. After stirring for 12 h, water was added to the reaction at 0 ºC. The resulting mixture was extracted with EtOAc. The combined organic layers were washed with brine, dried over anhydrous Na_2SO_4, filtered, and evaporated *in vacuo*. The residue was purified by silica-gel column chromatography to afford **1a** (67% yield) as a white solid. **^{1}H NMR** (400 MHz, $CDCl_3$): δ 8.72 (d, J = 8.2 Hz, 1H), 8.07 (d, J = 2.7 Hz, 1H), 7.99 (d, J = 7.8 Hz, 1H), 7.80 (d, J = 8.7 Hz, 1H), 7.7 (ddd, J = 7.8, 7.3, 0.9 Hz, 1H), 7.52 (d, J = 9.2 Hz, 1H), 7.47 (ddd, J = 7.8, 7.3, 0.9 Hz, 1H), 7.40-7.45 (m, 4H), 7.35 (d, J = 8.7 Hz, 1H), 6.99 (dd, J = 8.9, 2.5 Hz, 1H), 4.90 (s, 1H), 2.51 (s, 3H). **^{13}C NMR** (100 MHz, $CDCl_3$): δ 150.14, 139.48, 137.86, 135.65, 134.86, 130.61, 130.02, 129.31, 127.54, 127.07, 124.39, 123.14, 123.05, 114.90, 113.59, 112.01, 111.13, 107.41, 21.40 (Two carbons overlapped). **HRMS** (APCI): calcd for $C_{23}H_{18}NO$: *m/z* 324.1383 $[M + H]^+$, found 324.1380. **IR** (KBr): 3317, 3052, 3033, 2920, 1619, 1585, 1515, 1196, 1164, 819 cm^{-1}. **mp**: 95-97 °C.

7-Phenyl-7*H*-benzo[*c*]carbazol-10-ol **79b**

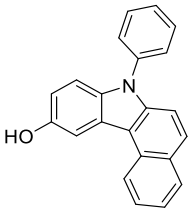

Following the same procedures as that of **79a**. **79b** (55% yield): a white solid. **^{1}H NMR** (400 MHz, $CDCl_3$): δ 8.73 (d, J = 8.7 Hz, 1H), 8.08 (d, J = 2.3 Hz, 1H), 7.99 (d, J = 8.2 Hz, 1H), 7.81 (d, J = 8.7 Hz, 1H), 7.71 (ddd, J = 7.8, 7.3, 0.9 Hz, 1H), 7.61-7.65 (m, 2H), 7.46-7.58 (m, 5H), 7.37 (d, J = 8.7 Hz, 1H), 7.00 (dd, J = 8.9, 2.5 Hz, 1H), 4.91 (s, 1H). **^{13}C NMR** (100 MHz, $CDCl_3$): δ 150.24, 139.34, 137.58, 135.50, 130.04, 130.00, 129.40, 129.34, 127.92, 127.74, 127.64, 127.13, 124.53, 123.15, 115.05, 113.63, 111.94, 111.11, 107.45 (One carbon overlapped). **HRMS** (APCI): calcd for $C_{22}H_{16}NO$: *m/z* 310.1226 $[M + H]^+$, found 310.1225. **IR** (KBr): 3318, 3062, 1620, 1589, 1503, 1446, 1388, 1197, 1156, 803 cm^{-1}. **mp**: 81-83 °C.

7-(4-Chlorophenyl)-7*H*-benzo[*c*]carbazol-10-ol **79c**

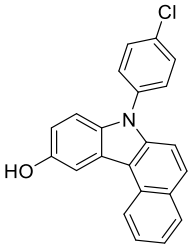

Following the same procedures as that of **79a**. **79c** (61% yield): a white solid. **^{1}H NMR** (400 MHz, $CDCl_3$): δ 8.70 (d, J = 8.2 Hz, 1H), 8.06 (d, J = 1.4 Hz, 1H), 7.99 (d, J = 7.8 Hz, 1H), 7.82 (d, J = 9.2 Hz, 1H), 7.71 (t, J = 7.6 Hz, 1H), 7.59 (d, J = 8.2 Hz, 2H), 7.48-7.50 (m, 4H), 7.32 (d, J = 8.7 Hz, 1H), 7.00 (dd, J = 8.7, 2.3 Hz, 1H), 4.94 (s, 1H). **^{13}C NMR** (100 MHz, $CDCl_3$): δ 150.42, 139.12, 136.12, 135.27, 133.55, 130.29, 129.92, 129.46, 129.36, 128.98, 127.83, 127.24, 124.68, 123.31, 123.15, 115.27, 113.79, 111.58, 110.86, 107.59. **HRMS** (APCI): calcd for $C_{22}H_{15}ClNO$: *m/z* 344.0837 $[M + H]^+$, found 344.0836. **IR** (KBr): 3326, 3063, 1621, 1586, 1496, 1474, 1198, 1163, 802, 741 cm^{-1}. **mp**: 88-90 °C.

7-(4-Bromophenyl)-7*H*-benzo[*c*]carbazol-10-ol **79d**

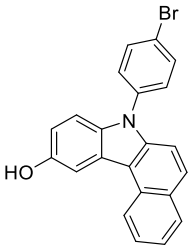

A mixture of **127** (2.5 mmol), *p*-quinone **128** (3.75 mmol), and *o*-phosphoric acid (130 µL, 2.5 mmol) in CH_2Cl_2 (25.0 mL) was stirred at rt. After stirring for 72 h, the reaction mixture was quenched by water and further extracted with CH_2Cl_2. The combined organic extracts were washed with brine and dried over anhydrous Na_2SO_4, filtered, and evaporated *in vacuo*. The crude product was purified by silica-gel column chromatography to afford **79d** (67% yield) as a white solid. **^{1}H NMR** (400 MHz, $CDCl_3$) δ 8.72 (d, J = 8.7 Hz, 1H), 8.06 (d, J = 2.3 Hz, 1H), 7.99 (d, J = 8.2 Hz, 1H), 7.82 (d, J = 8.7 Hz, 1H), 7.70-7.77 (m, 3H), 7.50 (d, J = 8.7 Hz, 2H), 7.46 (dd, J = 6.4, 1.8 Hz, 2H), 7.34 (d, J = 9.2 Hz, 1H), 7.00 (dd, J = 8.7, 2.3 Hz, 1H), 4.83 (s, 1H). **^{13}C NMR** (100 MHz, $CDCl_3$) δ 150.42, 139.05, 136.66, 135.21, 133.27, 129.92, 129.48, 129.36, 129.29, 127.84, 127.25, 124.73, 123.33, 123.15, 121.45, 115.32, 113.80, 111.56, 110.86, 107.62. **HRMS** (APCI): calcd for $C_{22}H_{15}BrNO$: *m/z* 388.0332 $[M + H]^+$, found 388.0345. **IR** (KBr): 3358, 3061, 2955, 2925, 1620, 1493, 1472, 1162, 803, 742 cm^{-1}. **mp**: 95-97 °C.

7-Methyl-7*H*-benzo[*c*]carbazol-10-ol **79e**

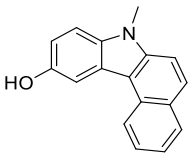

Following the same procedures as that of **79a**. **79e** (75% yield): a white solid. **^{1}H NMR** (400 MHz, $(CD_3)_2CO$): δ 8.68 (d, J = 8.2 Hz, 1H), 8.04-8.06 (m, 2H), 8.02 (s, 1H), 7.93 (d, J = 9.2 Hz, 1H), 7.80 (d, J = 8.7 Hz, 1H), 7.69 (ddd, J = 7.8, 7.3, 0.9 Hz, 1H), 7.54 (d, J = 9.2 Hz, 1H), 7.43 (ddd, J = 7.8, 7.3, 0.9 Hz, 1H), 7.10 (dd, J = 8.7, 2.3 Hz, 1H), 4.02 (s, 3H). **^{13}C NMR** (100 MHz, $(CD_3)_2CO$): δ 152.45, 139.96, 135.58, 130.94, 130.02, 129.65, 127.72, 127.59, 124.56, 123.45, 123.20, 114.71, 114.51, 112.03, 110.79, 107.53, 29.53. **HRMS** (APCI): calcd for $C_{17}H_{14}NO$: *m/z* 248.1070 $[M + H]^+$, found 248.1068. **IR** (KBr): 3189, 3072, 3036, 2923, 1616, 1528, 1479, 1173, 1156, 789 cm^{-1}. **mp**: 100-102 °C.

7-Benzyl-7*H*-benzo[*c*]carbazol-10-ol **79f**

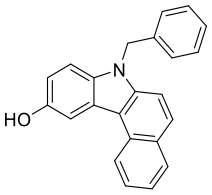

Following the same procedures used as that of **79a**. **79f** (80% yield): a white solid. **^{1}H NMR** (400 MHz, $CDCl_3$): δ 8.71 (d, J = 8.2 Hz, 1H), 8.06 (d, J = 2.3 Hz, 1H), 7.99 (d, J = 8.2 Hz, 1H), 7.85 (d, J = 8.7 Hz, 1H), 7.71 (ddd, J = 8.0, 7.6, 1.4 Hz, 1H), 7.58 (d, J = 9.2 Hz, 1H), 7.46 (ddd, J = 7.8, 7.3, 0.9 Hz, 1H), 7.36 (d, J = 8.7 Hz, 1H), 7.22-7.25 (m, 3H), 7.09 (d, J = 7.8 Hz, 2H), 7.02 (dd, J = 8.7, 2.3 Hz, 1H), 5.64 (s, 2H), 4.78 (s, 1H). **^{13}C NMR** (100 MHz, $CDCl_3$): δ 149.86, 139.01, 137.33, 134.8:6, 130.09, 129.31, 129.13, 128.61, 127.61, 127.33, 127.10, 126.29, 124.22, 122.99, 122.92, 114.64, 113.58, 111.07, 110.19, 107.68, 46.68. **HRMS** (APCI): calcd for $C_{23}H_{18}NO$: *m/z* 324.1383 $[M + H]^+$, found 324.1380. **IR** (KBr): 3335, 3061, 3033, 2926, 1698, 1620, 1475, 1353, 1170, 801 cm^{-1}. **mp**: 92-94 °C.

Synthesis of 79g-h

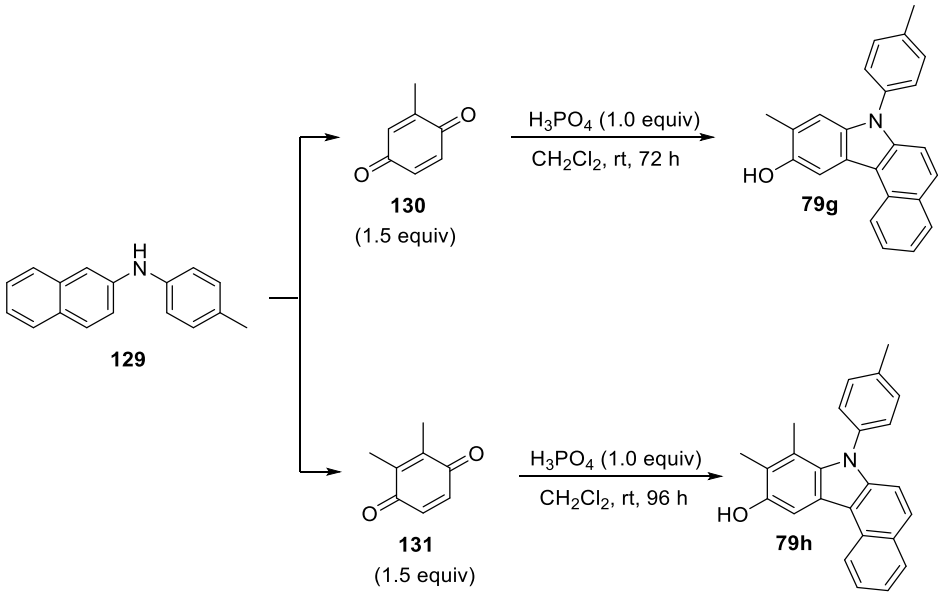

9-Methyl-7-(*p*-tolyl)-7*H*-benzo[*c*]carbazol-10-ol **79g**/8,9-Dimethyl-7-(*p*-tolyl)-7*H*-benzo[*c*]carbazol-10-ol **79h**

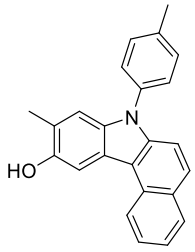

A mixture of **129** (582.8 mg, 2.5 mmol), corresponding dione **130**/**131** (3.75 mmol), and orthophosphoric acid (130 µL, 2.5 mmol) in CH_2Cl_2 (25.0 mL) was stirred at rt. After stirring for 72 h, the reaction mixture was quenched by water and further extracted with CH_2Cl_2. The combined organic extracts were washed with brine and dried over anhydrous Na_2SO_4, filtered, and evaporated *in vacuo*. The residue was purified by silica-gel column chromatography to afford **79g** (85% yield)/**79h** (70% yield) as white solids. **^{1}H NMR** (400 MHz, $CDCl_3$): δ 8.70 (d, J = 8.2 Hz, 1H), 8.01 (s, 1H), 7.98 (d, J = 8.2 Hz, 1H), 7.78 (d, J = 8.7 Hz, 1H), 7.69 (t, J = 7.6 Hz, 1H), 7.50 (d, J = 8.7 Hz, 1H), 7.44-7.48 (m, 5H), 7.23 (s, 1H), 4.79 (s, 1H), 2.52 (s, 3H), 2.43 (s, 3H). **^{13}C NMR** (100 MHz, $CDCl_3$): 148.83,

138.93, 137.75, 135.73, 135.03, 130.60, 129.84, 129.30, 129.24, 127.59, 126.84, 123.15, 122.91, 122.52, 122.36, 115.05, 111.98, 111.86, 107.02, 21.40, 17.06 (One carbon overlapped). **HRMS** (APCI): calcd for $C_{24}H_{20}NO$: *m/z* 338.1539 $[M + H]^+$, found 338.1533. **IR** (KBr): 3393, 3059, 3035, 2920, 2858, 1620, 1517, 1260, 1176, 803 cm^{-1}. **mp**: 73-74 °C.

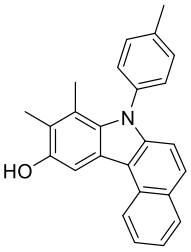

^{1}H NMR (400 MHz, $CDCl_3$): δ 8.72 (d, J = 8.7 Hz, 1H), 7.95-7.97 (m, 2H), 7.67-7.72 (m, 2H), 7.45 (t, J = 7.3 Hz, 1H), 7.36 (d, J = 8.2 Hz, 2H), 7.31 (d, J = 7.8 Hz, 2H), 7.22 (d, J = 8.7 Hz, 1H), 4.80 (s, 1H), 2.51 (s, 3H), 2.36 (s, 3H), 2.03 (s, 3H). **^{13}C NMR** (100 MHz, $CDCl_3$): δ 148.66, 141.26, 138.25, 137.89, 135.22, 130.09, 129.68, 129.41, 129.28, 129.21, 126.79, 126.77, 123.12, 122.85, 121.72, 121.61, 114.73, 112.37, 104.78, 21.45, 15.70, 12.52 (One carbon overlapped). **HRMS** (APCI): calcd for $C_{25}H_{22}NO$: *m/z* 352.1696 $[M + H]^+$, found 352.1694. **IR** (KBr): 3465, 3071, 2955, 2924, 2861, 1621, 1513, 1443, 1202, 822 cm^{-1}. **mp**: 90-92 °C.

Synthesis of 79i

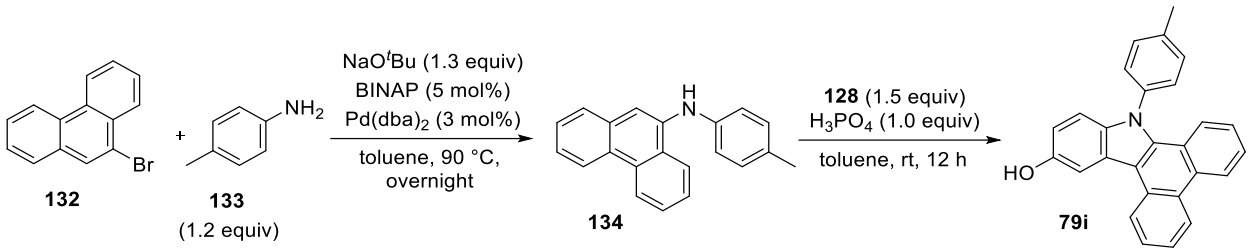

N-(*p*-Tolyl)phenanthren-9-amine **134**

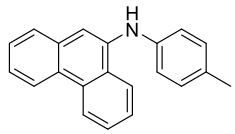

A toluene solution (30 mL) of **132** (30 mmol), *p*-toluidine **133** (3.8 g, 36 mmol), $Pd(dba)_2$ (3 mol%), BINAP (5 mol%), and NaO*t*-Bu (4.5 g, 40 mmol) was stirred at 90 °C under N_2 atmosphere. After stirring for 12 h, the reaction mixture was filtered and the filtrate was directly purified on silica-gel to give **134** (54% yield). **^{1}H NMR** (400 MHz, $CDCl_3$): δ 8.75 (d, J = 7.8 Hz, 1H), 8.62 (dd, J = 6.4, 2.8 Hz, 1H), 8.14 (d, J = 8.2 Hz, 1H), 7.67-7.72 (m, 2H), 7.63 (ddd, J = 7.8, 7.3, 0.9 Hz, 1H), 7.51-7.54 (m, 2H), 7.49 (s, 1H), 7.14 (d, J = 7.8 Hz, 2H), 7.02 (d, J = 8.2 Hz, 2H), 5.89 (s, 1H), 2.34 (s, 3H). **^{13}C NMR** (100 MHz, $CDCl_3$): δ 141.73, 137.87, 132.78, 131.44, 130.58, 129.98, 127.77, 127.41, 127.37, 126.92, 126.83, 126.58, 124.70, 123.31, 122.51, 122.14, 119.03, 112.67, 20.79. **HRMS** (APCI): calcd for $C_{21}H_{18}N$: *m/z* 284.1434 $[M + H]^+$, found 284.1439. **IR** (KBr): 3411, 3052, 3024, 2911, 2862, 1600, 1518, 1325, 1239, 818 cm^{-1}. **mp**: 110-112 °C.

9-(*p*-Tolyl)-9*H*-dibenzo[*a,c*]carbazol-12-ol **79i**

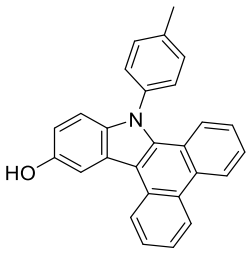

Following the same procedures as that of **79g**. **79i** (52% yield): a white solid. **^{1}H NMR** (400 MHz, $CDCl_3$): δ 8.77-8.81 (m, 3H), 8.07 (d, J = 2.3 Hz, 1H), 7.78 (ddd, J = 7.8, 7.3, 1.4 Hz, 1H), 7.60 (ddd, J = 7.8, 7.3, 0.9 Hz, 1H), 7.52-7.58 (m, 2H), 7.44 (d, J = 8.2 Hz, 2H), 7.38 (dd, J = 6.4, 1.8 Hz, 2H), 7.29 (ddd, J = 7.8, 7.3, 0.9 Hz, 1H), 7.07 (d, J = 9.2 Hz, 1H), 6.93 (dd, J = 8.7, 2.3 Hz, 1H), 4.82 (s, 1H), 2.56 (s, 3H). **^{13}C NMR** (100 MHz, $CDCl_3$): δ 150.52, 138.93, 137.75, 135.47, 131.01, 130.94, 130.08, 128.87, 127.47, 127.26, 126.02, 125.88, 124.28, 123.92, 123.89, 123.68, 123.60, 123.51, 123.37, 113.69, 113.33, 111.79, 106.92, 21.57 (One carbon overlapped). **HRMS** (APCI): calcd for $C_{27}H_{20}NO$: *m/z* 374.1539 $[M + H]^+$, found 374.1537. **IR** (KBr): 3382, 3086, 3034, 2924, 1701, 1609, 1512, 1375, 1202, 908 cm^{-1}. **mp**: 73-75 °C.

Synthesis of 79j

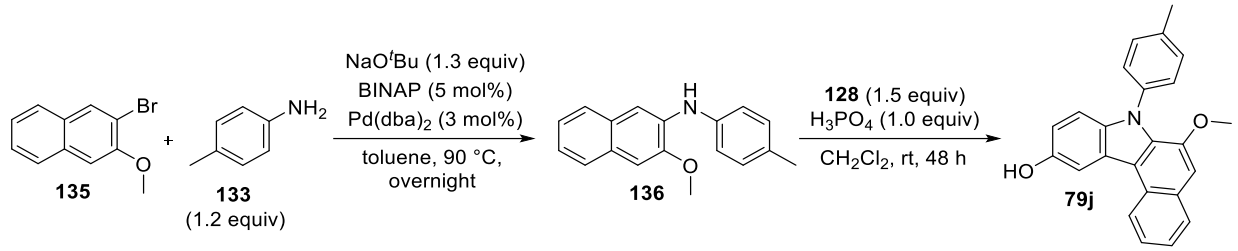

3-Methoxy-*N*-(*p*-tolyl)naphthalen-2-amine **136**

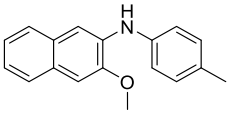

136 (89% yield): a white solid. **^{1}H NMR** (400 MHz, $CDCl_3$): δ 7.65 (dd, J = 7.8, 1.8 Hz, 1H), 7.55 (dd, J = 8.2, 1.8 Hz, 1H), 7.44 (s, 1H), 7.24-7.29 (m, 2H), 7.16-7.22 (m, 4H), 7.11 (s, 1H), 6.35 (s, 1H), 4.03 (s, 3H), 2.36 (s, 3H). **^{13}C NMR** (100 MHz, $CDCl_3$): δ 148.50, 139.28, 134.62, 131.98, 130.06, 129.81, 128.40, 126.36, 125.89, 124.22, 123.15, 120.77, 106.98, 105.33, 55.75, 20.94. **HRMS** (APCI): calcd for $C_{18}H_{18}NO$: *m/z* 264.1383 $[M + H]^+$, found 264.1382. **IR** (KBr): 3419, 3007, 2982, 2938, 2917, 1608, 1524, 1257, 1017, 751 cm^{-1}. **mp**: 76-78 °C.

6-Methoxy-7-(*p*-tolyl)-7*H*-benzo[*c*]carbazol-10-ol **79j**

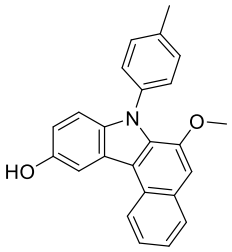

Following the same procedures as that of **79g**. **79j** (56% yield): a white solid. **^{1}H NMR** (400 MHz, $CDCl_3$): δ 8.66 (d, J = 8.2 Hz, 1H), 8.04 (d, J = 1.8 Hz, 1H), 7.87 (d, J = 8.0 Hz, 1H), 7.57 (ddd, J = 7.8, 7.3, 0.9 Hz, 1H), 7.44 (ddd, J = 7.8, 7.3, 0.9 Hz, 1H), 7.28-7.33 (m, 4H), 7.13 (d, J = 9.2 Hz, 1H), 7.11 (s, 1H), 6.95 (dd, J = 8.6, 2.2 Hz, 1H), 4.90 (s, 1H), 3.75 (s, 3H), 2.49 (s, 3H). **^{13}C NMR** (100 MHz, $CDCl_3$): δ 150.23, 147.81, 137.38, 137.29, 137.16, 131.41, 130.20, 129.13, 128.36, 127.66, 126.02, 124.61, 124.23, 123.53, 122.87, 117.12, 113.83, 111.78, 107.14, 104.83, 55.55, 21.43. **HRMS** (APCI): calcd for $C_{24}H_{20}NO_2$: *m/z* 354.1489 $[M + H]^+$, found 354.1486. **IR** (KBr): 3362, 3033, 2933, 2832, 1698, 1515, 1448, 1271, 1197, 812 cm^{-1}. **mp**: 75-77 °C.

Synthesis of 79k

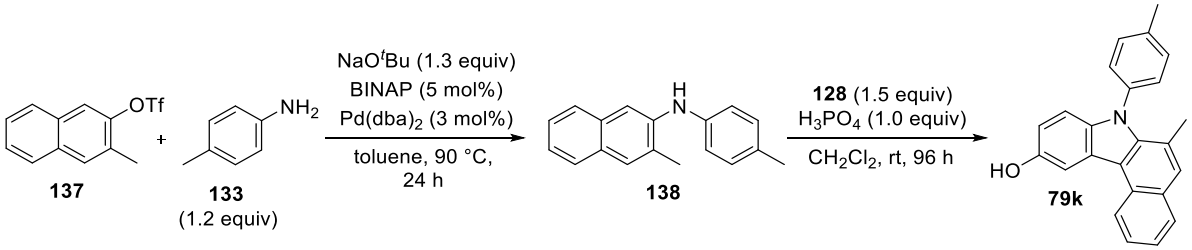

3-Methyl-*N*-(*p*-tolyl)naphthalen-2-amine **138**

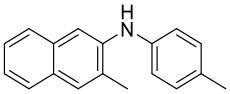

A coupling **137** with **133** was performed under the reported Buchwald–Hartwig amination conditions. **138** (82% yield): a white solid. **^{1}H NMR** (400 MHz, $CDCl_3$): δ 7.68 (d, J = 8.2 Hz, 1H), 7.64 (s, 1H), 7.58 (d, J = 8.2 Hz, 1H), 7.48 (s, 1H), 7.33 (ddd, J = 7.8, 7.3, 0.9 Hz, 1H), 7.27 (ddd, J = 7.8, 7.3, 0.9 Hz, 1H), 7.16 (d, J = 8.5 Hz, 2H), 7.08 (d, J = 8.2 Hz, 2H), 5.49 (s, 1H), 2.44 (s, 3H), 2.35 (s, 3H). **^{13}C NMR** (100 MHz, $CDCl_3$): δ 141.37, 140.50, 133.46, 131.51, 130.10, 129.13, 129.08, 127.71, 126.94, 126.22, 125.57, 123.37, 120.03, 110.38, 20.90, 18.45. **HRMS** (APCI): calcd for $C_{18}H_{18}N$: *m/z* 248.1434 $[M + H]^+$, found 248.1430. **IR** (KBr): 3423, 3055, 3019, 2918, 2860, 1613, 1524, 1313, 1248, 813 cm^{-1}. **mp**: 79-81 °C.

6-Methyl-7-(*p*-tolyl)-7*H*-benzo[*c*]carbazol-10-ol **79k**

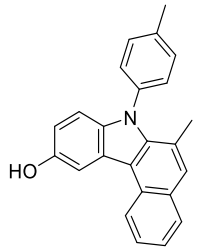

Following the same procedures used as that of **79g**. **79k** (69% yield): a white solid. **^{1}H NMR** (400 MHz, $CDCl_3$): δ 8.71 (d, J = 8.2 Hz, 1H), 8.07 (s, 1H), 7.90 (d, J = 7.8 Hz, 1H), 7.64 (ddd, J = 7.8, 7.3, 1.8 Hz, 1H), 7.54 (s, 1H), 7.45 (ddd, J = 8.1, 7.1, 2.3 Hz, 1H), 7.24-7.31 (m, 4H), 7.00 (dd, J = 8.7, 3.2 Hz, 1H), 6.94 (dt, J = 8.7, 2.8 Hz, 1H), 4.97 (s, 1H), 2.51 (s, 3H), 2.13 (s, 3H). **^{13}C NMR** (100 MHz, $CDCl_3$): δ 150.13, 139.27, 138.69, 137.70, 137.12, 129.88, 129.53, 129.33, 129.04, 128.77, 128.24, 126.16, 123.99, 123.36, 123.11, 122.84, 115.61, 113.51, 111.54, 107.14, 21.48, 20.64. **HRMS** (APCI): calcd for $C_{24}H_{20}NO$: *m/z* 338.1539 $[M + H]^+$, found 338.1536. **IR** (KBr): 3370, 3035, 2959, 2924, 1700, 1620, 1515, 1378, 1171, 740 cm^{-1}. **mp**: 82-84 °C.

Synthesis of 79l

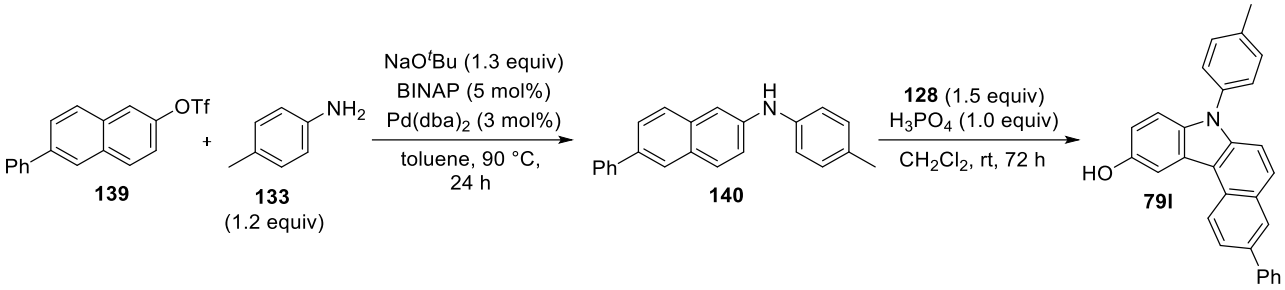

6-Phenyl-*N*-(*p*-tolyl)naphthalen-2-amine **140**

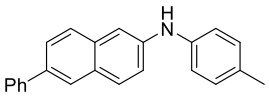

A coupling of **139** and **133** was performed following the same procedures used as that of **134**. **140** (51% yield): a white solid. **^{1}H NMR** (400 MHz, $CDCl_3$): δ 7.93 (s, 1H), 7.78 (d, J = 9.2 Hz, 1H), 7.67-7.71 (m, 4H), 7.47 (ddd, J = 7.8, 7.3, 1.4 Hz, 2H), 7.38 (d, J = 2.3 Hz, 1H), 7.35 (tt, J = 7.3, 1.5 Hz, 1H), 7.20 (dd, J = 8.7, 2.3 Hz, 1H), 7.10-7.16 (m, 4H), 5.82 (s, 1H), 2.34 (s, 3H). **^{13}C NMR** (100 MHz, $CDCl_3$): δ 142.02, 141.43, 140.10, 135.98, 134.07, 131.63, 130.11, 129.60, 129.17, 128.93, 127.26, 127.07, 126.99, 126.20, 125.70, 120.06, 119.61, 110.02, 20.90. **HRMS** (APCI): calcd for $C_{23}H_{20}N$: *m/z* 310.1590 $[M + H]^+$, found 310.1586. **IR** (KBr): 3421, 3060, 3021, 2922, 2857, 1605, 1523, 1445, 1307, 816 cm^{-1}. **mp**: 162-163 °C.

3-Phenyl-7-(*p*-tolyl)-7*H*-benzo[*c*]carbazol-10-ol **79l**

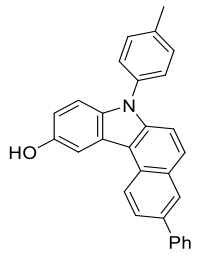

Following the same procedures used as that of **79g**. **79l** (61% yield): a white solid. **^{1}H NMR** (400 MHz, $CDCl_3$): δ 8.77 (d, J = 8.7 Hz, 1H), 8.20 (d, J = 1.8 Hz, 1H), 8.09 (d, J = 2.3 Hz, 1H), 7.98 (dd, J = 8.7, 1.8 Hz, 1H), 7.86 (d, J = 9.2 Hz, 1H), 7.79 (dd, J = 7.3,1.37 Hz, 2H), 7.49-7.55 (m, 3H), 7.43-7.46 (m, 4H), 7.38-7.41 (tt, J = 5.8, 1.15 Hz, 1H), 7.36 (d, J = 8.7 Hz, 1H), 7.01 (dd, J = 8.7, 2.3 Hz, 1H), 4.86 (s, 1H), 2.51 (s, 3H). **^{13}C NMR** (100 MHz, $CDCl_3$): δ 150.26, 141.42, 139.61, 137.90, 135.78, 135.68, 134.87, 130.63, 129.68, 129.15, 129.00, 127.85, 127.55, 127.40, 127.26, 127.13, 126.48, 124.41, 123.64, 114.90, 113.75, 112.44, 111.22, 107.45, 21.40. **HRMS** (APCI): calcd for $C_{29}H_{22}NO$: *m/z* 400.1696 $[M + H]^+$, found 400.1692. **IR** (KBr): 3355, 3058, 3032, 2922, 1698, 1588, 1516, 1366, 1167, 802 cm^{-1}. **mp**: 112-114 °C.

Synthesis of 79m

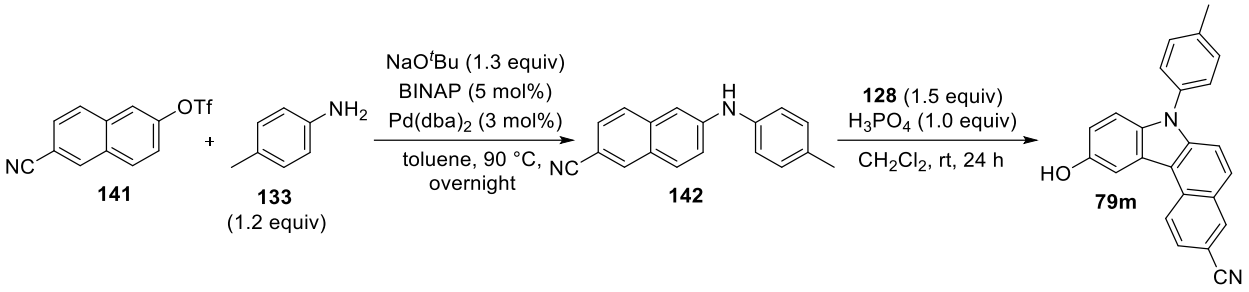

6-(*p*-tolylamino)-2-naphthonitrile **142**

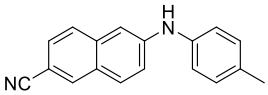

A coupling of **141** with **133** was performed following the same procedures as that of **134**. **142** (72% yield): a yellow solid. **^{1}H NMR** (600 MHz, $CDCl_3$): δ 8.05 (s, 1H), 7.73 (d, J = 8.9 Hz, 1H), 7.60 (d, J = 8.2 Hz, 1H), 7.47 (dd, J = 8.6, 1.7 Hz, 1H), 7.28 (d, J = 9.1 Hz, 1H), 7.18-7.22 (m, 3H), 7.13-7.16 (m, 2H), 5.99 (s, 1H), 2.37 (s, 3H). **^{13}C NMR** (150 MHz, $CDCl_3$): δ 145.27, 138.34, 136.73, 133.91, 133.41, 130.29, 129.99, 127.24, 127.22, 127.16, 121.35, 120.27, 120.12, 107.83, 105.48, 21.01. **HRMS** (APCI): calcd for $C_{18}H_{15}N_2$: m/z 259.1230 $[M + H]^+$, found 259.1230. **IR** (KBr): 3357, 3060, 3026, 2914, 2857, 2217, 1533, 1407, 1314, 816 cm^{-1}. **mp**: 170-172 °C.

10-Hydroxy-7-(p-tolyl)-7H-benzo[c]carbazole-3-carbonitrile **79m**

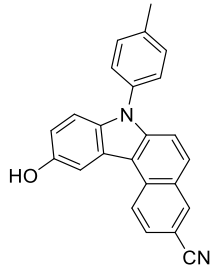

Following the same procedures used as that of **79g**. **79m** (52% yield): a yellow solid. **^{1}H NMR** (600 MHz, $(CD_3)_2CO$): δ 8.87 (d, J = 8.2 Hz, 1H), 8.54 (s, 1H), 8.34 (s, 1H), 8.09 (s, 1H), 8.00 (d, J = 8.9 Hz, 1H), 7.96 (d, J = 8.2 Hz, 1H), 7.64 (d, J = 8.9 Hz, 1H), 7.51-7.58 (m, 4H), 7.34 (d, J = 8.9 Hz, 1H), 7.11 (d, J = 8.2 Hz, 1H), 2.51 (s, 3H). **^{13}C NMR** (150 MHz, $(CD_3)_2CO$): δ 152.80, 140.44, 138.35, 134.82, 134.27, 131.63, 130.76, 128.37, 127.85, 127.39, 124.06, 123.86, 119.37, 114.87, 114.56, 113.71, 112.20, 111.36, 110.60, 106.75, 105.68, 20.41. **HRMS** (APCI): calcd for $C_{24}H_{17}N_2O$: m/z 349.1335 $[M + H]^+$, found 349.1323. **IR** (KBr): 3375, 3028, 3005, 2975, 2220, 1675, 1534, 1513, 1180, 798 cm^{-1}. **mp**: 135-137 °C.

Synthesis of 79n

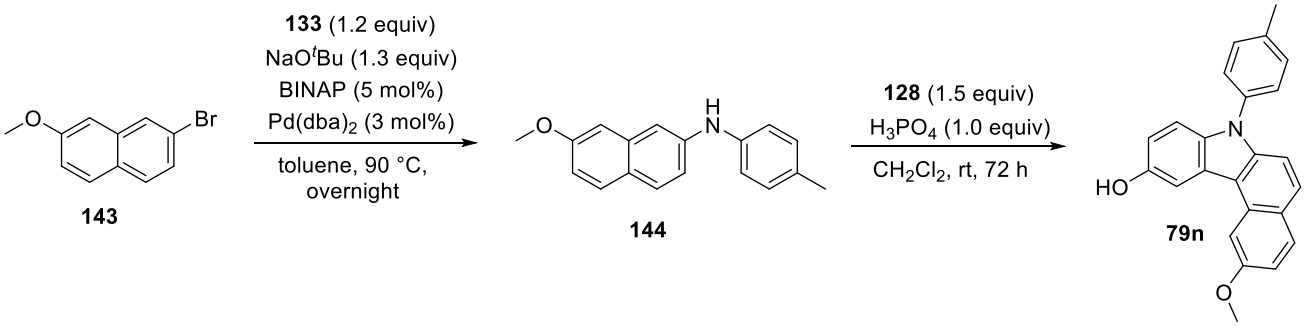

7-Methoxy-*N*-(*p*-tolyl)naphthalen-2-amine **144**

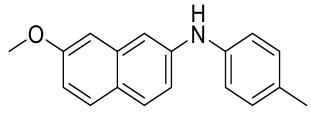

A coupling of **143** and **133** was performed following the same procedures used as that of **134**. **144** was obtained in 72% yield as a white solid. **^{1}H NMR** (400 MHz, $CDCl_3$): δ 7.60-7.65 (m, 2H), 7.26 (d, J = 2.3 Hz, 1H), 7.14 (d, J = 8.7 Hz, 2H), 7.10 (d, J = 8.3 Hz, 2H), 7.02 (dd, J = 8.7, 2.3 Hz, 1H), 6.93-6.96 (m, 2H), 5.75 (s, 1H), 3.89 (s, 3H), 2.34 (s, 3H). **^{13}C NMR** (100 MHz, $CDCl_3$): δ 158.36, 142.51, 140.18, 136.12, 131.56, 130.07, 129.25, 129.05, 124.38, 119.74, 117.16, 115.86, 109.45, 104.79, 55.35, 20.91. **HRMS** (APCI): calcd for $C_{18}H_{18}NO$: m/z 264.1383 $[M + H]^+$, found 264.1378. **IR** (KBr): 3387, 3027, 2998, 2922, 2861, 1631, 1514, 1214, 1030, 817 cm^{-1}. **mp**: 78-80 °C.

2-Methoxy-7-(*p*-tolyl)-7*H*-benzo[*c*]carbazol-10-ol **79n**

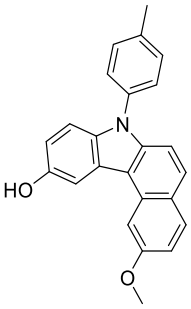

Following the same procedures used for preparation of compound **79g**. **79n** was obtained in 56% yield as a white solid. **^{1}H NMR** (600 MHz, $CDCl_3$): δ 8.01 (d, J = 2.1 Hz, 1H), 7.99 (d, J = 2.1 Hz, 1H), 7.88 (d, J = 8.9 Hz, 1H), 7.73 (d, J = 8.9 Hz, 1H), 7.40-7.44 (m, 4H), 7.36 (d, J = 8.9 Hz, 1H), 7.33 (d, J = 8.3 Hz, 1H), 7.13 (dd, J = 8.6, 1.7 Hz, 1H), 6.98 (dd, J = 8.6, 1.7 Hz, 1H), 5.13 (s, 1H), 4.06 (s, 3H), 2.50 (s, 3H). **^{13}C NMR** (150 MHz, $CDCl_3$): δ 158.88, 150.05, 140.09, 137.81, 135.61, 134.92, 131.20, 130.76, 130.59, 127.55, 127.35, 124.52, 124.35, 114.33, 114.22, 113.26, 111.00, 109.47, 107.14, 103.33, 55.61, 21.40. **HRMS** (APCI): calcd for $C_{24}H_{20}NO_2$: m/z 354.1489 $[M + H]^+$, found 354.1489. **IR** (KBr): 3381, 3035, 2954, 2923, 2853, 1624, 1516, 1228, 1157, 814 cm^{-1}. **mp**: 82-84 °C.

General procedure for the sequential preparation of dehydrohelicenes

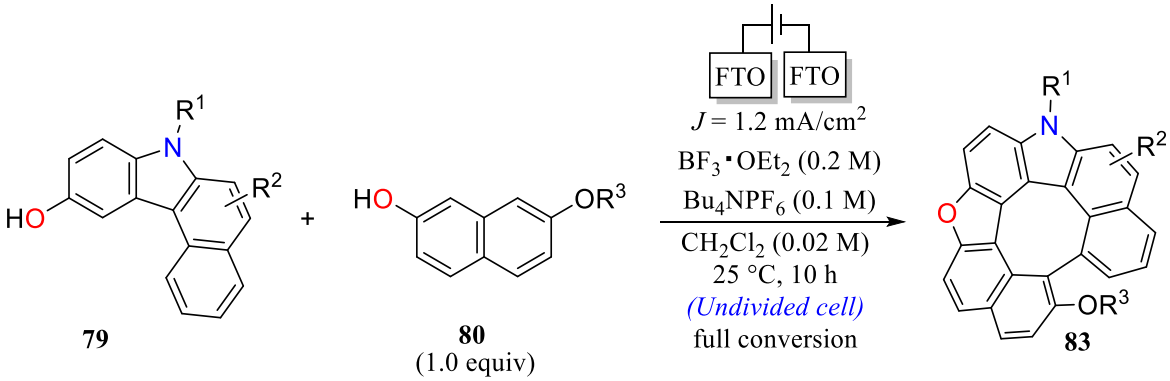

A solution of benzo[*c*]carbazol-10-ol derivatives **79** (0.1 mmol), 2-naphthols **80** (0.1 mmol), tetrabutylammonium hexafluorophosphate(V) (193.7 mg, 0.5 mmol) and $BF_3 \cdot EtO_2$ (0.2 M) in CH_2Cl_2 (5.0 mL) was transferred into an undivided electrolysis cell. This cell is equipped with two FTO electrodes (1.0 × 2.5 cm^2), which are connected to DC power supply. At rt, a constant current electrolysis with a current density of 1.20 mA/cm^2 was applied. After stirring for 10 h, the electrolysis was stopped and purification of the crude products by column chromatography (SiO_2, EtOAc/hexane) provided the desired dehydro[7]helicene **83**.

Dehydro[7]helicene **83aa**

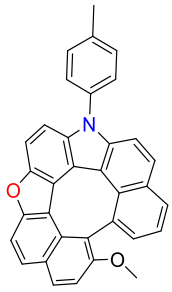

83aa (81% yield): a yellow solid.**^{1}H NMR** (400 MHz, $CDCl_3$): δ 7.93 (dd, J = 7.6, 1.1 Hz, 1H), 7.89 (d, J = 8.7 Hz, 1H), 7.84 (d, J = 8.7 Hz, 1H), 7.80 (d, J = 8.7 Hz, 1H), 7.71 (d, J = 8.7 Hz, 1H), 7.53 (d, J = 9.4 Hz, 1H), 7.50 (d, J = 8.7 Hz, 1H), 7.41-7.45 (m, 4H), 7.31-7.35 (m, 3H), 7.25 (d, J = 8.7 Hz, 1H), 3.24 (s, 3H), 2.51 (s, 3H). **^{13}C NMR** (100 MHz, $CDCl_3$): δ 161.99, 156.28, 151.31, 140.73, 138.33, 137.32, 136.95, 135.06, 132.66, 130.83, 130.75, 130.70, 129.73, 128.77, 128.40, 128.05, 128.00, 127.73, 126.84, 126.80, 122.24, 120.20, 118.85, 118.17, 117.48, 115.84, 112.23, 111.54, 108.15, 107.99, 58.47, 21.45. **HRMS** (APCI): calcd for $C_{34}H_{22}NO_2$: *m/z* 476.1645 $[M + H]^+$, found 476.1638. **IR** (KBr): 2955, 2925, 2853, 2321, 1516, 1457, 1296, 1269, 1020, 819 cm^{-1}. **mp**: 310-312 °C.

11-(2-Hydroxy-7-methoxynaphthalen-1-yl)-7-(p-tolyl)-7*H*-benzo[c]carbazol-10-ol (**81aa**)

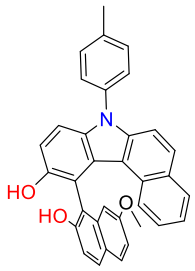

During the optimization of reaction conditions, intermediary diol **81aa** was formed as a yellow solid. **^{1}H NMR** (600 MHz, $CDCl_3$): δ 8.01 (d, J = 8.9 Hz, 1H), 7.88 (d, J = 8.9 Hz, 1H), 7.76 (d, J = 6.9 Hz, 1H), 7.72 (d, J = 8.9 Hz, 1H), 7.52 (d, J = 9.3 Hz, 1H), 7.47-7.51 (m, 4H), 7.43 (d, J = 8.9 Hz, 1H), 7.29 (d, J = 8.9 Hz, 1H), 7.20 (d, J = 8.9 Hz, 1H), 7.14 (ddd, J = 7.6, 6.9, 1.4 Hz, 1H), 7.06 (dd, J = 8.9, 2.7 Hz, 1H), 6.88 (d, J = 2.7 Hz, 1H), 6.76 (d, J = 8.9 Hz, 1H), 6.67 (ddd, J = 7.6, 6.9, 1.4 Hz, 1H), 5.25 (s, 1H), 4.95 (s, 1H), 3.61 (s, 3H), 2.55 (s, 3H). **^{13}C NMR** (150 MHz, $(CD_3)_2CO$): δ 159.22, 155.27, 150.99, 140.59, 139.05, 137.42, 136.76, 135.63, 131.54, 130.62, 130.53, 130.46, 130.38, 129.32, 128.99, 128.65, 126.34, 126.30, 125.68, 125.33, 122.92, 118.46, 117.37, 116.91, 115.49, 115.44, 114.95, 112.34, 111.84, 105.45, 55.03, 21.26. **HRMS** (APCI): calcd for $C_{34}H_{26}NO_3$: *m/z* 496.1907 $[M + H]^+$, found 496.1904. **IR** (KBr): 3498, 3331, 3059, 3032, 2940, 1624, 1516, 1276, 812, 747 cm^{-1}. **mp**: 275- 277 °C.

2-Methoxy-10-(*p*-tolyl)-10*H*-benzo[c]naphtho[1',2':4,5]furo[3,2-g]carbazole (**82aa**)

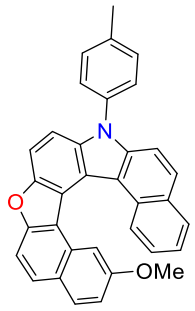

During the optimization of reaction conditions, intermediary helicene **82aa** was formed as a yellow solid. **^{1}H NMR** (400 MHz, $CDCl_3$): δ 8.49 (d, J = 8.2 Hz, 1H), 7.94 (d, J = 7.8 Hz, 1H), 7.91 (d, J = 8.7 Hz, 1H), 7.85 (d, J = 8.9 Hz, 1H), 7.84 (d, J = 9.2 Hz, 1H), 7.73 (d, J = 8.7 Hz, 1H), 7.71 (d, J = 8.7 Hz, 1H), 7.68 (d, J = 2.5 Hz, 1H), 7.58 (d, J = 8.7 Hz, 1H), 7.47-7.54 (m, 5H), 7.32 (ddd, J = 7.8, 7.3, 0.9 Hz, 1H), 7.02 (ddd, J = 7.8, 7.6, 1.2 Hz, 1H), 6.97 (dd, J = 8.7, 2.7 Hz, 1H), 2.62 (s, 3H), 2.55 (s, 3H). **^{13}C NMR** (100 MHz, $CDCl_3$): δ 154.58, 153.11, 139.16, 138.46, 138.30, 134.85, 130.77, 129.73, 129.50, 129.20, 128.57, 128.27, 128.13, 127.94, 127.91, 127.68, 124.86, 124.55, 124.25, 123.24, 120.17, 117.50, 117.40, 116.14, 112.61, 111.85, 109.29, 109.08, 29.85, 21.46 (Two carbons overlapped). **HRMS** (ESI): calcd for $C_{34}H_{24}NO_2$: *m/z* 478.1802 $[M + H]^+$, found 478.1792. **IR** (KBr): 3060, 2996, 2962, 2934, 1726, 1516, 1422, 1104, 1019, 803 cm^{-1}. **mp**: 276-278 °C.

Dehydro[7]helicene **83ba**

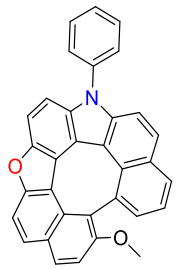

83ba (80% yield): a yellow solid. **^{1}H NMR** (400 MHz, $CDCl_3$): δ 7.96 (dd, J = 7.2, 1.9 Hz, 1H), 7.93 (d, J = 8.7 Hz, 1H), 7.88 (d, J = 8.7 Hz, 1H), 7.83 (d, J = 9.2 Hz, 1H), 7.73 (d, J = 8.7 Hz, 1H), 7.65-7.69 (m, 2H), 7.56-7.62 (m, 4H), 7.54 (d, J = 8.7 Hz, 1H), 7.31-7.38 (m, 3H), 7.28 (d, J = 8.7 Hz, 1H), 3.27 (s, 3H). **^{13}C NMR** (100 MHz, $(CDCl_3)$: δ 161.96, 156.31, 151.35, 140.57, 137.77, 137.35, 136.79, 132.68, 130.86, 130.79, 130.13, 129.75, 128.83, 128.50, 128.38, 128.24, 127.97, 127.71, 126.80, 126.78, 122.32, 120.16, 118.89, 118.25, 117.58, 115.76, 112.16, 111.55, 108.09, 58.44 (One carbon overlapped). **HRMS** (APCI): calcd for $C_{33}H_{20}NO_2$: *m/z* 462.1489 $[M + H]^+$, found 462.1483. **IR** (KBr): 3054, 2957, 2934, 2835, 1712, 1595, 1501, 1425, 1297, 821 cm^{-1}. **mp**: 312-314°C.

Dehydro[7]helicene **83ca**

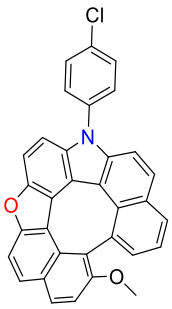

83ca (85% yield): a yellow solid. **^{1}H NMR** (600 MHz, $CDCl_3$): 7.95 (dd, J = 7.2, 1.7 Hz, 1H), 7.92 (d, J = 8.2 Hz, 1H), 7.87 (d, J = 8.9 Hz, 1H), 7.83 (d, J = 8.9 Hz, 1H), 7.72 (d, J = 8.9 Hz, 1H), 7.62 (d, J = 8.9 Hz, 2H), 7.52-7.55 (m, 3H), 7.49 (d, J = 8.9 Hz, 1H), 7.32-7.37 (m, 2H), 7.30 (d, J = 8.9 Hz, 1H), 7.27 (d, J = 8.9 Hz, 1H), 3.28 (s, 3H). **^{13}C NMR** (150 MHz, $CDCl_3$): δ 161.93, 156.35, 151.41, 140.36, 137.44, 136.60, 136.32, 134.10, 132.73, 130.91, 130.84, 130.40, 129.77, 129.52, 128.94, 128.70, 127.83, 127.65, 126.73, 122.48, 120.04, 118.98, 118.39, 117.81, 115.61, 111.79, 111.54, 108.22, 107.74, 58.35 (One carbon overlapped). **HRMS** (APCI): calcd for $C_{33}H_{19}ClNO_2$: *m/z* 496.1099 $[M + H]^+$, found 496.1092. **IR** (KBr): 3054, 2955, 2926, 2853, 1606, 1496, 1259, 1091, 819, 785 cm^{-1}. **mp**: 311-313 °C.

Dehydro[7]helicene **83da**

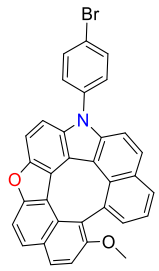

83da (79% yield): a yellow solid. **^{1}H NMR** (400 MHz, $CDCl_3$): δ 7.92-7.97 (m, 2H), 7.89 (d, J = 8.7 Hz, 1H), 7.85 (d, J = 9.2 Hz, 1H), 7.80 (d, J = 8.7 Hz, 2H), 7.73 (d, J = 8.7 Hz, 1H), 7.57 (d, J = 9.2 Hz, 1H), 7.49-7.51 (m, 3H), 7.32-7.36 (m, 3H), 7.29 (d, J = 8.7 Hz, 1H), 3.28 (s, 3H). **^{13}C NMR** (100 MHz, $CDCl_3$): δ 161.97, 156.38, 151.45, 140.32, 137.46, 136.88, 136.56, 133.40, 132.76, 131.03, 130.94, 130.84, 129.86, 129.78, 128.96, 128.72, 127.87, 127.68, 126.76, 122.50, 122.07, 120.06, 119.02, 118.45, 117.88, 115.67, 111.79, 111.56, 108.25, 107.76, 58.38. **HRMS** (APCI): calcd for $C_{33}H_{19}BrNO_2$: *m/z* 540.0594 $[M + H]^+$, found 540.0585. **IR** (KBr): 3054, 2957, 2928, 2854, 1731, 1605, 1493, 1259, 1022, 819 cm^{-1}. **mp**: 344-346 °C.

Dehydro[7]helicene **83ea**

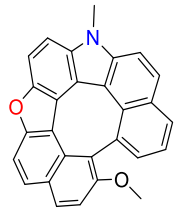

83ea (78% yield): a yellow solid. **^{1}H NMR** (400 MHz, $CDCl_3$): δ 7.96 (dd, J = 7.4, 1.7 Hz, 1H), 7.90-7.93 (m, 2H), 7.87 (d, J = 9.2 Hz, 1H), 7.73 (d, J = 7.3 Hz, 1H), 7.70 (d, J = 7.3 Hz, 1H), 7.64 (d, J = 8.7 Hz, 1H), 7.47 (d, J = 8.7 Hz, 1H), 7.28-7.35 (m, 3H), 4.05 (s, 3H), 3.24 (s, 3H). **^{13}C NMR** (150 MHz, $CDCl_3$): δ 161.95, 156.22, 150.93, 140.39, 137.30, 136.50, 132.37, 130.72, 130.30, 129.78, 128.77, 128.34, 128.13, 127.76, 126.92, 126.80, 122.02, 120.12, 118.95, 117.82, 117.10, 115.91, 111.53, 110.95, 107.73, 106.71, 58.51, 30.18. **HRMS** (APCI): calcd for $C_{28}H_{18}NO_2$: *m/z* 400.1332 $[M + H]^+$, found 400.1333. **IR** (KBr): 3039, 2957, 2927, 2853, 1518, 1460, 1259,1018, 819, 782 cm^{-1}. **mp**: 300-302 °C.

Dehydro[7]helicene **83fa**

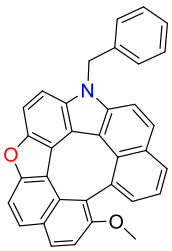

83fa (86% yield): a yellow solid. **^{1}H NMR** (400 MHz, $CDCl_3$): δ 7.95 (dd, J = 7.6, 1.6 Hz, 1H), 7.92 (d, J = 8.7 Hz, 1H), 7.87 (d, J = 8.7 Hz, 2H), 7.72 (d, J = 8.7 Hz, 1H), 7.65 (d, J = 9.2 Hz, 1H), 7.59 (d, J = 8.7 Hz, 1H), 7.41 (d, J = 8.7 Hz, 1H), 7.32-7.37 (m, 2H), 7.23-7.30 (m, 4H), 7.11-7.13 (m, 2H), 5.73 (s, 2H), 3.27 (s, 3H). **^{13}C NMR** (100 MHz, $CDCl_3$): δ 161.90, 156.30, 151.10, 139.93, 137.33, 137.20, 135.89, 132.47, 130.78, 130.53, 129.78, 128.98, 128.84, 128.56, 128.00, 127.73, 127.69, 126.90, 126.77, 126.37, 122.13, 120.09, 119.05, 118.03, 117.34, 115.62, 111.55, 111.24, 108.01, 107.14, 58.37, 47.18. **HRMS** (APCI): calcd for $C_{34}H_{22}NO_2$: *m/z* 476.1645 $[M + H]^+$, found 476.1640. **IR** (KBr): 3057, 2956, 2925, 1517, 1376, 1184, 1091, 819, 832, 755 cm^{-1}. **mp**: 320-322 °C.

Dehydro[7]helicene **83ga**

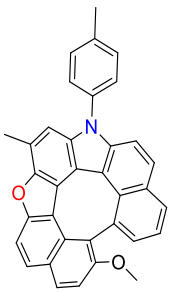

83ga (76% yield): a yellow solid. **^{1}H NMR** (600 MHz, $CDCl_3$): δ 7.95 (dd, J = 7.2, 1.7 Hz, 1H), 7.91 (d, J = 8.9 Hz, 1H), 7.86 (d, J = 8.9 Hz, 1H), 7.79 (d, J = 8.9 Hz, 1H), 7.75 (d, J = 8.9 Hz, 1H), 7.45-7.55 (m, 5H), 7.35 (dd, J = 7.2, 1.7 Hz, 1H), 7.33 (d, J = 7.6 Hz, 1H), 7.27 (d, J = 8.2 Hz, 1H), 7.16 (s, 1H), 3.24 (s, 3H), 2.70 (s, 3H), 2.54 (s, 3H). **^{13}C NMR** (150 MHz, $CDCl_3$): δ 161.99, 156.09, 150.37, 140.22, 138.23, 137.20, 137.14, 135.21, 132.67, 130.81, 130.69, 129.67, 128.57, 128.10, 128.05, 127.94, 127.66, 126.81, 126.77, 122.16, 120.48, 118.62, 118.23, 117.58, 116.27, 115.89, 112.19, 111.59, 108.66, 58.51, 21.46, 16.11 (One carbon overlapped). **HRMS** (APCI): calcd for $C_{35}H_{24}NO_2$: *m/z* 490.1802 $[M + H]^+$, found 490.1801. **IR** (KBr): 3036, 2955, 2925, 2854, 1516, 1456, 1292, 1258, 1017, 819 cm^{-1}. **mp**: 317-319 °C.

Dehydro[7]helicene **83ha**

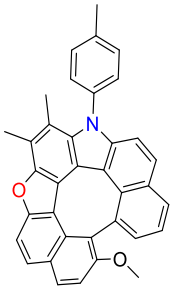

83ha (79% yield): a yellow solid. **^{1}H NMR** (600 MHz, $CDCl_3$): δ 7.92 (dd, J = 6.9, 2.1 Hz, 1H), 7.89 (d, J = 8.2 Hz, 1H), 7.83 (d, J = 8.9 Hz, 1H), 7.74 (d, J = 6.9 Hz, 1H), 7.72 (d, J = 6.9 Hz, 1H), 7.62-7.45 (m, 1H), 7.29-7.44 (m, 5H), 7.25 (d, J = 8.9 Hz, 1H), 7.23 (d, J = 8.9 Hz, 1H), 3.21 (s, 3H), 2.62 (s, 3H), 2.53 (s, 3H), 2.06 (s, 3H). **^{13}C NMR** (150 MHz, $CDCl_3$): δ 161.75, 155.57, 150.89, 142.18, 138.57, 137.98, 137.04, 136.27, 132.82, 130.86, 130.57, 130.09, 129.61, 128.12, 127.92, 127.83, 127.55, 126.71, 126.60, 122.15, 120.82, 118.31, 117.76, 117.33, 116.95, 116.00, 115.86, 112.63, 111.59, 58.58, 21.52, 15.58, 12.63 (One carbon overlapped). **HRMS** (APCI): calcd for $C_{36}H_{26}NO_2$: m/z 504.1958 $[M + H]^+$, found 504.1957. **IR** (KBr): 3043, 2953, 2924, 2854, 1602, 1514, 1167, 1019, 818, 750 cm^{-1}. **mp**: 335-337 °C.

Dehydro[7]helicene **83ia**

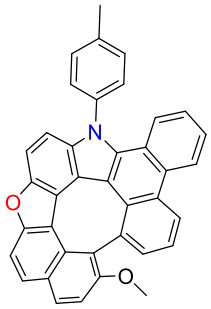

83ia (80% yield): a yellow solid. **^{1}H NMR** (600 MHz, $CDCl_3$): δ 8.67 (d, J = 8.2 Hz, 1H), 8.58 (d, J = 7.6 Hz, 1H), 7.94 (d, J = 8.2 Hz, 1H), 7.87 (d, J = 8.9 Hz, 1H), 7.72-7.74 (m, 2H), 7.54-7.59 (m, 2H), 7.50 (d, J = 8.9 Hz, 1H), 7.42 (dd, J = 8.3, 1.4 Hz, 1H), 7.39 (t, J = 7.9 Hz, 1H), 7.31 (dd, J = 8.3, 2.1 Hz, 1H), 7.27-7.29 (m, 2H), 7.23 (dd, J = 6.9, 1.4 Hz, 1H), 7.06 (d, J = 8.9 Hz, 1H), 6.90 (dd, J = 7.9, 2.4 Hz, 1H), 3.37 (s, 3H), 2.56 (s, 3H). **^{13}C NMR** (150 MHz, $CDCl_3$): δ 161.34, 156.23, 151.96, 139.14, 138.29, 137.14, 136.87, 135.59, 132.80, 132.27, 131.00, 130.76, 130.56, 129.56, 129.30, 128.81, 128.43, 127.65, 127.59, 127.50, 126.33, 126.27, 125.72, 124.77, 123.73, 123.39, 123.12, 122.54, 120.46, 118.42, 118.35, 116.32, 114.99, 111.55, 108.68, 107.75, 58.20, 21.61. **HRMS** (APCI): calcd for $C_{38}H_{24}NO_2$: *m/z* 526.1802 $[M + H]^+$, found 526.1792. **IR** (KBr): 3052, 2955, 2925, 2854, 1733, 1595, 1501, 1426, 1296, 821 cm^{-1}. **mp**: 325-327 °C.

Dehydro[7]helicene **83ja**

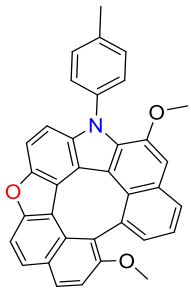

83ja (82% yield): a yellow solid. **^{1}H NMR** (600 MHz, $CDCl_3$): δ 7.91 (d, J = 8.2 Hz, 1H), 7.86 (d, J = 8.9 Hz, 1H), 7.83 (d, J = 7.6 Hz, 1H), 7.71 (d, J = 8.9 Hz, 1H), 7.51 (d, J = 8.9 Hz, 1H), 7.26-7.34 (m, 6H), 7.18 (d, J = 7.6 Hz, 1H), 7.13 (d, J = 8.9 Hz, 1H), 7.11 (s, 1H), 3.79 (s, 3H), 3.27 (s, 3H), 2.51 (s, 3H). **^{13}C NMR** (150 MHz, $CDCl_3$): δ 161.87, 156.25, 151.44, 147.43, 138.18, 137.77, 137.38, 135.04, 132.70, 132.08, 131.91, 130.59, 129.31, 128.64, 128.53, 128.46, 128.13, 127.96, 127.81, 126.67, 123.17, 122.76, 120.28, 119.60, 118.76, 118.08, 115.85, 111.52, 108.85, 108.25, 105.18, 58.54, 55.53, 21.51. **HRMS** (APCI): calcd for $C_{35}H_{24}NO_3$: *m/z* 506.1751 $[M + H]^+$, found 506.1744. **IR** (KBr): 3035, 2957, 2925, 2854, 1606, 1514, 1299, 1259, 1038, 819 cm^{-1}. **mp**: 319-321 °C.

Dehydro[7]helicene **83ka**

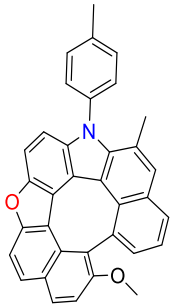

83ka (80% yield): a yellow solid. **^{1}H NMR** (600 MHz, $CDCl_3$): δ 7.91 (d, J = 8.2 Hz, 1H), 7.85-7.87 (m, 2H), 7.72 (d, J = 8.2 Hz, 1H), 7.56 (s, 1H), 7.53 (d, J = 7.6 Hz, 1H), 7.50 (d, J = 8.2 Hz, 1H), 7.40 (d, J = 8.2 Hz, 1H), 7.36 (d, J = 8.2 Hz, 1H), 7.27-7.31 (m, 3H), 7.24 (d, J = 8.2 Hz, 1H), 7.03 (d, J = 8.9 Hz, 1H), 3.24 (s, 3H), 2.53 (s, 3H), 2.16 (s, 3H). **^{13}C NMR** (150 MHz, $CDCl_3$): δ 161.84, 156.20, 151.47, 140.03, 139.02, 138.51, 137.18, 136.40, 132.29, 130.80, 130.58, 130.03, 129.83, 129.46, 129.41, 128.59, 128.53, 128.12, 127.75, 126.63, 125.98, 122.88, 122.33, 120.34, 118.60, 118.18, 117.78, 115.83, 111.52, 108.67, 107.93, 58.50, 21.53, 20.21. **HRMS** (APCI): calcd for $C_{35}H_{24}NO_2$: *m/z* 490.1802 $[M + H]^+$, found 490.1794. **IR** (KBr): 3047, 2959, 2935, 2844, 1723, 1585, 1505, 1429, 1298, 827 cm^{-1}. **mp**: 311-313 °C.

Dehydro[7]helicene **83la**

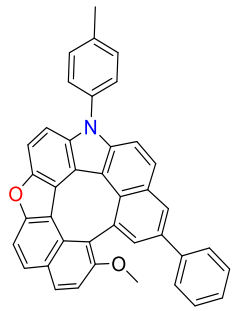

83la (84% yield): a yellow solid. **^{1}H NMR** (400 MHz, $CDCl_3$): δ 8.18 (s, 1H), 7.95 (d, J = 8.7 Hz, 1H), 7.89 (dd, J = 8.9, 1.6 Hz, 2H), 7.75 (d, J = 8.7 Hz, 1H), 7.64-7.69 (m, 3H), 7.56 (td, J = 8.3, 0.9 Hz, 2H), 7.41-7.50 (m, 6H), 7.36 (d, J = 9.6 Hz, 1H), 7.29-7.33 (m, 2H), 3.32 (s, 3H), 2.54 (s, 3H). **^{13}C NMR** (150 MHz, $CDCl_3$): δ 162.04, 156.38, 151.35, 140.87, 140.80, 138.40, 137.01, 136.89, 135.03, 134.75, 133.23, 131.17, 130.89, 130.74, 128.87, 128.84, 128.73, 128.00, 127.87, 127.75, 127.44, 127.22, 127.03, 126.77, 126.06, 120.09, 118.85, 118.06, 117.41, 115.50, 112.66, 111.59, 108.20, 108.11, 58.36, 21.48. **HRMS** (APCI): calcd for $C_{40}H_{26}NO_2$: *m/z* 552.1958 $[M + H]^+$, found 552.1955. **IR** (KBr): 3031, 2962, 2925, 2835, 1604, 1515, 1437, 1259, 1022, 796 cm^{-1}. **mp**: 338-340 °C.

Dehydro[7]helicene **83ma**

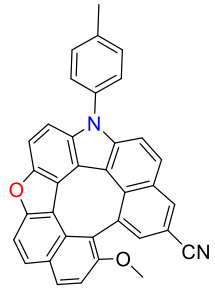

83ma (67% yield): a yellow solid. **^{1}H NMR** (400 MHz, $CDCl_3$): δ 8.26 (d, J = 1.4 Hz, 1H), 7.99 (d, J = 8.7 Hz, 1H), 7.89 (d, J = 8.7 Hz, 1H), 7.83 (d, J = 8.7 Hz, 1H), 7.74 (d, J = 8.7 Hz, 1H), 7.60 (d, J = 8.7 Hz, 1H), 7.59 (d, J = 9.2 Hz, 1H), 7.54 (d, J = 1.6 Hz, 1H), 7.47 (d, J = 7.3 Hz, 4H), 7.34 (d, J = 8.7 Hz, 1H), 7.31 (d, J = 8.7 Hz, 1H), 3.54 (s, 3H), 2.54 (s, 3H). **^{13}C NMR** (150 MHz, $CDCl_3$): δ 161.48, 156.59, 151.61, 144.08, 141.90, 138.94, 137.74, 137.08, 134.40, 134.05, 134.02, 131.76, 130.88, 129.15, 128.21, 127.24, 126.55, 125.56, 119.80, 119.63, 119.14, 118.91, 117.68, 117.46, 113.98, 113.59, 111.74, 108.90, 108.43, 104.78, 100.05, 57.46, 21.49. **HRMS** (APCI): calcd for $C_{35}H_{21}N_2O_2$: *m/z* 501.1598 $[M + H]^+$, found 501.1601. **IR** (KBr): 2954, 2925, 2870, 2853, 2224, 1712, 1600, 1516, 1260, 818 cm^{-1}. **mp**: 340-342 °C.

Dehydro[7]helicene **83na**

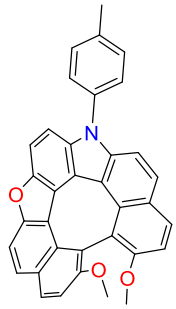

83na (27% yield): a yellow solid. **^{1}H NMR** (400 MHz, $CDCl_3$): δ 7.95 (d, J = 8.7 Hz, 1H), 7.91 (d, J = 8.7 Hz, 1H), 7.88 (d, J = 8.7 Hz, 1H), 7.76 (d, J = 9.2 Hz, 1H), 7.71 (d, J = 9.2 Hz, 1H), 7.54 (d, J = 8.7 Hz, 1H), 7.45 (s, 4H), 7.40 (d, J = 8.7 Hz, 1H), 7.31 (d, J = 8.7 Hz, 1H), 7.22 (d, J = 8.7 Hz, 1H), 7.15 (d, J = 8.7 Hz, 1H), 3.48 (s, 3H), 3.45 (s, 3H), 2.53 (s, 3H). **^{13}C NMR** (150 MHz, $CDCl_3$): δ 162.32, 162.09, 156.55, 151.56, 141.07, 138.26, 136.80, 135.15, 131.07, 130.96, 130.67, 128.81, 128.45, 128.19, 128.01, 127.88, 127.15, 126.17, 121.40, 120.50, 119.88, 119.19, 118.20, 117.61, 113.80, 112.09, 111.29, 110.41, 107.69, 107.67, 57.95, 29.85, 21.46. **HRMS** (APCI): calcd for $C_{35}H_{24}NO_3$: *m/z* 506.1751 $[M + H]^+$, found 506.1747. **IR** (KBr): 2958, 2922, 2851, 1712, 1596, 1516, 1457, 1261, 1024, 815 cm^{-1}. **mp**: 278-280 °C.

Dehydro[7]helicene **83ab**

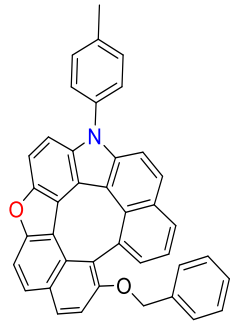

83ab (79% yield): a yellow solid. **^{1}H NMR** (600 MHz, $CDCl_3$): δ 7.98 (d, J = 7.6 Hz, 1H), 7.91 (d, J = 8.9 Hz, 1H), 7.88 (d, J = 8.9 Hz, 1H), 7.84 (d, J = 8.9 Hz, 1H), 7.75 (d, J = 8.9 Hz, 1H), 7.57 (d, J = 8.9 Hz, 1H), 7.54 (d, J = 8.9 Hz, 1H), 7.45-7.48 (m, 5H), 7.34-7.36 (m, 2H), 7.33 (d, J = 8.9 Hz, 1H), 7.18-7.21 (m, 3H), 6.93 (dd, J = 7.6, 2.1 Hz, 2H), 4.46 (d, J = 11.7 Hz, 1H), 4.07 (d, J = 11.7 Hz, 1H), 2.54 (s, 3H). **^{13}C NMR** (150 MHz, $CDCl_3$): δ 160.94, 156.26, 151.34, 140.77, 138.40, 137.66, 137.39, 136.97, 135.04, 132.47, 130.97, 130.82, 130.74, 129.85, 129.19, 128.78, 128.38, 128.21, 128.03, 127.74, 127.65, 127.48, 127.23, 126.93, 122.50, 120.33, 118.85, 118.17, 117.93, 117.46, 112.34, 111.81, 108.24, 108.07, 73.50, 21.48. **HRMS** (APCI): calcd for $C_{40}H_{26}NO_2$: *m/z* 552.1958 $[M + H]^+$, found 552.1956. **IR** (KBr): 3044, 2947, 2944, 2837, 1718, 1597, 1505, 1427, 1299, 823 cm^{-1}. **mp**: 332-334 °C.

Dehydro[7]helicene **83ac**

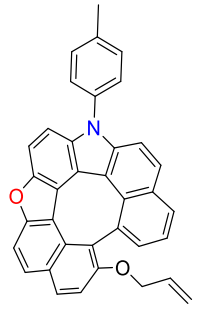

83ac (80% yield): a yellow solid. **^{1}H NMR** (600 MHz, $CDCl_3$): δ 7.95 (d, J = 6.9 Hz, 1H), 7.91 (d, J = 8.2 Hz, 1H), 7.88 (d, J = 8.9 Hz, 1H), 7.83 (d, J = 8.9 Hz, 1H), 7.74 (d, J = 8.9 Hz, 1H), 7.56 (d, J = 8.9 Hz, 1H), 7.53 (d, J = 8.9 Hz, 1H), 7.45-7.50 (m, 4H), 7.40 (dd, J = 6.9, 1.4 Hz, 1H), 7.32-7.35 (m, 2H), 7.29 (d, J = 8.2 Hz, 1H), 5.58-5.64 (m, 1H), 4.96 (dq, J = 10.7, 1.6 Hz, 1H), 4.89 (dq, J = 17.2, 1.6 Hz, 1H), 3.95-3.98 (m, 1H), 3.67-3.70 (m, 1H), 2.54 (s, 3H). **^{13}C NMR** (150 MHz, $CDCl_3$): δ 160.79, 156.25, 151.33, 140.73, 138.37, 137.53, 136.95, 135.06, 133.53, 132.47, 130.87, 130.72, 129.77, 128.93, 128.76, 128.39, 128.02, 127.71, 127.07, 126.86, 122.36, 120.28, 118.84, 118.15, 117.46, 117.35, 116.82, 112.25, 111.72, 108.19, 108.02, 72.16, 21.47 (One carbon overlapped). **HRMS** (APCI): calcd for $C_{36}H_{24}NO_2$: *m/z* 502.1802 $[M + H]^+$, found 502.1794. **IR** (KBr): 3038, 2961, 2924, 2855, 1725, 1604, 1516, 1260, 1018, 820 cm^{-1}. **mp**: 346-348 °C.

Dehydro[7]helicene **83bb**

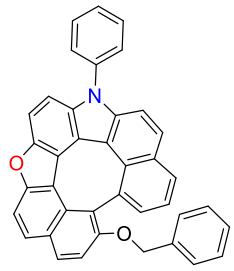

83bb (82% yield): a yellow solid. **^{1}H NMR** (400 MHz, $CDCl_3$): δ 7.98 (d, J = 6.9 Hz, 1H), 7.91 (d, J = 8.7 Hz, 1H), 7.89 (d, J = 9.2 Hz, 1H), 7.85 (d, J = 9.2 Hz, 1H), 7.75 (d, J = 8.7 Hz, 1H), 7.54-7.69 (m, 7H), 7.48 (dd, J = 6.9, 0.9 Hz, 1H), 7.35-7.38 (m, 2H), 7.33 (d, J = 8.2 Hz, 1H), 7.18-7.20 (m, 3H), 6.92-6.94 (m, 2H), 4.47 (d, J = 11.4 Hz, 1H), 4.09 (d, J = 11.9 Hz, 1H). **^{13}C NMR** (150 MHz, $CDCl_3$): δ 160.94, 156.29, 151.40, 140.63, 137.77, 137.69, 137.38, 136.84, 132.52, 131.03, 130.83, 130.15, 129.85, 129.15, 128.82, 128.45, 128.41, 128.26, 128.20, 127.74, 127.65, 127.46, 127.22, 126.92, 122.56, 120.31, 118.91, 118.29, 117.86, 117.61, 112.24, 111.81, 108.14, 73.47 (One carbon overlapped). **HRMS** (APCI): calcd for $C_{39}H_{24}NO_2$: *m/z* 538.1802 $[M + H]^+$, found 538.1794. **IR** (KBr): 3060, 3034, 2925, 2859, 1595, 1500, 1296, 1020, 820, 744 cm^{-1}. **mp**: 301-303 °C.

Dehydro[7]helicene **83bc**

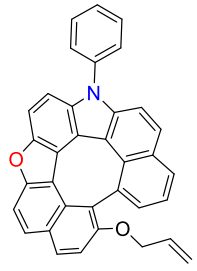

83bc (81% yield): a yellow solid. **^{1}H NMR** (600 MHz, $CDCl_3$): δ 7.96 (d, J = 8.2 Hz, 1H), 7.92 (d, J = 8.9 Hz, 1H), 7.89 (d, J = 8.9 Hz, 1H), 7.84 (d, J = 8.9 Hz, 1H), 7.75 (d, J = 8.9 Hz, 1H), 7.67 (t, J = 7.9 Hz, 2H), 7.60-7.63 (m, 2H), 7.56-7.58 (m, 2H), 7.54 (d, J = 8.9 Hz, 1H), 7.41 (dd, J = 6.9, 1.4 Hz, 1H), 7.37 (d, J = 8.9 Hz, 1H), 7.34 (t, J = 7.2 Hz, 1H), 7.29 (d, J = 8.9 Hz, 1H), 5.61 (qd, J = 10.9, 5.2 Hz, 1H), 4.96 (dd, J = 11.7, 1.4 Hz, 1H), 4.89 (dd, J = 17.2, 1.4 Hz, 1H), 3.97 (dd, J = 12.7, 5.2 Hz, 1H), 3.70 (dd, J = 12.7, 5.2 Hz, 1H). **^{13}C NMR** (150 MHz, $CDCl_3$) δ 160.79, 156.28, 151.38, 140.57, 137.77, 137.56, 136.80, 133.51, 132.51, 130.92, 130.74, 130.15, 129.79, 128.87, 128.82, 128.48, 128.40, 128.26, 127.70, 127.05, 126.84, 122.44, 120.27, 118.89, 118.25, 117.58, 117.29, 116.84, 112.17, 111.72, 108.12, 108.11, 72.13. **HRMS** (APCI): calcd for $C_{35}H_{22}NO_2$: *m/z* 488.1645 $[M + H]^+$, found 488.1645. **IR** (KBr): 3051, 2955, 2925, 2853, 1595, 1501, 1425, 1296, 821, 734 cm^{-1}. **mp**: 317-319 °C.

Dehydro[7]helicene **83cb**

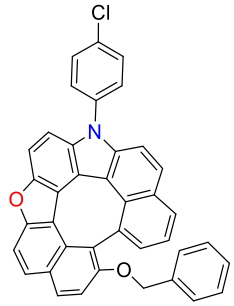

83cb (84% yield): a yellow solid. **^{1}H NMR** (600 MHz, $CDCl_3$): δ 7.98 (dd, J = 8.3, 1.4 Hz, 1H), 7.91 (d, J = 8.2 Hz, 1H), 7.88 (d, J = 8.9 Hz, 1H), 7.86 (d, J = 9.6 Hz, 1H), 7.75 (d, J = 8.9 Hz, 1H), 7.64 (d, J = 8.9 Hz, 2H), 7.54-7.58 (m, 3H), 7.51 (d, J = 8.9 Hz, 1H), 7.47 (dd, J = 6.9, 1.4 Hz, 1H), 7.36 (t, J = 7.6 Hz, 1H), 7.32-7.33 (m, 2H), 7.18-7.21 (m, 3H), 6.92-6.93 (m, 2H), 4.48 (d, J = 11.7 Hz, 1H), 4.11 (d, J = 11.7 Hz, 1H). **^{13}C NMR** (150 MHz, $CDCl_3$): δ 160.93, 156.34, 151.46, 140.43, 137.78, 137.32, 136.66, 136.31, 134.17, 132.57, 131.07, 130.88, 130.43, 129.88, 129.55, 128.99, 128.95, 128.66, 128.22, 127.70, 127.68, 127.42, 127.18, 126.84, 122.74, 120.20, 119.01, 118.44, 117.83, 117.75, 111.90, 111.81, 108.31, 107.85, 73.39. **HRMS** (APCI): calcd for $C_{39}H_{23}ClNO_2$: *m/z* 572.1412 $[M + H]^+$, found 572.1413. **IR** (KBr): 3033, 2955, 2925, 2855, 1605, 1495, 1292, 1091, 1017, 819 cm^{-1}. **mp**: 324-326 °C.

Dehydro[7]helicene **83cc**

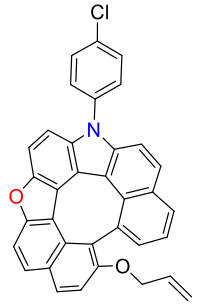

83cc (75% yield): a yellow solid. **^{1}H NMR** (600 MHz, $CDCl_3$): δ 7.95 (d, J = 6.9 Hz, 1H), 7.91 (d, J = 8.9 Hz, 1H), 7.88 (d, J = 8.9 Hz, 1H), 7.85 (d, J = 8.9 Hz, 1H), 7.74 (d, J = 8.9 Hz, 1H), 7.64 (d, J = 8.9 Hz, 2H), 7.54-7.57 (m, 3H), 7.50 (d, J = 8.9 Hz, 1H), 7.40 (dd, J = 7.6, 1.4 Hz, 1H), 7.35 (d, J = 7.6 Hz, 1H), 7.31 (d, J = 8.9 Hz, 1H), 7.28 (d, J = 8.9 Hz, 1H), 5.58-5.64 (m, 1H), 4.96 (dd, J = 10.7, 1.7 Hz, 1H), 4.88 (dd, J = 17.2, 1.4 Hz, 1H), 3.98 (dq, J = 13.6, 1.9 Hz, 1H), 3.72 (qd, J = 12.0, 4.8 Hz, 1H). **^{13}C NMR** (150 MHz, $CDCl_3$): δ 160.77, 156.33, 151.44, 140.37, 137.65, 136.63, 136.33, 134.15, 133.45, 132.57, 130.97, 130.80, 130.41, 129.81, 129.54, 128.93, 128.72, 128.68, 127.65, 127.02, 126.77, 122.60, 120.15, 119.00, 118.40, 117.81, 117.15, 116.84, 111.82, 111.72, 108.26, 107.80, 72.04. **HRMS** (APCI): calcd for $C_{35}H_{21}ClNO_2$: *m/z* 522.1255 $[M + H]^+$, found 522.1247. **IR** (KBr): 3049, 2955, 2925, 2855, 1496, 1425, 1298, 1091, 1016, 819 cm^{-1}. **mp**: 314-316 °C.

Dehydro[7]helicene **83db**

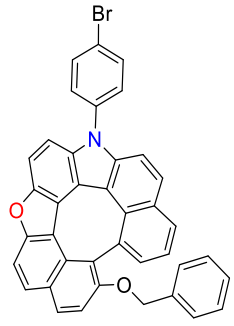

83db (81% yield): a yellow solid. **^{1}H NMR** (600 MHz, $CDCl_3$): δ 7.98 (dd, J = 7.6, 1.4 Hz, 1H), 7.91 (d, J = 8.9 Hz, 1H), 7.87 (d, J = 8.2 Hz, 1H), 7.86 (d, J = 8.9 Hz, 1H), 7.78 (d, J = 8.9 Hz, 2H), 7.74 (d, J = 8.9 Hz, 1H), 7.56 (d, J = 7.9 Hz, 1H), 7.46-7.51 (m, 4H), 7.36 (t, J = 7.6 Hz, 1H), 7.31-7.33 (m, 2H), 7.18-7.21 (m, 3H), 6.92 (dd, J = 7.2, 2.4 Hz, 2H), 4.48 (d, J = 11.7 Hz, 1H), 4.11 (d, J = 11.7 Hz, 1H). **^{13}C NMR** (150 MHz, $CDCl_3$) δ 160.90, 156.33, 151.45, 140.32, 137.77, 137.31, 136.83, 136.54, 133.40, 132.57, 131.07, 130.87, 129.87, 128.94, 128.65, 128.21, 127.67, 127.40, 127.15, 126.82, 122.74, 122.08, 120.17, 119.00, 118.45, 117.85, 117.70, 111.88, 111.79, 108.30, 107.82, 73.36 (Three carbons overlapped). **HRMS** (APCI): calcd for $C_{39}H_{23}BrNO_2$: *m/z* 616.0907 $[M + H]^+$, found 616.0909. **IR** (KBr): 3061, 3034, 2925, 2856, 1605, 1496, 1247, 1091, 1017, 819 cm^{-1}. **mp**: 348-350 °C.

Dehydro[7]helicene **83dc**

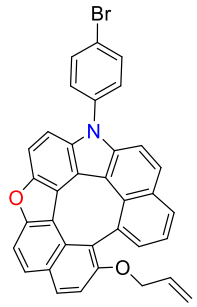

83dc (72% yield): a yellow solid. **^{1}H NMR** (400 MHz, $CDCl_3$): δ 7.96 (dd, J = 7.6, 1.1 Hz, 1H), 7.92 (d, J = 8.2 Hz, 1H), 7.89 (d, J = 8.7 Hz, 1H), 7.85 (d, J = 8.7 Hz, 1H), 7.80 (d, J = 8.7 Hz, 2H), 7.74 (d, J = 9.2 Hz, 1H), 7.57 (d, J = 8.7 Hz, 1H), 7.49-7.52 (m, 3H), 7.41 (dd, J = 7.3, 1.4 Hz, 1H), 7.32-7.36 (m, 2H), 7.29 (d, J = 8.7 Hz, 1H), 5.56-5.66 (m, 1H), 4.96 (dq, J = 10.5, 1.5 Hz, 1H), 4.88 (dq, J = 17.3, 1.7 Hz, 1H), 3.98 (dtd, J = 12.8, 3.3, 1.7 Hz, 1H), 3.71 (dtd, J = 12.8, 3.4, 1.7 Hz, 1H). **^{13}C NMR** (175 MHz, $CDCl_3$): δ 160.77, 156.33, 151.44, 140.30, 137.65, 136.85, 136.54, 133.41, 132.56, 131.06, 130.97, 130.80, 129.87, 129.82, 128.95, 128.70, 127.64, 127.01, 126.75, 122.62, 122.09, 120.14, 119.00, 118.43, 118.25, 117.84, 117.17, 116.85, 111.82, 111.72, 108.28, 107.80, 72.05. **HRMS** (APCI): calcd for $C_{35}H_{21}BrNO_2$: *m/z* 566.0750 $[M + H]^+$, found 566.0751. **IR** (KBr): 3050, 3017, 2925, 2854, 1605, 1496, 1298, 1091, 820, 733 cm^{-1}. **mp**: 342-344 °C.

Dehydro[7]helicene **83eb**

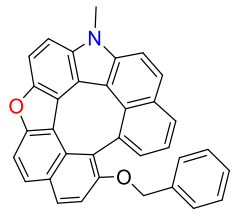

83eb (71% yield): a yellow solid. **^{1}H NMR** (400 MHz, $CDCl_3$): δ 7.99 (dd, J = 7.6, 1.1 Hz, 1H), 7.94 (d, J = 8.7 Hz, 1H), 7.86-7.91 (m, 2H), 7.74 (d, J = 6.9 Hz, 1H), 7.72 (d, J = 6.9 Hz, 1H), 7.66 (d, J = 8.7 Hz, 1H), 7.49 (d, J = 8.7 Hz, 1H), 7.45 (dd, J = 7.3, 1.4 Hz, 1H), 7.34 (d, J = 7.8 Hz, 1H), 7.31 (d, J = 8.7 Hz, 1H), 7.17-7.21 (m, 3H), 6.91 (dd, J = 6.6, 2.5 Hz, 2H), 4.41 (d, J = 11.4 Hz, 1H), 4.06 (s, 3H), 4.04 (d, J = 11.9 Hz, 1H). **^{13}C NMR** (150 MHz, $CDCl_3$): δ 160.91, 158.74, 156.20, 151.26, 150.99, 140.47, 137.65, 137.39, 136.72, 136.53, 132.21, 130.76, 130.13, 129.89, 129.16, 128.80, 128.30, 128.20, 127.93, 127.65, 127.50, 122.28, 118.08, 116.98, 114.77, 111.79, 111.04, 107.81, 106.78, 105.90, 73.52, 70.30. **HRMS** (APCI): calcd for $C_{34}H_{22}NO_2$: *m/z* 476.1645 $[M + H]^+$, found 476.1639. **IR** (KBr): 3062, 3033, 2926, 2854, 1702, 1625, 1515, 1455, 1018, 820 cm^{-1}. **mp**: 335-337 °C.

Dehydro[7]helicene **83ec**

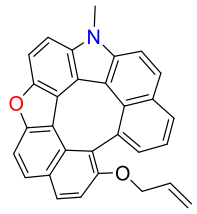

83ec (62% yield): a yellow solid. **^{1}H NMR** (600 MHz, $CDCl_3$): δ 7.96 (dd, J = 7.6, 1.4 Hz, 1H), 7.92 (d, J = 8.9 Hz, 1H), 7.90 (d, J = 8.9 Hz, 1H), 7.87 (d, J = 8.9 Hz, 1H), 7.73 (d, J = 8.2 Hz, 1H), 7.71 (d, J = 8.9 Hz, 1H), 7.64 (d, J = 8.9 Hz, 1H), 7.46 (d, J = 8.9 Hz, 1H), 7.38 (dd, J = 6.9, 1.4 Hz, 1H), 7.31 (t, J = 7.6 Hz, 1H), 7.27 (d, J = 8.2 Hz, 1H), 5.56-5.62 (m, 1H), 4.94 (dq, J = 10.3, 1.4 Hz, 1H), 4.86 (dq, J = 17.2, 1.8 Hz, 1H), 4.04 (s, 3H), 3.91 (dtd, J = 12.7, 3.4, 1.7 Hz, 1H), 3.64-3.67 (dtd, J = 12.8, 3.3, 1.7 Hz, 1H). **^{13}C NMR** (150 MHz, $CDCl_3$): δ 160.75, 156.19, 150.96, 140.36, 137.51, 136.49, 133.54, 132.21, 130.67, 130.37, 129.82, 129.06, 128.75, 128.30, 127.75, 127.09, 126.96, 122.14, 120.24, 118.96, 117.82, 117.52, 117.10, 116.88, 111.70, 110.96, 107.76, 106.74, 72.22, 30.17. **HRMS** (APCI): calcd for $C_{30}H_{20}NO_2$: *m/z* 426.1489 $[M + H]^+$, found 426.1488. **IR** (KBr): 3036, 2925, 2888, 2855, 1604, 1517, 1257, 1144, 816, 782 cm^{-1}. **mp**: 323-325 °C.

Dehydro[7]helicene **83fb**

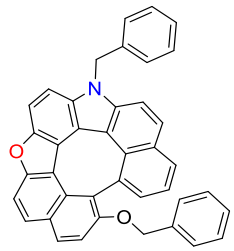

83fb (77% yield): a yellow solid. **^{1}H NMR** (600 MHz, $CDCl_3$): δ 7.98 (dd, J = 7.6, 1.4 Hz, 1H), 7.91 (d, J = 8.9 Hz, 1H), 7.88 (t, J = 8.9 Hz, 2H), 7.74 (d, J = 8.9 Hz, 1H), 7.66 (d, J = 8.9 Hz, 1H), 7.59 (d, J = 8.9 Hz, 1H), 7.47 (dd, J = 6.9, 1.4 Hz, 1H), 7.42 (d, J = 8.9 Hz, 1H), 7.35 (d, J = 7.6 Hz, 1H), 7.32 (d, J = 8.2 Hz, 1H), 7.23-7.27 (m, 3H), 7.18-7.19 (m, 3H), 7.13 (d, J = 6.2 Hz, 2H), 6.92 (dd, J = 7.2, 2.4 Hz, 2H), 5.73 (s, 2H), 4.46 (d, J = 11.7 Hz, 1H), 4.10 (d, J = 11.7 Hz, 1H). **^{13}C NMR** (150 MHz, $CDCl_3$): δ 160.85, 156.28, 151.14, 139.98, 137.64, 137.34, 137.18, 135.93, 132.32, 130.82, 130.68, 129.88, 129.19, 129.00, 128.83, 128.80, 128.50, 128.19, 127.71, 127.65, 127.48, 127.22, 127.04, 126.39, 122.38, 120.26, 119.07, 118.08, 117.80, 117.37, 111.79, 111.31, 108.07, 107.22, 73.39, 47.23. **HRMS** (APCI): calcd for $C_{40}H_{26}NO_2$: *m/z* 552.1958 $[M + H]^+$, found 552.1951. **IR** (KBr): 3060, 3031, 2925, 1624, 1516, 1378, 1183, 1001, 831, 754 cm^{-1}. **mp**: 309-311 °C.

Dehydro[7]helicene **83fc**

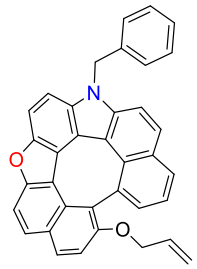

83fc (79% yield): a yellow solid. **^{1}H NMR** (600 MHz, $CDCl_3$): δ 7.95 (dd, J = 7.6, 1.4 Hz, 1H), 7.91 (d, J = 8.2 Hz, 1H), 7.88 (d, J = 8.9 Hz, 1H), 7.87 (d, J = 9.3 Hz, 1H), 7.73 (d, J = 8.2 Hz, 1H), 7.66 (d, J = 8.9 Hz, 1H), 7.59 (d, J = 8.2 Hz, 1H), 7.42 (d, J = 8.9 Hz, 1H), 7.40 (dd, J = 7.4, 1.7 Hz, 1H), 7.32 (t, J = 7.6 Hz, 2H), 7.25-7.29 (m, 3H), 7.13 (d, J = 6.9 Hz, 2H), 5.75 (s, 2H), 5.57-5.64 (m, 1H), 4.96 (dq, J = 10.3, 1.4 Hz, 1H), 4.88 (dq, J = 17.2, 1.6 Hz, 1H), 3.94-3.98 (m, 1H), 3.69-3.72 (m, 1H). **^{13}C NMR** (175 MHz, $CDCl_3$): δ 160.69, 156.25, 151.10, 139.92, 137.51, 137.18, 135.89, 133.47, 132.28, 130.73, 130.56, 129.82, 129.00, 128.87, 128.81, 128.53, 127.70, 127.03, 126.94, 126.37, 122.25, 120.18, 119.04, 118.03, 117.34, 117.19, 116.87, 111.71, 111.24, 108.03, 107.18, 72.04, 47.22 (One carbon overlapped). **HRMS** (APCI): calcd for $C_{36}H_{24}NO_2$: *m/z* 502.1802 $[M + H]^+$, found 502.1802. **IR** (KBr): 3060, 3032, 2925, 2855, 1604, 1518, 1453, 1216, 819, 781 cm^{-1}. **mp**: 322-324 °C.

Dehydro[7]helicene **83oa**

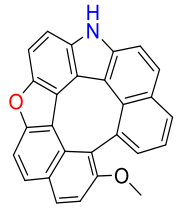

A solution of **83fa** (22.38 mg, 0.05 mmol) in anisole (1 mL) was added to a suspension of $AlCl_3$ (26.67 mg, 0.2 mmol) in anisole (0.5 mL) at 0 °C under nitrogen atmosphere. After stirring at 25 °C for 72 h, the mixture was poured into water and extracted with ethyl acetate. The organic layer was washed successively with 5% $NaHCO_3$, brine, dried over Na_2SO_4 and evaporated to dryness *in vacuo*. The residue was purified on column chromatography (SiO_2, EtOAc/ hexane) to give **83oa** (67% yield) as a yellow solid. **^{1}H NMR** (600 MHz, $CDCl_3$): δ 8.44 (s, 1H), 7.92 (d, J = 6.9 Hz, 1H), 7.89 (d, J = 8.2 Hz, 1H), 7.84 (d, J = 8.9 Hz, 1H), 7.78 (d, J = 8.9 Hz, 1H), 7.70 (d, J = 8.9 Hz, 1H), 7.55 (d, J = 8.9 Hz, 1H), 7.52 (d, J = 8.9 Hz, 1H), 7.36 (d, J = 8.2 Hz, 1H), 7.29-7.33 (m, 2H), 7.25 (d, J = 8.9 Hz, 1H), 3.24 (s, 3H). **^{13}C NMR** (150 MHz, $CDCl_3$): δ 161.88, 156.13, 150.93, 139.34, 137.29, 134.88, 132.59, 130.77, 130.62, 129.77, 128.76, 128.40, 127.91, 127.59, 126.78, 126.76, 122.12, 120.02, 118.78, 118.50, 117.82, 115.63, 112.86, 111.52, 108.66, 107.94, 58.38. **HRMS** (APCI): calcd for $C_{27}H_{16}NO_2$: *m/z* 386.1176 $[M + H]^+$, found 386.1170. **IR** (KBr): 3409, 3045, 2960, 2934, 2836, 1605, 1518, 1257, 1020, 820 cm^{-1}. **mp**: 313-315 °C.

Dehydro[7]helicene **83pa**

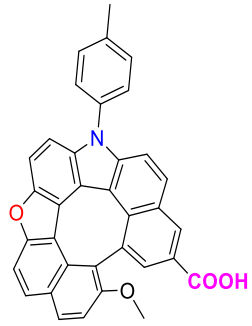

An aqueous solution of NaOH (10 M, 1 mL) was added to ethanol solution (1 mL) of **83ma** (25.03 mg, 0.05 mmol). After refluxing for 48 h, the solution was acidified by (1 M) HCl, and extracted with EtOAc. The organic layer was dried over Na_2SO_4, filtered, and concentrated *in vacuo*. The residue was purified by column chromatography (SiO_2, EtOAc/hexane) to give **83pa** (65% yield) as a yellow solid. **^{1}H NMR** (400 MHz, $CDCl_3$): δ 8.51 (d, J = 1.8 Hz, 1H), 7.96 (d, J = 8.7 Hz, 1H), 7.90 (d, J = 9.2 Hz, 1H), 7.89 (d, J = 9.4 Hz, 1H), 7.74 (d, J = 8.7 Hz, 1H), 7.71 (d, J = 1.8 Hz, 1H), 7.58 (d, J = 8.7 Hz, 1H), 7.57 (d, J = 8.9 Hz, 1H), 7.45-7.49 (m, 4H), 7.35 (d, J = 8.7 Hz, 1H), 7.30 (d, J = 8.7 Hz, 1H), 3.40 (s, 3H), 2.54 (s, 3H). **^{13}C NMR** (175 MHz, $CDCl_3$) δ 169.25, 161.73, 156.47, 151.47, 141.65, 138.69, 136.98, 134.69, 134.63, 133.07, 131.22, 130.81, 130.25, 129.73, 129.20, 129.03, 128.97, 127.93, 127.48, 127.06, 126.64, 126.14, 119.82, 118.83, 117.86, 117.37, 114.82, 113.30, 111.68, 108.49, 108.33, 58.05, 21.50. **HRMS** (APCI): calcd for $C_{34}H_{22}NO_4$: *m/z* 520.1543 $[M + H]^+$, found 520.1533. **IR** (KBr): 3368, 2955, 2925, 2853, 1657, 1603, 1515, 1022, 817, 782 cm^{-1}. **mp**: 319-321°C.

Synthesis of aza-dioxa[8]circulene 86

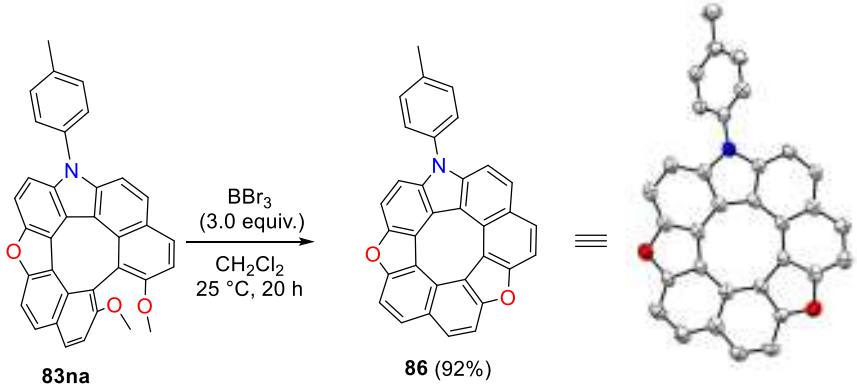

To a dry round bottom flask, **83na** (50.5 mg, 0.1 mmol) was charged. The reaction flask was evacuated and purged with argon three times. After **83na** was dissolved in dry dichloromethane (40 mL), 1.0 M boron tribromide solution in dichloromethane (0.3 mL, 0.3 mmol, 3.0 equiv.) was added via syringe at 0 °C, and the reaction mixture was stirred at room temperature for 20 h. After quenched with saturated aqueous sodium bicarbonate solution, the mixture was extracted with THF three times and the combined organic layers were washed with water, brine and dried over anhydrous sodium sulfate. After removal of the solvents *in vacuo*, the

residue was purified by column chromatography on silica with ethyl acetate/*n*-hexane as eluent to give product **86** as a yellowish white solid in 92% yield. **^{1}H NMR** (700 MHz, $CDCl_3$): δ 8.31 (m, 3H), 8.21 (d, J = 9.0 Hz, 1H), 8.06 (d, J = 8.6 Hz, 1H), 8.03 (d, J = 8.4 Hz, 1H), 8.02 (d, J = 8.6 Hz, 1H), 7.93 (d, J = 8.6 Hz, 1H), 7.72 (d, J = 8.6 Hz, 1H), 7.69 (d, J = 8.6 Hz, 1H), 7.60 (d, J = 7.7 Hz, 2H), 7.54 (d, J = 8.2 Hz, 2H), 2.59 (s, 3H). **^{13}C NMR** (175 MHz, $CDCl_3$) δ 155.96, 155.87, 155.56, 151.15, 141.15, 138.76, 136.72, 134.88, 131.00, 130.84, 130.75, 130.42, 130.40, 128.68, 127.39, 126.51, 123.02, 122.14, 117.61, 117.17, 116.82, 115.69, 114.58, 114.52, 110.86, 110.60, 110.02, 109.59, 108.71, 108.46, 21.56. **HRMS** (APCI): calcd for $C_{33}H_{18}NO_2$: *m/z* 460.1332 [M + H]$^+$, found 460.1328. **IR** (KBr): 2956, 2923, 2869, 2850, 1604, 1516, 1262, 1099, 1026, 817 cm^{-1}. **mp**: 295-297 °C.

Synthesis of 8-Methoxy-17-(*p*-tolyl)-7,13-dioxa-17-aza-3,4 methanobenzo[*jk*]naphtho[1',8':6,7,8]cycloocta[1,2,3,4-def]phenanthrene 87aa

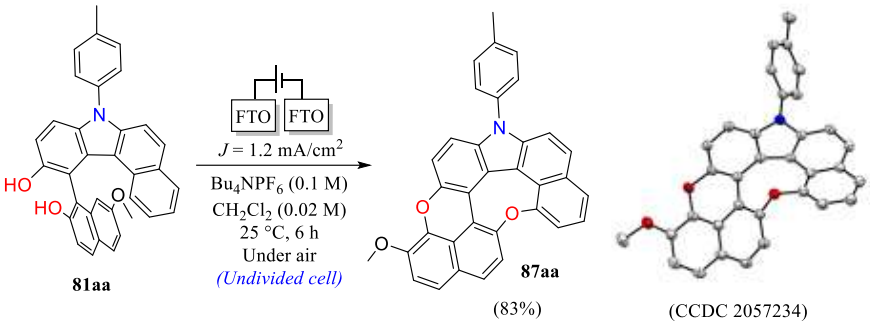

A solution of **81aa** (0.1 mmol), tetrabutylammonium hexafluorophosphate(V) (193.7 mg, 0.5 mmol) in CH_2Cl_2 (0.02 M) was transferred into an undivided electrolysis cell. This cell is equipped with two FTO electrodes, which are connected to DC power supply. At 25 °C temperature, a constant current electrolysis with a current density of 1.2 mA/cm^2 was performed. After 6 h, the electrolysis was stopped and a purification of the crude products by column chromatography (SiO_2, EtOAc/hexane) provided **87aa** (83% yield) as a yellow solid. **^{1}H NMR** (400 MHz, $CDCl_3$): δ 7.81 (d, J = 7.8 Hz, 1H), 7.72-7.74 (m, 2H), 7.65 (d, J = 9.2 Hz, 1H), 7.56 (d, J = 8.7 Hz, 1H), 7.32-7.48 (m, 8H), 7.30 (d, J = 8.7 Hz, 1H), 7.18 (d, J = 9.2 Hz, 1H), 4.02 (s, 3H), 2.52 (s, 3H). **^{13}C NMR** (100 MHz, $CDCl_3$): δ 152.78, 151.28, 149.45, 141.32, 140.00, 138.99, 138.82, 138.73, 134.15, 131.53, 130.79, 127.45, 127.04, 126.61, 125.79, 125.61, 123.31, 121.36, 120.94, 119.80, 119.20, 118.43, 116.39, 115.16, 114.57, 114.38, 112.48, 112.33, 57.43, 21.45 (Two carbons overlaped). **HRMS** (APCI): calcd for $C_{34}H_{22}NO_3$: *m/z* 492.1594 [M + H]$^+$, found 492.1593. **IR** (KBr): 3060, 2954, 2925, 2853, 1724, 1604, 1515, 1249, 822, 806 cm^{-1}. **mp**: 310-312 °C.

Synthesis of 89a

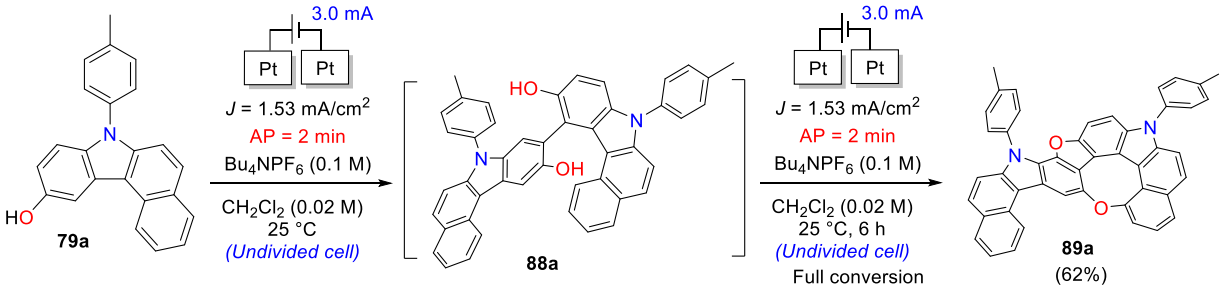

A solution of **79a** (0.1 mmol), tetrabutylammonium hexafluorophosphate(V) (193.7 mg, 0.5 mmol) in CH_2Cl_2 (0.02 M) was transferred into an undivided electrolysis cell. This cell is equipped with two Pt electrodes, which are connected to DC power supply (alternating polarity every 2 mins). At 25 °C temperature, a constant current

electrolysis with a current density of 1.53 mA/cm^2 was performed. After 6 h, the electrolysis was stopped and a purification of the crude products by column chromatography (SiO_2, EtOAc/hexane) provided **89a** (62% yield) as a yellow solid. **^{1}H NMR** (400 MHz, $CDCl_3$): δ 9.08 (d, J = 8.2 Hz, 1H), 8.83 (s, 1H), 8.19 (dd, J = 7.3, 0.9 Hz, 1H), 8.06 (d, J = 7.3 Hz, 1H), 7.83-7.92 (m, 4H), 7.64-7.67 (m, 3H), 7.55-7.61 (m, 3H), 7.46-7.54 (m, 7H), 7.43 (d, J = 8.7 Hz, 1H), 2.59 (s, 3H), 2.54 (s, 3H). **^{13}C NMR** (100 MHz, $CDCl_3$): δ 155.75, 151.04, 147.63, 142.41, 140.67, 139.30, 138.39, 138.03, 137.68, 137.50, 135.43, 134.89, 133.75, 133.39, 132.34, 130.75, 130.11, 129.79, 129.69, 129.43, 127.93, 127.90, 127.27, 127.21, 127.09, 126.47, 125.50, 123.84, 123.54, 123.49, 122.15, 118.83, 117.56, 117.10, 116.77, 114.14, 112.75, 112.11, 109.57, 108.80, 21.57, 21.47. **HRMS** (APCI): calcd for $C_{46}H_{28}N_2O_2$: *m/z* 641.2224 $[M + H]^+$, found 641.2222.

Synthesis of 90

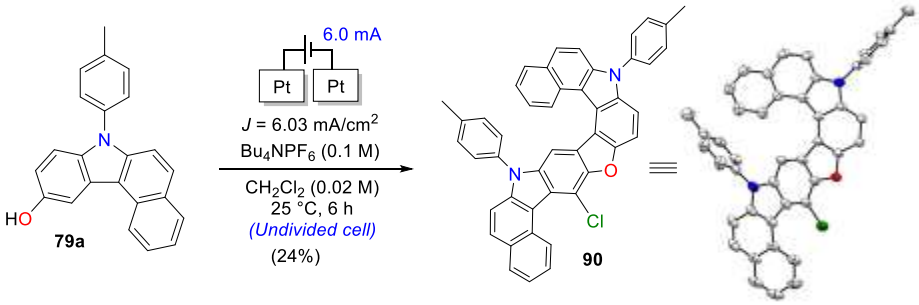

A solution of **79a** (0.1 mmol), tetrabutylammonium hexafluorophosphate(V) (193.7 mg, 0.5 mmol) in CH_2Cl_2 (0.02 M) was transferred into an undivided electrolysis cell. This cell is equipped with two Pt electrodes, which are connected to DC power supply. At 25 °C temperature, a constant current electrolysis with a current density of 3.06 mA/cm^2 was performed. After 6 h, the electrolysis was stopped and a purification of the crude products by column chromatography (SiO_2, EtOAc/hexane) provided **90** (24% yield) as a yellow solid. **^{1}H NMR** (400 MHz, $CDCl_3$): δ 9.92 (d, J = 8.7 Hz, 1H), 8.51 (d, J = 8.2 Hz, 1H), 8.12 (s, 1H), 8.00 (t, J = 7.6 Hz, 2H), 7.91 (d, J = 9.2 Hz, 1H), 7.88 (d, J = 8.7 Hz, 1H), 7.84 (d, J = 8.7 Hz, 1H), 7.76-7.80 (m, 1H), 7.49-7.60 (m, 4H), 7.45-7.47 (m, 4H), 7.37-7.43 (m, 3H), 7.32-7.35 (m, 2H), 7.17 (td, J = 7.6, 1.4 Hz, 1H), 2.54 (s, 3H), 2.51 (s, 3H). **HRMS** (APCI): calcd for $C_{46}H_{29}ClN_2O$: *m/z* 661.2041 $[M + H]^+$, found 661.2039.

Synthesis of dicarbazole 118a

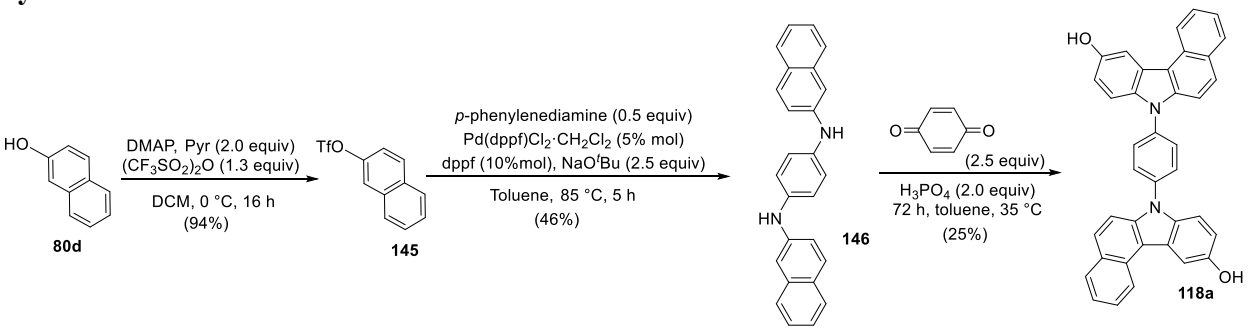

118a (25% yield): a gray white solid. **^{1}H NMR** (400 MHz, $CDCl_3$): δ 8.77 (d, J = 8.2 Hz, 2H), 8.12 (d, J = 2.3 Hz, 2H), 8.04 (d, J = 7.8 Hz, 2H), 7.90 (d, J = 9.2 Hz, 2H), 7.85 (s, 4H), 7.76 (td, J = 7.7, 1.2 Hz, 2H), 7.72 (d, J = 9.2 Hz, 2H), 7.51-7.57 (m, 4H), 7.08 (dd, J = 8.6, 2.4 Hz, 2H), 4.84 (s, 2H). **^{13}C NMR** (100 MHz, $CDCl_3$): δ 150.77, 139.19, 136.87, 135.25, 130.03, 129.58, 129.40, 128.97, 127.86, 127.28, 123.36, 123.22, 116.29, 115.59, 115.48, 113.93, 112.23, 111.76, 111.05, 107.70, 106.27. **HRMS** (APCI): calcd for $C_{38}H_{24}N_2O_2$: *m/z* 541.1911 $[M + H]^+$, found 541.1912.

Synthesis of dicarbazole 118b

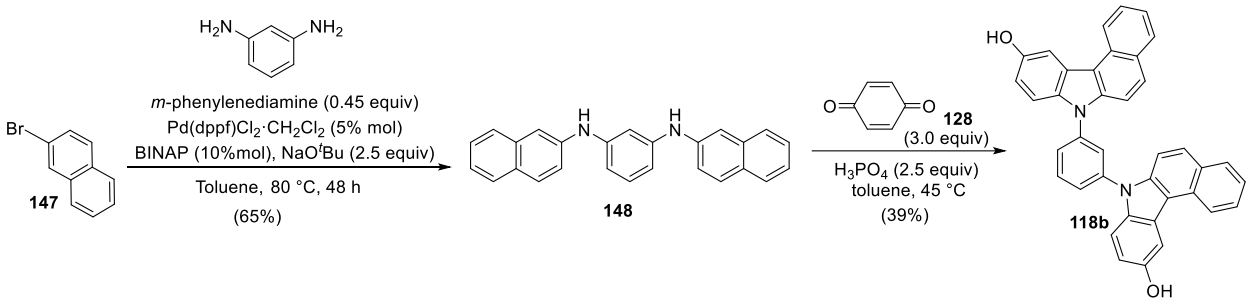

118a (39% yield): brown solid. **HRMS** (APCI): calcd for $C_{38}H_{24}N_2O_2$: *m/z* 541.1911 $[M + H]^+$, found 541.1910.

Synthesis of dicarbazole 119

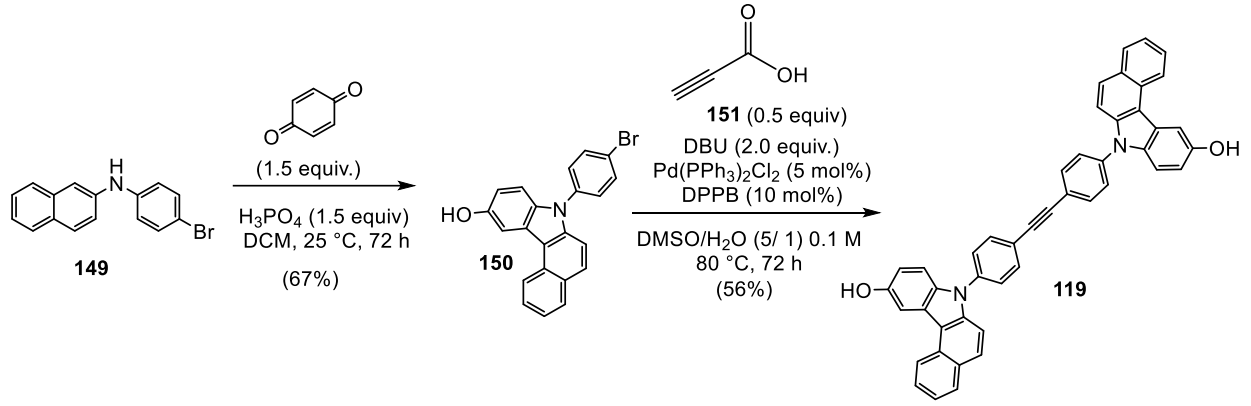

119 (56% yield): yellow solid. **^{1}H NMR** (400 MHz, $CDCl_3$): δ 8.74 (d, J = 8.7 Hz, 2H), 8.09 (d, J = 2.3 Hz, 2H), 8.01 (d, J = 7.8 Hz, 2H), 7.84-7.87 (m, 6H), 7.74 (td, J = 7.6, 1.4 Hz, 2H), 7.62-7.64 (m, 4H), 7.60 (d, J = 9.2 Hz, 2H), 7.49-7.53 (m, 2H), 7.44 (d, J = 8.7 Hz, 2H), 7.03 (dd, J = 8.9, 2.5 Hz, 2H), 4.79 (s, 2H). **HRMS** (APCI): calcd for $C_{46}H_{28}N_2O_2$: *m/z* 641.2224 $[M + H]^+$, found 641.2213.

Synthesis of multiple helicenes and dehydrohelicenes

100 (26% yield): yellow solid. **^{1}H NMR** (600 MHz, $CDCl_3$): δ 8.38 (d, J = 8.2 Hz, 2H), 8.31 (d, J = 8.2 Hz, 2H), 8.00-8.04 (m, 12H), 7.92 (d, J = 8.9 Hz, 2H), 7.85 (d, J = 8.9 Hz, 4H), 7.77 (d, J = 8.9 Hz, 2H), 7.34-7.39 (m, 4H), 6.95-7.00 (m, 4H). **^{13}C NMR** (150 MHz, $CDCl_3$): δ 154.74, 153.30, 138.79, 137.92, 137.33, 130.84, 129.90, 129.85, 129.80, 129.72, 129.48, 129.14, 128.59, 128.10, 128.04, 125.12, 124.66, 124.37, 123.61, 120.06, 117.96, 117.76, 116.63, 112.65, 111.58, 109.45, 109.06 (One carbon overlapped). **HRMS** (APCI): calcd for $C_{58}H_{32}N_2O_2$: *m/z* 789.2538 $[M + H]^+$, found 789.2542.

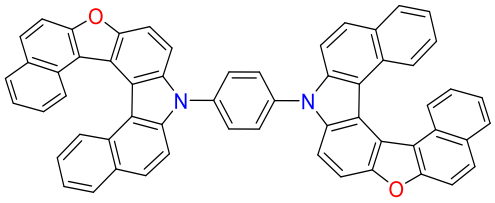

101 (31% yield): yellow solid. **^{1}H NMR** (600 MHz, $CDCl_3$): δ 8.02 (dd, J = 7.2, 1.7 Hz, 2H), 7.90-7.96 (m, 10H), 7.76 (t, J = 8.6 Hz, 4H), 7.67 (d, J = 8.9 Hz, 2H), 7.58 (dd, J = 8.3, 1.4 Hz, 2H), 7.37-7.41 (m, 4H), 7.31 (d, J = 8.9 Hz, 2H), 3.33 (s, 6H). **^{13}C NMR** (150 MHz, $CDCl_3$): δ 161.96, 156.45, 151.57, 140.38, 137.50, 136.62, 132.82, 131.05, 130.89, 129.85, 129.69, 129.04, 128.95, 128.86, 127.84, 127.70, 126.80, 126.76, 122.58, 120.09, 119.14, 118.60, 118.03, 115.56, 111.98, 111.60, 108.37, 107.94, 58.36. **HRMS** (APCI): calcd for $C_{60}H_{32}N_2O_4$: *m/z* 845.2435 $[M + H]^+$, found 845.2421.

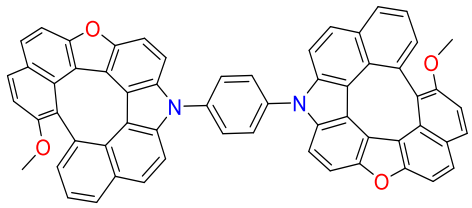

102 (44% yield): yellow solid. **^{1}H NMR** (600 MHz, $CDCl_3$): δ 8.34 (d, J = 8.2 Hz, 2H), 8.27 (d, J = 8.2 Hz, 2H), 8.01 (d, J = 8.2 Hz, 2H), 7.99 (d, J = 8.2 Hz, 4H), 7.96 (d, J = 8.9 Hz, 2H), 7.93 (d, J = 8.2 Hz, 4H), 7.91 (d, J = 8.9 Hz, 2H), 7.78 (d, J = 8.9 Hz, 2H), 7.71-7.76 (m, 4H), 7.69 (d, J = 8.9 Hz, 2H), 7.62 (d, J = 8.2 Hz, 2H), 7.36 (t, J = 7.2 Hz, 2H), 7.33 (t, J = 6.9 Hz, 2H), 6.93-6.97 (m, 4H). **^{13}C NMR** (150 MHz, $CDCl_3$): δ 154.70, 153.24, 138.67, 137.79, 137.65, 133.56, 130.82, 129.68, 129.65, 129.48, 129.13, 128.56, 128.51, 128.36, 128.28, 127.99, 127.91, 126.67, 125.05, 124.63, 124.34, 123.54, 123.06, 120.06, 117.87, 117.66, 116.56, 112.64, 111.58, 109.35, 109.07. **HRMS** (APCI): calcd for $C_{66}H_{36}N_2O_2$: *m/z* 889.2849 $[M + H]^+$, found 889.2847.

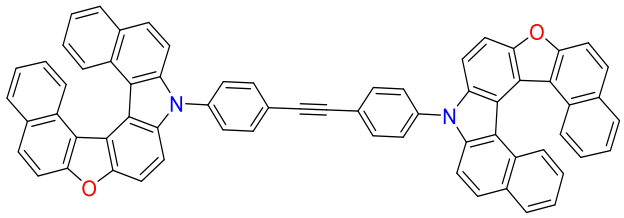

104 (18% yield): yellow solid. **^{1}H NMR** (600 MHz, $CDCl_3$): δ 8.33 (d, J = 8.2 Hz, 2H), 8.25 (d, J = 8.2 Hz, 2H), 7.97-8.01 (m, 10H), 7.89 (d, J = 8.2 Hz, 2H), 7.80-7.83 (m, 4H), 7.72-7.77 (m, 4H), 7.30-7.36 (m, 4H), 6.91-6.95 (m, 4H). **HRMS** (APCI): calcd for $C_{58}H_{32}N_2O_2$: *m/z* 789.2537 $[M + H]^+$, found 789.2535.

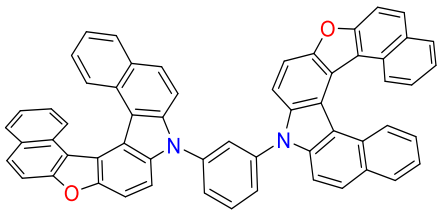

X-ray crystallographic analysis

83aa (CCDC 2091483) with ellipsoids at 30% probability. (H atoms were omitted for clarity).

Empirical formula	$C_{34}H_{21}NO_2$
Formula weight	475.551
Temperature/K	173
Crystal system	monoclinic
Space group	$P2_1$
a/Å	9.1897(1)
b/Å	23.1326(3)
c/Å	10.5732(2)
α/°	90
β/°	91.282(1)
γ/°	90
Volume/Å^3	2247.11(6)
Z	4
ρ_{calc}g/cm^3	1.406
μ/mm^{-1}	0.686
F(000)	995.2
Crystal size/mm^3	0.082 × 0.042 × 0.022
Radiation	CuKα (λ = 1.54184)
2Θ range for data collection/°	7.64 to 161.2
Index ranges	$-11 \le h \le 11$, $-29 \le k \le 28$, $-13 \le l \le 13$
Reflections collected	59505
Independent reflections	9585 [R_{int} = 0.0383, R_{sigma} = 0.0254]
Data/restraints/parameters	9585/1/671
Goodness-of-fit on F^2	1.051
Final R indexes [I>=2σ (I)]	R_1 = 0.0358, wR_2 = 0.0866
Final R indexes [all data]	R_1 = 0.0406, wR_2 = 0.0900
Largest diff. peak/hole / e Å^{-3}	0.16/-0.18
Flack parameter	-0.02(6)

Datablock: 200514Im-6

Bond precision: C-C = 0.0027 A Wavelength=1.54184

Cell: a=9.1897(1) b=23.1326(3) c=10.5732(2)
alpha=90 beta=91.282(1) gamma=90
Temperature: 173 K

	Calculated	Reported
Volume	2247.11(6)	2247.11(6)
Space group	P 21	P 1 21 1
Hall group	P 2yb	P 2yb
Moiety formula	C34 H21 N O2	C34 H21 N O2
Sum formula	C34 H21 N O2	C34 H21 N O2
Mr	475.52	475.55
Dx,g cm-3	1.406	1.406
Z	4	4
Mu (mm-1)	0.686	0.686
F000	992.0	995.2
F000'	994.84	
h,k,lmax	11,29,13	11,29,13
Nref	9866[5058]	9585
Tmin,Tmax	0.966,0.985	0.862,1.000
Tmin'	0.945	

Correction method= # Reported T Limits: Tmin=0.862 Tmax=1.000
AbsCorr = MULTI-SCAN

Data completeness= 1.90/0.97 Theta(max)= 80.600

R(reflections)= 0.0358(8733) wR2(reflections)= 0.0900(9585)

S = 1.051 Npar= 671

The following ALERTS were generated. Each ALERT has the format
test-name_ALERT_alert-type_alert-level.
Click on the hyperlinks for more details of the test.

Alert level G

PLAT005_ALERT_5_G	No Embedded Refinement Details Found in the CIF	Please Do !
PLAT068_ALERT_1_G	Reported F000 Differs from Calcd (or Missing)...	Please Check
PLAT073_ALERT_1_G	H-atoms ref, but _hydrogen_treatment Reported as	constr Check
PLAT398_ALERT_2_G	Deviating C-O-C Angle From 120 for O13 .	105.6 Degree
PLAT398_ALERT_2_G	Deviating C-O-C Angle From 120 for O50 .	105.5 Degree
PLAT769_ALERT_4_G	CIF Embedded explicitly supplied scattering data	Please Note
PLAT912_ALERT_4_G	Missing # of FCF Reflections Above STh/L= 0.600	68 Note
PLAT960_ALERT_3_G	Number of Intensities with I < - 2*sig(I) ...	1 Check
PLAT978_ALERT_2_G	Number C-C Bonds with Positive Residual Density.	2 Info
PLAT982_ALERT_1_G	The C-f'= 0.0192 Deviates from IT-value =	0.0181 Check
PLAT982_ALERT_1_G	The N-f'= 0.0326 Deviates from IT-value =	0.0311 Check
PLAT982_ALERT_1_G	The O-f'= 0.0524 Deviates from IT-value =	0.0492 Check
PLAT983_ALERT_1_G	The O-f"= 0.0338 Deviates from IT-Value =	0.0322 Check

---

0 **ALERT level A** = Most likely a serious problem - resolve or explain
0 **ALERT level B** = A potentially serious problem, consider carefully
0 **ALERT level C** = Check. Ensure it is not caused by an omission or oversight
13 **ALERT level G** = General information/check it is not something unexpected

6 ALERT type 1 CIF construction/syntax error, inconsistent or missing data
3 ALERT type 2 Indicator that the structure model may be wrong or deficient
1 ALERT type 3 Indicator that the structure quality may be low
2 ALERT type 4 Improvement, methodology, query or suggestion
1 ALERT type 5 Informative message, check

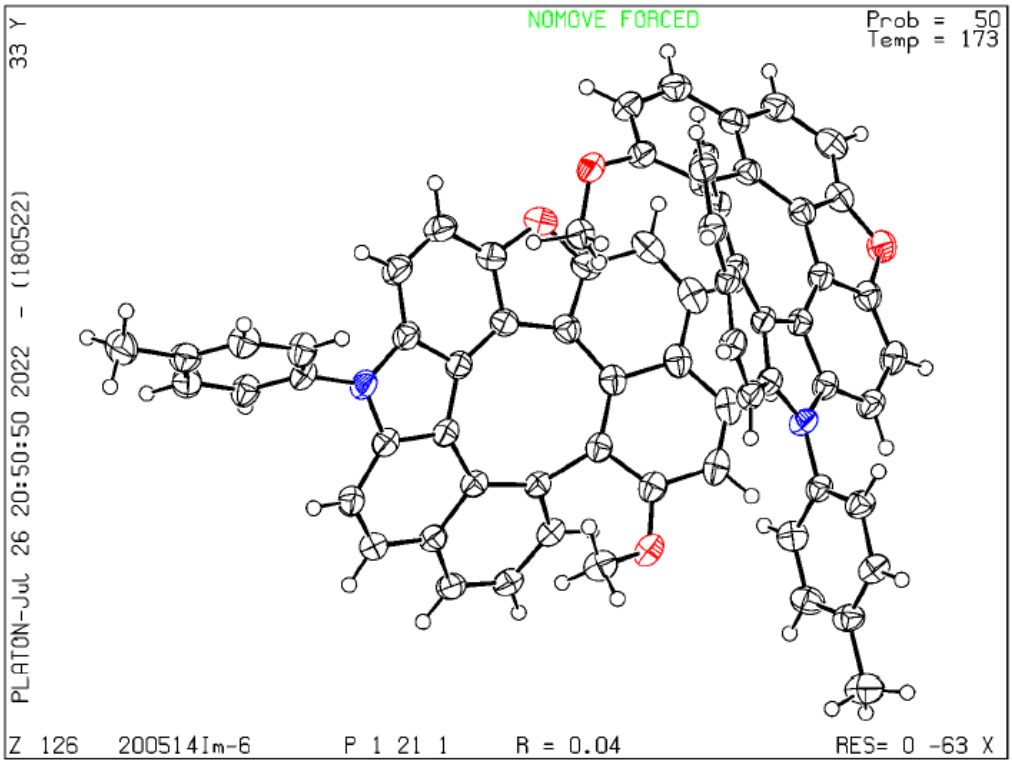

82aa (CCDC 2128351) with ellipsoids at 30% probability. (H atoms were omitted for clarity).

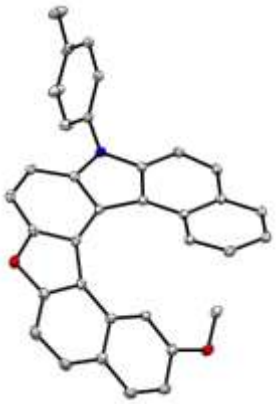

Empirical formula	$C_{34}H_{23}NO_2$
Formula weight	477.567
Temperature/K	100
Crystal system	triclinic
Space group	P-1
a/Å	10.2477(5)
b/Å	11.5049(6)
c/Å	11.5650(5)
α/°	66.563(5)
β/°	76.852(4)
γ/°	68.746(4)
Volume/Å^3	1160.37(11)
Z	2
ρ_{calc}g/cm^3	1.367
μ/mm^{-1}	0.664
F(000)	501.6
Crystal size/mm^3	0.12 × 0.04 × 0.03
Radiation	CuKα (λ = 1.54184)
2Θ range for data collection/°	8.38 to 151.94
Index ranges	$-12 \leq h \leq 12$, $-12 \leq k \leq 14$, $-14 \leq l \leq 14$
Reflections collected	11350
Independent reflections	4657 [R_{int} = 0.0313, R_{sigma} = 0.0423]
Data/restraints/parameters	4657/0/337
Goodness-of-fit on F^2	1.023
Final R indexes [I>=2σ (I)]	R_1 = 0.0419, wR_2 = 0.0977
Final R indexes [all data]	R_1 = 0.0532, wR_2 = 0.1027
Largest diff. peak/hole / e Å^{-3}	0.27/-0.23

Datablock: Req143-1

Bond precision: C-C = 0.0023 A Wavelength=1.54184

Cell: a=10.2477(5) b=11.5049(6) c=11.5650(5)
alpha=66.563(5) beta=76.852(4) gamma=68.746(4)
Temperature: 100 K

	Calculated	Reported
Volume	1160.37(11)	1160.37(11)
Space group	P -1	P -1
Hall group	-P 1	-P 1
Moiety formula	C34 H23 N O2	C34 H23 N O2
Sum formula	C34 H23 N O2	C34 H23 N O2
Mr	477.53	477.57
Dx,g cm-3	1.367	1.367
Z	2	2
Mu (mm-1)	0.664	0.664
F000	500.0	501.6
F000'	501.42	
h,k,lmax	12,14,14	12,14,14
Nref	4846	4657
Tmin,Tmax	0.969,0.980	0.925,1.000
Tmin'	0.923	

Correction method= # Reported T Limits: Tmin=0.925 Tmax=1.000
AbsCorr = MULTI-SCAN

Data completeness= 0.961 Theta(max)= 75.970

R(reflections)= 0.0419(3861) wR2(reflections)= 0.1027(4657)

S = 1.023 Npar= 337

The following ALERTS were generated. Each ALERT has the format
test-name_ALERT_alert-type_alert-level.
Click on the hyperlinks for more details of the test.

Alert level C

```
PLAT906_ALERT_3_C Large K Value in the Analysis of Variance ......      4.801 Check
PLAT911_ALERT_3_C Missing FCF Refl Between Thmin & STh/L=    0.600         21 Report
```

Alert level G

```
PLAT005_ALERT_5_G No Embedded Refinement Details Found  in the CIF     Please Do !
PLAT068_ALERT_1_G Reported F000 Differs from Calcd (or Missing)...     Please Check
PLAT073_ALERT_1_G H-atoms ref, but _hydrogen_treatment Reported as     constr Check
PLAT398_ALERT_2_G Deviating  C-O-C   Angle From 120 for O002     .      105.4 Degree
PLAT720_ALERT_4_G Number of Unusual/Non-Standard Labels .........        60 Note
PLAT769_ALERT_4_G CIF Embedded explicitly supplied scattering data     Please Note
PLAT912_ALERT_4_G Missing # of FCF Reflections Above STh/L=  0.600      169 Note
PLAT978_ALERT_2_G Number C-C Bonds with Positive Residual Density.      11 Info
PLAT982_ALERT_1_G The  C-f'=    0.0192 Deviates from  IT-value =      0.0181 Check
PLAT982_ALERT_1_G The  N-f'=    0.0326 Deviates from  IT-value =      0.0311 Check
PLAT982_ALERT_1_G The  O-f'=    0.0524 Deviates from  IT-value =      0.0492 Check
PLAT983_ALERT_1_G The  O-f"=    0.0338 Deviates from  IT-Value =      0.0322 Check
```

```
  0 ALERT level A = Most likely a serious problem - resolve or explain
  0 ALERT level B = A potentially serious problem, consider carefully
  2 ALERT level C = Check. Ensure it is not caused by an omission or oversight
 12 ALERT level G = General information/check it is not something unexpected

  6 ALERT type 1 CIF construction/syntax error, inconsistent or missing data
  2 ALERT type 2 Indicator that the structure model may be wrong or deficient
  2 ALERT type 3 Indicator that the structure quality may be low
  3 ALERT type 4 Improvement, methodology, query or suggestion
  1 ALERT type 5 Informative message, check
```

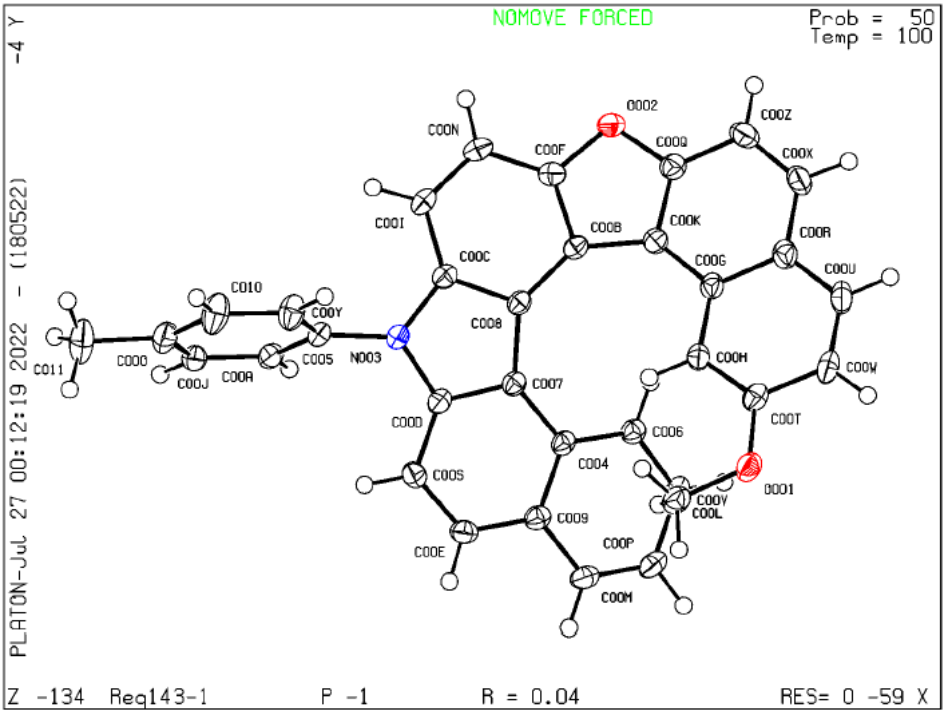

83ma (CCDC 2158892) with ellipsoids at 30% probability. (H atoms were omitted for clarity).

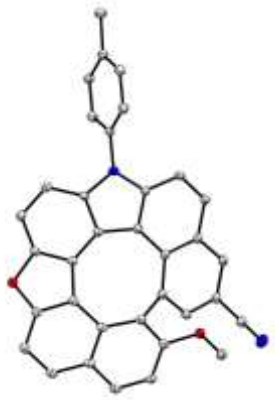

Empirical formula	$C_{46.67}H_{26.67}N_{2.67}O_{2.67}$
Formula weight	667.415
Temperature/K	100
Crystal system	monoclinic
Space group	$P2_1/c$
a/Å	12.7952(2)
b/Å	13.3698(2)
c/Å	14.2802(2)
α/°	90
β/°	104.075(2)
γ/°	90
Volume/Å^3	2369.56(6)
Z	3
ρ_{calc}g/cm^3	1.403
μ/mm^{-1}	0.694
F(000)	1043.4
Crystal size/mm^3	0.06 × 0.05 × 0.04
Radiation	CuKα (λ = 1.54184)
2Θ range for data collection/°	7.12 to 151.88
Index ranges	-12 ≤ h ≤ 15, -13 ≤ k ≤ 16, -17 ≤ l ≤ 17
Reflections collected	13617
Independent reflections	4808 [R_{int} = 0.0262, R_{sigma} = 0.0326]
Data/restraints/parameters	4808/0/355
Goodness-of-fit on F^2	1.017
Final R indexes [I>=2σ (I)]	R_1 = 0.0375, wR_2 = 0.0903
Final R indexes [all data]	R_1 = 0.0484, wR_2 = 0.0967
Largest diff. peak/hole / e Å^{-3}	0.24/-0.21

Datablock: Req148-1

Bond precision: C-C = 0.0020 A Wavelength=1.54184

Cell: a=12.7952(2) b=13.3698(2) c=14.2802(2)
alpha=90 beta=104.075(2) gamma=90
Temperature: 100 K

	Calculated	Reported
Volume	2369.56(6)	2369.56(6)
Space group	P 21/c	P 1 21/c 1
Hall group	-P 2ybc	-P 2ybc
Moiety formula	C35 H20 N2 O2	1.333(C35 H20 N2 O2)
Sum formula	C35 H20 N2 O2	C46.667 H26.667 N2.667 O2.667
Mr	500.53	667.41
Dx,g cm-3	1.403	1.403
Z	4	3
Mu (mm-1)	0.694	0.694
F000	1040.0	1043.4
F000'	1043.01	
h,k,lmax	16,16,17	15,16,17
Nref	4935	4808
Tmin,Tmax	0.959,0.973	0.692,1.000
Tmin'	0.959	

Correction method= # Reported T Limits: Tmin=0.692 Tmax=1.000
AbsCorr = MULTI-SCAN

Data completeness= 0.974 Theta(max)= 75.940

R(reflections)= 0.0375(3942) wR2(reflections)= 0.0967(4808)

S = 1.017 Npar= 355

The following ALERTS were generated. Each ALERT has the format
test-name_ALERT_alert-type_alert-level.
Click on the hyperlinks for more details of the test.

Alert level C

```
PLAT911_ALERT_3_C Missing FCF Refl Between Thmin & STh/L=    0.600         14 Report
```

Alert level G

```
FORMU01_ALERT_1_G  There is a discrepancy between the atom counts in the
           _chemical_formula_sum and _chemical_formula_moiety. This is
           usually due to the moiety formula being in the wrong format.
           Atom count from _chemical_formula_sum:   C46.66699 H26.66699 N2.667 O2
           Atom count from _chemical_formula_moiety:C46.65499 H26.66 N2.666 O2.66
PLAT005_ALERT_5_G No Embedded Refinement Details Found  in the CIF     Please Do !
PLAT045_ALERT_1_G Calculated and Reported Z Differ by a Factor ...      1.333 Check
PLAT068_ALERT_1_G Reported F000 Differs from Calcd (or Missing)...     Please Check
PLAT073_ALERT_1_G H-atoms ref, but _hydrogen_treatment Reported as     constr Check
PLAT230_ALERT_2_G Hirshfeld Test Diff for    C015     --C025     .        5.4 s.u.
PLAT398_ALERT_2_G Deviating  C-O-C   Angle From 120 for O001     .      105.4 Degree
PLAT720_ALERT_4_G Number of Unusual/Non-Standard Labels .....          59 Note
PLAT769_ALERT_4_G CIF Embedded explicitly supplied scattering data     Please Note
PLAT912_ALERT_4_G Missing # of FCF Reflections Above STh/L=  0.600     109 Note
PLAT960_ALERT_3_G Number of Intensities with I  <   - 2*sig(I) ...       2 Check
PLAT978_ALERT_2_G Number C-C Bonds with Positive Residual Density.       8 Info
PLAT982_ALERT_1_G The  C-f'=    0.0192 Deviates from  IT-value =      0.0181 Check
PLAT982_ALERT_1_G The  N-f'=    0.0326 Deviates from  IT-value =      0.0311 Check
PLAT982_ALERT_1_G The  O-f'=    0.0524 Deviates from  IT-value =      0.0492 Check
PLAT983_ALERT_1_G The  O-f"=    0.0338 Deviates from  IT-Value =      0.0322 Check
```

```
   0 ALERT level A = Most likely a serious problem - resolve or explain
   0 ALERT level B = A potentially serious problem, consider carefully
   1 ALERT level C = Check. Ensure it is not caused by an omission or oversight
  16 ALERT level G = General information/check it is not something unexpected

   8 ALERT type 1 CIF construction/syntax error, inconsistent or missing data
   3 ALERT type 2 Indicator that the structure model may be wrong or deficient
   2 ALERT type 3 Indicator that the structure quality may be low
   3 ALERT type 4 Improvement, methodology, query or suggestion
   1 ALERT type 5 Informative message, check
```

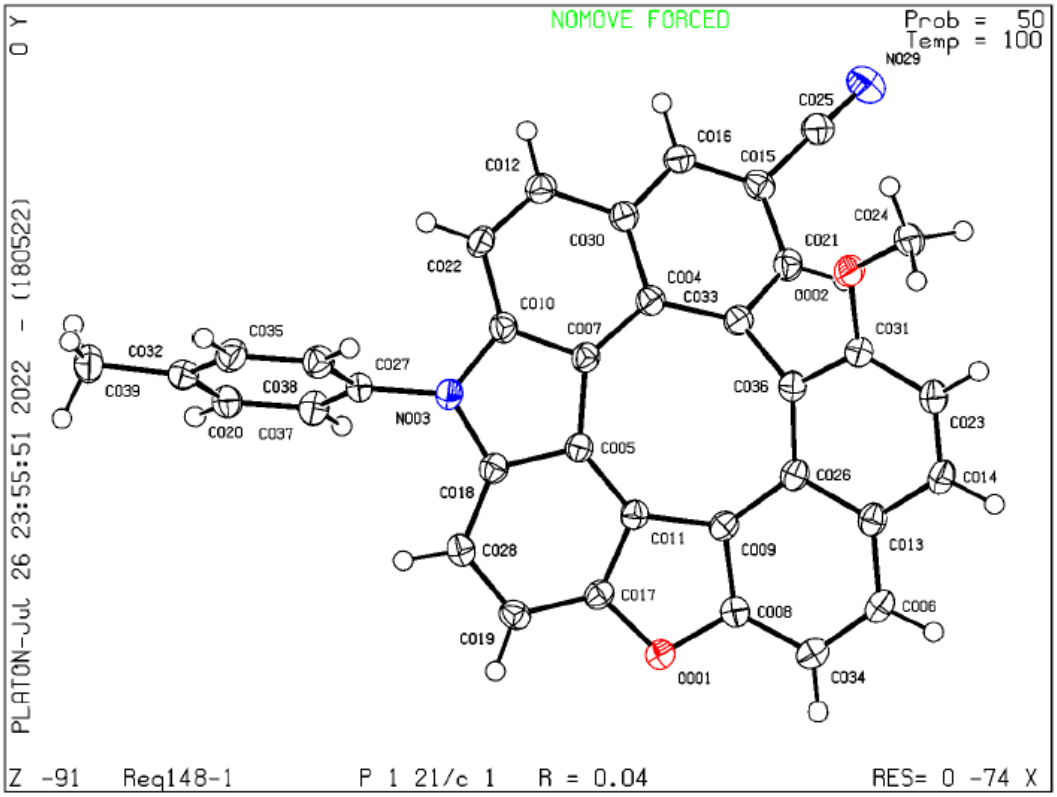
NOMOVE FORCED
Prob = 50
Temp = 100
PLATON-Jul 26 23:55:51 2022 - (180522)
0 Y
Z -91 Req148-1 P 1 21/c 1 R = 0.04 RES= 0 -74 X
N029
C025
C016
C015
C012
C024
C030
C021
C022
C004
C033
O002
C010
C007
C031
C035
C032
C027
C036
C039
C038
N003
C023
C020
C037
C005
C026
C014
C018
C011
C009
C013
C028
C017
C008
C006
C019
O001
C034

86 (CCDC 2183557) with ellipsoids at 30% probability. (H atoms were omitted for clarity).

Empirical formula	$C_{33}H_{17}NO_2$
Formula weight	459.508
Temperature/K	100
Crystal system	triclinic
Space group	P-1
a/Å	8.0973(4)
b/Å	11.6061(5)
c/Å	11.6897(5)
α/°	77.674(3)
β/°	75.721(4)
γ/°	76.630(4)
Volume/Å^3	1021.42(8)
Z	2
ρ_{calc}g/cm^3	1.494
μ/mm^{-1}	0.736
F(000)	477.5
Crystal size/mm^3	0.13 × 0.03 × 0.02
Radiation	CuKα (λ = 1.54184)
2Θ range for data collection/°	7.92 to 152.68
Index ranges	$-10 \leq h \leq 9$, $-11 \leq k \leq 14$, $-14 \leq l \leq 14$
Reflections collected	10181
Independent reflections	4043 [R_{int} = 0.0342, R_{sigma} = 0.0524]
Data/restraints/parameters	4043/0/326
Goodness-of-fit on F^2	1.053
Final R indexes [I>=2σ (I)]	R_1 = 0.0670, wR_2 = 0.1839
Final R indexes [all data]	R_1 = 0.0831, wR_2 = 0.1994
Largest diff. peak/hole / e Å^{-3}	0.80/-0.34

Datablock: req214-1

Bond precision: C-C = 0.0043 A Wavelength=1.54184

Cell: a=8.0973(4) b=11.6061(5) c=11.6897(5)
alpha=77.674(3) beta=75.721(4) gamma=76.630(4)

Temperature: 100 K

	Calculated	Reported
Volume	1021.42(8)	1021.42(8)
Space group	P -1	P -1
Hall group	-P 1	-P 1
Moiety formula	C33 H17 N O2	C33 H17 N O2
Sum formula	C33 H17 N O2	C33 H17 N O2
Mr	459.48	459.48
Dx,g cm-3	1.494	1.494
Z	2	2
Mu (mm-1)	0.736	0.736
F000	476.0	476.0
F000'	477.39	
h,k,lmax	10,14,14	10,14,14
Nref	4287	4043
Tmin,Tmax	0.974,0.985	0.751,1.000
Tmin'	0.909	

Correction method= # Reported T Limits: Tmin=0.751 Tmax=1.000 AbsCorr = MULTI-SCAN

Data completeness= 0.943 Theta(max)= 76.342

R(reflections)= 0.0675(3171) wR2(reflections)= 0.2246(4043)

S = 0.798 Npar= 326

The following ALERTS were generated. Each ALERT has the format
test-name_ALERT_alert-type_alert-level.
Click on the hyperlinks for more details of the test.

Alert level C

DIFMX02_ALERT_1_C The maximum difference density is > 0.1*ZMAX*0.75
The relevant atom site should be identified.

GOODF01_ALERT_2_C The least squares goodness of fit parameter lies outside the range 0.80 <> 2.00
Goodness of fit given = 0.798

PLAT094_ALERT_2_C Ratio of Maximum / Minimum Residual Density .... 2.32 Report

PLAT097_ALERT_2_C Large Reported Max. (Positive) Residual Density 0.72 eA-3

PLAT230_ALERT_2_C Hirshfeld Test Diff for O1 --C019 . 6.9 s.u.

PLAT230_ALERT_2_C Hirshfeld Test Diff for C021 --C023 . 5.5 s.u.
PLAT340_ALERT_3_C Low Bond Precision on C-C Bonds ..... 0.00429 Ang.
PLAT906_ALERT_3_C Large K Value in the Analysis of Variance ..... 4.054 Check
PLAT911_ALERT_3_C Missing FCF Refl Between Thmin & STh/L= 0.600 56 Report

Alert level G

PLAT005_ALERT_5_G No Embedded Refinement Details Found in the CIF Please Do !
PLAT072_ALERT_2_G SHELXL First Parameter in WGHT Unusually Large 0.17 Report
PLAT398_ALERT_2_G Deviating C-O-C Angle From 120 for O1 . 104.2 Degree
PLAT398_ALERT_2_G Deviating C-O-C Angle From 120 for O2 . 105.6 Degree
PLAT720_ALERT_4_G Number of Unusual/Non-Standard Labels ..... 50 Note
PLAT912_ALERT_4_G Missing # of FCF Reflections Above STh/L= 0.600 189 Note
PLAT978_ALERT_2_G Number C-C Bonds with Positive Residual Density. 13 Info

0 **ALERT level A** = Most likely a serious problem - resolve or explain
0 **ALERT level B** = A potentially serious problem, consider carefully
9 **ALERT level C** = Check. Ensure it is not caused by an omission or oversight
7 **ALERT level G** = General information/check it is not something unexpected

1 ALERT type 1 CIF construction/syntax error, inconsistent or missing data
9 ALERT type 2 Indicator that the structure model may be wrong or deficient
3 ALERT type 3 Indicator that the structure quality may be low
2 ALERT type 4 Improvement, methodology, query or suggestion
1 ALERT type 5 Informative message, check

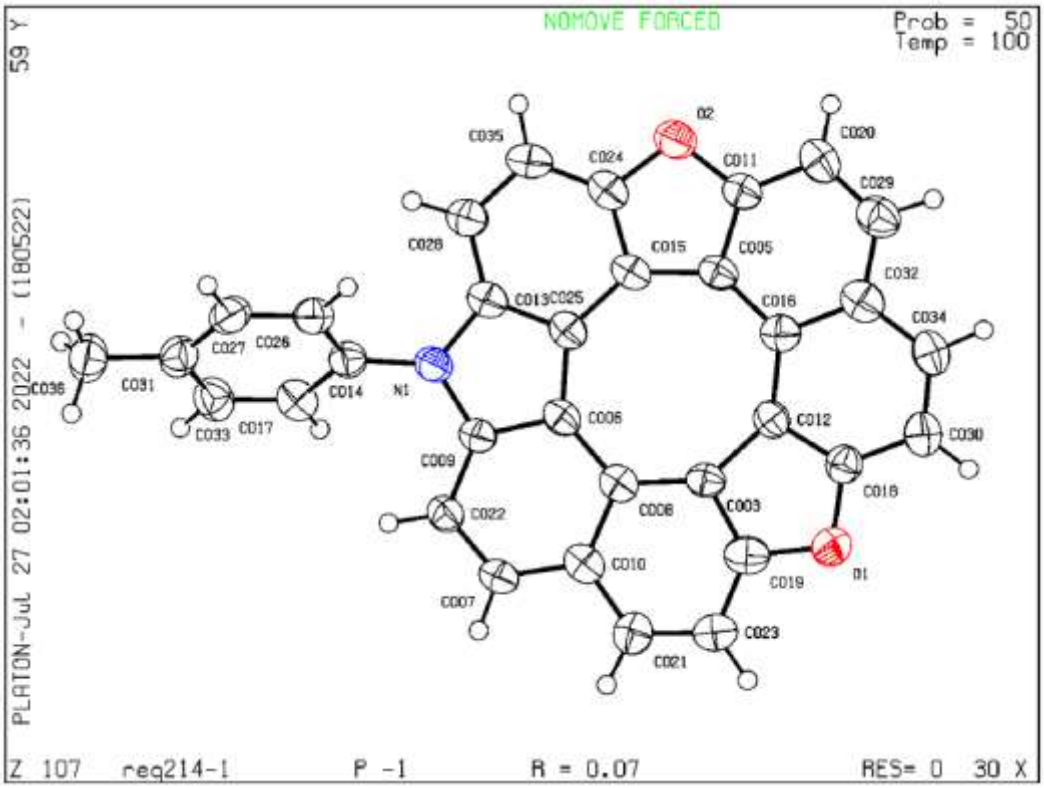

87aa (CCDC 2057234) with ellipsoids at 30% probability. (H atoms were omitted for clarity).

Empirical formula	$C_{34}H_{21}NO_3$
Formula weight	491.550
Temperature/K	100
Crystal system	triclinic
Space group	P-1
a/Å	7.8183(2)
b/Å	10.4498(3)
c/Å	14.6113(4)
α/°	90.337(2)
β/°	102.930(2)
γ/°	99.636(2)
Volume/Å^3	1145.89(6)
Z	2
ρ_{calc}g/cm^3	1.425
μ/mm^{-1}	0.725
F(000)	513.7
Crystal size/mm^3	0.106 × 0.073 × 0.039
Radiation	CuKα (λ = 1.54184)
2Θ range for data collection/°	6.22 to 151.76
Index ranges	$-9 \le h \le 9$, $-13 \le k \le 13$, $-18 \le l \le 18$
Reflections collected	24136
Independent reflections	4643 [R_{int} = 0.0476, R_{sigma} = 0.0348]
Data/restraints/parameters	4643/0/345
Goodness-of-fit on F^2	1.041
Final R indexes [I>=2σ (I)]	R_1 = 0.0414, wR_2 = 0.1052
Final R indexes [all data]	R_1 = 0.0503, wR_2 = 0.1110
Largest diff. peak/hole / e Å^{-3}	0.21/-0.23

Datablock: No2020-7-3

Bond precision: C-C = 0.0020 A Wavelength=1.54184

Cell: a=7.8183(2) b=10.4498(3) c=14.6113(4)
alpha=90.337(2) beta=102.930(2) gamma=99.636(2)
Temperature: 100 K

	Calculated	Reported
Volume	1145.89(6)	1145.89(6)
Space group	P -1	P -1
Hall group	-P 1	-P 1
Moiety formula	C34 H21 N O3	C34 H21 N O3
Sum formula	C34 H21 N O3	C34 H21 N O3
Mr	491.52	491.55
Dx,g cm-3	1.425	1.425
Z	2	2
Mu (mm-1)	0.725	0.725
F000	512.0	513.7
F000'	513.52	
h,k,lmax	9,13,18	9,13,18
Nref	4768	4643
Tmin,Tmax	0.938,0.972	0.862,1.000
Tmin'	0.926	

Correction method= # Reported T Limits: Tmin=0.862 Tmax=1.000
AbsCorr = MULTI-SCAN

Data completeness= 0.974 Theta(max)= 75.880

R(reflections)= 0.0414(3881) wR2(reflections)= 0.1110(4643)

S = 1.041 Npar= 345

The following ALERTS were generated. Each ALERT has the format
test-name_ALERT_alert-type_alert-level.
Click on the hyperlinks for more details of the test.

Alert level C

PLAT906_ALERT_3_C Large K Value in the Analysis of Variance	2.296	Check
PLAT911_ALERT_3_C Missing FCF Refl Between Thmin & STh/L= 0.600	15	Report

---

Alert level G

PLAT005_ALERT_5_G No Embedded Refinement Details Found in the CIF	Please	Do !
PLAT068_ALERT_1_G Reported F000 Differs from Calcd (or Missing)...	Please	Check
PLAT073_ALERT_1_G H-atoms ref, but _hydrogen_treatment Reported as	constr	Check
PLAT154_ALERT_1_G The s.u.'s on the Cell Angles are Equal ..(Note)	0.002	Degree
PLAT720_ALERT_4_G Number of Unusual/Non-Standard Labels	59	Note
PLAT769_ALERT_4_G CIF Embedded explicitly supplied scattering data	Please	Note
PLAT912_ALERT_4_G Missing # of FCF Reflections Above STh/L= 0.600	111	Note
PLAT978_ALERT_2_G Number C-C Bonds with Positive Residual Density.	7	Info
PLAT982_ALERT_1_G The C-f'= 0.0192 Deviates from IT-value =	0.0181	Check
PLAT982_ALERT_1_G The N-f'= 0.0326 Deviates from IT-value =	0.0311	Check
PLAT982_ALERT_1_G The O-f'= 0.0524 Deviates from IT-value =	0.0492	Check
PLAT983_ALERT_1_G The O-f"= 0.0338 Deviates from IT-Value =	0.0322	Check

---

0 **ALERT level A** = Most likely a serious problem - resolve or explain
0 **ALERT level B** = A potentially serious problem, consider carefully
2 **ALERT level C** = Check. Ensure it is not caused by an omission or oversight
12 **ALERT level G** = General information/check it is not something unexpected

7 ALERT type 1 CIF construction/syntax error, inconsistent or missing data
1 ALERT type 2 Indicator that the structure model may be wrong or deficient
2 ALERT type 3 Indicator that the structure quality may be low
3 ALERT type 4 Improvement, methodology, query or suggestion
1 ALERT type 5 Informative message, check

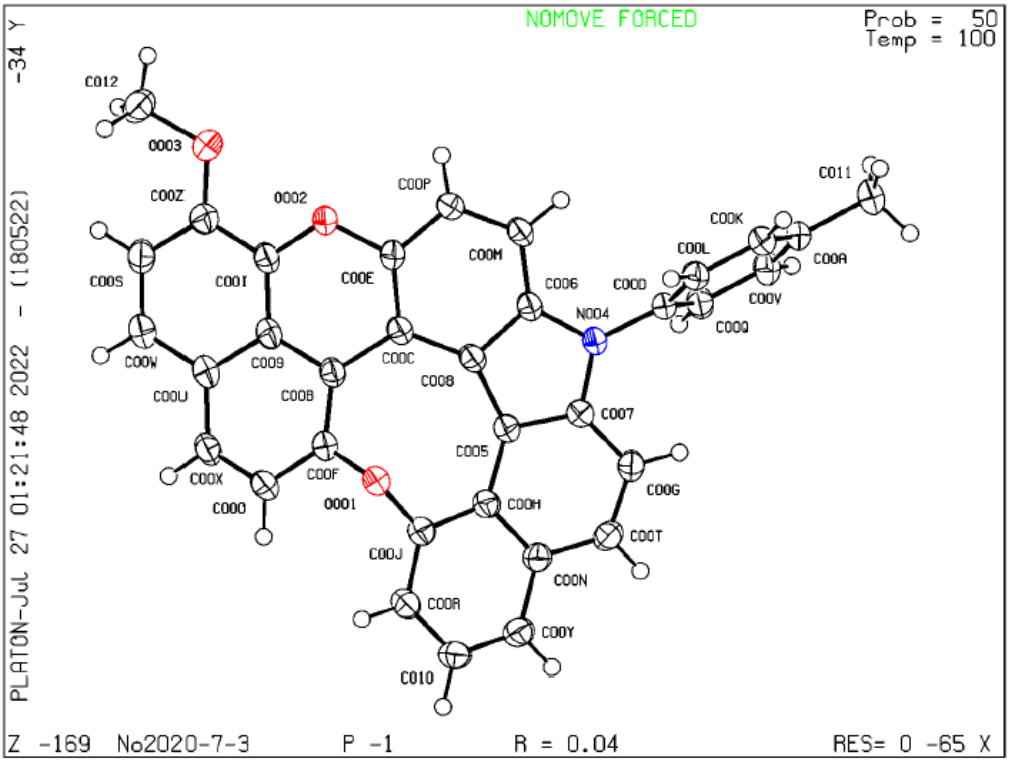

89a with ellipsoids at 30% probability. (H atoms were omitted for clarity).

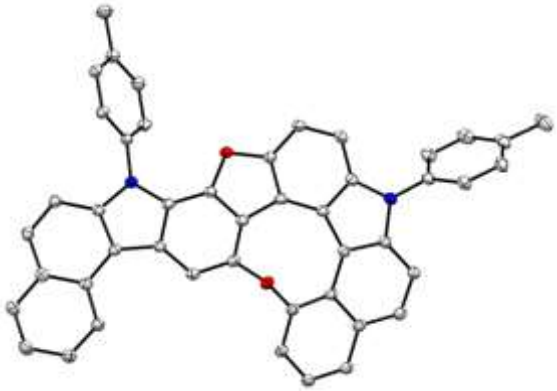

Empirical formula	$C_{52.57}H_{32}N_{2.29}O_{2.29}$
Formula weight	732.23
Temperature/K	100
Crystal system	monoclinic
Space group	C2/c
a/Å	19.3733(3)
b/Å	18.8934(3)
c/Å	17.7205(2)
α/°	90
β/°	101.3490(10)
γ/°	90
Volume/Å^3	6359.36(16)
Z	7
ρ_{calc}g/cm^3	1.338
μ/mm^{-1}	0.643
F(000)	2672.0
Crystal size/mm^3	0.185 × 0.091 × 0.067
Radiation	CuKα (λ = 1.54184)
2Θ range for data collection/°	6.598 to 150.796
Index ranges	$-22 \leq h \leq 24$, $-23 \leq k \leq 22$, $-22 \leq l \leq 21$
Reflections collected	31903
Independent reflections	6466 [R_{int} = 0.0280, R_{sigma} = 0.0218]
Data/restraints/parameters	6466/0/453
Goodness-of-fit on F^2	1.045
Final R indexes [I>=2σ (I)]	R_1 = 0.0415, wR_2 = 0.1106
Final R indexes [all data]	R_1 = 0.0446, wR_2 = 0.1129
Largest diff. peak/hole / e Å^{-3}	0.28/-0.24

Datablock: req133-1

Bond precision: C-C = 0.0019 A Wavelength=1.54184

Cell: a=19.3733(3) b=18.8934(3) c=17.7205(2)
alpha=90 beta=101.349(1) gamma=90

Temperature: 100 K

	Calculated	Reported
Volume	6359.37(16)	6359.36(16)
Space group	C 2/c	C 1 2/c 1
Hall group	-C 2yc	-C 2yc
Moiety formula	C46 H28 N2 O2 [+ solvent]	1.143(C46 H28 N2 O2)
Sum formula	C46 H28 N2 O2 [+ solvent]	C46 H28 N2 O2
Mr	640.70	640.70
Dx,g cm-3	1.338	1.171
Z	8	7
Mu (mm-1)	0.643	0.562
F000	2672.0	2338.0
F000'	2679.55	
h,k,lmax	24,23,22	24,23,22
Nref	6584	6466
Tmin,Tmax	0.940,0.963	0.958,1.000
Tmin'	0.901	

Correction method= # Reported T Limits: Tmin=0.958 Tmax=1.000
AbsCorr = MULTI-SCAN

Data completeness= 0.982 Theta(max)= 75.398

R(reflections)= 0.0408(5936) wR2(reflections)= 0.1158(6466)

S = 1.025 Npar= 453

```
The following ALERTS were generated. Each ALERT has the format
       test-name_ALERT_alert-type_alert-level.
Click on the hyperlinks for more details of the test.
```

Alert level C

```
PLAT906_ALERT_3_C Large K Value in the Analysis of Variance ......      2.203 Check
PLAT911_ALERT_3_C Missing FCF Refl Between Thmin & STh/L=    0.600          8 Report
```

Alert level G

```
FORMU01_ALERT_1_G  There is a discrepancy between the atom counts in the
            _chemical_formula_sum and _chemical_formula_moiety. This is
            usually due to the moiety formula being in the wrong format.
            Atom count from _chemical_formula_sum:   C46 H28 N2 O2
            Atom count from _chemical_formula_moiety:C52.57799 H32.00400 N2.286 O2
FORMU01_ALERT_2_G  There is a discrepancy between the atom counts in the
            _chemical_formula_sum and the formula from the _atom_site* data.
            Atom count from _chemical_formula_sum:C46 H28 N2 O2
            Atom count from the _atom_site data:  C52.57143 H32 N2.285714 O2.28571
CELLZ01_ALERT_1_G Difference between formula and atom_site contents detected.
CELLZ01_ALERT_1_G ALERT: Large difference may be due to a
            symmetry error - see SYMMG tests
           From the CIF: _cell_formula_units_Z    7
           From the CIF: _chemical_formula_sum  C46 H28 N2 O2
           TEST: Compare cell contents of formula and atom_site data

           atom    Z*formula  cif sites diff
           C        322.00    368.00  -46.00
           H        196.00    224.00  -28.00
           N         14.00     16.00   -2.00
           O         14.00     16.00   -2.00
PLAT041_ALERT_1_G Calc. and Reported SumFormula    Strings  Differ     Please Check
PLAT042_ALERT_1_G Calc. and Reported Moiety Formula Strings Differ     Please Check
PLAT045_ALERT_1_G Calculated and Reported Z Differ by a Factor ...       1.14 Check
PLAT051_ALERT_1_G Mu(calc) and Mu(CIF) Ratio Differs from 1.0 by .      14.33 %
PLAT398_ALERT_2_G Deviating  C-O-C    Angle From 120 for O002           105.0 Degree
PLAT605_ALERT_4_G Largest Solvent Accessible VOID in the Structure        41 A**3
PLAT720_ALERT_4_G Number of Unusual/Non-Standard Labels ..........        78 Note
PLAT912_ALERT_4_G Missing # of FCF Reflections Above STh/L=  0.600       110 Note
PLAT941_ALERT_3_G Average HKL Measurement Multiplicity ...........       4.9 Low
PLAT978_ALERT_2_G Number C-C Bonds with Positive Residual Density.        11 Info
```

```
  0 ALERT level A = Most likely a serious problem - resolve or explain
  0 ALERT level B = A potentially serious problem, consider carefully
  2 ALERT level C = Check. Ensure it is not caused by an omission or oversight
 14 ALERT level G = General information/check it is not something unexpected

  7 ALERT type 1 CIF construction/syntax error, inconsistent or missing data
  3 ALERT type 2 Indicator that the structure model may be wrong or deficient
  3 ALERT type 3 Indicator that the structure quality may be low
  3 ALERT type 4 Improvement, methodology, query or suggestion
  0 ALERT type 5 Informative message, check
```

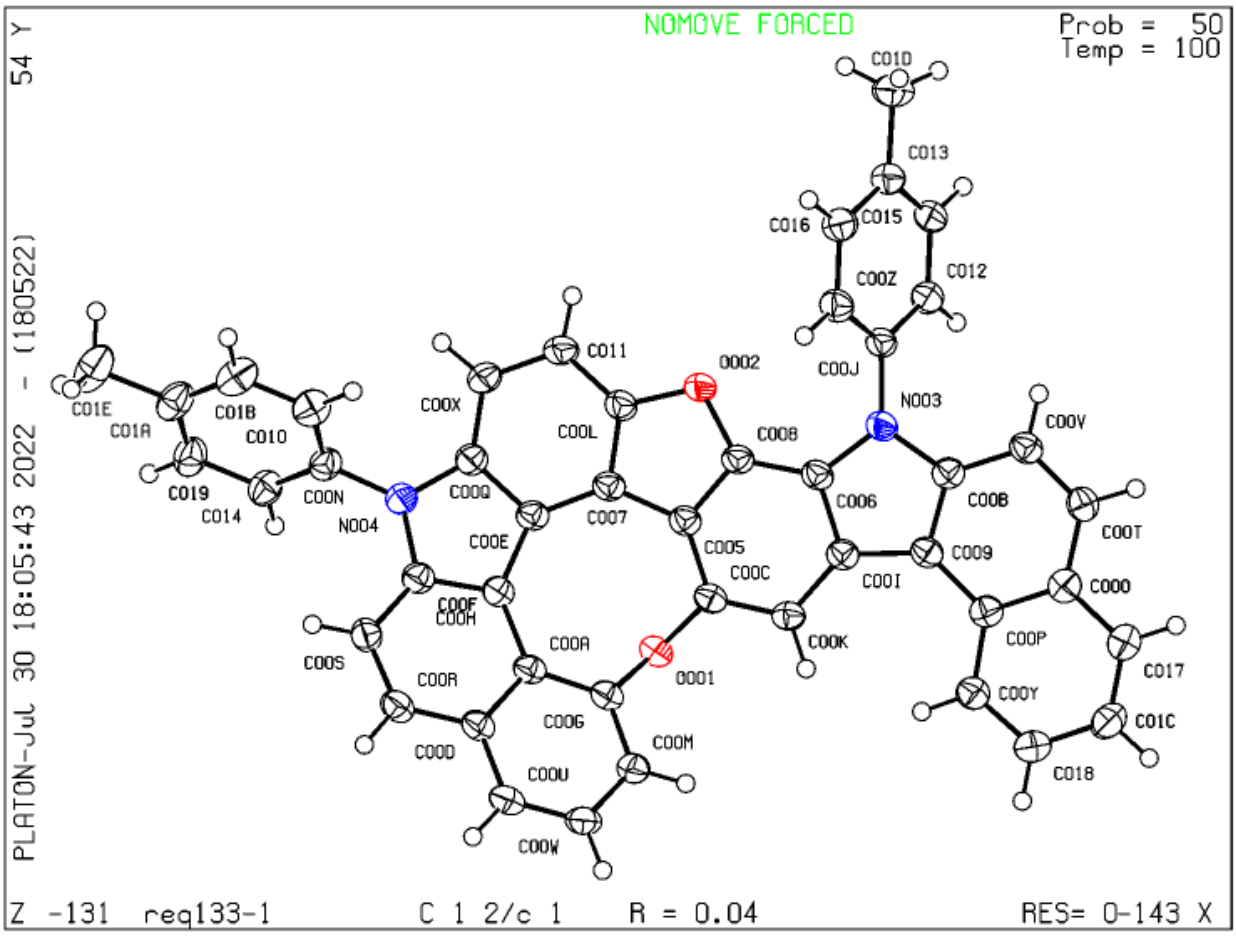
NOMOVE FORCED
Prob = 50
Temp = 100
54 Y
PLATON-Jul 30 18:05:43 2022 - (180522)
Z -131 req133-1
C 1 2/c 1
R = 0.04
RES= 0-143 X
C01D
C013
C016
C015
C012
C00Z
C00J
O002
N003
C011
C00X
C00L
C008
C00V
C01E
C01A
C01B
C010
C019
C014
C00N
N004
C00Q
C007
C006
C00B
C00T
C00E
C005
C00C
C00I
C009
C000
C00F
C00H
C00A
C00K
C00P
C017
C00S
C00R
O001
C00Y
C01C
C00G
C00D
C00M
C00U
C018
C00W

90 with ellipsoids at 30% probability. (H atoms were omitted for clarity).

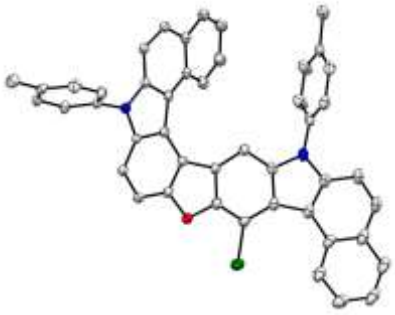

Empirical formula	$C_{46}H_{29}ClN_2O$
Formula weight	755.61
Temperature/K	293(2)
Crystal system	monoclinic
Space group	Pn
a/Å	13.6336(2)
b/Å	29.1177(3)
c/Å	17.1765(2)
α/°	90
β/°	104.7280(10)
γ/°	90
Volume/Å^3	6594.67(14)
Z	7
ρ_{calc}g/cm^3	1.332
μ/mm^{-1}	1.340
F(000)	2752.0
Crystal size/mm^3	0.16 × 0.04 × 0.03
Radiation	Cu Kα (λ = 1.54184)
2Θ range for data collection/°	6.07 to 152.444
Index ranges	-16 ≤ h ≤ 17, -36 ≤ k ≤ 36, -21 ≤ l ≤ 20
Reflections collected	69213
Independent reflections	69213 [R_{int} = ?, R_{sigma} = 0.0583]
Data/restraints/parameters	69213/2/1810
Goodness-of-fit on F^2	0.818
Final R indexes [I>=2σ (I)]	R_1 = 0.0474, wR_2 = 0.1288
Final R indexes [all data]	R_1 = 0.0548, wR_2 = 0.1361
Largest diff. peak/hole / e Å^{-3}	1.74/-0.49
Flack parameter	0.029(4)

Datablock: req186-1

Bond precision: C-C = 0.0076 A Wavelength=1.54184

Cell: a=13.6336(2) b=29.1177(3) c=17.1765(2)
alpha=90 beta=104.728(1) gamma=90

Temperature: 293 K

	Calculated	Reported
Volume	6594.67(14)	6594.67(14)
Space group	P n	P 1 n 1
Hall group	P -2yac	P -2yac
Moiety formula	C46 H29 Cl N2 O	1.143(C46 H29 Cl N2 O)
Sum formula	C46 H29 Cl N2 O	C52.57 H33.14 Cl1.14 N2.29 O1.14
Mr	661.16	755.61
Dx,g cm-3	1.332	1.332
Z	8	7
Mu (mm-1)	1.340	1.340
F000	2752.0	2752.0
F000'	2762.09	
h,k,lmax	17,36,21	17,36,21
Nref	27622[13829]	24560
Tmin,Tmax	0.938,0.961	0.975,1.000
Tmin'	0.807	

Correction method= # Reported T Limits: Tmin=0.975 Tmax=1.000 AbsCorr = MULTI-SCAN

Data completeness= 1.78/0.89 Theta(max)= 76.222

R(reflections)= 0.0537(22251) wR2(reflections)= 0.1593(24560)

S = 1.035 Npar= 1809

The following ALERTS were generated. Each ALERT has the format
test-name_ALERT_alert-type_alert-level.
Click on the hyperlinks for more details of the test.

Alert level C

DIFMX02_ALERT_1_C The maximum difference density is > 0.1*ZMAX*0.75
The relevant atom site should be identified.
PLAT094_ALERT_2_C Ratio of Maximum / Minimum Residual Density .... 3.43 Report
PLAT097_ALERT_2_C Large Reported Max. (Positive) Residual Density 1.68 eA-3
PLAT241_ALERT_2_C High 'MainMol' Ueq as Compared to Neighbors of C05E Check
PLAT241_ALERT_2_C High 'MainMol' Ueq as Compared to Neighbors of C04V Check
PLAT250_ALERT_2_C Large U3/U1 Ratio for Average U(i,j) Tensor .... 2.3 Note
PLAT340_ALERT_3_C Low Bond Precision on C-C Bonds ..... 0.00757 Ang.
PLAT601_ALERT_2_C Unit Cell Contains Solvent Accessible VOIDS of . 75 Ang**3
PLAT911_ALERT_3_C Missing FCF Refl Between Thmin & STh/L= 0.600 5 Report

PLAT971_ALERT_2_C Check Calcd Resid. Dens. 1.50Ang From C043 1.63 eA-3
PLAT987_ALERT_1_C The Flack x is >> 0 - Do a BASF/TWIN Refinement Please Check

Alert level G

CELLZ01_ALERT_1_G Difference between formula and atom_site contents detected.
CELLZ01_ALERT_1_G ALERT: check formula stoichiometry or atom site occupancies.
From the CIF: _cell_formula_units_Z 7
From the CIF: _chemical_formula_sum C52.57 H33.14 Cl1.14 N2.29 O1.14
TEST: Compare cell contents of formula and atom_site data

atom	Z*formula	cif sites	diff
C	367.99	368.00	-0.01
H	231.98	232.00	-0.02
Cl	7.98	8.00	-0.02
N	16.03	16.00	0.03
O	7.98	8.00	-0.02

PLAT045_ALERT_1_G Calculated and Reported Z Differ by a Factor ... 1.143 Check
PLAT199_ALERT_1_G Reported _cell_measurement_temperature ..... (K) 293 Check
PLAT200_ALERT_1_G Reported _diffrn_ambient_temperature ..... (K) 293 Check
PLAT398_ALERT_2_G Deviating C-O-C Angle From 120 for O006 . 104.1 Degree
And 3 other PLAT398 Alerts
More ...
PLAT720_ALERT_4_G Number of Unusual/Non-Standard Labels ..... 313 Note
PLAT790_ALERT_4_G Centre of Gravity not Within Unit Cell: Resd. # 2 Note
C46 H29 Cl N2 O
PLAT910_ALERT_3_G Missing # of FCF Reflection(s) Below Theta(Min). 1 Note
PLAT912_ALERT_4_G Missing # of FCF Reflections Above STh/L= 0.600 181 Note
PLAT915_ALERT_3_G No Flack x Check Done: Low Friedel Pair Coverage 79 %
PLAT933_ALERT_2_G Number of HKL-OMIT Records in Embedded .res File 7 Note
PLAT978_ALERT_2_G Number C-C Bonds with Positive Residual Density. 0 Info

0 **ALERT level A** = Most likely a serious problem - resolve or explain
0 **ALERT level B** = A potentially serious problem, consider carefully
11 **ALERT level C** = Check. Ensure it is not caused by an omission or oversight
16 **ALERT level G** = General information/check it is not something unexpected

7 ALERT type 1 CIF construction/syntax error, inconsistent or missing data
13 ALERT type 2 Indicator that the structure model may be wrong or deficient
4 ALERT type 3 Indicator that the structure quality may be low
3 ALERT type 4 Improvement, methodology, query or suggestion
0 ALERT type 5 Informative message, check

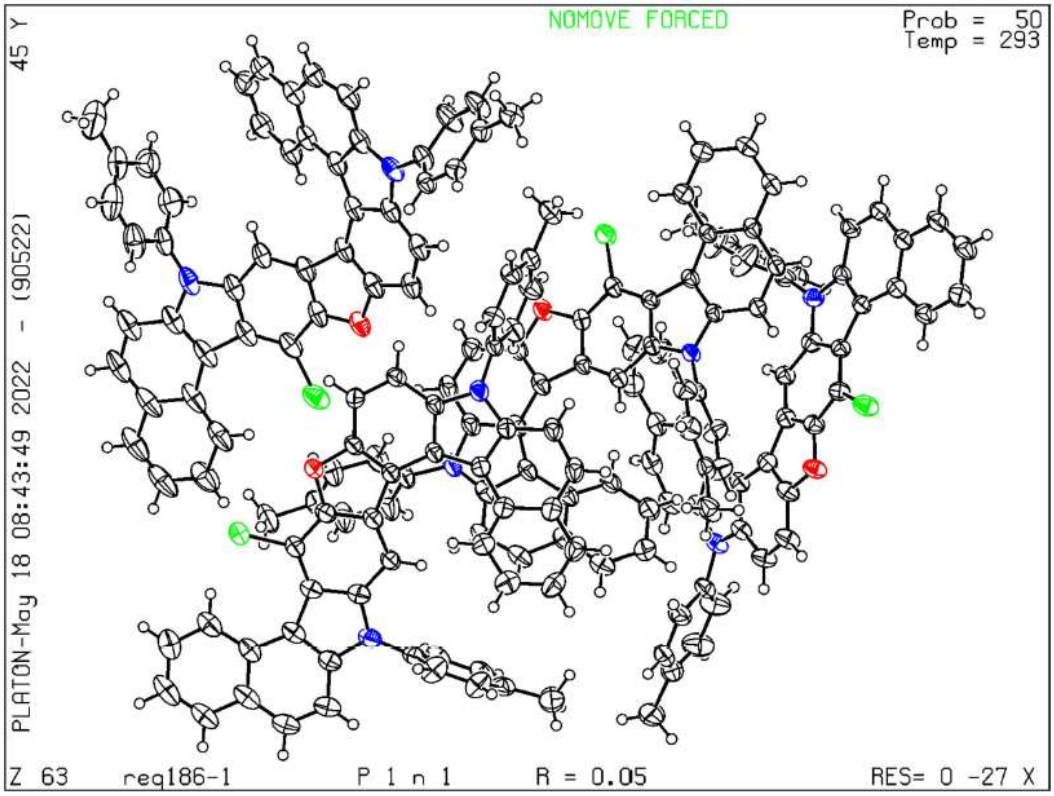
NOMOVE FORCED
Prob = 50
Temp = 293
45 Y
PLATON-May 18 08:43:49 2022 - (90522)
Z 63
req186-1
P 1 n 1
R = 0.05
RES= 0 -27 X

100 (CCDC 2156335) with ellipsoids at 30% probability. (H atoms were omitted for clarity).

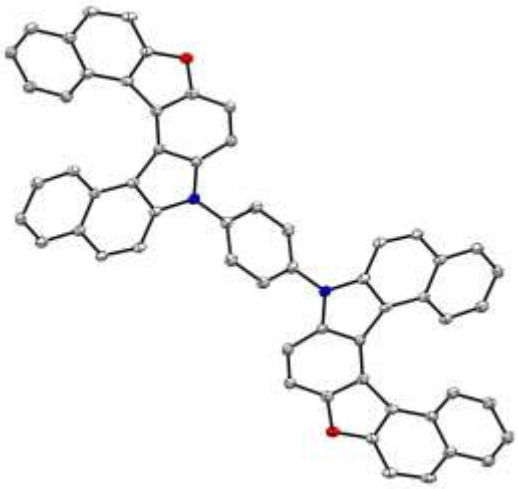

Empirical formula	$C_{77.33}H_{42.67}N_{2.67}O_{2.67}$
Formula weight	1051.81
Temperature/K	293(2)
Crystal system	monoclinic
Space group	I2/a
a/Å	22.2530(10)
b/Å	4.4560(2)
c/Å	37.5710(18)
α/°	90
β/°	91.972(4)
γ/°	90
Volume/Å^3	3723.3(3)
Z	3
ρ_{calc}g/cm^3	1.407
μ/mm^{-1}	0.665
F(000)	1640.0
Crystal size/mm^3	0.09 × 0.08 × 0.05
Radiation	CuKα (λ = 1.54184)
2Θ range for data collection/°	4.548 to 151.27
Index ranges	$-27 \leq h \leq 26$, $-5 \leq k \leq 5$, $-45 \leq l \leq 47$
Reflections collected	9555
Independent reflections	3700 [R_{int} = 0.0380, R_{sigma} = 0.0486]
Data/restraints/parameters	3700/0/281
Goodness-of-fit on F^2	1.077
Final R indexes [I>=2σ (I)]	R_1 = 0.0948, wR_2 = 0.2554
Final R indexes [all data]	R_1 = 0.1204, wR_2 = 0.2737
Largest diff. peak/hole / e Å^{-3}	0.51/-0.42

Datablock: req161-2

Bond precision: C-C = 0.0066 A Wavelength=1.54184

Cell: a=22.253(1) b=4.4560(2) c=37.5710(18)
alpha=90 beta=91.972(4) gamma=90

Temperature: 293 K

	Calculated	Reported
Volume	3723.3(3)	3723.3(3)
Space group	I 2/a	I 1 2/a 1
Hall group	-I 2ya	-I 2ya
Moiety formula	C58 H32 N2 O2	1.333(C58 H32 N2 O2)
Sum formula	C58 H32 N2 O2	C77.33 H42.67 N2.67 O2.67
Mr	788.86	1051.81
Dx,g cm-3	1.407	1.407
Z	4	3
Mu (mm-1)	0.665	0.665
F000	1640.0	1640.0
F000'	1644.60	
h,k,lmax	27,5,47	27,5,47
Nref	3875	3700
Tmin,Tmax	0.942,0.967	0.772,1.000
Tmin'	0.942	

Correction method= # Reported T Limits: Tmin=0.772 Tmax=1.000 AbsCorr = MULTI-SCAN

Data completeness= 0.955 Theta(max)= 75.635

R(reflections)= 0.0948(2707) wR2(reflections)= 0.2737(3700)

S = 1.077 Npar= 281

The following ALERTS were generated. Each ALERT has the format
test-name_ALERT_alert-type_alert-level.
Click on the hyperlinks for more details of the test.

Alert level C

PLAT084_ALERT_3_C High wR2 Value (i.e. > 0.25) ..... 0.27 Report
PLAT340_ALERT_3_C Low Bond Precision on C-C Bonds ..... 0.00658 Ang.
PLAT906_ALERT_3_C Large K Value in the Analysis of Variance ..... 4.284 Check
PLAT911_ALERT_3_C Missing FCF Refl Between Thmin & STh/L= 0.600 30 Report

Alert level G

FORMU01_ALERT_1_G There is a discrepancy between the atom counts in the
_chemical_formula_sum and _chemical_formula_moiety. This is
usually due to the moiety formula being in the wrong format.
Atom count from _chemical_formula_sum: C77.33 H42.67 N2.67 O2.67
Atom count from _chemical_formula_moiety:C77.31399 H42.65599 N2.666 O2
PLAT012_ALERT_1_G No _shelx_res_checksum Found in CIF ..... Please Check
PLAT042_ALERT_1_G Calc. and Reported Moiety Formula Strings Differ Please Check
PLAT045_ALERT_1_G Calculated and Reported Z Differ by a Factor ... 1.333 Check
PLAT072_ALERT_2_G SHELXL First Parameter in WGHT Unusually Large 0.13 Report
PLAT083_ALERT_2_G SHELXL Second Parameter in WGHT Unusually Large 23.24 Why ?
PLAT199_ALERT_1_G Reported _cell_measurement_temperature ..... (K) 293 Check
PLAT200_ALERT_1_G Reported _diffrn_ambient_temperature ..... (K) 293 Check
PLAT398_ALERT_2_G Deviating C-O-C Angle From 120 for O001 . 105.4 Degree
PLAT720_ALERT_4_G Number of Unusual/Non-Standard Labels ..... 47 Note
PLAT870_ALERT_4_G ALERTS Related to Twinning Effects Suppressed .. ! Info
PLAT912_ALERT_4_G Missing # of FCF Reflections Above STh/L= 0.600 145 Note
PLAT955_ALERT_1_G Reported (CIF) and Actual (FCF) Lmax Differ by . 1 Units

0 **ALERT level A** = Most likely a serious problem - resolve or explain
0 **ALERT level B** = A potentially serious problem, consider carefully
4 **ALERT level C** = Check. Ensure it is not caused by an omission or oversight
13 **ALERT level G** = General information/check it is not something unexpected

7 ALERT type 1 CIF construction/syntax error, inconsistent or missing data
3 ALERT type 2 Indicator that the structure model may be wrong or deficient
4 ALERT type 3 Indicator that the structure quality may be low
3 ALERT type 4 Improvement, methodology, query or suggestion
0 ALERT type 5 Informative message, check

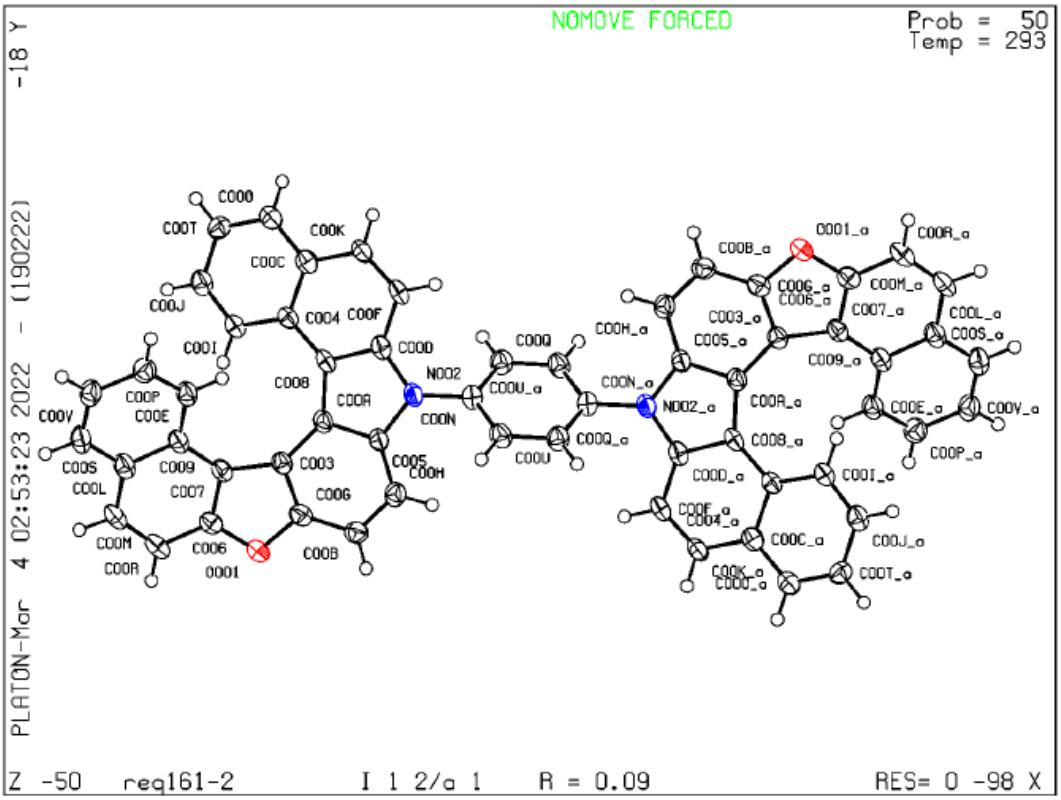
NOMOVE FORCED
Prob = 50
Temp = 293
PLATON-Mar 4 02:53:23 2022 - (190222) -18 Y
Z -50 req161-2 I 1 2/a 1 R = 0.09 RES= 0 -98 X
C000
C00T
C00K
C00C
C00J
C004
C00F
C001
C00D
C008
C00A
NO02
C00N
C00Q
C00U_a
C00H_a
C00N_a
NO02_a
C00Q_a
C00U
C00P
C00E
C00V
C00S
C00L
C009
C007
C003
C005
C00H
C00M
C00R
C006
0001
C00B
0001_a
C00R_a
C00B_a
C006_a
C00M_a
C007_a
C00L_a
C003_a
C005_a
C009_a
C00S_a
C00R_a
C00E_a
C00V_a
C00P_a
C00B_a
C00I_a
C00D_a
C00F_a
C004_a
C00C_a
C00J_a
C00K_a
C000_a
C00T_a

Acknowledgment

During my Ph.D. journey, I received a lot of support, tips, and guidance, through which I learned a lot and avoided making many mistakes. I will remain indebted throughout my life to many people who helped me during this long journey, whom I will certainly not be able to count. I would like to express my sincere gratitude to my supervisors: Prof. Hiroaki Sasai, and Prof. Takayoshi Suzuki for the great opportunity they gave me to work under their guidance and for their continuous support and endless help during my Ph.D. study. I am also so appreciative for my co-supervisor Associate Prof. Shinobu Takizawa, who gave me all kinds of support and help from the first moment and presented me with every possible opportunity to learn. I owe him most of my chemical knowledge and lab skills and this is something I will remember for the rest of my life. Without their valuable suggestions and smart guidance, I could never achieve any real progress in my project.

I would like to thank all committee members for my doctoral defense, Prof. Takashi Kubo, Prof. Hironobu Hojo, and Associate Prof. Takeyuki Suzuki for their kindness, precious time, and dedicated efforts to review my work and to give fruitful suggestions to improve its quality.

I am also so grateful to Dr. Md.Imrul Khalid and Dr. Makoto Sako for their continuous support and valuable guidance that helped me to complete this research. Additionally, I would like to thank all the former staff of Sasai laboratory, especially Dr. Masaru Kondo for continuous assistance. My sincere thanks to the technical staff of the Comprehensive Analysis Center (CAC) at Osaka University and Prof. Masahiro Miura, and Mr. Shotaro Nakamura for the CPL analysis of the dehydrohelicens.

I would like to thank all my friends in the laboratory, for helping me with their tips, and advice and for encouraging me with their kind words. I would like to make a special mention of the secretaries Mrs. Ayaka Honda and Mrs. Kaya Yoshino for caring about our daily office work and various tasks.

It's been a long and hard path but enjoyable at the same time. When I think of the circumstances that led me to this path to come from a faraway place here and study, I feel immense gratitude to all those people who helped me and definitely, this would never be possible without the generous support of the Japanese government (MEXT) scholarship. They open up a great opportunity for me with their financial support to focus on research only.

I cannot forget to acknowledge all my teachers during all educational levels, and this is a good opportunity to remember and appreciate my master's supervisor, prof. Mohamed Mokhtar, who passed away during my Ph.D. study. I will be always indebted for all that you have taught me, and all the learning opportunities that you have created for me. Finally, I would like to express my gratitude and love for the unconditional and endless support of my family and my friends. Without their love, support, and prayers I could never succeed.

Mohamed Salem
Osaka University
2022